Online ISSN 2716-9650
Print ISSN 2676-5837

Volume 2, Dec. 25, 2020

Journal of
Composites and Compounds

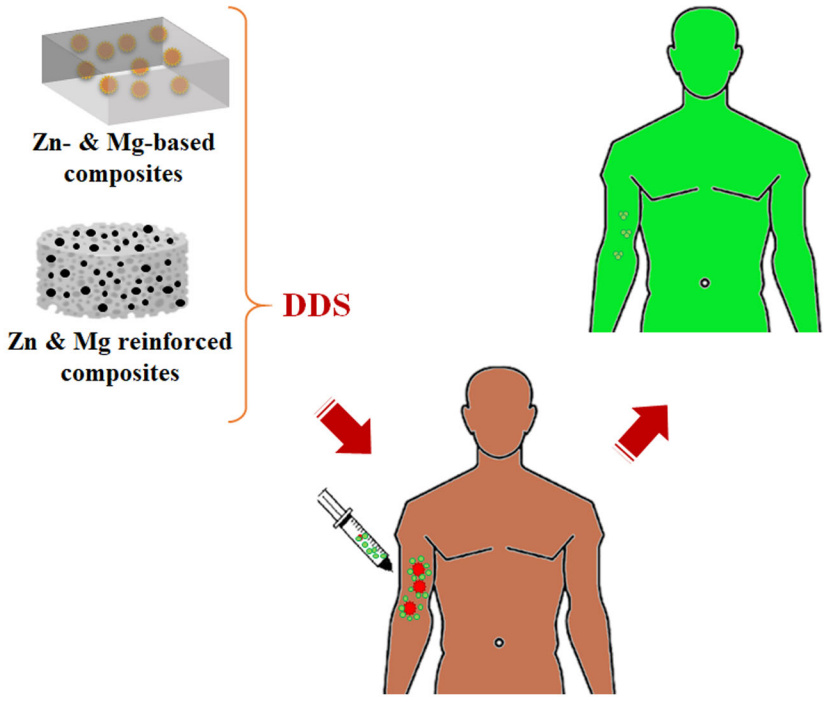

Editor-in-Chief: N. Parvin

www.JOURCC.com

Journal of
Composites and Compounds

Online ISSN 2716-9650
Print ISSN 2676-5837
Dec. 25, 2020
Volume 2
No. 5

Available online at www.jourcc.com

Janatabad St., Tehran, Iran

+982144473176

Journal of
Composites and Compounds
Online ISSN 2716-9650
Print ISSN 2676-5837
Dec. 25, 2020
Volume 2
No. 5

Table of contents

Available online at www.jourcc.com

Janatabad St., Tehran, Iran
+982144473176

Available online at www.jourcc.com

Journal homepage: www.JOURCC.com

Journal of Composites and Compounds

Characterization of TiB_2 reinforced aluminum matrix composite synthesized by in situ stir casting method

Fereshteh Barragh Jam[a], *Hadi Bangi Houri*[b]*, *Morteza Ferdosi*[c]

[a] *Department of Chemical Engineering, Faculty of Engineering, University of Maragheh, Maragheh, Iran*
[b] *Department of Materials and Metallurgical Engineering, Ferdowsi University of Mashhad, Mashhad, Iran*
[c] *Faculty of Materials and Metallurgical Engineering, Semnan University, Semnan, Iran*

ABSTRACT

In this study, TiB_2 reinforced Al-matrix composite was fabricated by in situ stir casting route, and the effect of processing parameters was investigated. X-ray diffraction (XRD) and field emission scanning electron microscopy (FE-SEM) equipped with energy-dispersive X-ray spectroscopy (EDX) were used to study the composition and microstructure of the samples. Finally, to investigate the tribological and electrochemical behavior of the samples, wear tests (pin-on-disk) and potentiodynamic polarization tests (PDP) were used, respectively. Results showed that by increasing stirring time, both tribological and mechanical behavior of the samples improved. Also, it was found that by increasing the stirring speed of the melt to 180 rpm, the mechanical and tribological behavior of the samples improved, and by further increasing the stirring speed to 300 rpm, they were decreased. Consequently, samples containing lower than 7 wt. % TiB_2 showed better metallurgical properties, due to lack of agglomeration.

Peer review under responsibility of jourcc

ARTICLE INFORMATION

Article history:
Received 8 November 2020
Received in revised form 3 December 2020
Accepted 17 December 2020

Keywords:
In situ
Composite
TiB_2
Wear resistance
Stir casting

1. Introduction

One of the most abundant metallic element in nature, after O_2 and Si, is aluminum, which makes up 8.13% of the Earth's crust. Aluminum is a white-silvery and soft metal that is a chemical element with an atomic number of 13. Also, under normal conditions, it is insoluble in water [1]. This metal is found in combination with other elements such as phosphate [2], sulfate [3], silicate [4], and hydroxide [5], and there is no pure state of this metal due to its high reactivity with other chemical elements. Al can also be found in clays, soils, minerals and rocks, and even in food and water. The outstanding features of this metal are its malleability and ductility. The Greek word alum that means astringent in medicine, is the root of the name aluminum [6]. During the reaction of Al with O_2, water, and other oxidants, an Al_2O_3 film is formed on its surface which prevents corrosion of the metal [7]. Al_2O_3 is insoluble in water while easily soluble in strong alkalis and mineral acids, unlike aluminum sulfate, nitrate, and chloride that are dissolved in water [8, 9].

Due to the good wear resistance, high specific strength-to-weight ratio, superior damping capacity, and excellent dimensional stability of Al-based metal matrix composites (MMCs) that are reinforced with ceramic particles, it has been noticed by researchers [10-12]. The incorporation of externally synthesized reinforcements, like TiC, Al_2O_3, and SiC, to the matrix alloys, is commonly applied for preparing Al-based composites (ex-situ composites) [13-16]. In this method, without proper modification of the ceramic particle, the addition of reinforcements could cause poor adhesion at the interface, thermodynamic instability, and segregation of the reinforcements [17, 18]. The superior bonding in the interface of matrix and reinforcement, uniform distribution of smaller particles, process economy, and thermodynamical stability of the reinforcing particles are the advantages of the in-situ synthesized MMCs because the reinforcement formation takes place within the matrix [4, 19, 20]. For the fabrication of the Al-based MMCs, many in-situ formed ceramic particulates including TiC, TiB_2, and Al_2O_3 can be used [21-23].

Due to the outstanding wear resistance, high hardness (3400 HV), high elastic modulus (534 GPa), and high melting point (3225 °C) of TiB_2, it is an advanced strengthening phase for Al matrix [24]. Moreover, TiB_2 does not show any reaction with Al to form detrimental products at the interface of the matrix and reinforcement and this is a special reason for their application [18, 25]. The mechanical erosion resistance, oxidation stability, and excellent heat conductivity are the properties of TiB_2 as a hard ceramic. TiB_2 reacts with sulfuric acid, nitric acid, and alkalis, however, it is not oxidized in the air above 1100 °C and also in hydrofluoric and hydrochloric acids [26-29].

To prepare in-situ composites of Al/TiB_2 with enhanced dispersion of the reinforcing agent, a new method of mechanical stirring at the interface of Al and the salts was developed by Chen et al. [30]. They reported that the improvement in the distribution of TiB_2 particles in the aluminum matrix was due to the interface mechanical stirring. The speed of 180 rpm stirring was applied for both first 15 min and last 15min of the

* *Corresponding author: Hadi Bangi Houri; E-mail: Pers73hadi@gmail.com*
https://doi.org/10.29252/jcc.2.4.1

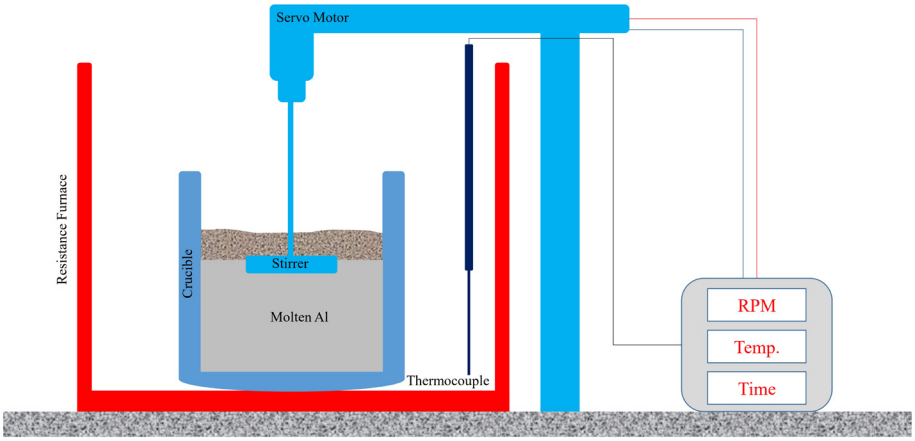

Fig. 1. The schematic representation of the installed equipment.

60 min for the synthesis process.

Pazhouhanfar et al. [31] synthesized the composite of Al-TiB_2 with 3, 6, and 9 wt. % of TiB_2 reinforcement by the method of stir casting. They analyzed the mechanical and microstructure properties of the composites. They reported that using the optimized process parameters leads to a uniform distribution without agglomeration for reinforcements in the aluminum matrix. Furthermore, preheating of TiB_2 powders and the addition of K_2TiF_6 results in a strong bonding.

The clusters of particles in the cast of MMCs are formed due to the combination of reinforcement settling effect and the particle rejection by the matrix dendrites while growing into the remaining melt during the solidification process [32]. In this work, the vortex casting method was applied for in-situ preparation of Al/TiB_2 composites which is an attractive method because of flexibility in using raw materials and the condition of processing. Also it has economic benefits of large-scale manufacturing. The amount of reinforcing particles, sample cooling rate, stirring start time, and stirring time are the process parameters.

2. Materials and methods

Aluminum matrix composite reinforced with TiB_2 particles has been produced through exothermic reactions, using Halide salts of KBF_4 – K_2TiF_6 within molten aluminum. This composite is produced through the following reactions.

$$3K_2TiF_6 + 13Al \rightarrow 3KAlF_4 + K_3AlF_6 + 3TiAl_3 \quad (1)$$

$$2KBF_4 + 3Al \rightarrow 2KAlF_4 + AlB_2 \quad (2)$$

$$TiAl_3 + AlB_2 \rightarrow TiB_2 + 4Al \quad (3)$$

The aluminum used here was %99.8 pure aluminum. %99 pure KBF_4 and K_2TiF_6 have been used as well. Fig. 1 displays the schematic representation of the equipment used for composite production. For any experiment, 1.5kg of aluminum has been melted and maintained in a graphite-clay crucible under a temperature of 850 °C. The powders used in this study have been dried up for two hours under a temperature of 200 °C. The powders have been mixed afterward with a Ti/B stoichiometric ratio of 1.2 and have been added to the molten mixture. After the powders have been fully solved in the molten mixture, a pre-heated four-bladed stirrer has been used to fully mix the molten material and composite-maker powders and stirred the mixture under different conditions. To prevent the entry of impure elements including Fe inside the molten mixture, the stirrer blades have been coated with nickel.

Different stirring velocities of the molten mixture were 0, 60, 180, and 300 rpm for 5, 15, 30, and 60 minutes respectively. To study the impacts of the time starting from the rest time until the start of stirring on mechanical and tribological properties of the samples, 0, 15, 30 and 45 minutes have passed after adding the reinforcing particles to the molten mixture and stirring operation has been conducted then. It's noteworthy that the molten mixture's temperature has been conserved throughout these time durations to prevent the solidification of the mixture. To study the impact of reinforcing particle's amount on the properties of composites being produced, samples with different percentages of reinforcing particles (0, 1, 4, 7, and 9 wt. %) have been produced. The first series of samples being investigated were samples with different percentages of reinforcing materials which have been investigated after identifying the best reinforcing percentage of other remaining samples. Table 1 displays the characteristics of samples under investigation.

To study the phases involved in composites being produced, X-Ray Diffraction (XRD) procedure has been used. The device used here was Empyrean with Cu- Kα and its radiation operated at 40 Kv and 40 mA. To study the microstructures, the samples have been sanded with 200-2000 sand and they have been polished then using felt and alumina powder (in micrometer scale) for 10 minutes. Finally, the FESEM device, Quanta 200 model has been used for imaging purposes.

Study the mechanical behavior of the samples, hardness and tensile assays have been used. Hardness testing has been undertaken using the Brinel device, made in Koopa. The study samples selected for hardness

Table 1.
The properties of samples produced under different conditions

Sample	TiB_2 wt. %.	RPM	Time (min)	Time to Mix (min)
S1	Al Pure	-	-	-
S2	1	180	15	0
S3	4	180	15	0
S4	7	180	15	0
S5	9	180	15	0
S6	7	0	15	0
S7	7	60	15	0
S8	7	300	15	0
S9	7	180	5	0
S10	7	180	30	0
S11	7	180	60	0
S12	7	180	15	15
S13	7	180	15	30
S14	7	180	15	45

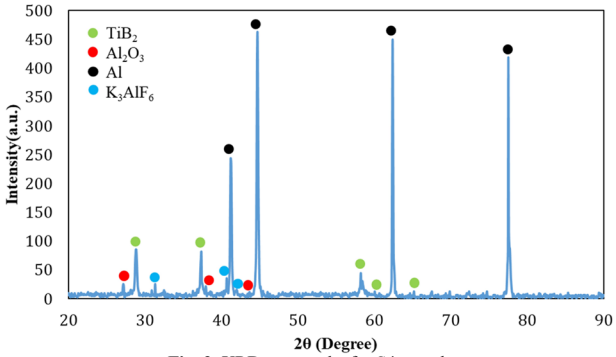

Fig. 2. XRD test results for S4 sample

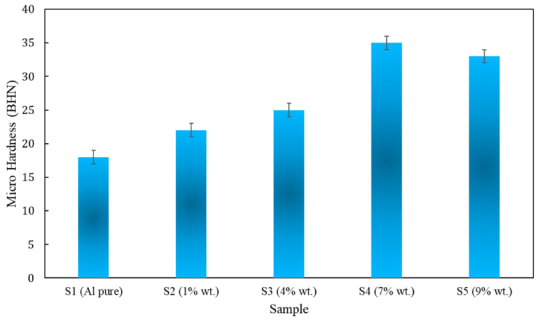

Fig. 4. The results of hardness testing for composites with different percentages of reinforcing particles

testing have been all prepared based on the ASTM E8M-04 standard. Finally, to study the tensile behavior of the samples, Universal tensile testing device, the TB model has been used. The tensile strength of the samples has been tested under a velocity of 0.05 mm/s.

To study the tribological behavior of the samples, a pin on disk wear test has been used. The device used to conduct this test was the wear device, the Bong Shin model. This test has been conducted under room temperature and humidity. The wear velocity was 0.125 m/s and he wear distance was 200 m. the pin used in this study was made up of hardened steel with a hardness ratio of 50 HRC/ finally to test for the impact of reinforcing particles on the electrochemical behavior of the composites being produced, potentiodynamic polarization (PDP) test has been conducted in 3.5 wt. % NaCl solution. This test has been implemented using Origa Flex, made in France with a three-electrode system. The reference electrode used in this test was SCE. The scanning rate in this test was 0.5 mv/s. To develop balance in the Open Circuit Potential (OCP) of the samples, the samples have been immersed in a test solution for one hour.

3. Result and discussion

3.1. Characterization of composites with different TiB_2 content

3.1.1. XRD Analyses

Fig. 2 displays the XRD analysis of the S4 sample. This figure contains the peaks related to TiB_2 as a reinforcing particle. This peak illustrates that the produced composite is an in-place type of composite because the intended phase has been produced inside the molten material and through the reactions between the particles being added and the matrix. The rest of the results illustrate that the main phases being produced are related to TiB_2 and Al phases. Considering the aluminum matrix used in this study, the presence of the main Al peak is not surprising. The presence of TiB_2 as the main peak suggests that the generated Gibbs energy involved in the formation of TiB_2 is far less than the Gibbs energy involved in $AlTi_3$ and AlB_2 formation [25, 33]. The emergence of this peak confirms reactions 1-3. The present study didn't report any intermediate product of $TiAl_3$ or AlB_2. Considering the Ti-B proportion, only 2.1 will be inferred which suggests that no significant portion of KBF_4 or K_2TiF_6 will be synthesized or oxidized during the reactions.

3.1.2. Morphology

Fig. 3 displays the FESEM images produced from S2, S3, S4, and S5. It can be inferred from these figures that reinforcing particles are present within the aluminum matrix. The presence of such particles leads to significant changes in the engineering properties of the samples. According to these figures, it can be concluded that in percentages higher than %7 of TiB_2 particle, agglomeration and clotting behavior occurred within the system. This may lead to the disappearance of sales' engineering behavior because pieces' properties are different in various parts of the samples and we can't record a uniform behavior of the sample. Considering the figures, it can be inferred that the matrix's particles became finer upon the presence of reinforcing particles. The further fineness of the matrix under the influence of reinforcing particles can be studied in two different parts. The first part concerns the initiation of solidification in which the reinforcing particles act as germinating particles and result in I further fineness of the system's particles. The second part concerns the process of solidification itself through which the presence of reinforcing particles inhibits the growth of germinations being developed.

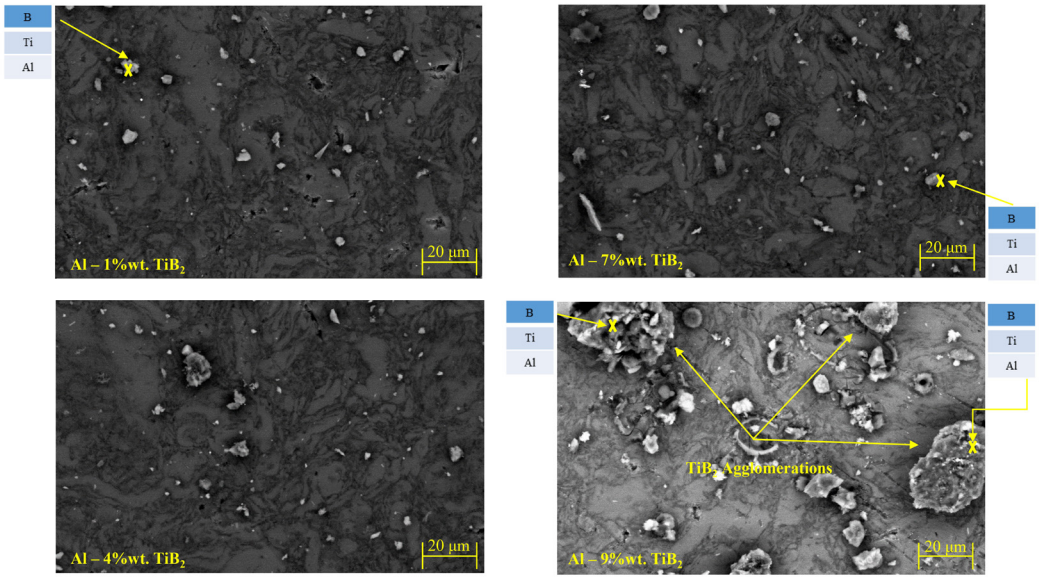

Fig. 3. FESEM images taken from aluminum matrix composites reinforced with different wt. % of TiB_2

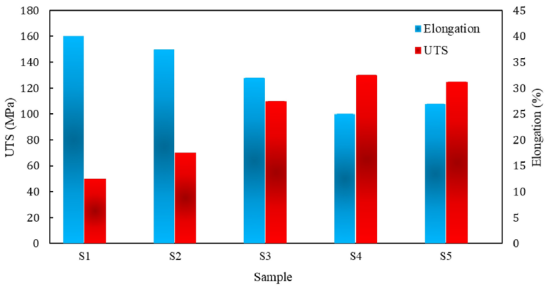

Fig. 5. The results of tensile strength tests for composites including different percentages of reinforcing particles

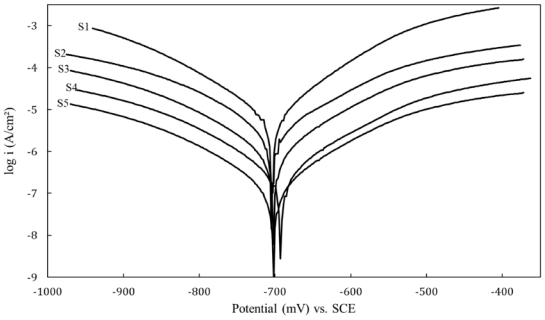

Fig. 7. Polarization diagram related to PDP test

To put it differently, the developed particles are surrounded by these particles and can't grow any further. It's crystal clear that the fineness of the matrix will contribute to improving the mechanical properties of study samples [34, 35].

3.1.3. Hardness

Fig. 4 displays the hardness test results. From this figure, it can be inferred that the presence of reinforcing particles resulted in the higher hardness of study samples compared with pure aluminum. This suggests that the presence of reinforcing particles under any conditions results in increased hardness of the study samples. Besides, the increased number of these particles resulted in increased hardness of the samples. The results of hardness tests illustrated that for values higher than 7 wt. % of reinforcing particles, composites' hardness has been reduced. This may be related to agglomeration and clotting of the particles the hardness reduction and weakening of composites' mechanical behavior upon the presence of reinforcing particles' agglomeration has been proved in the literature as well [29-32]. The presence of reinforcing particles resulted in the development of a higher energy level within the system which will finally result in increased hardness upon locking up the misplacements and development of blockages against misplacements. The mechanism involved in hardness testing is based on the plastic deformity on the surface of the study samples. The plastic deformation required the motion of misplacements; meanwhile, in case any factor prohibits the motion of misplacements, it will result in plastic deformity which will finally contribute to increased hardness.

3.1.4. Tensile

Fig. 5 displays the variations of tensile behavior of the composite samples with different percentages of reinforcing particles. It can be inferred that the presence of reinforcing particles up to 7% wt. of TiB_2 resulted in increased strength of the study samples and upon increasing the amount of reinforcing particles to %9 wt. resulted in decreased strength of the amole. The main reason behind the weakness of the sample's mechanical properties for higher percentages of reinforcing particles can be

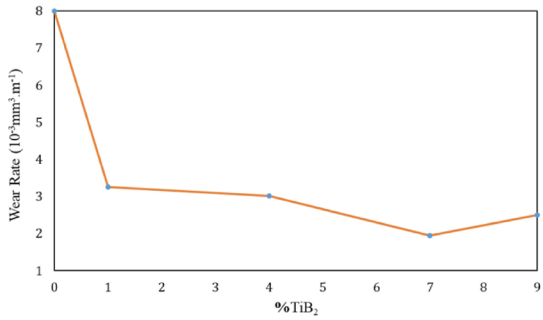

Fig. 6. Wear rate for composites containing different percentages of reinforcing particles

traced back to the agglomeration of reinforcing particles, which has been approved in FESEM images for %9 wt. of reinforcing particles. It can be inferred from Fig. 5 that the use of reinforcing particles resulted in the deceased elongation of the composites being produced. It's clear that the presence of reinforcing particles resulted in misplacements being locked up and therefore their motion potential will be reduced and this was the main reason for higher strength, misplacement lock up and finally decreased composite formation.

Finally, to study the mechanical behavior of the composites being produced (such as hardness and strength) which vary according to the presence of reinforcing particles can be discussed in two main parts [21]. First, based on the (continuous) transfer of matrix load to particles which has been developed through the favorable linking between the soft matrix and TiB_2 particles as strong and non-deficient particles. Whenever tension is incurred on a composite, it will be transferred to reinforcing particles from the matrix. As a result of such transfer of force, the soft and formable matrix will tolerate fewer loads and the reinforced particles will bear a significant portion of the force which will finally lead to improved behavior of the composite behavior. Another related factor is the reinforcing impact of TiB_2 particles on the surrender strength of the aluminum matrix. The impact of reinforcing particles on the composite strength (i.e. $\sigma_{ys)\ can\ be\ analyzed\ based}$ on the following equation [11, 21].

$$\sigma_{yc} = \sigma_{ys} [V_p (1+S/2) + (1-V_p)] \quad (4)$$

Where σ_{yc} is the matrix's strength, V_p is the volumetric fraction of the reinforcing particles, and S is the superficial proportion of reinforcing particles which will be considered as equal to 1 for similar particles. The micromechanics involved in the increased strength of the composites may be originated from the following.

Any variation in the size of matrix particles (further fineness of the matrix) which based on Hall-Petch equation, the boundary of the increased particle will result in the development of obstructions against the motion of misplacements and will finally lock up the misplacements and decrease their motion which is itself the main origin for increased hardness and strength. The second point concerning the boundaries is the resource for misplacement generation. In other words, the boundary itself results in the development of misplacements and increased misplacement density which will lead to misplacement jungle, and locking up the misplacements will result in increased strength as well ($_{Hall\text{-}Petch}\Delta\sigma$).

Orowan mechanism. based on the Orowan mechanism, the use of reinforcing particles will itself contribute to misplacement lock up and obstructs their motion. The pinning of the misplacements through using reinforcing particles will result in increased strength of the composites $\Delta\sigma_{Orowan}$ [33, 34].

The difference in heat expansion coefficient between reinforcing particles and the matrix leads to irregularities in the crystal and will generate misplacements. The increased density of misplacements will

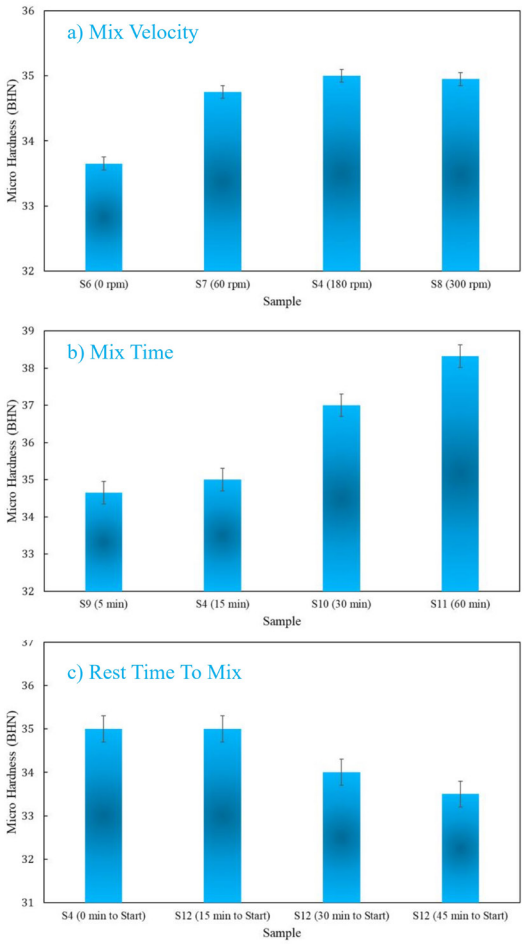

Fig. 8. Variations in samples' hardness under different conditions for the production of Al – 7% wt. TiB2 composite; a) different stirring velocities; b) different stirring durations; c) different resting times and reactions between molten mixtures and aluminum

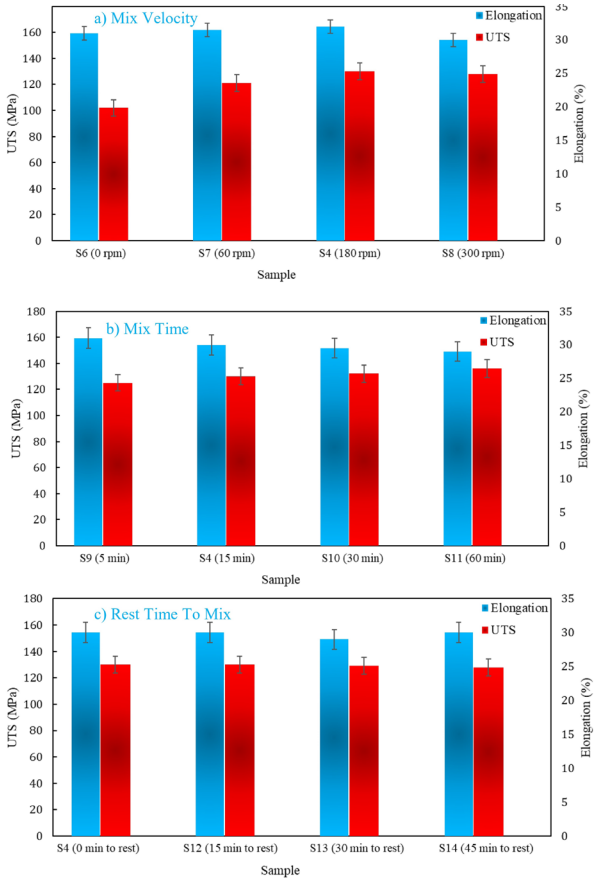

Fig. 9. The tensile behavior of the sample under different conditions for the production of Al – 7% wt. TiB2 composite; a) different stirring velocities; b) different stirring durations; c) different resting times and reactions between molten mixtures and aluminum

lead to the formation of different misplacements locks which will finally contribute to decreased formability and strength of the samples ($_{CTE}\Delta\sigma$).

3.1.5. Wear

Fig. 6 displays the tribological behavior of the composites being produced using different percentages of reinforcing particles. It can be inferred from this figure that composites containing different percentages of reinforcing particles displays different tribological behavior. The figure suggests that the presence of reinforcing particles resulted in a decreased wear rate of the composites. Besides, increasing the amount of reinforcing particles up to 7 wt. %. resulted in decreased wear rate and improved tribological behavior of the composite. Decreased rate of wear and improved tribological behavior of aluminum matrix composites has been proved in other studied available in the literature. A review of the related literature suggests that TiB_2-reinforced composites displayed favorable wear properties compared with composites reinforced with SiC [36-39]. Considering the study conducted by Prasada Rao et al.[40], It has been proved that the presence of TiB_2 particles resulted in decreased wear rate of aluminum matrix composites. According to Prasada Rao et al., the wear rate of the Al-7Si / TiB_2 composite depends upon the size of particles, the distance between dendrites, and the size of Si particles. In other words, in case any factors result in further fineness of system's particles during solidification process and finally, particles in lower dimensions will be developed, the wear properties will be improved and wear rate will be decreased. In this study, the use of reinforcing particles resulted in a decreased wear rate which will consequently lead to a reduction of grains' size. In other words, the presence of TiB_2 particles modifies the particles' morphology and makes them smaller. Finally, the produced composite displays improved wear properties. Meanwhile, increasing the number of particles to higher than 7-9 wt. % results in higher wear rate and diminished sample's tribological behavior. The reason behind the increased wear rate in higher percentages of TiB_2 particles can be traced back to the agglomeration of the particles.

Considering the results obtained from mechanical and tribological tests, it has been suggested that the best parentage to produce aluminum matrix composite reinforced with TiB_2 particles, is 7 wt. % of TiB_2.

3.1.6. Corrosion

The potentiodynamic polarization (PDP) electrochemical test was used to study the effect of TiO_2 particles on the electrochemical properties of the produced composite, which the results are presented in Fig. 7. As shown, the presence of reinforcing particles results in changing the electrochemical behavior of particles. Also, their existence and an increase in their amount in composites lead to the formation of Tafel branches with low flows. In other words, their presence results in decreasing corrosion flow density (Table 2). Based on Fig. 7 and Table 2, adding the reinforcing particles fails to change the slope of Tafel branches and they are produced in lower flow density in parallel, which indicates no change in corrosion mechanism in the existence of the reinforcing particles. Their presence leads to no change in the mechanism of cathodic (e.g., hydrogen reduction) and anodic reactions (e.g., aluminum dissolution) although it only results in decreasing their rate and kinetics [41]. As represented in Table 7, the change in the amount of the reinforcing particles, and their presence or absence fail to vary the corrosion potential of the samples significantly, which represents no change in the thermodynamic of electrochemical reactions in the presence of the

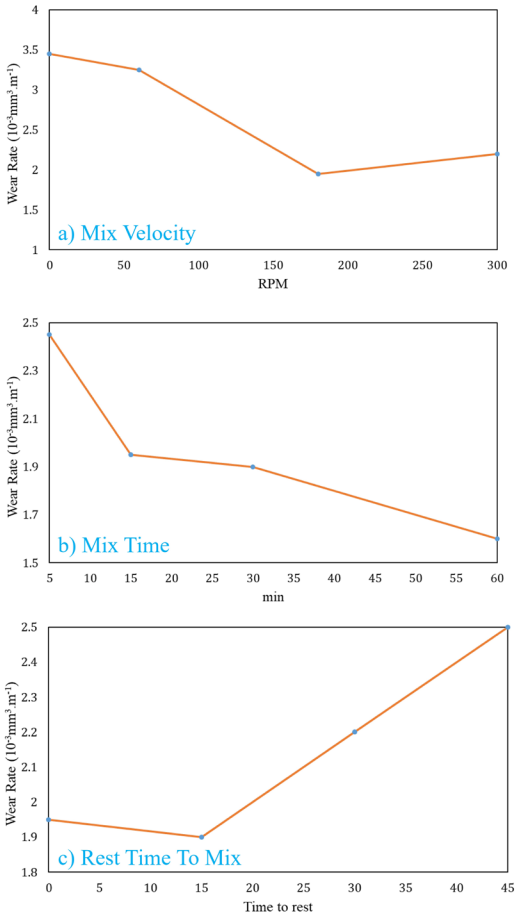

Fig. 10. Wear rate of the study sample under different conditions of Al – 7% wt. TiB2 composite production; 1) different stirring velocities; b) different stirring durations; c) different resting times and implementation of reactions between molten mixture and aluminum

particles [42-44]. Finally, their existence only alters the kinetics of electrochemical reactions. The blockage of the cavities and micro-cracks existing in the structure of aluminum-based by TiO_2 is considered as a reason for reducing the rate of electrochemical reactions (decreasing corrosion flow density) in the existence of the particles. The dangerous ions such as Cl^- can easily pass through each micro-crack due to their small radius (angstrom), which leads to corrosion in the system. The reinforcing particles reduce the diffusion rate of aggressive ions such as Cl^- because of blocking the micro-cracks, leading to a decrease in corrosion rate.

3.2. Characterization of composites with the different condition of fabrication

3.2.1. Mechanical Properties

Figs. 8-9 display the tensile and hardness behavior of the samples produced with different stirring velocity (a), stirring duration (b), and the resting time until the beginning of stirring (c). According to this figure, one can declare that making changes in any of the above parameters resulted in different tensile and hardness behavior of the samples. In other words, making changes in composite production conditions resulted in different mechanical properties of the composites.

To study the impact of stirring speed on the properties of the composites being produced, a reinforced version of the composite containing 7 wt. % of TiB_2 has been produced under different stirring velocities. According to Figs. 8-a,b, stirring contributes to higher hardness and mechanical strength of the composites which suggests that stirring and

Table 2.
Results obtained from PDP test through tafel method

Sample	i_{Corr} (A.cm^{-2})	E_{Corr} (mV)	β_a (mV.decade^{-1})	β_c (mV.decade^{-1})
S1	2.7×10^{-4}	-701	78	-90
S2	7.9×10^{-5}	-700	75	-89
S3	1.36×10^{-5}	-703	74	-91
S4	9.32×10^{-6}	-695	75	-88
S5	1.02×10^{-6}	-699	75	-92

complete mixture of the molten material and reinforcing particles results in optimized mechanical properties of the samples. It's also clear that upon increasing stirring velocity up to 180 rpm, samples' hardness and strength have been increased. On the other hand, increased stirring velocity didn't affect hardness and samples' strength significantly. Improved hardness and strength of the study samples as a result of increased stirring velocity up to 180 rpm can be analyzed through two different points; first, under higher stirring velocities, more uniform scattering of the reinforcing particles will be developed in the matrix which will finally contribute to improved mechanical properties of the samples. Second, higher stirring velocities lead to the formation of finer-grained structures within the matrix. This fine-grained structure results in improved mechanical properties of the composite (Hall-Petch). It has been turned out that increased stirring velocity up to 180 rpm results in decreased mechanical properties of the samples which may be due to excessive turbulence and absorption of developed oxides on the surface of molten material and their entrance into that, such that under higher stirring velocities, the developed oxides on the surface of the molten material will be absorbed and imprisoned which finally results in the production of a deficient piece, with its mechanical properties being weakened. Accordingly, it has been made clear that the best stirring speed for the production aluminum matrix composite reinforced with 7% wt of TiB_2 is 180 rpm.

To study the impact of stirring duration, the sample was reinforced with 7 wt. % of reinforcing particles has been stirred for different time durations. Figs. 8-a, b display the samples' varied hardness and strength upon changing stirring time required for molten material. According to this figure, increased stirring duration resulted in higher hardness and strength of the composites. Improved strength and hardness of the composites upon increased time duration for stirring can be discussed in two levels. First, increasing stirring duration will contribute to better scatteredness of the particles within the system which will finally lead to better mechanical properties of the composite being produced. Second, fine-grained particles affect the system to a great extent. It has been found that upon increasing stirring duration, the microstructure, as well as the matrix's morphology, became finer and therefore the density of particles located on the boundaries will be higher. It's clear that a higher density of the boundary particles results in decreased motion of misplacements and therefore sample's strength will be increased as well. Accordingly, it's expected that samples' deformity and length increase will decrease during the tensile tests. The results of tensile tests all confirm this phenomenon.

To study the rest duration and the reactions that occurred between the added particles and molten material, different time durations have been established and samples have been produced under different resting times. In other words, the samples have been located inside the kiln under different time intervals of 0, 15, 30, and 45 minutes of stirring after the addition of reinforcing particles to the molten mixture. After these times, the mixture has been stirred once again and the molten mixture including the reinforcing particles has been loaded. Figs. 8-c and 9-c display the hardness and strength variations of the composites produced

under different resting times for the molten mixture and addition of reinforcing particles. It has been found that during the primary minutes, the molten mixture undertook required reactions and after some time has been passed, i.e. from 0-15 minutes, no significant changes have been made in samples' mechanical properties. Increased reaction duration between reinforcing particles and the matrix resulted in decreased mechanical properties of the samples. It suggests that increased duration of the reaction between reinforcing materials and the molten mixture results in unwanted reactions inside the molten mixture which will consequently lead to the production of an unfavorable phase. Finally, the presence of such unfavorable phases results in the devastation of the mechanical properties of the samples being produced.

Upon the comparison made between the hardness test results in Figs. 8b-c, it's clear that higher durations of stirring didn't result in a significant change in mechanical properties. Meanwhile, over time in static mode, the composite's hardness is decreased. It suggests that higher stirring durations prohibit the formation of unfavorable phases as well as the development of unwanted reactions and will finally contribute to the formation of a structure with unfavorable phases.

3.2.2. Wear

Fig. 10 displays the variations in wear rate for the samples being produced under different loading conditions. According to Fig. 10-a, it can be inferred that increased velocity for stirring the molten mixture resulted in lower wear resistance. Besides, increased stirring velocity of the molten mixture up to 180 rpm resulted in an increased wear rate. Weakened mechanical properties of the samples under increased stirring velocities have been confirmed in hardness and tensile tests. The reason behind the weakened wear behavior of the composites being produced under higher stirring velocities can be related to the ceramic and fragile phases which have entered inside the molten mixture from the slag due to turbulence. Molten mixture's turbulence will be increased under higher stirring velocities and the paths for oxygen penetration inside the molten mixture will be increased. Therefore, unfavorable oxidized phased will be formed inside the molten mixture which will finally contribute to lowered wear quality of the composite.

It's clear from Fig. 10-b that increased stirring duration resulted in a lower wear rate of the composite. The results of mechanical tests illustrated that increased mixing time for molten mixture and reinforcing particles will contribute to the development of a more uniformly scattered matrix of the reinforcing materials. This will also lead to a decreased risk of formation of reinforcing clots within the matrix and will lower down agglomeration risk as well.

Finally, Fig. 10-c displays that increased resting time results in weakened wear properties of the sample and increases the wear rate. This can be due to the formation of unfavorable phases under higher resting times, such that increased resting time and incomplete mixing of the molten mixture through this low time duration results in the formation of unfavorable phases which will consequently lead to weakened engineering properties of the samples including their wear properties.

4. Conclusions

1. Production of aluminum matrix composite reinforced with TiB_2 particles through the in-place method is possible through using $KBF_4 – K_2TiF_6$ Halide salts.
2. The presence of reinforcing particles within aluminum matrix composite resulted in heightened engineering properties (including hardness, wear, tensile, and corrosion) of the sample composites being produced.
3. The best combination protocol for the production of aluminum matrix composite reinforced with TiB_2 particles is Al / 7% wt. TiB_2.
4. It has been found out that increasing the percentage of TiB_2 particles up to 7 wt. % resulted in the agglomeration of the particles within the composite and weakened its engineering properties.
5. The reinforcing particles obstruct the entrance of dangerous ions such a Cl- upon the obstruction of micro-cracks and pores existing on the surface of the composites and improved samples' electrochemical properties.
6. TiB_2 particles resulted in improved engineering properties of the samples by blocking the misplacements and blocking the particles' growth during solidification.
7. The mechanisms governing the improved strength and hardness of the composites reinforced with TiB_2 particles include Orowan and Hall-Petch.
8. Upon increasing stirring velocity, samples' engineering properties have been weakened as a result of the formation of oxidized phases and turbulence and solution of oxygen within the molten phase.
9. Increased stirring duration improved composites' engineering properties due to uniform scattering of the reinforcing particles inside the composite matrix.
10. Upon increasing the time interval between the moment of adding reinforcing particles to the loading moment (up to 15 minutes), samples' engineering properties will be weakened due to the occurrence of unwanted reactions and the formation of unfavorable phases.

REFERENCES

[1] A.M. Davitoiu, E. Truta, A.M. Mitu, A.A. Bojescu, F. Grama, M. Ionica, The Role of Aluminum in the Symptomatology of Attention Deficit Hyperactivity Disorder Children, Res. & Sci. Today 1 (2018) 115.

[2] C.C.T. Leussa, L. Libessart, C. Djelal, C.N. Djangang, A. Elimbi, Pozzolanic activity of kaolins containing aluminum hydroxide, Scientific Reports 10(1) (2020) 1-12.

[3] A. Bigham, A.H. Aghajanian, M. Movahedi, M. Sattary, M. Rafienia, L. Tayebi, A 3D nanostructured calcium-aluminum-silicate scaffold with hierarchical meso-macroporosity for bone tissue regeneration: Fabrication, sintering behavior, surface modification and in vitro studies, Journal of the European Ceramic Society (2020).

[4] L.S. Fard, N.S. Peighambardoust, H.W. Jang, A. Dehghan, N.N.K. Saligheh, M. Iranpour, M.I. Rajabi, The rechargeable aluminum-ion battery with different composite cathodes: A review, Journal of Composites and Compounds 2(4) (2020) 138-146.

[5] D.-L. Vu, N. Kim, Y. Myung, M. Yang, J.-w. Lee, Aluminum phosphate as a bifunctional additive for improved cycling stability of Li-S batteries, Journal of Power Sources 459 (2020) 228068.

[6] J.L. Domingo, J. Llobet, M. Gomez, J. Tomas, J. Corbella, Nutritional and toxicological effects of short-term ingestion of aluminum by the rat, Research communications in chemical pathology and pharmacology 56(3) (1987) 409.

[7] V.T. Targhi, H. Omidvar, F. Sharifianjazi, A. Paksereshat, Hot corrosion behavior of aluminized and Si-modified aluminized coated IN-738LC produced by a novel hot-dip process, Surfaces and Interfaces 21 (2020) 100599.

[8] M.G. Soni, S.M. White, W.G. Flamm, G.A. Burdock, Safety evaluation of dietary aluminum, Regulatory toxicology and pharmacology 33(1) (2001) 66-79.

[9] E.H. Jazi, R. Esalmi-Farsani, G. Borhani, F.S. Jazi, Synthesis and Characterization of In Situ Al-$Al_{13}Fe_4$-Al_2O_3-TiB_2 Nanocomposite Powder by Mechanical Alloying and Subsequent Heat Treatment, Synthesis and Reactivity in Inorganic, Metal-Organic, and Nano-Metal Chemistry 44(2) (2014) 177-184.

[10] Y. Zhang, N. Ma, H. Wang, Y. Le, X. Li, Damping capacity of in situ TiB_2 particulates reinforced aluminium composites with Ti addition, Materials & design 28(2) (2007) 628-632.

[11] S. Jayalakshmi, S. Gupta, S. Sankaranarayanan, S. Sahu, M. Gupta, Structural and mechanical properties of Ni60Nb40 amorphous alloy particle reinforced Al-based composites produced by microwave-assisted rapid sintering, Materials

Science and Engineering: A 581 (2013) 119-127.
[12] S. Rahimi, F. SharifianJazi, A. Esmaeilkhanian, M. Moradi, A.H.S. Samghabadi, Effect of SiO_2 content on Y-TZP/Al_2O_3 ceramic-nanocomposite properties as potential dental applications, Ceramics International (2020).
[13] S.A. Sajjadi, H.R. Ezatpour, M. Torabi Parizi, Comparison of microstructure and mechanical properties of A356 aluminum alloy/Al_2O_3 composites fabricated by stir and compo-casting processes, Materials & Design 34 (2012) 106-111.
[14] P. Poddar, V.C. Srivastava, P.K. De, K.L. Sahoo, Processing and mechanical properties of SiC reinforced cast magnesium matrix composites by stir casting process, Materials Science and Engineering: A 460-461 (2007) 357-364.
[15] S. Gopalakrishnan, N. Murugan, Production and wear characterisation of AA 6061 matrix titanium carbide particulate reinforced composite by enhanced stir casting method, Composites Part B: Engineering 43(2) (2012) 302-308.
[16] B. Leila, S. Mostafa, S. Arman, A review of carbon nanotube/TiO_2 composite prepared via sol-gel method, Journal of Composites and Compounds 1(1) (2019).
[17] S. Kumar, M. Chakraborty, V. Subramanya Sarma, B.S. Murty, Tensile and wear behaviour of in situ Al–7Si/TiB_2 particulate composites, Wear 265(1) (2008) 134-142.
[18] C.S. Ramesh, A. Ahamed, Friction and wear behaviour of cast Al 6063 based in situ metal matrix composites, Wear 271(9) (2011) 1928-1939.
[19] M. Emamy, M. Mahta, J. Rasizadeh, Formation of TiB_2 particles during dissolution of $TiAl_3$ in Al–TiB_2 metal matrix composite using an in situ technique, Composites Science and Technology 66(7) (2006) 1063-1066.
[20] S. Lakshmi, L. Lu, M. Gupta, In situ preparation of TiB_2 reinforced Al based composites, Journal of Materials Processing Technology 73(1) (1998) 160-166.
[21] Q. Zhang, B.L. Xiao, W.G. Wang, Z.Y. Ma, Reactive mechanism and mechanical properties of in situ composites fabricated from an Al–TiB_2 system by friction stir processing, Acta Materialia 60(20) (2012) 7090-7103.
[22] D.G. Zhao, X.F. Liu, Y.C. Pan, X.F. Bian, X.J. Liu, Microstructure and mechanical properties of in situ synthesized (TiB_2+Al_2O_3)/Al–Cu composites, Journal of Materials Processing Technology 189(1) (2007) 237-241.
[23] A. Masoudian, A. Tahaei, A. Shakiba, F. Sharifianjazi, J.A. Mohandesi, Microstructure and mechanical properties of friction stir weld of dissimilar AZ31-O magnesium alloy to 6061-T6 aluminum alloy, Transactions of nonferrous metals society of China 24(5) (2014) 1317-1322.
[24] H. Morteza Ferdosi, E. Sara, D. Alireza, Ni-Cu matrix composite reinforced with CNTs: preparation, characterization, wear and corrosion behavior, inhibitory effects, Journal of Composites and Compounds 2(4) (2020).
[25] S. Suresh, N. Shenbag, V. Moorthi, Aluminium-Titanium Diboride (Al-TiB_2) Metal Matrix Composites: Challenges and Opportunities, Procedia Engineering 38 (2012) 89-97.
[26] A.C. Reddy, Investigation of the Clustering Behavior of Titanium Diboride Particles in TiB_2/AA2024 Alloy Metal Matrix Composites, 4th International Conference on Composite Materials and Characterization, Hyderabad, India, 2003, pp. 216-220.
[27] B. Basu, G. Raju, A. Suri, Processing and properties of monolithic TiB_2 based materials, International materials reviews 51(6) (2006) 352-374.
[28] A. Aliasghar, M. Mostafa, The Effect of Cu-substitution on the microstructure and magnetic properties of Fe-15%Ni alloy prepared by mechanical alloying, Journal of Composites and Compounds 1(1) (2019).
[29] E. Sharifi Sedeh, S. Mirdamadi, F. Sharifianjazi, M. Tahriri, Synthesis and evaluation of mechanical and biological properties of scaffold prepared from Ti and Mg with different volume percent, Synthesis and Reactivity in Inorganic, Metal-Organic, and Nano-Metal Chemistry 45(7) (2015) 1087-1091.
[30] F. Chen, Z. Chen, F. Mao, T. Wang, Z. Cao, TiB_2 reinforced aluminum based in situ composites fabricated by stir casting, Materials Science and Engineering: A 625 (2015) 357-368.
[31] Y. Pazhouhanfar, B. Eghbali, Microstructural characterization and mechanical properties of TiB_2 reinforced Al6061 matrix composites produced using stir casting process, Materials Science and Engineering: A 710 (2018) 172-180.
[32] A.C. Reddy, Fracture behaviour of brittle matrix and alumina trihydrate particulate composites, (2002).
[33] Z. Sadeghian, M.H. Enayati, P. Beiss, In situ production of Al–TiB_2 nanocomposite by double-step mechanical alloying, Journal of Materials Science 44(10) (2009) 2566-2572.
[34] L. Lu, M.O. Lai, F.L. Chen, Al-4 wt% Cu Composite reinforced with in-situ TiB2 particles, Acta Materialia 45(10) (1997) 4297-4309.
[35] H.B. Michael Rajan, S. Ramabalan, I. Dinaharan, S.J. Vijay, Synthesis and characterization of in situ formed titanium diboride particulate reinforced AA7075 aluminum alloy cast composites, Materials & Design 44 (2013) 438-445.
[36] M. Huang, X. Li, H. Yi, N. Ma, H. Wang, Effect of in situ TiB_2 particle reinforcement on the creep resistance of hypoeutectic Al–12Si alloy, Journal of alloys and compounds 389(1-2) (2005) 275-280.
[37] P.L. Schaffer, L. Arnberg, A.K. Dahle, Segregation of particles and its influence on the morphology of the eutectic silicon phase in Al–7 wt.% Si alloys, Scripta materialia 54(4) (2006) 677-682.
[38] J. Wood, P. Davies, J. Kellie, Properties of reactively cast aluminium–TiB_2 alloys, Materials science and technology 9(10) (1993) 833-840.
[39] M. Zhao, G. Wu, L. Jiang, Z. Dou, Friction and wear properties of TiB_2P/Al composite, Composites Part A: Applied Science and Manufacturing 37(11) (2006) 1916-1921.
[40] A.P. Rao, K. Das, B. Murty, M. Chakraborty, Effect of grain refinement on wear properties of Al and Al–7Si alloy, Wear 257(1-2) (2004) 148-153.
[41] M. Behpour, S. Ghoreishi, M. Khayatkashani, N. Soltani, The effect of two oleo-gum resin exudate from Ferula assa-foetida and Dorema ammoniacum on mild steel corrosion in acidic media, Corrosion science 53(8) (2011) 2489-2501.
[42] M.F. Heragh, S. Eskandarinezhad, A. Dehghan, Ni-Cu matrix composite reinforced with CNTs: preparation, characterization, wear and corrosion behavior, inhibitory effects, Journal of Composites and Compounds 2(4) (2020) 123-128.
[43] M.F. Heragh, H. Tavakoli, Electrochemical properties of a new green corrosion inhibitor derived from Prosopis farcta for St37 steel in 1 M hydrochloric acid, Metals and Materials International (2019) 1-10.
[44] A. Satapathy, G. Gunasekaran, S. Sahoo, K. Amit, P. Rodrigues, Corrosion inhibition by Justicia gendarussa plant extract in hydrochloric acid solution, Corrosion science 51(12) (2009) 2848-2856.

Available online at www.jourcc.com

Journal homepage: www.JOURCC.com

Journal of Composites and Compounds

Synthesis and mechanical properties of Bi_2O_3-$Al_4Bi_2O_9$ nanopowders

Shayan Askari[a], Majid Ghashang[a], Ghazal Sohrabi[a]*

[a] *Department of Chemistry, Najafabad Branch, Islamic Azad University, Isfahan, Iran*

A B S T R A C T

As a result of great surface area and a great number of energetic sites, ceramic nanocomposites are being considered as good adsorbents and catalysts. Al_2O_3 nanoparticles are widely used in high-tech applications owing to their excellent properties. Besides, Bi-based oxides have been the center of attention for applications such as remediation of hazardous wastes and wastewater photochemical degradation of organic contaminants and remediation of hazardous wastes. In this research, the synthesis of Bi_2O_3-$Al_4Bi_2O_9$ nanocomposite and its mechanical properties as a novel composition were investigated. The results showed that the prepared Bi_2O_3-Al4Bi_2O_9 sample exhibited the $Al_4Bi_2O_9$ crystalline peaks. Additionally, the prepared nanocomposite showed no impurities. The mechanical properties of the Bi_2O_3-$Al_4Bi_2O_9$ sample were improved in comparison with Al_2O_3, Bi_2O_3, and Bi_2O_3- Al_2O_3, which offer it as a promising alternative to Bi_2O_3-Al_2O_3 composite ceramic.

Peer review under responsibility of jourcc

A R T I C L E I N F O R M A T I O N

Article history:
Received 2 November 2020
Received in revised form 7 December 2020
Accepted 19 December 2020

Keywords:
Nanocomposite
Catalyst
Al_2O_3
Bi_2O_3-$Al_4Bi_2O_9$
Novel composition

1. Introduction

Due to significant advances in the production of nanostructured materials with new properties, many researchers have focused on the engineering of multi-functional macroscopic materials by structure design at the nanometer scale. One of the fast-growing areas of composites research is the development of nanocomposites [1, 2].

Novel material properties can be achieved by decreasing the particle size to the nanometer scale [3]. In addition to the properties of the matrix and reinforcement, the properties of nanocomposite depend on the morphology and interfacial characteristics of the constituents [4, 5]. The surface area to volume ratio of reinforcements is a morphological property determining the relationship between the structure and property of nanocomposites [3].

Nanocrystalline ceramics have the potential to be used as catalyst supports [6, 7] and adsorbents [8-11] owing to possessing a large surface area and a high number of energetic sites for the interaction with contaminants [12, 13]. Due to the excellent properties of Al_2O_3 nanoparticles, they have found ways to the ceramic industry and high-tech applications [14]. Crystal phases of Al_2O_3 include η, δ, θ, γ, and α-Al_2O_3, and among all these phases, the strongest absorption belongs to α and γ due to possessing the highest surface area for the majority of photocatalytic reactions [15-18].

Owing to properties such as good environmental compatibility, dielectric permittivity, low toxicity, high retractile indicator, and convenient band gap energy about 2.8 eV, Bi-based oxides, especially Bi_2O_3, have been widely studied. These oxides are good candidates for different green applications including remediation of hazardous waste substances and photochemical (visible light) degradation of organic contaminants in wastewater [18-25] Bi_2O_3 is used in some industries including optical coatings, gas sensors, optoelectronics, and solid oxide fuel cells [26, 27]. Trivedi et al. [28] studied the thermal, physical, and atomic properties of Bi_2O_3 treated by biofield energy [29]. According to the results, the physical and atomic characteristics of Bi_2O_3 changed by biofield energy treatment, which makes it more useful to be used in solid oxide fuel cells [30].

Dehkordi et al. [31] used Transient Liquid Phase (TLP) route by Bi_2O_3 reinforcement to join alumina to alumina. Bi_2O_3 was used because of its low melting point [32]. A thin interlayer of Bi_2O_3 was placed between the ceramic bodies [33]. The results showed the interfacial compound growth between Bi_2O_3 and Al_2O_3 at 880 °C upon the TLP process [34]. Higher mechanical properties of the interfaces were observed for longer joining times. Neiman et al. [35] studied differences between the interaction of microsized Al_2O_3 or nanosized Al_2O_3 with microsized Bi_2O_3 [36]. Nano-Al_2O_3 showed higher reactivity and stronger adhesion to micro-Bi_2O_3 leading to the encapsulation of micro-Bi_2O_3 in a shell composed of Al_2O_3 and interaction products [37]. Above 400 °C, the presence of $BiAlO_3$, $Al_2Bi_{24}O_{39}$, and $Al_4Bi_2O_9$ phases was confirmed, and at higher temperatures, the main complex intermediate was $Al_4Bi_2O_9$. At 730 °C, phase transfer from α-Bi2O3 to δ-Bi2O3 was achieved. By further increase in the temperature to 780 °C, the solid phase was decomposed in interaction products, and the δ-Bi_2O_3 phase was separated. The grains of δ-Bi_2O_3 [38] with high conductivity formed a connected charge percolation resulting in a 2.5-fold conductivity increase between 770 °C to 800 °C.

Different methods are employed for the production of metal oxide nanoparticles including electrodeposition, precipitation, sol-gel, hydrothermal, and combustion methods [39, 40]. A common synthesis method is the sol-gel route. Homogeneity and the production of high purity

* *Corresponding author: Shayan Askari ; E-mail: shayan_askari@ymail.com*
https://doi.org/10.29252/jcc.2.4.2

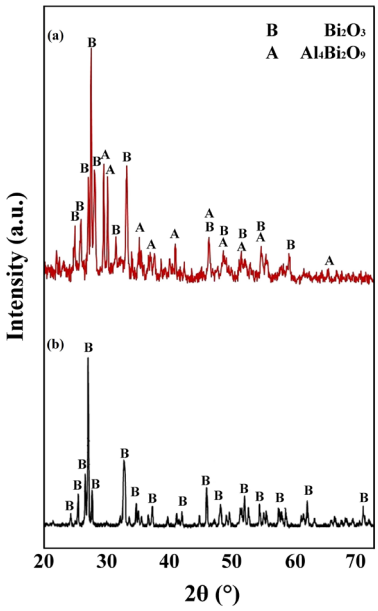

Fig. 1. XRD patterns of the (a) Bi_2O_3-$Al_4Bi_2O_9$ and (b) Bi_2O_3 nanopowders.

materials are some advantages of the sol-gel method [41, 42]. In this study, Bi_2O_3-$Al_4Bi_2O_9$ nanocomposite was synthesized using the sol-gel method and its mechanical properties were evaluated. Based on previous studies regarding the phases formed in Bi_2O_3 and Al_2O_3 nanocomposites, this new nanocomposite is expected to have improved mechanical properties and can be utilized as novel and efficient materials for various applications.

2. Materials and methods

2.1. Materials

All reagents and chemicals i.e. Bismuth (III) nitrate ($Bi(NO_3)_3$, Aluminum nitrate nonahydrate ($Al(NO_3)_3$) and Ethanolamine (2-Aminoethanol) C_2H_7NO in this research were obtained from Merck (Darmstadt, Germany) without further purification. All Glass containers underwent alkali washing and rinsing before application.

Synthesis procedure

To prepare the samples, 300 mmol of 2-aminoethanol was added to 50 ml of water. Then, the solution was added dropwise to a solution containing aluminum nitrate (40 mmol) and $Bi(NO_3)_3$ (40 mmol) in distilled water (200 ml) while the solution was stirred during mixing. Stirring continued for another 60 min. Finally, the precipitates were filtered, washed, and heat-treated at 600 °C for 3 h.

2.2. Characterization

The tensile properties of the nanocomposites were evaluated as per D3039-ASTM at room temperature at a crosshead speed of 5 mm/min using an Instron 6025 device. The samples were prepared by sintering (600 °C for 3 h) with dimensions of 150 × 25 × 3 mm. A three-point bending tester (Instron 6025) was used to measure the bending strength of the nanocomposites. The test was performed according to D790-ASTM at a crosshead speed of 2 mm/ min at room temperature. The length, width, and thickness of the samples were 90 mm, 10 mm, and 3 mm, respectively. A Zwick pendulum impact tester was used to study the impact strength of the samples. The results are the average of five repetitions.

The Vickers hardness of the samples was measured at ambient temperature using Instron, Wilson-Wolpert Tukon 2100B. The applied load

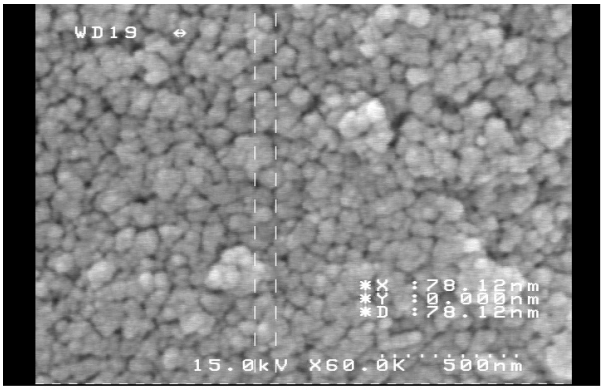

Fig. 2. SEM micrographs of the Bi_2O_3-$Al_4Bi_2O_9$ nanopowder.

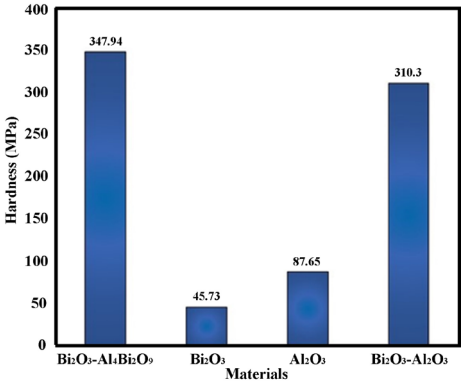

Fig. 3. Vickers hardness of the Bi_2O_3, Al_2O_3, Bi_2O_3-Al_2O_3, and Bi_2O_3-$Al_4Bi_2O_9$ samples.

and loading time was 10 N and 10 s, respectively. The samples were polished prior to the measurement and the measurement was repeated three times for each sample. The structure of the powders was studied using X-ray diffraction analysis (XRD) (Philips X' Pert, The Netherlands) operating at 30 mA and 40 kV. Cu-Kα radiation with λ = 15.405 nm was used, and the step size was 0.02˚. X'Pert HighScore software was utilized to identify the crystalline phases of the powder [43]. The gold-coated fracture surface of the samples was studied by the scanning electron microscopy **(**SEM) analysis (Hitachi S-3400N, Japan). The operating voltage of the microscope was 15 kV [44, 45].

3. Results and discussion

3.1. Microstructural analysis

To identify the crystal structure and parameters, the quantitative and non-destructive method of XRD is widely used. The XRD diffraction pattern of the prepared powder is illustrated in Fig.1. The peaks appeared at 2θ of 24.79°, 25.85°, 27.13°, 27.66°, 28.09°, 31.45°, 33.20°, and 46.51° are related to the Bi_2O_3 phase and the peaks at 15.83°, 29.64°, 30.21°, 35.21°, 41.10°, 48.82, 52.01, 54.91, and 59.35° represent the presence of $Al_4Bi_2O_9$. The $Al_4Bi_2O_9$ and Bi_2O_3 phases have monoclinic and orthorhombic crystal structures, respectively. Additionally, no impurities were detected in the powder composition. The average crystal sizes of the powder estimated from the Debye-Scherrer equation was obtained to be around 24 nm. The microstructure of the Bi_2O_3-$Al_4Bi_2O_9$ nanopowder is illustrated in Fig. 2. As seen, the particle size of the nanopowder is in the range of 30-60 nm.

3.2. Mechanical properties

The results of Vickers hardness for Al_2O_3, Bi_2O_3, Bi_2O_3-Al_2O_3, and Bi_2O_3-$Al_4Bi_2O_9$ are represented in Fig. 3. According to the results, the Bi_2O_3-$Al_4Bi_2O_9$ sample showed the highest hardness compared to other

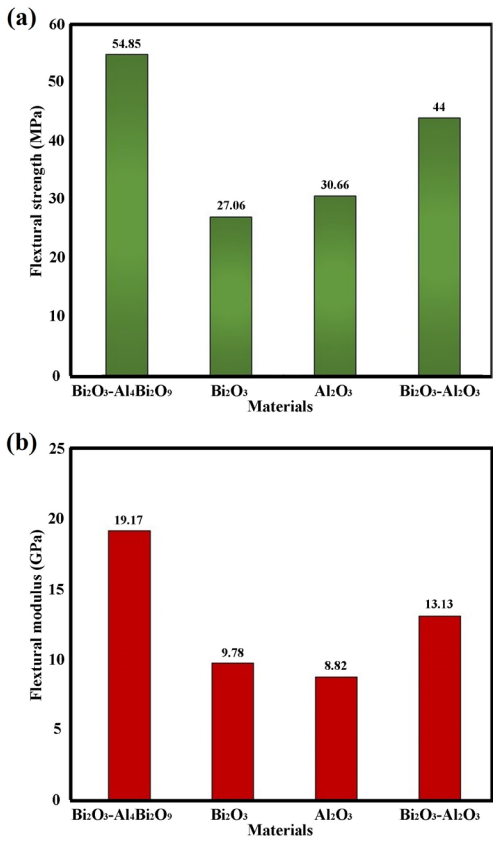

Fig. 4. (a) Flexural strength and (b) flexural modulus of the Bi_2O_3, Al_2O_3, Bi_2O_3-Al_2O_3, and Bi_2O_3-$Al_4Bi_2O_9$ samples

samples, revealing that the Bi_2O_3-$Al_4Bi_2O_9$ composite can be considered as a good alternative to the Al_2O_3-Bi_2O_3 composite. The Vickers hardness data indicated that Bi-O chemical bonds in Bi_2O_3-$Al_4Bi_2O_9$ composite are considerably strong. The Bi_2O_3-$Al_4Bi_2O_9$ samples exhibited 260.29, 302.21, and 37.64 MPa enhancement in Vickers hardness compared to Al_2O_3, Bi_2O_3, and Bi_2O_3-Al_2O_3, respectively. The increase in hardness in the composite indicates a good bond between the Bi_2O_3 and Al_2O_3.

The bending test was carried out to measure the flexural modulus and flexural strength of the samples. The flexural modulus and flexural strength of Al_2O_3, Bi_2O_3, Bi_2O_3-Al_2O_3, and Bi_2O_3-$Al_4Bi_2O_9$ samples are observed in Fig. 4. The results show that the highest value of bending strength is associated with Bi_2O_3-$Al_4Bi_2O_9$. Significant increase in flexural modulus and flexural strength of Bi_2O_3-$Al_4Bi_2O_9$ sample exhibited in Fig. 4. When we use Bi_2O_3 its impact on its mechanical properties such as flexural modulus and flexural strength can be seen. The good effect of Bi_2O_3-$Al_4Bi_2O_9$ can be attributed to the proper relationship created between Al_2O_3 and Bi_2O_3.

Failure toughness of the samples is obtained from the impact test. As shown in Fig.5, The fracture toughness of the Al_2O_3, Bi_2O_3, Bi_2O_3-Al_2O_3, and Bi_2O_3-$Al_4Bi_2O_9$ samples are 0.5, 0.6, 0.8, and 1.8, respectively. The Bi_2O_3-$Al_4Bi_2O_9$ samples showed the highest fracture toughness compared to other samples and Bi_2O_3 show the lowest fracture toughness. The most important reason that can be the cause of this result is the formation of agglomerates and agglomerates at Bi_2O_3, where failure occurs earlier than expected.

4. Conclusions

In this research, Bi_2O_3-$Al_4Bi_2O_9$ nanocomposite was synthesized via the sol-gel method. The formation of the $Al_4Bi_2O_9$ was confirmed by the XRD analysis without any impurities in the composite structure. The

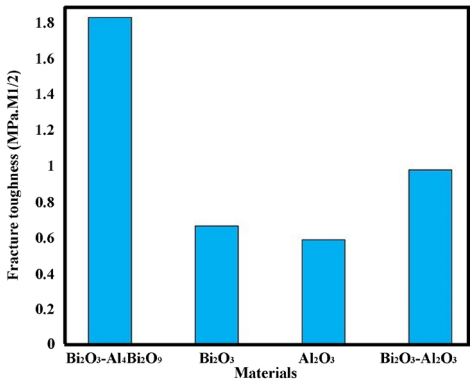

Fig. 4. Fracture toughness of the Bi_2O_3, Al_2O_3, Bi_2O_3-Al_2O_3, and Bi_2O_3-$Al_4Bi_2O_9$ samples

mechanical properties of the Al_2O_3, Bi_2O_3, Bi_2O_3-Al_2O_3, and Bi_2O_3-$Al_4Bi_2O_9$ samples were evaluated and the results showed that Vickers hardness, bending strength, and failure toughness of Bi_2O_3-$Al_4Bi_2O_9$ was the highest amount among other samples. Therefore, this ceramic composite can be a good alternative to the Bi_2O_3-Al_2O_3 composite.

REFERENCES

[1] L. Bazli, A. Khavandi, M.A. Boutorabi, M. Karrabi, Morphology and viscoelastic behavior of silicone rubber/EPDM/Cloisite 15A nanocomposites based on Maxwell model, Iranian Polymer Journal 25(11) (2016) 907-918.

[2] L. Bazli, A. Khavandi, M.A. Boutorabi, M. Karrabi, Correlation between viscoelastic behavior and morphology of nanocomposites based on SR/EPDM blends compatibilized by maleic anhydride, Polymer 113 (2017) 156-166.

[3] E. Thostenson, C. Li, T. Chou, Nanocomposites in context, Composites Science and Technology 65(3-4) (2005) 491-516.

[4] F. Hussain, M. Hojjati, M. Okamoto, R.E. Gorga, Review article: Polymer-matrix Nanocomposites, Processing, Manufacturing, and Application: An Overview, Journal of Composite Materials 40(17) (2006) 1511-1575.

[5] L. Bazli, M.H. Bagherian, M. Karrabi, F. Abbassi-Sourki, H. Azizi, Effect of starch ratio and compatibilization on the viscoelastic behavior of POE/starch blends, Journal of Applied Polymer Science 137(29) (2020) 48877.

[6] J.R. Gaudet, A. de la Riva, E.J. Peterson, T. Bolin, A.K. Datye, Improved Low-Temperature CO Oxidation Performance of Pd Supported on La-Stabilized Alumina, ACS Catalysis 3(5) (2013) 846-855.

[7] H. Purón, J.L. Pinilla, C. Berrueco, J.A. Montoya de la Fuente, M. Millán, Hydrocracking of Maya Vacuum Residue with NiMo Catalysts Supported on Mesoporous Alumina and Silica–Alumina, Energy & Fuels 27(7) (2013) 3952-3960.

[8] M.M. Ibrahim, Cr_2O_3/Al_2O_3 as adsorbent: Physicochemical properties and adsorption behaviors towards removal of Congo red dye from water, Journal of Environmental Chemical Engineering 7(1) (2019) 102848.

[9] L.M. Camacho, A. Torres, D. Saha, S. Deng, Adsorption equilibrium and kinetics of fluoride on sol–gel-derived activated alumina adsorbents, Journal of Colloid and Interface Science 349(1) (2010) 307-313.

[10] J. Li, L. Xu, P. Sun, P. Zhai, X. Chen, H. Zhang, Z. Zhang, W. Zhu, Novel application of red mud: Facile hydrothermal-thermal conversion synthesis of hierarchical porous AlOOH and Al_2O_3 microspheres as adsorbents for dye removal, Chemical Engineering Journal 321 (2017) 622-634.

[11] K. Yang, Y. Li, Z. Zhao, Z. Tian, Y. Lai, Amorphous porous layered-Al_2O_3 derived from AlFu MOFs as an adsorbent for removing fluorine ions in industrial $ZnSO_4$ solution, Chemical Engineering Research and Design 153 (2020) 562-571.

[12] A. Khaleel, P.N. Kapoor, K.J. Klabunde, Nanocrystalline metal oxides as new adsorbents for air purification, Nanostructured Materials 11(4) (1999) 459-468.

[13] K. Hristovski, A. Baumgardner, P. Westerhoff, Selecting metal oxide nanomaterials for arsenic removal in fixed bed columns: From nanopowders to aggregated nanoparticle media, Journal of Hazardous Materials 147(1) (2007) 265-274.

[14] F. Mirjalili, M. Hasmaliza, L.C. Abdullah, Size-controlled synthesis of nano α-alumina particles through the sol–gel method, Ceramics International 36(4) (2010) 1253-1257.

[15] S. Motaghi, M. Farahmandjou, Structural and optoelectronic properties of Ce–Al_2O_3 nanoparticles prepared by sol-gel precursors, Materials Research Express 6(4) (2019) 045008.

[16] M. Farahmandjou, N. Golabiyan, Synthesis and characterization of Alumina (Al_2O_3) nanoparticles prepared by simple sol-gel method, International Journal of Bio-Inorganic Hybrid Nanomaterials 5(1) (2016) 73-77.

[17] M. Salehi, E. Arabsarhangi, Solution combustion synthesis using Schiff-base aluminum complex without fuel and optical property investigations of alumina nanoparticles, International Nano Letters 5(3) (2015) 141-146.
[18] M. Hakimi, M. Morvaridi, H.A. Hosseini, P. Alimard, Preparation, characterization, and photocatalytic activity of Bi_2O_3–Al_2O_3 nanocomposite, Polyhedron 170 (2019) 523-529.
[19] Z.N. Adamian, H.V. Abovian, V.M. Aroutiounian, Smoke sensor on the base of Bi_2O_3 sesquioxide, Sensors and Actuators B: Chemical 35(1) (1996) 241-243.
[20] L. Leontie, M. Caraman, M. Alexe, C. Harnagea, Structural and optical characteristics of bismuth oxide thin films, Surface Science 507-510 (2002) 480-485.
[21] L. Leontie, M. Caraman, M. Delibaş, G.I. Rusu, Optical properties of bismuth trioxide thin films, Materials Research Bulletin 36(9) (2001) 1629-1637.
[22] V. Fruth, M. Popa, D. Berger, R. Ramer, M. Gartner, A. Ciulei, M. Zaharescu, Deposition and characterisation of bismuth oxide thin films, Journal of the European Ceramic Society 25(12) (2005) 2171-2174.
[23] D. Kulkarni, I.E. Wachs, Isopropanol oxidation by pure metal oxide catalysts: number of active surface sites and turnover frequencies, Applied Catalysis A: General 237(1) (2002) 121-137.
[24] T.-K. Tseng, J. Choi, D.-W. Jung, M. Davidson, P.H. Holloway, Three-Dimensional Self-Assembled Hierarchical Architectures of Gamma-Phase Flowerlike Bismuth Oxide, ACS Applied Materials & Interfaces 2(4) (2010) 943-946.
[25] B. Yang, M. Mo, H. Hu, C. Li, X. Yang, Q. Li, Y. Qian, A Rational Self-Sacrificing Template Route to β-Bi_2O_3 Nanotube Arrays, European Journal of Inorganic Chemistry 2004(9) (2004) 1785-1787.
[26] K. Karthik, K.S. Devi, D. Pinheiro, S. Sugunan, Influence of surfactant on the phase transformation of Bi_2O_3 and its photocatalytic activity, Australian Journal of Chemistry 72(4) (2019) 295-304.
[27] M. Al-Buriahi, F. El-Agawany, C. Sriwunkum, H. Akyıldırım, H. Arslan, B. Tonguc, R. El-Mallawany, Y. Rammah, Influence of Bi_2O_3/PbO on nuclear shielding characteristics of lead-zinc-tellurite glasses, Physica B: Condensed Matter 581 (2020) 411946.
[28] M.K. Trivedi, R.M. Tallapragada, A. Branton, D. Trivedi, G. Nayak, O. Latiyal, S. Jana, Evaluation of atomic, physical, and thermal properties of bismuth oxide powder: An impact of biofield energy treatment, (2015).
[29] S. Thakur, V. Thakur, A. Kaur, L. Singh, Synthesis and the study of structural, thermal and optical properties of (100-x) Bi_2O_3-x (BaO-TiO_2) glass system, Optik 223 (2020) 165646.
[30] B.-H. Yun, Study on Bismuth-based Oxide Ion Conductors with High Performance and Durability for Lower Temperature Solid Oxide Fuel Cells, DGIST, 2020.
[31] O.B. Dehkordi, A.M. Hadian, Joining of Alumina to Alumina Using Bismuth Oxide Nano Powder, Procedia Materials Science 11 (2015) 733-737.
[32] K. Kohama, Joining of alumina ceramics using silicon–magnesium composite filler for high-temperature applications, Science and Technology of Welding and Joining 25(5) (2020) 383-390.
[33] F. Cui, Z. Xu, R. Chu, X. He, X. Guo, G. Li, Low temperature sintering ZnO-Bi_2O_3 based varistor ceramics with low electrical breakdown voltage and high nonlinear coefficient, Ceramics International (2020).
[34] Y. Liao, Y. Wang, Z. Chen, X. Wang, J. Li, R. Guo, C. Liu, G. Gan, G. Wang, Y. Li, Microstructure and enhanced magnetic properties of low-temperature sintered LiZnTiMn ferrite ceramics with Bi_2O_3-Al_2O_3 additive, Ceramics International 46(1) (2020) 487-492.
[35] A.Y. Neiman, A.V. Tanskaya, E.V. Tsipis, L.M. Fyodorova, B.D. Antonov, Effect of size factor on mechanism of interaction between Al_2O_3 and Bi_2O_3 and conductivity of composite on their basis, Nanotechnologies in Russia 6(3-4) (2011) 218-226.
[36] I. Zālīte, L. Grase, S. Lagzdina, D. Rašmane, Porous Ceramics from Al_2O_3 Nanopowders, Key Engineering Materials 850 (2020) 273-278.
[37] S.K. Shubham, R. Purohit, P. Yadav, R. Rana, Study of nano-fillers embedded in polymer matrix composites to enhance its properties–A review, Materials Today: Proceedings (2020).
[38] Y. Dong, A. Ma, D. Zhang, Y. Gao, H. Li, Preparation of high-performance α-Bi_2O_3 photocatalysts and their photocatalytic activity, Surface Innovations (2020) 1-9.
[39] V. Amendola, I.D. Amans, Y. Ishikawa, N. Koshizaki, S. Scirè, G. Compagnini, S. Reichenberger, I.S. Barcikowski, Room-Temperature Laser Synthesis in Liquid of Oxide, Metal-Oxide Core-Shells, and Doped Oxide Nanoparticles, Chemistry (Weinheim an der Bergstrasse, Germany) 26(42) (2020) 9206.
[40] M. Parashar, V.K. Shukla, R. Singh, Metal oxides nanoparticles via sol–gel method: a review on synthesis, characterization and applications, Journal of Materials Science: Materials in Electronics (2020) 1-21.
[41] P. Karasiński, A. Domanowska, E. Gondek, A. Sikora, C. Tyszkiewicz, M. Skolik, Homogeneity of sol-gel derived silica-titania waveguide films–Spectroscopic and AFM studies, Optics & Laser Technology 121 (2020) 105840.
[42] H. Ibrahimov, L. Afandiyeva, S. Malikli, G. Rustamli, R. Babali, Obtaining of nanostructured γ-Al_2O_3 by sol-gel method, Thermam (2020) 83.
[43] S. Rahimi, F. SharifianJazi, A. Esmaeilkhanian, M. Moradi, A.H.S. Samghabadi, Effect of SiO_2 content on Y-TZP/Al_2O_3 ceramic-nanocomposite properties as potential dental applications, Ceramics International (2020).
[44] A. Masoudian, M. Karbasi, F. SharifianJazi, A. Saidi, Developing Al_2O_3-TiC in-situ nanocomposite by SHS and analyzingtheeffects of Al content and mechanical activation on microstructure, Journal of Ceramic Processing Research 14(4) (2013) 486-491.
[45] A. Kazemzadeh, M.A. Meshkat, H. Kazemzadeh, M. Moradi, R. Bahrami, R. Pouriamanesh, Preparation of graphene nanolayers through surfactant-assisted pure shear milling method, Journal of Composites and Compounds 1(1) (2019) 25-30.

Available online at www.jourcc.com

Journal homepage: www.JOURCC.com

Journal of Composites and Compounds

Thermal conductivity, viscosity, and heat transfer process in nanofluids: A critical review

Saeed Noorzadeh[a], Farhad Sadegh Moghanlou[a], Mohammad Vajdi[a], Mohammad Ataei[a]*

[a] *Department of Mechanical Engineering, University of Mohaghegh Ardabili, Ardabil, Iran*

A B S T R A C T

Heat transfer efficiency has always been at the center of attractions for many researchers and industries, and demand for higher efficiency methods and materials are increased in the last decades. Among the different methods of heat transfer enhancement, using nanofluids has proven to be an effective technique. In the present paper, the properties of nanofluids including viscosity, thermal conductivity as well as convective heat transfer are discussed and useful conclusions about the reported results by different researchers are presented. The effect of volume fraction, temperature, size and shape of particles, base fluid properties, and other factors on viscosity, and thermal conductivity of nanofluids are reviewed. Also, in the present manuscript, the methods of stable nanofluid preparation, and the effective factors on the stability of nanofluids are exhibited in detail. Besides, a summarized number of experimental and mathematical studies on the properties, and stability of nanofluids are listed, compared, and analyzed. The works about the Nusselt number in fluids and nanofluids are presented in detail to determine the future challenges of nanofluids.

Peer review under responsibility of jourcc

A R T I C L E I N F O R M A T I O N

Article history:
Received 30 August 2020
Received in revised form 6 October 2020
Accepted 16 December 2020

Keywords:
Nanofluid
Heat transfer
Convection
Thermal conductivity

Table of contents

1. Introduction

The rising energy demands and concerns about environmental pollutions have motivated the engineers to utilize new sources of energy such as solar, wind, and biogas [1–4]. The optimization of thermal systems is inevitable to increase the efficiency and reduce the cost and air pollution [2, 5–9]. The energy-efficient systems are obtained by enhancing the heat transfer rate using different passive or active methods [10, 11]. Active methods benefit the external energies such as electric or magnetic field, vibrating surface, or a mechanical mixer. However, the passive methods don't need external sources and the heat transfer enhancement is obtained by a change in geometry or fluid properties [12, 13]. The miniaturization of the channels, using the fins, or utilizing nanofluids are some common passive methods [11, 14–17]. In the last decades, due to the developments of miniaturized devices, such as computer electronic components, the old techniques of cooling became inadequate [15, 18–20]. Besides, the evolutions in technology have created an urgent demand for new and efficient cooling methods to maintain the device temperatures below the critical area. This need for new methods has motivated the researchers to study and find a profitable way. Nanofluid, which is the mixture of nano-sized particles in the base fluid, proved to be a novel heat transfer method in heat transfer issues [21].

Nanofluids are known as a new generation of fluids with hidden and unknown thermal capabilities.

Choi [22, 23] introduced nanofluids and claimed that they showed better heat transfer characteristics than their base fluids. Adding nanoparticles to the base fluid is a passive method for improving heat transfer processes [24]. The volume fraction of the nanoparticles as well as their size and type are significant factors that result in the mentioned improvements. Also, the working temperature and type of fluid play role in enhancement [25, 26].

* *Corresponding author: Farhad Sadegh Moghanloua; E-mail: f_moghanlou@uma.ac.ir*

https://doi.org/10.29252/jcc.2.4.3

Nomenclature

A	Area (m2)	vol	Volume fraction
c_p	Heat capacity (J/kg.K)	wt	Weight fraction
CTAB	Cetyltrimethylammonium bromide		
d	Diameter (m)	*Greek Letters*	
EG	Ethylene glycol	α	Thermal diffusivity
EO	Engine oil	β	A constant
GA	Gum Arabic	μ	Dynamic viscosity (Pa.s)
h	Convective heat transfer coefficient (W/m2 K)	ρ	density (kg/m^3)
k	Thermal conductivity (W/m.K)	σ	A constant
L	Length (m)	ϕ	Particle volume fraction
n	Shape factor	ψ	Sphericity
Nu	Nusselt number		
PG	Propylene glycol	*Subscripts*	
Pr	Prandtl number	bf	Base fluid
PVP	Polyvinyl pyrrolidone nanofluids	c	Critical
R	Thermal resistance (m² K/W)	eff	Effective
r	Radius (m)	l	Laminar
Re	Reynolds number	p	Particle
SDBS	Sodium dodecylbenzene sulfonate	t	turbulent
SDS	Sodium dodecyl sulfate		
T	Temperature (K)		

Nowadays, nanofluids have been used in many fields of industries such as electronic, nuclear, medicine, and transportation systems [27].

Nanofluids preparation, stability, characterizations, thermal features, conduction, and convection heat transfer processes have been studied widely by the researchers [28]. For the first time, Choi [22] dispersed the nano-sized particles in a base fluid and called the mixture as nanofluid. After introducing nanofluids, Lee et al. [29], Eastman et al. [30], Yu et al. [31], and many other researchers investigated the thermal behavior of nanofluids, and heat transfer rate enhancement by use of nanofluids was proved. It was also shown that the unique behavior of nanofluids may originate from some mechanisms such as the Brownian motion of nanoparticles and decreases in the thermal boundary layer [32].

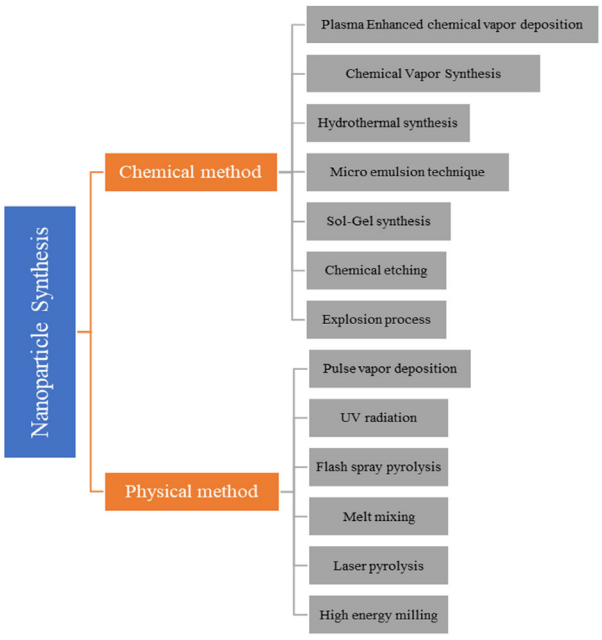

Fig. 1. Synthesizing methods of nanoparticles [21].

As mentioned above, the stability of nanofluids is a crucial factor that determines the applicability of nanofluids. Researchers always looking for stable nanofluids. So, many stability tests have been accomplished and the results showed the three main different methods to prepare a stable suspension, that is surfactants, ultrasonic bath, and pH control [33–35]. Also, there are other factors such as viscosity that are critically related to the pumping power of nanofluid. Although there are a lot of experimental studies of the nanofluids behavior, numerical methods are still a strong tool to obtain detailed information about the investigated phenomenon and have wide applications in heat and mass transfer, biomechanics, and solid mechanics [36, 37, 46, 38–45].

In the present paper, a critical review of the preparation, characterization, and heat transfer enhancement nanofluids has been done. We are attempting to provide a comprehensive review of the factors that affect the thermos-physical properties of nanofluids. Also, the experimental correlations and results have been compiled. The present review mainly aims to summarize the recent researches on thermophysical properties and the stability of nanofluids and applications of nanofluids in various industries and devices.

2. Nanofluids

2.1. Preparation methods

Nanofluids are recognized with their unique thermal properties, such as viscosity, thermal conductivity, and many other properties, compared to common fluids. Many types of nanoparticles are used for synthesizing nanofluids including carbon nanotubes, metals, metal oxides, ceramics, etc. metals generally have considerably high thermal conductivities than fluids, however, some types of advanced ceramics offer interestingly high thermal conductivities even more than common metal, such as ZrB_2 [47, 48, 57–66, 49, 67–76, 50, 77–86, 51, 87–96, 52, 97–102, 53–56], TiB_2 [103, 104, 113–121, 105–112], SiC, AlN [122–125], TiC [126, 127, 136, 128–135], and HfB_2 [137]. These ceramics have proved remarkable thermos-mechanical behaviors in different branches of industry [138, 139, 148–157, 140, 158–164, 141–147]. One of the important factors,

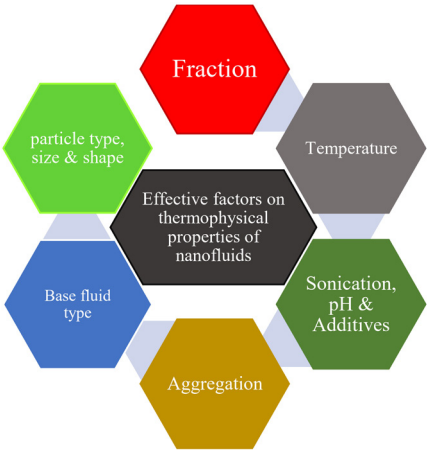

Fig. 2. Effective parameters on thermophysical properties of nanofluids.

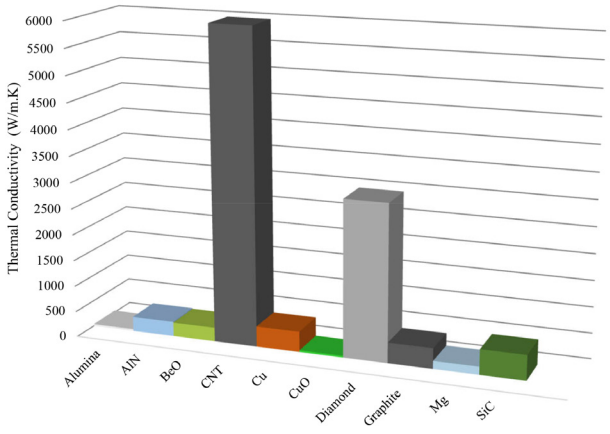

Fig. 3. Thermal conductivity of various materials at 25°C [211].

which affects the final properties od nanofluids, is the preparation of the nanoparticles [165]. Some of the synthesizing methods of nanoparticles are presented in Fig. 1.

Also, there are various methods for analyzing nanoparticles. The most common methods are Transmission Electron Microscope (TEM), Scanning Electron Microscope (SEM), Optical spectroscopy, X-ray Diffraction (XRD), Infrared and Raman Spectroscopy [166].

The synthesis of a nanofluid is a key role task in researches. The main goal of preparing nanofluids is to obtain a stable suspension without any agglomeration in a specified period and temperature. The agglomeration of nanoparticles in a nanofluid is a significant problem in all nanofluid investigations. Two main methods involved with preparing nanofluids are One-step and Two-step methods [167]. The purpose of the mentioned methods is to generate good nanoparticle suspensions. The unique heat transfer improvements by using nanofluids directly depend on the quality of the suspension. The quality of nanofluid is a function of the synthesis method and the homogeneity of nanoparticles in the base fluid [166]. Overcoming the mentioned problems has become more important in higher nanoparticle concentrations [168].

In the One-step method, in a single process, the nanoparticles are formed and dispersed in the base fluid. In the Two-step method, nanoparticles are prepared in the first step and after that, in the second step, the prepared particles are dispersed in a fluid [167]. From an economical point of view, the Two-step method takes lower costs [169]. In the two-

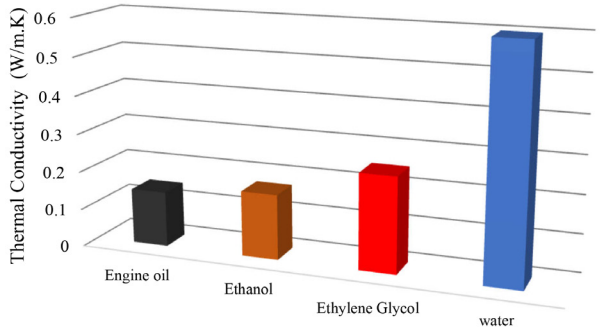

Fig. 4. Thermal Conductivity of various fluids at 25°C [211].

step method, nanoparticles can be synthesized and dispersed in base fluid chemically or mechanically [170]. In chemical dispersion, surfactants are commonly are added to the fluid, whereas in mechanical dispersion, sonication is often employed to disperse nanoparticles [171]. Besides, there are other significant factors that have remarkable effects on a suspension's quality. According to various studies such as Sonawane et al. [172], and Buonomo et al. [173], particle size and sonication time are

Table 1.
Some of the reported synthesis studies of nanofluids

Synthesis method	Authors	Publish year	Nanoparticle/Base fluid	Particle size (nm)	Fraction (Vol% or wt%)
	Eastman et al. [30]	2001	Cu/EG	10	0.3
	Hong et al. [174]	2005	Fe/EG	10	0.55
One-Step	Liu et al. [175]	2006	Cu/Water	75~100	0.1
	Paul et al. [176]	2012	Ag/Water	-	1
	De Robertis et al. [177]	2012	Cu/EG	-	-
	Choi et al. [178]	2001	CNT/Poly oil	25*50000	2
	Murshed et al. [179]	2005	TiO_2/Water	15	5
	Meibodi et al. [180]	2010	CNT/Water	1-4	0.12
	Lee et al. [181]	2011	SiC/Water	<100nm	0.001-3
Two-Step	Singh et al. [182]	2012	Al_2O_3/EG&Water	130,211,300	0.25-1
	Fazeli et al. [183]	2012	SiO_2/Water	18	3.5-5
	Zeinali Heris et al. [184]	2015	MWCNT/Water	10*20000	0.55
	Choudhary et al. [185]	2016	Al_2O_3/Water	40	0.1-2
	Irani et al. [186]	2018	GO/Water+MDEA	-	0.1 & 0.2

other critical factors that affect the dispersion level of nanoparticles and lead to better thermophysical properties of nanofluids. Some of the synthesized nanofluids utilizing one-step and two-step methods reported in various articles are presented in Table 1.

2.2. Stability of nanofluids

Synthesizing a stable and durable homogenous nanofluid has always been challenging for researchers due to the agglomeration of nanoparticles as a result of the van der Waals forces [187]. To avoid particle agglomeration, some physical and chemical methods have been proposed and investigated [165]. The most common method that researchers use while confronting agglomerations is adding surfactants which is a chemical method [188]. The addition of surfactants makes hydrophobic materials disperse in an aqueous suspension better than normal situations [189]. There are many types of surfactants such as Gum Arabic, CTAB, SDS, SDBS, NADDBS, CMC, HCTAB, TX-100, etc. [190]. Besides, the fraction of surfactants that are used for making a suspension stable is very important. If used less than the limit, causes inadequate stability and if overused, causes agglomeration of nanoparticles in the suspension due to the osmotic pressure [191].

Also, there are other methods that enhance the stability of nanofluid. Li and Xuan [192] suggested the ultrasonic waves for increasing the stability of nanofluids in addition to surfactants. Peng et al. [193] defined and studied the important factors of the preparation of stable nanofluids. They showed that the dispersion method, volume fraction of nanoparticles, the viscosity of the base fluid, the value of pH, density of nanofluid, type of nanoparticles, and size of nanoparticles in conjunction with ultrasonic waves affect the stability of nanofluids.

The main purpose of all methods is to prevent particle clustering by changing the surface properties of particles, which results in a stable nanofluid. An ultrasonic bath, which is used widely by researchers [35], is a powerful instrument for breaking the agglomerations. A conclusion of researches, which has utilized an ultrasonic bath to prepare stable nanofluids, is presented Table 2.

The stability of an aqueous nanofluid directly depends on electro-kinetic properties. The high surface charge density of the nanoparticles may result in strong repulsive forces and consequently, bring up better dispersion of nanoparticles in suspensions [35].

In the isoelectric point (IEP), the concentration ions that play a role in zeta potential is zero. In the isoelectric point, surface charge density is equal to electron charge density and because of that, the zeta potential is zero. The pH value has to be considered to attain the isoelectric point [206]. It has been observed that pH control makes a nanofluid to be stable for a long time [207]. By controlling the repulsive force between nanoparticles, the zeta potential is decreased to zero at a particular pH value at the isoelectric point and it is a negative problem for the stability of nanofluids [35]. The pH deviation of a prepared suspension from the isoelectric point increases the stability of colloidal particles and causes the changes in the thermal conductivity of the nanofluid [208]. Jorge et al. [209] investigated the MWCNT/water nanofluid at pH values of 2 and 5.5 and reported that the mentioned nanofluids were stable because of the deposition of amines on the MWCNT surface. Zareei et al. [210] evaluated the stability of Al_2O_3/water nanofluid at various pH values and showed that the Al_2O_3/water nanofluid had the highest stability at pH=4 while pH=10 showed less stability. Each type of nanoparticle became stably dispersed at its optimized pH value that leads to optimum thermal properties. At an optimum pH, the repulsive force between nanoparticles increases and prevents the sedimentations and agglomerations [211].

Among the various methods to evaluate the stability of nanofluids the most common techniques are: zeta potential, absorbency, stratification observing, sedimentation observing, and particle size-changing [212]. When almost all of the particles have high zeta potential values, there is no tendency for agglomeration and consequently, the suspension becomes stable [213]. In the zeta potential method, a Laser Doppler Velocimetry (LDV) records the movement of nanoparticles under an electrical field. Nowadays most of the investigations about the stability of nanofluids are done with the zeta potential method [181]. The acceptable values of zeta potential are shown in Table 3 [214]

2.3. Thermophysical properties of nanofluids

The main idea of the synthesis of nanofluids is to enhance the thermophysical behavior of the base fluids. Thermal properties of the working fluid play an essential role in the heat transfer rate of a thermal system. The working fluid commonly has weak thermal properties, therefore the improvements of these properties increase the efficiency of thermal devices, reduce costs, and results in more compact and miniaturized devices [20]. The properties of some of the base fluids that are utilized commonly in various investigations are presented in Table 4 [187, 215–218]. The dispersion of nanoparticles in the base fluid is one of the attractive methods in the enhancement of the fluid properties. Many factors affect the thermophysical properties of nanofluids that are presented in Fig. 2 [219]. Kolade et al. [220] investigated the effect of

Table 2.
Investigations of nanofluid stability

Authors	Publish year	Nanoparticles/Base fluid	Particle size(nm)	Fraction (vol% or wt%)	Sedimentation	surfactant
Patel et al. [194]	2005	Al_2O_3/Water	11	0.8	-	-
Lee et al. [195]	2006	CuO/Water	25	0.3	-	-
Zhu et al. [189]	2007	Graphite/Water	20	0.5	-	PVP
Li et al. [188]	2008	Cu/Water	25	0.1	-	SDBS
Chen et al. [196]	2009	Titanate NT/EG	10*100	0.5-8	>2 months	-
Yu et al. [197]	2010	Fe_3O_4/Kerosene	15	0.1-2	-	Oleic acid
Chandareskar [198]	2010	Al_2O_3/Water	43	033-5	-	-
Aravind et al. [199]	2011	MWCNT/Water	-	0.005-0.03	-	-
Shanbedi et al. [200]	2012	MWCNT/Water	15*10000	0-1.5	>6 months	-
Shanbedi et al. [201]	2013	MWCNT/Water	15*10000	0-1	>6 months	GA
Amiri et al. [202]	2015	Graphene/Water	3.74*3000	0-0.1	1 month	SDBS
Mustafizur [203]	2016	SiO_2/Methanol	5-15	0.005-0.05	24 hours	-
Cacua et al. [204]	2017	Al_2O_3/Water	-	0.1-0.5	30 days	SDBS-CTAB
Krishnan et al. [205]	2019	MgO/Water-EG	-	0.05-0.6	20 days	-

Table 3.
The acceptable values of zeta potential [70]

Zeta potential (mv)	Stability
0	No stability or little stability
15	Some stability but settling lightly
30	Moderate stability
45	Good stability with settling possibility
60	Excellent stability

the particle fraction on the effective thermal conductivity of Al_2O_3-water and MWCNT-water nanofluids and reported 6% and 10% enhancement at 2% and 0.2% fractions, respectively. Das et al. [221] reported that temperature increment results in higher thermal conductivity of nanofluids. Also, Shou et al. [222] indicated that an increase in thermal conductivity had a linear proportion with temperature. Chon et al. [223] studied the effect of nanoparticles size on the thermal conductivity of nanofluids for spherical nanoparticles with the size of 10-50 nm and showed that the thermal conductivity of nanofluids increased with a decrease in particles size.

2.3.1. Thermal conductivity

In the last decades, the thermal conductivity of the fluids containing nanoparticles has become a point of attraction for many researchers and various numerical and experimental studies have done about nanofluids [220]. The results of various studies show that the thermal conductivity of nanofluids improves by diverse factors like volume fraction, nanoparticle type and size, the thermal conductivity of nanoparticles and base fluid, temperature, viscosity, Brownian motion, pH value, and the quality of dispersion[224]

The Brownian movement of nanoparticles at nano-sized levels and molecular scales plays a key role in the thermal behavior of solid-fluid suspensions including nanofluids. The increases in thermal conductivity of nanofluids are related to local convections that caused by Brownian motions of nanoparticles [225].

Solid materials have generally higher thermal conductivities than fluids. Metals possess considerably high thermal conductivity, however, some types of advanced ceramics offer considerable thermal conductivities such as ZrB_2, AlN, BeO, and TiB_2 [226–231]. Since the thermal conductivity of solid nanoparticles is very higher than fluids, it is expected that dispersing nanoparticles in a base fluid enhances the thermal conductivity and the heat transfer functions of the fluid. The approximate thermal conductivity of some materials and base fluids is shown in Fig. 3 and Fig. 4, respectively [211].

The experimental studies exhibited that nanofluids do not conform with general correlations and the thermal conductivity of nanofluids depends on many factors that some of them are still unknown. Jana et al. [232] studied various nanofluids and showed that the Cu-water nanofluid brings up to 74% enhancement in thermal conductivity. Xie et al. [233] investigated the effect of using CNT, CuO, and Al_2O_3 nanoparticles in a base fluid and showed that regardless of the type of the base fluid, Carbon nanotube suspensions demonstrated better thermal conductivity values in the same volume fractions [233]. Wang et al. [234] compared the diverse data for Al_2O_3 and CuO nanoparticles by considering water, vacuum pump fluid, engine oil, and ethylene glycol as base fluids and showed that the thermal conductivity of nanofluids increased with a decrease in nanoparticle size. Abareshi et al. [235] investigated the thermal conductivity of Fe3O4-water nanofluid and highlighted that the thermal conductivity of nanofluids improved with increment in temperature due to the increases in the activity of molecules to transfer energy. Lai et al. [236] and Zhu et al. [237] claimed that the pH value is very effective on the thermal conductivity of suspensions. In Table 5 found., the thermal conductivity enhancement reported by some researchers is presented.

Table 4.
Thermophysical properties of common base fluids that utilized in nanofluids [187, 215–218]

Base fluid	cp (J/kg.K)	k (W/m.K)	ρ (kg/m³)	μ (N.s/m²)
Distilled water	4184	0.599	998	1.00E-04
Ethylene Glycol	2383	0.25	1117	2.20E-02
Engine oil	1881	0.145	888	8.40E-01
Propylene glycol	4019	0.34	1036	4.20E-02
EG + water (X=0.5)	3473	0.316	1094	28.00E-04

Many studies reported the enhancement of thermal conductivity by utilizing and dispersing nanoparticles in the base fluid [220]. Although the researchers presented many models to predict the thermal conductivity of nanofluids, however, comparing the experimental data with theoretical models shows the need for more investigations to explain the abnormal improvements in the thermal conductivity of nanofluids.

Maxwell [251] for the first time presented a mathematical model to determine the thermal conductivity of a solid-fluid suspension by assuming spherical shape for all solid particles as follow:

$$k_{eff} = \frac{k_p + 2k_{bf} + 2(k_p - k_{bf})\phi}{k_p + 2k_{bf} - (k_p - k_{bf})\phi} k_{bf} \quad (1)$$

where φ is the volume fraction and k_{bf} and k_p are the thermal conductivity of the fluid and particles, respectively.

Researchers also developed various mathematical models by considering different parameters that affect thermal conductivity. Hamilton and Crosser [252] considered the shape of the particles and justified the Maxwell model as below:

$$k_{eff} = \frac{k_p + (n-1)k_{bf} + (n-1)(k_p - k_{bf})\phi}{k_p + (n-1)k_{bf} - (k_p - k_{bf})\phi} k_{bf} \quad (2)$$

where n is the shape factor given as

$$n = \frac{3}{\psi} \quad (3)$$

ψ is defined as the sphericity of the solid particles. A series of mathematical models considering the different involving factors are presented by several researchers. A conclusion of various presented models suggested by researchers is shown in Table 6.

2.3.2. Viscosity

The viscosity is a significant and important characteristic of all types of fluids that shows the resistance of a fluid flow against shear stress. Because of that, the viscosity has a great effect on the rheological and thermal behaviors of nanofluids as a special type of fluids. The viscosity affects the friction between the fluid molecules and the contact surface of nanoparticles and plays a key role in fluid flow and heat transfer phenomena. The pumping power and convective heat transfer rate are directly related to the value of viscosity [267].

The viscosity depends on various factors such as dispersing method, nanoparticle diameter, nanoparticle type, temperature, and nanoparticle concentration which the effect of concentration is more than other factors [268, 269]. Ghazvini et al. [270] showed that the viscosity of nanofluids increased by up to 20% in high nanoparticle concentrations. Ding et al. [271] investigated the viscosity of carbon nanotube-water nanofluid as a function of shear stress and indicated that the viscosity of

Table 5.
The overview of the result of some studies on the thermal conductivity of nanofluids

Authors	Publish year	Particle/Base fluid	Fraction (vol% or wt%)	Particle size (nm)	Additives	Enhancement (%)
Xuan & Li [192]	2000	Cu/water	2.5-7.5	100	Laurate salt	22-75
Xie et al. [238]	2002	Al_2O_3/water	1.8-5	60.4	-	7-21
Patel et al. [239]	2003	Ag/water	0.001	60-70	-	3% at 30°C 4% at 60°C
Das et al. [221]	2003	Al_2O_3/water	1-4	38.4	-	2-9% at 21°C 10-24% at 51°C
Wen & Ding [240]	2004	Al_2O_3/water	0.19-1.59	42	SDBS	1-10
Hong et al. [174]	2005	Fe/EG	0.2-0.55	10	-	13-18
Putnam et al. [241]	2006	Au/ethanol	0.01-0.07	4	Alkanrthiolate	0.3-1.3
Lee et al. [195]	2006	CuO/water	0.03-0.3	25	-	4-12% at pH=3 2-7% at pH=6
Li et al. [188]	2008	Cu/water	0.02-1 wt%	25	SDBS	10.7
Godson et al. [242]	2010	Ag/water	0.3-0.9	60	-	10-30% (50 to 90°C)
Kole & Dey [243]	2010	Al_2O_3/water	0.001-0.035	50	Oleic acid	10.5%
Colla et al. [244]	2012	Fe_3O_4/water	5-20 wt%	67	-	0-7% at 10°C 1-10% at 30°C 5-11% at 50°C 3-15% at 70°C
Manna et al. [245]	2012	SiC/water	0.01-0.1	60	-	7.5-11.5%
Teng [246]	2013	Al_2O_3/water	0,0.5,1,3	20	Chitosan	1-9% decrease
Amiri et al. [202]	2015	Geraphene/water	0.025-0.1 wt%	3.74*3000	SDBS	Up to 26.2
Sinha et al. [247]	2017	ZnO/water	0.1-5	-	-	33
Micali et al. [248]	2018	CuO-water	2.5	-	-	Up to 18
Ranjbarzadeh et al. [249]	2019	SiO_2/water	0.1-3	-	-	Up to 38.2
Riahi et al. [250]	2020	Al_2O_3/water	0.7	9	-	8.6

nanofluids increases with increments in concentration on the one hand and also, decrements in temperature on the other hand. Zeinali Heris et al. [272] showed that the viscosity value of CuO-water nanofluid is greater than Al_2O_3-water nanofluid because of the bigger size of CuO nanoparticles.

Nguyen et al. [273] investigated the effect of temperature, concentration, and size of nanoparticles on the dynamic viscosity of Al_2O_3-water and CuO-water nanofluids. The results showed that the viscosity of prepared nanofluids was a function of temperature and volume fraction of nanoparticles.

A conclusion of experimental researches about the viscosity of nanofluids is presented in Table 7. Also, there are some mathematical correlations for predicting the effective viscosity of nanofluids. A summary of the significant viscosity correlations is presented in Table 8.

2.4. Convective heat transfer process in nanofluids

Using nanofluids in various devices is an effective method to reach high efficiencies in the cooling procedure. In the previous sections, the synthesis and some thermophysical properties of nanofluids have been explained, however, convective heat transfer needs many studies about the flow regime, heat transfer process, and other significant factors [295]. The convective heat transfer coefficient of nanofluids increases with increment in conductive heat transfer rate, intensification of turbulence, stopping the growth of the boundary layer, etc. [24]. A decrease in the thermal boundary layer can lead to the stimulation of the particles around the wall and migration of the particles toward the center of the duct and this subject will decrease the viscosity near the wall [296]. Numerous studies have been performed to investigate the convective heat transfer using nanofluids. A constant heat flux or constant wall temperature is usually considered as the boundary condition for studying the heat transfer of nanofluids [297].

By using nanofluids, complicated behaviors such as Brownian motion, rotation of the particles, and micro-displacements of nanoparticles emerge [297]. These mechanisms make it necessary to find new correlations to cover the convective heat transfer of the nanofluids.

Jung et al. [298] investigated the Al_2O_3-water nanofluid in a microchannel with considering the laminar flow regime and showed a 32% increase in the convective heat transfer coefficient in comparison with used base fluids. Zeinali heris et al. [299] investigated the Cu-water nanofluids in a tube with a laminar flow regime at constant wall temperature condition as a boundary condition and indicated that with increases in volume fraction, the convective heat transfer coefficient values improved as 45% at 2% volume fraction. Faulkner et al. [300] investigated the convective heat transfer in a microchannel by utilizing CNT-water. The results showed that the convective heat transfer coefficient improves with an increase in volume fraction. Aravind et al [199] synthesized the CNT-water nanofluids at 0.005% and 0.03% volume fractions and showed that the convective heat transfer coefficient increases with an increase in Reynolds number and volume fraction. Naraki et al. [301] investigated the CuO-water nanofluid in a car radiator and presented an 8% enhancement in the heat transfer rate.

Several mathematical correlations are presented by researchers for predicting the Nusselt number of single-phase fluids in a tube at laminar and turbulent flow regimes. A conclusion of some correlations for the Nusselt number is shown in Table 9.

2.5. Future Challenges

As the researches about nanofluid progress over time, many chal-

Table 6.
A conclusion of models proposed for thermal conductivity of nanofluids

Reference	Year	Correlation	Dependent Parameters
Maxwell et al [251]	1890	$k_{eff}=\frac{k_p+2k_{bf}+2(k_p-k_{bf})\phi}{k_p+2k_{bf}-(k_p-k_{bf})\phi}k_{bf}$	Volume fraction
Bruggeman [253]	1937	$k_{eff}=\frac{1}{4}[(3\phi-1)k_p+(2-3\phi)k_{bf}]+\frac{k_{bf}}{4}\sqrt{\Delta}$ $\Delta=\left[(3\phi-1)^2\left(\frac{k_p}{k_{bf}}\right)+(2-3\phi)^2+2(2+9\phi-9\phi^2)\left(\frac{k_p}{k_{bf}}\right)\right]$	Volume fraction
Hamilton & Crosser [252]	1962	$k_{eff}=\frac{k_p+(n-1)k_{bf}+(n-1)(k_p-k_{bf})\phi}{k_p+(n-1)k_{bf}-(k_p-k_{bf})\phi}k_{bf}$	Volume fraction Shape factor
Wasp [254]	1977	$k_{eff}=\frac{k_p+2k_{bf}-2(k_{bf}-k_p)\phi}{k_p+2k_{bf}+(k_{bf}-k_p)\phi}k_{bf}$	Volume fraction
Lu and Lin [255]	1996	$k_{eff}=\left[1+\frac{k_p}{k_{bf}}\phi+\frac{k_p-k_{bf}}{k_p+2k_{bf}}\phi^2\right]k_{bf}$	Volume fraction
Yu and Choi [256]	2003	$k_{eff}=\frac{k_{pe}+2k_{bf}+2(k_{pe}-k_{bf})(1+\beta)^3\phi}{k_{pe}+2k_{bf}-(k_{pe}-k_{bf})(1+\beta)^3\phi}k_{bf}$ $k_{pe}=\frac{[2(1-\gamma)+(1+\beta)^3(1+2\gamma)\gamma]}{[-(1-\gamma)+(1+\beta)^3(1+2\gamma)]}k_p$	Interfacial layer Volume fraction
Nan [257]	2003	$\frac{k_{eff}}{k_{bf}}=\frac{3+\phi(\frac{k_p}{k_{bf}})}{3-2\phi}$	Volume fraction
Wang et al [258]	2003	$k_{eff}=\frac{(1-\phi)+3\phi\int_0^\infty\frac{k_{c1}(r)n(r)}{k_{c1}(r)+2k_{bf}}dr}{(1-\phi)+3\phi\int_0^\infty\frac{k_{bf}(r)n(r)}{k_{c1}(r)+2k_{bf}}dr}k_{bf}$	Size effect Surface adsorption
Kumar et al [259]	2004	$k_{eff}=k_{bf}+c\frac{2k_BT}{\pi\nu d_p^2}\frac{\phi r_b}{k_{bf}(1-\phi)r_p}k_{bf}$	Temperature, Density, Specific heat capacity, Viscosity, Radius of nanoparticle, Volume fraction
Xie et al [260]	2005	$k_{eff}=\left(1+3\Theta\phi_T+\frac{3\Theta^2\phi_T^2}{1-\Theta\phi_T}\right)k_{bf}$ $\Theta=\frac{\beta_{1b}[(1+\gamma^3)-\frac{\beta_{p1}}{\beta_{b1}}]}{(1+\gamma)^3+2\beta_{p1}\beta_{b1}}$	Interfacial nanolayer Volume fraction
Prasher [261]	2005	$\frac{k_{eff}}{k_{bf}}=1+64.7\phi^{0.746}(\frac{d_{bf}}{d_p})^{0.369}(\frac{k_p}{k_{bf}})^{0.7476}\times\mathrm{Pr}^{0.9955}\times\mathrm{Re}^{1.2321}$	Reynolds number Prandtl number Particle size Volume fraction
Murshed [262]	2006	$\frac{k_{eff}}{k_{bf}}=\frac{[1+0.27\phi^{1.3}\left(\frac{k_p}{k_{bf}}-1\right)][1+\frac{0.52\phi}{1-\phi^{0.3}}\left(\frac{k_p}{k_{bf}}-1\right)}{1+\phi^{1.3}\left(\frac{k_p}{k_{bf}}-1\right)\left(\frac{0.52}{1-\phi^{0.3}}+0.27\phi^{0.3}+0.27\right)}$	Volume fraction

Continuation of Table 5

Reference	Year	Correlation	Dependent Parameters
Li [263]	2008	$k_{eff} = k_{static} + k_{Brownian}$ $k_{static} = \frac{k_p + 2k_{bf} + 2(k_p - k_{bf})\phi}{k_p + 2k_{bf} - (k_p - k_{bf})\phi} k_{bf}$ $k_{Brownian} = 50000\phi(\rho c_p)_{bf}\sqrt{\frac{k_B T}{\rho_p d_p}} g(T,\phi,d_p)$ $g(T,\phi,d_p) = (a + b\ln(d_p) + c\ln(\phi) + d\ln(\phi)\ln(d_p)$ $+e\ln(d_p)^2)\ln(T) + (g + h\ln(d_p) + i\ln(\phi) + j\ln(\phi)\ln(d_p) + k\ln(d_p)^2)$	Brownian motion Particle diameter Temperature Volume fraction
Vajjha [264]	2010	$k_{eff} = \frac{k_p + 2k_{bf} - 2(k_{bf} - k_p)\phi}{k_p + 2k_{bf} + (k_{bf} - k_p)\phi} k_{bf} + 5\times10^4 \beta\phi\rho_{bf} c_{pf}\sqrt{\frac{kT}{\rho_p d_p}} f(T,\phi)$	Temperature Nanoparticle type Volume fraction
Suganthi [265]	2014	$\frac{k_{eff}}{k_{bf}} = 1 + 7.926\phi$ $\frac{k_{eff}}{k_{bf}} = 1 + 8.195\phi$	Volume fraction
Gao [266]	2018	$\frac{k_{eff}}{k_{bf}} = \frac{3 + 2\eta^2\phi}{\frac{k_f}{k_{bf}}(\frac{2R_k}{L} + 13.4\sqrt{t}) \over 3 - \eta\phi}$	Thickness Length Thermal resistance Flatness ratio

Table 7.
A conclusion of experimental studies on the viscosity of nanofluids

Authors	Year	Particles/Base fluid	Fraction	Particle size(nm)	Additives	Viscosity increase
Godson et al. [242]	2010	Ag/water	0.3-0.9	20	-	6-23% at 50°C 10-35% at 70°C 20-43% at 90°C
Aravind [199]	2011	MWCNT/water	0.005-0.03	-	-	3-15% at 40°C 4-20% at 60°C 6-11% at 40°C 4-16% at 60°C
Colla et al. [244]	2012	Fe_2O_3/water	5-20 wt%	67	-	21-36% at 10°C 24-49% at 30°C 21-36% at 50°C 32-72% at 70°C
Syam Sundar et al. [274]	2013	Fe_3O_4/water	0.2-2	13	CTAB	6.3-108% at 20°C 1.8-107% at 40°C 10-196.6% at 60°C
Shanbedi et al. [275]	2015	MWCNT/water	0.1 wt%	10*30000	GA SDS CTAB	Temperature increase led to lower viscosity values
Chiam et al. [276]	2017	Al_2O_3/water+EG	0.2-1	-	-	Up to 50%
Yashawantha et al. [277]	2019	Graphite/EG	0.2, 0.8, 2	<50	-	58% decrease by increasing temperature (25°C-60°C)

lenges in nanofluid studies and applications still exist. Firstly, the synthesis of nanofluids must take lower costs on the one hand and give more stable nanofluids on the other hand. So, there is a critical need for more studies about the mechanisms and methods to earn information about the unique behavior of nanofluids and give more stable nanofluids that make them more commercial and applicable.

Secondly, many mathematical and experimental correlations are presented to predict the thermal and rheological properties of nanofluids. Some of them have properly validated, however, all mechanisms involved in the heat transfer of nanofluids are still unknown and unexplored. Considering optimal parameters for prospecting the behavior of nanofluids is very necessary to extract the maximum potential of nanofluids.

From the heat transfer aspect, nanofluids have developed in many heat transfer processes and instruments such as medical sciences, biomechanics, electronics, etc. [311]. Researchers are studying and investigating the various facets of the nanofluids to make nanofluids more reliable and marketable [312].

Nowadays, nanofluids are utilizing in heat transfer and other fields widely. However, this unique type of suspension is still under the investigation to be more applicable. Finding ways to give more stable and high-efficiency nanofluids will lead to a revolution in the heat transfer in industry and many other fields.

Table 8.
A conclusion of mathematical correlations for the viscosity of nanofluids

Authors	Year	Correlation	Dependent parameters
Einstein [278]	1906	$\mu_{eff} = (1+2.5\phi)\mu_{bf}$	Volume fraction
Robinson [279]	1949	$\mu_{eff} = \left(1+\frac{c_p\phi}{1-S_r\phi}\right)\mu$	Volume fraction Special heat capacity
Brinkman [279]	1952	$\mu_{eff} = \frac{\mu_f}{(1-\phi)^{2.5}}$	Volume fraction
Eshelby [280]	1957	$\mu_{eff} = \left(1+\frac{7.5(1-\sigma)}{4-5\sigma}\phi\right)\mu_{bf}$ $\sigma = 0.333$	Volume fraction
Krieger [281]	1959	$\mu_{eff} = \mu_{bf}(1-\frac{\phi}{\phi_m})^{-[\eta]\phi_m}$	Volume fraction Shear stress Particle packing
Frankel and Acrivos [282]	1967	$\mu_{eff} = 1.125\left[\frac{\left(\frac{\phi}{\phi_m}\right)^{0.333}}{1-\left(\frac{\phi}{\phi_m}\right)^{0.333}}\right]\mu_{bf}$	Volume fraction
Jeffrey et al [283]	1976	$\mu_{eff} = \mu_{bf}\left(3+\frac{4}{3}\left(\frac{\phi r^2}{\ln\left(\frac{r}{\phi}\right)}\right)\right)$	Volume fraction
Graham [284]	1981	$\frac{\mu_{eff}}{\mu_{bf}} = 1+2.5\phi+\frac{4.5}{\left(\frac{h}{d_p}\right)\left(2+\frac{h}{d_p}\right)\left(1+\frac{h}{d_p}\right)^2}$	Particle diameter Inter-particle spacing
Chow [285]	1993	$\frac{\mu_{eff}}{\mu_{bf}} = \left[\exp\left(\frac{2.5\phi}{1-\phi}\right)+\frac{A\phi^2}{1-A\phi^2\phi_{\max}}\right]$	Volume fraction
Pak and Cho [286]	1998	$\mu_{eff} = (108.2\phi^2+5.45\phi+1)\mu_{bf}$	Volume fraction
Liu [287]	1999	$\frac{\mu_{eff}}{\mu_{bf}} = \left\{\left(\frac{1-\phi}{\phi_{\max}}\right)^2+\left(\frac{k_1-2}{\phi_{\max}}\right)\phi+\left(\frac{k_2-6}{\phi_{\max}^2}\right)\phi^2\right\}$	Volume fraction
Noni [288]	2002	$\frac{\mu_{eff}}{\mu_{bf}} = \left(1+b\left(\frac{\phi}{1-\phi_m}\right)^n\right)$	Volume fraction Bidimensional forces
Orozco and Castillo [289]	2003	$\frac{\mu_{eff}}{\mu_{bf}} = 1+2.5\phi+6.17\phi^2$	Volume fraction
Nguyen [290]	2007	$\frac{\mu_{eff}}{\mu_{bf}} = 0.904^{0.1483\phi}$	Volume fraction
Bobbo [291]	2012	$\frac{\mu_{eff}}{\mu_{bf}} = \left(1+a\phi+b\phi^2\right)$	Volume fraction
Aberoumand [292]	2016	$\frac{\mu_{eff}}{\mu_{bf}} = 1.15+1.061\phi-0.5442\phi^2+0.1181\phi^3$	Volume fraction
Karimipour [293]	2018	$\frac{\mu_{eff}}{\mu_{bf}} = 0.995246-0.000293119T.w+0.125761w$	Weight fraction temperature
Esfe [294]	2019	$\mu_{eff} = 6.35+2.56\phi-0.24T-0.068\phi T+0.905\phi^2+0.0027T^2$	Volume fraction temperature

Table 9.
A summary of correlations presented for Nusselt number

Author	Year	Correlation	Conditions
Dittus-Boelter [302]	1930	$Nu = 0.023\,\mathrm{Re}^{0.8}\,\mathrm{Pr}^{n}$	Turbulent flow n=0.3 for cooling n=0.4 for heating $2500<\mathrm{Re}<1.25\times10^{5}$ $0.6<\mathrm{Pr}<160$
Hausen [303]	1943	$Nu = 3.66 + \frac{0.0668(d/L)\,\mathrm{Re}\,\mathrm{Pr}}{1+0.04[(d/L)\,\mathrm{Re}\,\mathrm{Pr}]^{2/3}}$	Laminar flow Const. wall temperature
Lyon [304]	1952	$Nu = 7 + 0.025(\mathrm{Re}\,\mathrm{Pr})^{0.8}$	Const. heat flux
Lubarsky and Kaufman [305]	1955	$Nu = 0.625\,\mathrm{Re}^{0.4}\,\mathrm{Pr}^{0.4}$	-
Churchill and Ugasi [306]	1972	$Nu^{10} = Nu_l^{10} + \left[\exp\left(\frac{2200-(\mathrm{Re}/365)}{Nu_c^{2}} + \frac{1}{Nu_t^{2}}\right)\right]^{-5}$	-
Notter-Sleicher [307]	1972	$Nu = 5 + 0.015\,\mathrm{Re}^{0.856}\,\mathrm{Pr}^{0.347}$	$0<\mathrm{Pr}<10^{4}$ $10^{4}<\mathrm{Re}<10^{5}$
Pak and Cho [286]	1998	$Nu = 0.021\,\mathrm{Re}^{0.8}\,\mathrm{Pr}^{0.5}$	$10^{4}<\mathrm{Re}<10^{5}$ $6.54<\mathrm{Pr}<12.33$ $0<\phi<3\%$
Maiga et al. [308]	2004	$Nu = 0.086\,\mathrm{Re}^{0.55}\,\mathrm{Pr}^{0.5}$ $Nu = 0.28\,\mathrm{Re}^{0.35}\,\mathrm{Pr}^{0.36}$	Const. heat flux Const. wall temperature
Suresh et al. [309]	2012	$Nu = 0.031(\mathrm{Re}\,\mathrm{Pr})^{0.68}(1+\phi)^{95.73}$	$\mathrm{Re}<2300$ $0<\phi<0.1\%$
Sundar et al. [310]	2012	$Nu = 0.02172\,\mathrm{Re}^{0.8}\,\mathrm{Pr}^{0.5}(1+\phi)^{0.5181}$	$3000<\mathrm{Re}<22000$ $3.72<\mathrm{Pr}<6.5$ $0<\phi<0.6\%$

3. Conclusion

Cooling performance is a major demand of many industries and because of that, the need for fluids with enhanced thermophysical properties and reliable stability is more vital than the past. The present review gives a piece of summarized information about the nanofluids and heat transfer phenomena in nanofluids and make nanofluids more understanding and displays the recent developments in nanofluids.

Many rheological and thermal properties of nanofluid have taken into account to make nanofluids more applicable. Although, the thermal conductivity, viscosity, stability, and heat transfer processes are reviewed in the present paper. Also, summarized experimental studies and mathematical correlations about the mentioned properties are brought in the present review. The parameters that affect the thermal behavior of nanofluids are particle size, volume and weight fraction, fluid type, nanoparticle type, temperature, viscosity, stability, and preparation method. Nanofluids have a huge potential to be used in many fields and industries but, there is more need for study on the hidden and unknown mechanisms of nanofluids to make them more applicable. Also, more investigations are needed to simplify the preparation methods and enhance the thermos-physical properties of nanofluids.

Conflict of interests

The Author(s) declare(s) that there is no conflict of interest.

REFERENCES

[1] T. Gholizadeh, M. Vajdi, H. Rostamzadeh, A new trigeneration system for power, cooling, and freshwater production driven by a flash-binary geothermal heat source, Renew. Energy. 148 (2020) 31–43. doi:10.1016/j.renene.2019.11.154.

[2] T. Gholizadeh, M. Vajdi, F. Mohammadkhani, Thermodynamic and thermoeconomic analysis of basic and modified power generation systems fueled by biogas, Energy Convers. Manag. 181 (2019) 463–475. doi:10.1016/j.enconman.2018.12.011.

[3] T. Gholizadeh, M. Vajdi, H. Rostamzadeh, Freshwater and cooling production via integration of an ethane ejector expander transcritical refrigeration cycle and a humidification-dehumidification unit, Desalination. 477 (2020) 114259. doi:10.1016/j.desal.2019.114259.

[4] T. Gholizadeh, M. Vajdi, H. Rostamzadeh, A new biogas-fueled bi-evaporator electricity/cooling cogeneration system: Exergoeconomic optimization, Energy Convers. Manag. 196 (2019) 1193–1207. doi:10.1016/j.enconman.2019.06.053.

[5] F. Yekani, S., Abdi Aghdam, E., Sadegh Moghanlo, Experimental study of The Performance and e xhaust gas emissions Response of A Spark Ignition Engine to Adding Natural Gas to Gasoline in CR=11., Int. J. Ind. Math. 11 (2019) 307–317.

[6] T. Gholizadeh, M. Vajdi, H. Rostamzadeh, Energy and exergy evaluation of a new bi-evaporator electricity/cooling cogeneration system fueled by biogas, J. Clean. Prod. 233 (2019) 1494–1509. doi:10.1016/j.jclepro.2019.06.086.

[7] T. Gholizadeh, M. Vajdi, H. Rostamzadeh, Exergoeconomic optimization of a new trigeneration system driven by biogas for power, cooling, and freshwater production, Energy Convers. Manag. 205 (2020) 112417. doi:10.1016/j.enconman.2019.112417.

[8] S.M.F. Yekani S, Abdi Aghdam E, Performance Response of a Spark Ignition Engine to Adding Natural Gas to Gasoline on Lean-Burn Condition in 10 Compression Ratio., Modares Mech. Eng. 20 (2020) 1691–1699.

[9] M. Namazizadeh, M. Talebian Gevari, M. Mojaddam, M. Vajdi, Optimization of the Splitter Blade Configuration and Geometry of a Centrifugal Pump Impeller using Design of Experiment, J. Appl. Fluid Mech. 13 (2020) 89–101. doi:10.29252/jafm.13.01.29856.

[10] F.S. Moghanlou, A.S. Khorrami, E. Esmaeilzadeh, H. Aminfar, Experimental study on electrohydrodynamically induced heat transfer enhancement in a minichannel, Exp. Therm. Fluid Sci. 59 (2014) 24–31. doi:10.1016/j.expthermflusci.2014.07.019.

[11] R.L. Webb, N.-H. Kim, principles enhanced heat transfer, CRC Press, 2005.

[12] J.S. Moghanlou FS, Ghazanfari Jajin E, Vajdy Hokmabad M, On the Experimental and Numerical Droplet Generation in the Ordinary and Modified Micro

channels with Oval Obstacle, Modares Mech. Eng. 20 (2020).
[13] Y. Sui, P.S. Lee, C.J. Teo, An experimental study of flow friction and heat transfer in wavy microchannels with rectangular cross section, Int. J. Therm. Sci. 50 (2011) 2473–2482. doi:10.1016/j.ijthermalsci.2011.06.017.
[14] M. Shahedi Asl, M. Sakkaki, F. Sadegh Moghanlou, S. Parvizi, H. Baghbanijavid, A. Babapoor, Phase change materials as quenching media for heat treatment of 42CrMo4 steels, J. Cent. South Univ. (2020).
[15] M. Fattahi, K. Vaferi, M. Vajdi, F. Sadegh Moghanlou, A. Sabahi Namini, M. Shahedi Asl, Aluminum nitride as an alternative ceramic for fabrication of microchannel heat exchangers: A numerical study, Ceram. Int. 46 (2020) 11647–11657. doi:10.1016/j.ceramint.2020.01.195.
[16] T. Dehghani, F. Sadegh Moghanlou, M. Vajdi, M. Shahedi Asl, M. Shokouhimehr, M. Mohammadi, Mixing enhancement through a micromixer using topology optimization, Chem. Eng. Res. Des. 161 (2020) 187–196. doi:10.1016/j.cherd.2020.07.008.
[17] M. Namazizadeh, R. Haghighi khoshkhoo, F. Joda, Effect of Air Gap on thermohydraulic performance of finned tube bundles, Therm. Sci. Eng. Prog. 20 (2020) 100687. doi:10.1016/j.tsep.2020.100687.
[18] M. Vajdi, M. Shahedi Asl, S. Nekahi, F. Sadegh Moghanlou, S. Jafargholinejad, M. Mohammadi, Numerical assessment of beryllium oxide as an alternative material for micro heat exchangers, Ceram. Int. 46 (2020) 19248–19255. doi:10.1016/j.ceramint.2020.04.263.
[19] M. Vajdi, F. Sadegh Moghanlou, E. Ranjbarpour Niari, M. Shahedi Asl, M. Shokouhimehr, Heat transfer and pressure drop in a ZrB2 microchannel heat sink: A numerical approach, Ceram. Int. 46 (2020) 1730–1735. doi:10.1016/j.ceramint.2019.09.146.
[20] F. Sadegh Moghanlou, S. Noorzadeh, M. Ataei, M. Vajdi, M. Shahedi Asl, E. Esmaeilzadeh, Experimental investigation of heat transfer and pressure drop in a minichannel heat sink using Al_2O_3 and TiO_2–water nanofluids, J. Brazilian Soc. Mech. Sci. Eng. 42 (2020) 315. doi:10.1007/s40430-020-02403-5.
[21] M.U. Sajid, H.M. Ali, Recent advances in application of nanofluids in heat transfer devices: A critical review, Renew. Sustain. Energy Rev. 103 (2019) 556–592. doi:10.1016/j.rser.2018.12.057.
[22] J.A. Choi, S U.S.; Eastman, No Title, in: Enhancing Therm. Conduct. Fluids with Nanoparticles, n.d.: pp. 99–106.
[23] W.H. Choi S. Siginer DA, Developments and Applications of Non-Newtonian Flows, 1995.
[24] M. Ataei, F. Sadegh Moghanlou, S. Noorzadeh, M. Vajdi, M. Shahedi Asl, Heat transfer and flow characteristics of hybrid Al_2O_3/TiO_2–water nanofluid in a minichannel heat sink, Heat Mass Transf. 56 (2020) 2757–2767. doi:10.1007/s00231-020-02896-9.
[25] S. Chakraborty, An investigation on the long-term stability of TiO_2 nanofluid, Mater. Today Proc. 11 (2019) 714–718. doi:10.1016/j.matpr.2019.03.032.
[26] H. Zhang, S. Wang, Y. Lin, M. Feng, Q. Wu, Stability, thermal conductivity, and rheological properties of controlled reduced graphene oxide dispersed nanofluids, Appl. Therm. Eng. 119 (2017) 132–139. doi:10.1016/j.applthermaleng.2017.03.064.
[27] W. Yu, D.M. France, S.U.S. Choi, J.L. Routbort, Review and assessment of nanofluid technology for transportation and other applications., Argonne, IL, 2007. doi:10.2172/919327.
[28] C.G. Granqvist, R.A. Buhrman, J. Wyns, A.J. Sievers, Far-Infrared Absorption in Ultrafine Al Particles, Phys. Rev. Lett. 37 (1976) 625–629. doi:10.1103/PhysRevLett.37.625.
[29] J.-H. Lee, K.S. Hwang, S.P. Jang, B.H. Lee, J.H. Kim, S.U.S. Choi, C.J. Choi, Effective viscosities and thermal conductivities of aqueous nanofluids containing low volume concentrations of Al_2O_3 nanoparticles, Int. J. Heat Mass Transf. 51 (2008) 2651–2656. doi:10.1016/j.ijheatmasstransfer.2007.10.026.
[30] J.A. Eastman, S.U.S. Choi, S. Li, W. Yu, L.J. Thompson, Anomalously increased effective thermal conductivities of ethylene glycol-based nanofluids containing copper nanoparticles, Appl. Phys. Lett. 78 (2001) 718–720. doi:10.1063/1.1341218.
[31] W. Yu, H. Xie, L. Chen, Y. Li, Investigation of thermal conductivity and viscosity of ethylene glycol based ZnO nanofluid, Thermochim. Acta. 491 (2009) 92–96. doi:10.1016/j.tca.2009.03.007.
[32] Y. Hwang, J.K. Lee, C.H. Lee, Y.M. Jung, S.I. Cheong, C.G. Lee, B.C. Ku, S.P. Jang, Stability and thermal conductivity characteristics of nanofluids, Thermochim. Acta. 455 (2007) 70–74. doi:10.1016/j.tca.2006.11.036.
[33] M.A. Khairul, K. Shah, E. Doroodchi, R. Azizian, B. Moghtaderi, Effects of surfactant on stability and thermo-physical properties of metal oxide nanofluids, Int. J. Heat Mass Transf. 98 (2016) 778–787. doi:10.1016/j.ijheatmasstransfer.2016.03.079.
[34] V. Fuskele, R.M. Sarviya, Recent developments in Nanoparticles Synthesis, Preparation and Stability of Nanofluids, Mater. Today Proc. 4 (2017) 4049–4060. doi:10.1016/j.matpr.2017.02.307.
[35] A. Ghadimi, R. Saidur, H.S.C. Metselaar, A review of nanofluid stability properties and characterization in stationary conditions, Int. J. Heat Mass Transf. 54 (2011) 4051–4068. doi:10.1016/j.ijheatmasstransfer.2011.04.014.
[36] M. Sakkaki, F. Sadegh Moghanlou, M. Vajdi, M. Shahedi Asl, M. Mohammadi, M. Shokouhimehr, Numerical simulation of heat transfer during spark plasma sintering of zirconium diboride, Ceram. Int. 46 (2020) 4998–5007. doi:10.1016/j.ceramint.2019.10.240.
[37] F. Sadegh Moghanlou, M. Vajdi, J. Sha, A. Motallebzadeh, M. Shokouhimehr, M. Shahedi Asl, A numerical approach to the heat transfer in monolithic and SiC reinforced HfB_2, ZrB_2 and TiB_2 ceramic cutting tools, Ceram. Int. (2019). doi:10.1016/j.ceramint.2019.05.095.
[38] M. Vajdi, F. Sadegh Moghanlou, F. Sharifianjazi, M. Shahedi Asl, M. Shokouhimehr, A review on the Comsol Multiphysics studies of heat transfer in advanced ceramics, J. Compos. Compd. 2 (2020) 35–44. doi:10.29252/jcc.2.1.5.
[39] M. Fattahi, M. Najafi Ershadi, M. Vajdi, F. Sadegh Moghanlou, A. Sabahi Namini, M. Shahedi Asl, On the simulation of spark plasma sintered TiB_2 ultra high temperature ceramics: A numerical approach, Ceram. Int. 46 (2020) 14787–14795. doi:10.1016/j.ceramint.2020.03.003.
[40] F. Sadegh Moghanlou, M. Vajdi, A. Motallebzadeh, J. Sha, M. Shokouhimehr, M. Shahedi Asl, Numerical analyses of heat transfer and thermal stress in a ZrB2 gas turbine stator blade, Ceram. Int. 45 (2019) 17742–17750. doi:10.1016/j.ceramint.2019.05.344.
[41] S. Nekahi, K. Vaferi, M. Vajdi, F. Sadegh Moghanlou, M. Shahedi Asl, M. Shokouhimehr, A numerical approach to the heat transfer and thermal stress in a gas turbine stator blade made of HfB_2, Ceram. Int. (2019). doi:10.1016/j.ceramint.2019.08.112.
[42] F. Sadegh Moghanlou, M. Vajdi, J. Sha, A. Motallebzadeh, M. Shokouhimehr, M. Shahedi Asl, A numerical approach to the heat transfer in monolithic and SiC reinforced HfB2, ZrB2 and TiB_2 ceramic cutting tools, Ceram. Int. 45 (2019) 15892–15897. doi:10.1016/j.ceramint.2019.05.095.
[43] Z. Hajati, F. Sadegh Moghanlou, M. Vajdi, E. Razavi, S. Matin, Fluid Structure Interaction of blood flow around a vein valve, BioImpacts. (2020).
[44] S. Mohammad Bagheri, M. Vajdi, F. Sadegh Moghanlou, M. Sakkaki, M. Mohammadi, M. Shokouhimehr, M. Shahedi Asl, Numerical modeling of heat transfer during spark plasma sintering of titanium carbide, Ceram. Int. 46 (2020) 7615–7624. doi:10.1016/j.ceramint.2019.11.262.
[45] M. Sakkaki, F. Sadegh Moghanlou, M. Vajdi, F. Pishgar, M. Shokouhimehr, M. Shahedi Asl, The effect of thermal contact resistance on the temperature distribution in a WC made cutting tool, Ceram. Int. 45 (2019) 22196–22202. doi:10.1016/j.ceramint.2019.07.241.
[46] K. Vaferi, M. Vajdi, S. Nekahi, S. Nekahi, F. Sadegh Moghanlou, M. Shahedi Asl, M. Mohammadi, Thermo-mechanical simulation of ultrahigh temperature ceramic composites as alternative materials for gas turbine stator blades, Ceram. Int. (2020). doi:10.1016/j.ceramint.2020.08.164.
[47] M. Jaberi Zamharir, M. Shahedi Asl, N. Pourmohammadie Vafa, M. Ghassemi Kakroudi, Significance of hot pressing parameters and reinforcement size on densification behavior of ZrB_2–25vol% SiC UHTCs, Ceram. Int. 41 (2015) 6439–6447. doi:10.1016/j.ceramint.2015.01.082.
[48] M. Shahedi Asl, B. Nayebi, M. Akhlaghi, Z. Ahmadi, S.A. Tayebifard, E. Salahi, M. Shokouhimehr, M. Mohammadi, A novel ZrB2-based composite manufactured with Ti_3AlC_2 additive, Ceram. Int. (2020). doi:10.1016/j.ceramint.2020.08.193.
[49] C. Xia, S.A. Delbari, Z. Ahmadi, M. Shahedi Asl, M. Ghassemi Kakroudi, Q. Van Le, A. Sabahi Namini, M. Mohammadi, M. Shokouhimehr, Electron microscopy study of ZrB_2–SiC–AlN composites: Hot-pressing vs. pressureless sintering, Ceram. Int. (2020). doi:10.1016/j.ceramint.2020.08.054.
[50] Z. Ahmadi, M. Zakeri, A. Habibi-Yangjeh, M. Shahedi Asl, A novel ZrB2–C_3N_4 composite with improved mechanical properties, Ceram. Int. 45 (2019) 21512–21519. doi:10.1016/j.ceramint.2019.07.144.
[51] N. Pourmohammadie Vafa, B. Nayebi, M. Shahedi Asl, M. Jaberi Zamharir, M. Ghassemi Kakroudi, Reactive hot pressing of ZrB_2-based composites with changes in ZrO_2/SiC ratio and sintering conditions. Part II: Mechanical behavior, Ceram. Int. 42 (2016) 2724–2733. doi:10.1016/j.ceramint.2015.10.166.
[52] Z. Ahmadi, B. Nayebi, M. Shahedi Asl, M. Ghassemi Kakroudi, Fractographical characterization of hot pressed and pressureless sintered AlN-doped ZrB_2–SiC composites, Mater. Charact. 110 (2015) 77–85. doi:10.1016/j.matchar.2015.10.016.
[53] C. Xia, M. Shahedi Asl, A. Sabahi Namini, Z. Ahmadi, S.A. Delbari, Q. Van Le, M. Shokouhimehr, M. Mohammadi, Enhanced fracture toughness of ZrB_2–SiCw ceramics with graphene nano-platelets, Ceram. Int. 46 (2020) 24906–24915. doi:10.1016/j.ceramint.2020.06.275.

[54] N.P. Vafa, M. Shahedi Asl, M. Jaberi Zamharir, M. Ghassemi Kakroudi, Reactive hot pressing of ZrB_2-based composites with changes in ZrO_2/SiC ratio and sintering conditions. Part I: Densification behavior, Ceram. Int. 41 (2015) 8388–8396. doi:10.1016/j.ceramint.2015.03.033.

[55] M.S. Asl, B. Nayebi, Z. Ahmadi, M.J. Zamharir, M. Shokouhimehr, Effects of carbon additives on the properties of ZrB_2–based composites: A review, Ceram. Int. 44 (2018) 7334–7348. doi:10.1016/j.ceramint.2018.01.214.

[56] B. Nayebi, M. Shahedi Asl, M. Ghassemi Kakroudi, M. Shokouhimehr, Temperature dependence of microstructure evolution during hot pressing of ZrB_2–30 vol.% SiC composites, Int. J. Refract. Met. Hard Mater. 54 (2016) 7–13. doi:10.1016/j.ijrmhm.2015.06.017.

[57] M. Shahedi Asl, Microstructure, hardness and fracture toughness of spark plasma sintered ZrB_2–SiC–Cf composites, Ceram. Int. 43 (2017) 15047–15052. doi:10.1016/j.ceramint.2017.08.030.

[58] B. Nayebi, N. Parvin, J. Aghazadeh Mohandesi, M. Shahedi Asl, Densification and toughening mechanisms in spark plasma sintered ZrB_2-based composites with zirconium and graphite additives, Ceram. Int. 46 (2020) 13685–13694. doi:10.1016/j.ceramint.2020.02.156.

[59] M. Shahedi Asl, Y. Pazhouhanfar, A. Sabahi Namini, S. Shaddel, M. Fattahi, M. Mohammadi, Role of graphite nano-flakes on the characteristics of ZrB_2-based composites reinforced with SiC whiskers, Diam. Relat. Mater. 105 (2020) 107786. doi:10.1016/j.diamond.2020.107786.

[60] T.P. Nguyen, M. Ghassemi Kakroudi, M. Shahedi Asl, Z. Ahmadi, A. Sabahi Namini, S.A. Delbari, Q. Van Le, M. Shokouhimehr, Influence of SiAlON addition on the microstructure development of hot-pressed ZrB_2–SiC composites, Ceram. Int. 46 (2020) 19209–19216. doi:10.1016/j.ceramint.2020.04.258.

[61] M. Jaberi Zamharir, M. Shahedi Asl, M. Ghassemi Kakroudi, N. Pourmohammadie Vafa, M. Jaberi Zamharir, Significance of hot pressing parameters and reinforcement size on sinterability and mechanical properties of ZrB_2–25vol% SiC UHTCs, Ceram. Int. 41 (2015) 9628–9636. doi:10.1016/j.ceramint.2015.04.027.

[62] B. Nayebi, N. Parvin, J. Aghazadeh Mohandesi, M. Shahedi Asl, Effect of Zr and C co-addition on the characteristics of ZrB_2-based ceramics: Role of spark plasma sintering temperature, Ceram. Int. 46 (2020) 24975–24985. doi:10.1016/j.ceramint.2020.06.283.

[63] M. Shahedi Asl, M.J. Zamharir, Z. Ahmadi, S. Parvizi, Effects of nano-graphite content on the characteristics of spark plasma sintered ZrB_2–SiC composites, Mater. Sci. Eng. A. 716 (2018) 99–106. doi:10.1016/j.msea.2018.01.038.

[64] Y. Azizian-Kalandaragh, A.S. Namini, Z. Ahmadi, M. Shahedi Asl, Reinforcing effects of SiC whiskers and carbon nanoparticles in spark plasma sintered ZrB_2 matrix composites, Ceram. Int. 44 (2018) 19932–19938. doi:10.1016/j.ceramint.2018.07.258.

[65] M. Shahedi Asl, B. Nayebi, A. Motallebzadeh, M. Shokouhimehr, Nanoindentation and nanostructural characterization of ZrB_2–SiC composite doped with graphite nano-flakes, Compos. Part B Eng. 175 (2019) 107153. doi:10.1016/j.compositesb.2019.107153.

[66] H. Istgaldi, B. Nayebi, Z. Ahmadi, P. Shahi, M. Shahedi Asl, Characterization of ZrB_2–TiC composites reinforced with short carbon fibers, Ceram. Int. 46 (2020) 23155–23164. doi:10.1016/j.ceramint.2020.06.095.

[67] M. Shahedi Asl, M. Ghassemi Kakroudi, F. Golestani-Fard, H. Nasiri, A Taguchi approach to the influence of hot pressing parameters and SiC content on the sinterability of ZrB_2-based composites, Int. J. Refract. Met. Hard Mater. 51 (2015) 81–90. doi:10.1016/j.ijrmhm.2015.03.002.

[68] B. Mohammadpour, Z. Ahmadi, M. Shokouhimehr, M. Shahedi Asl, Spark plasma sintering of Al-doped ZrB_2–SiC composite, Ceram. Int. 45 (2019) 4262–4267. doi:10.1016/j.ceramint.2018.11.098.

[69] V.-H. Nguyen, S.A. Delbari, Z. Ahmadi, M. Shahedi Asl, M. Ghassemi Kakroudi, Q. Van Le, A. Sabahi Namini, M. Mohammadi, M. Shokouhimehr, Electron microscopy characterization of porous ZrB_2–SiC–AlN composites prepared by pressureless sintering, Ceram. Int. 46 (2020) 25415–25423. doi:10.1016/j.ceramint.2020.07.011.

[70] M. Shahedi Asl, B. Nayebi, Z. Ahmadi, P. Pirmohammadi, M. Ghassemi Kakroudi, Fractographical characterization of hot pressed and pressureless sintered SiAlON-doped ZrB_2–SiC composites, Mater. Charact. 102 (2015) 137–145. doi:10.1016/j.matchar.2015.03.002.

[71] M.S. Asl, M.G. Kakroudi, S. Noori, Hardness and toughness of hot pressed ZrB2–SiC composites consolidated under relatively low pressure, J. Alloys Compd. 619 (2015) 481–487. doi:10.1016/j.jallcom.2014.09.006.

[72] Z. Ahmadi, B. Nayebi, M. Shahedi Asl, M. Ghassemi Kakroudi, I. Farahbakhsh, Sintering behavior of ZrB_2–SiC composites doped with Si_3N_4: A fractographical approach, Ceram. Int. 43 (2017) 9699–9708. doi:10.1016/j.ceramint.2017.04.144.

[73] T.P. Nguyen, M. Shahedi Asl, S.A. Delbari, A. Sabahi Namini, Q. Van Le, M. Shokouhimehr, M. Mohammadi, Electron microscopy investigation of spark plasma sintered ZrO_2 added ZrB_2–SiC composite, Ceram. Int. 46 (2020) 19646–19649. doi:10.1016/j.ceramint.2020.04.292.

[74] M. Shahedi Asl, F. Golmohammadi, M. Ghassemi Kakroudi, M. Shokouhimehr, Synergetic effects of SiC and Csf in ZrB_2-based ceramic composites. Part I: Densification behavior, Ceram. Int. 42 (2016) 4498–4506. doi:10.1016/j.ceramint.2015.11.139.

[75] M. Shahedi Asl, M. Ghassemi Kakroudi, Fractographical assessment of densification mechanisms in hot pressed ZrB_2-SiC composites, Ceram. Int. 40 (2014) 15273–15281. doi:10.1016/j.ceramint.2014.07.023.

[76] M. Khoeini, A. Nemati, M. Zakeri, M. Shahedi Asl, Pressureless sintering of ZrB2 ceramics codoped with TiC and graphite, Int. J. Refract. Met. Hard Mater. 81 (2019) 189–195. doi:10.1016/j.ijrmhm.2019.02.026.

[77] S. Parvizi, Z. Ahmadi, M.J. Zamharir, M. Shahedi Asl, Synergistic effects of graphite nano-flakes and submicron SiC particles on the characteristics of spark plasma sintered ZrB_2 nanocomposites, Int. J. Refract. Met. Hard Mater. 75 (2018) 10–17. doi:10.1016/j.ijrmhm.2018.03.017.

[78] M. Shahedi Asl, M. Ghassemi Kakroudi, R. Abedi Kondolaji, H. Nasiri, Influence of graphite nano-flakes on densification and mechanical properties of hot-pressed ZrB_2–SiC composite, Ceram. Int. 41 (2015) 5843–5851. doi:10.1016/j.ceramint.2015.01.014.

[79] E. Ghasali, M. Shahedi Asl, Microstructural development during spark plasma sintering of ZrB_2–SiC–Ti composite, Ceram. Int. 44 (2018) 18078–18083. doi:10.1016/j.ceramint.2018.07.011.

[80] Y. Orooji, M.R. Derakhshandeh, E. Ghasali, M. Alizadeh, M. Shahedi Asl, T. Ebadzadeh, Effects of ZrB_2 reinforcement on microstructure and mechanical properties of a spark plasma sintered mullite-CNT composite, Ceram. Int. 45 (2019) 16015–16021. doi:10.1016/j.ceramint.2019.05.113.

[81] B. Nayebi, M.S. Asl, M.G. Kakroudi, I. Farahbakhsh, M. Shokouhimehr, Interfacial phenomena and formation of nano-particles in porous ZrB_2–40 vol% B_4C UHTC, Ceram. Int. 42 (2016) 17009–17015. doi:10.1016/j.ceramint.2016.07.208.

[82] F. Adibpur, S.A. Tayebifard, M. Zakeri, M. Shahedi Asl, Co-reinforcing of ZrB_2–SiC ceramics with optimized ZrC to Cf ratio, Ceram. Int. 46 (2020) 22661–22673. doi:10.1016/j.ceramint.2020.06.029.

[83] N. Pourmohammadie Vafa, M. Ghassemi Kakroudi, M. Shahedi Asl, Advantages and disadvantages of graphite addition on the characteristics of hot-pressed ZrB_2–SiC composites, Ceram. Int. 46 (2020) 8561–8566. doi:10.1016/j.ceramint.2019.12.086.

[84] H. Istgaldi, M. Shahedi Asl, P. Shahi, B. Nayebi, Z. Ahmadi, Solid solution formation during spark plasma sintering of ZrB_2–TiC–graphite composites, Ceram. Int. 46 (2020) 2923–2930. doi:10.1016/j.ceramint.2019.09.287.

[85] Y. Orooji, A. Alizadeh, E. Ghasali, M.R. Derakhshandeh, M. Alizadeh, M.S. Asl, T. Ebadzadeh, Co-reinforcing of mullite-TiN-CNT composites with ZrB_2 and TiB_2 compounds, Ceram. Int. 45 (2019) 20844–20854. doi:10.1016/j.ceramint.2019.07.072.

[86] M. Shahedi Asl, A statistical approach towards processing optimization of ZrB_2–SiC–graphite nanocomposites. Part I: Relative density, Ceram. Int. 44 (2018) 6935–6939. doi:10.1016/j.ceramint.2018.01.122.

[87] F. Adibpur, S.A. Tayebifard, M. Zakeri, M. Shahedi Asl, Spark plasma sintering of quadruplet ZrB_2–SiC–ZrC–Cf composites, Ceram. Int. 46 (2020) 156–164. doi:10.1016/j.ceramint.2019.08.243.

[88] M. Shahedi Asl, B. Nayebi, Z. Ahmadi, S. Parvizi, M. Shokouhimehr, A novel ZrB_2–VB_2–ZrC composite fabricated by reactive spark plasma sintering, Mater. Sci. Eng. A. 731 (2018) 131–139. doi:10.1016/j.msea.2018.06.008.

[89] M. Shahedi Asl, Y. Azizian-Kalandaragh, Z. Ahmadi, A. Sabahi Namini, A. Motallebzadeh, Spark plasma sintering of ZrB_2-based composites co-reinforced with SiC whiskers and pulverized carbon fibers, Int. J. Refract. Met. Hard Mater. 83 (2019) 104989. doi:10.1016/j.ijrmhm.2019.104989.

[90] V.-H. Nguyen, S.A. Delbari, M. Shahedi Asl, A. Sabahi Namini, M. Ghassemi Kakroudi, Y. Azizian-Kalandaragh, Q. Van Le, M. Mohammadi, M. Shokouhimehr, Role of hot-pressing temperature on densification and microstructure of ZrB_2–SiC ultrahigh temperature ceramics, Int. J. Refract. Met. Hard Mater. 93 (2020) 105355. doi:10.1016/j.ijrmhm.2020.105355.

[91] M. Ghassemi Kakroudi, M. Dehghanzadeh Alvari, M. Shahedi Asl, N. Pourmohammadie Vafa, T. Rabizadeh, Hot pressing and oxidation behavior of ZrB_2–SiC–TaC composites, Ceram. Int. 46 (2020) 3725–3730. doi:10.1016/j.ceramint.2019.10.093.

[92] B. Nayebi, Z. Ahmadi, M. Shahedi Asl, S. Parvizi, M. Shokouhimehr, Influence of vanadium content on the characteristics of spark plasma sintered ZrB_2–SiC–V composites, J. Alloys Compd. 805 (2019) 725–732. doi:10.1016/j.jallcom.2019.07.117.

[93] V.-H. Nguyen, S. Ali Delbari, Z. Ahmadi, M. Shahedi Asl, M. Ghassemi Kak-

roudi, Q. Van Le, A. Sabahi Namini, M. Shokouhimehr, M. Mohammadi, W. Peng, TEM characterization of hot-pressed ZrB_2-SiC-AlN composites, Results Phys. 19 (2020) 103348. doi:10.1016/j.rinp.2020.103348.

[94] Y. Pazhouhanfar, A. Sabahi Namini, S. Shaddel, Z. Ahmadi, M. Shahedi Asl, Combined role of SiC particles and SiC whiskers on the characteristics of spark plasma sintered ZrB_2 ceramics, Ceram. Int. 46 (2020) 5773–5778. doi:10.1016/j.ceramint.2019.11.027.

[95] M. Ghassemi Kakroudi, N. Pourmohammadie Vafa, M. Shahedi Asl, M. Shokouhimehr, Effects of SiC content on thermal shock behavior and elastic modulus of cordierite–mullite composites, Ceram. Int. 46 (2020) 23780–23784. doi:10.1016/j.ceramint.2020.06.153.

[96] Z. Balak, M. Shahedi Asl, M. Azizieh, H. Kafashan, R. Hayati, Effect of different additives and open porosity on fracture toughness of ZrB_2–SiC-based composites prepared by SPS, Ceram. Int. 43 (2017) 2209–2220. doi:10.1016/j.ceramint.2016.11.005.

[97] M. Shahedi Asl, M. Ghassemi Kakroudi, B. Nayebi, A fractographical approach to the sintering process in porous ZrB_2–B_4C binary composites, Ceram. Int. 41 (2015) 379–387. doi:10.1016/j.ceramint.2014.08.081.

[98] M. Fattahi, Y. Azizian-Kalandaragh, S.A. Delbari, A. Sabahi Namini, Z. Ahmadi, M. Shahedi Asl, Nano-diamond reinforced ZrB_2–SiC composites, Ceram. Int. 46 (2020) 10172–10179. doi:10.1016/j.ceramint.2020.01.008.

[99] M. Shahedi Asl, B. Nayebi, M.G. Kakroudi, M. Shokouhimehr, Investigation of hot pressed ZrB_2–SiC–carbon black nanocomposite by scanning and transmission electron microscopy, Ceram. Int. 45 (2019) 16759–16764. doi:10.1016/j.ceramint.2019.05.211.

[100] M. Shahedi Asl, B. Nayebi, M. Shokouhimehr, TEM characterization of spark plasma sintered ZrB_2–SiC–graphene nanocomposite, Ceram. Int. 44 (2018) 15269–15273. doi:10.1016/j.ceramint.2018.05.170.

[101] M. Shahedi Asl, M. Ghassemi Kakroudi, M. Rezvani, F. Golestani-Fard, Significance of hot pressing parameters on the microstructure and densification behavior of zirconium diboride, Int. J. Refract. Met. Hard Mater. 50 (2015) 140–145. doi:10.1016/j.ijrmhm.2015.01.004.

[102] M. Shahedi Asl, M. Ghassemi Kakroudi, B. Nayebi, H. Nasiri, Taguchi analysis on the effect of hot pressing parameters on density and hardness of zirconium diboride, Int. J. Refract. Met. Hard Mater. 50 (2015) 313–320. doi:10.1016/j.ijrmhm.2014.09.006.

[103] A. Sabahi Namini, S.A.A. Dilawary, A. Motallebzadeh, M. Shahedi Asl, Effect of TiB_2 addition on the elevated temperature tribological behavior of spark plasma sintered Ti matrix composite, Compos. Part B Eng. 172 (2019) 271–280. doi:10.1016/j.compositesb.2019.05.073.

[104] S.A. Delbari, A. Sabahi Namini, M. Shahedi Asl, Hybrid Ti matrix composites with TiB_2 and TiC compounds, Mater. Today Commun. 20 (2019) 100576. doi:10.1016/j.mtcomm.2019.100576.

[105] Z. Ahmadi, B. Nayebi, M. Shahedi Asl, I. Farahbakhsh, Z. Balak, Densification improvement of spark plasma sintered TiB_2-based composites with micron-, submicron- and nano-sized SiC particulates, Ceram. Int. 44 (2018) 11431–11437. doi:10.1016/j.ceramint.2018.03.202.

[106] M. Shahedi Asl, Z. Ahmadi, S. Parvizi, Z. Balak, I. Farahbakhsh, Contribution of SiC particle size and spark plasma sintering conditions on grain growth and hardness of TiB_2 composites, Ceram. Int. 43 (2017) 13924–13931. doi:10.1016/j.ceramint.2017.07.121.

[107] A. Sabahi Namini, Z. Ahmadi, A. Babapoor, M. Shokouhimehr, M. Shahedi Asl, Microstructure and thermomechanical characteristics of spark plasma sintered TiC ceramics doped with nano-sized WC, Ceram. Int. 45 (2019) 2153–2160. doi:10.1016/j.ceramint.2018.10.125.

[108] Y. Orooji, E. Ghasali, M. Moradi, M.R. Derakhshandeh, M. Alizadeh, M.S. Asl, T. Ebadzadeh, Preparation of mullite-TiB_2-CNTs hybrid composite through spark plasma sintering, Ceram. Int. 45 (2019) 16288–16296. doi:10.1016/j.ceramint.2019.05.154.

[109] M. Shahedi Asl, A. Sabahi Namini, M. Ghassemi Kakroudi, Influence of silicon carbide addition on the microstructural development of hot pressed zirconium and titanium diborides, Ceram. Int. 42 (2016) 5375–5381. doi:10.1016/j.ceramint.2015.12.072.

[110] A. Sabahi Namini, S.N. Seyed Gogani, M. Shahedi Asl, K. Farhadi, M. Ghassemi Kakroudi, A. Mohammadzadeh, Microstructural development and mechanical properties of hot pressed SiC reinforced TiB_2 based composite, Int. J. Refract. Met. Hard Mater. 51 (2015) 169–179. doi:10.1016/j.ijrmhm.2015.03.014.

[111] M. Shahedi Asl, S.A. Delbari, F. Shayesteh, Z. Ahmadi, A. Motallebzadeh, Reactive spark plasma sintering of TiB_2–SiC–TiN novel composite, Int. J. Refract. Met. Hard Mater. 81 (2019) 119–126. doi:10.1016/j.ijrmhm.2019.02.022.

[112] Z. Hamidzadeh Mahaseni, M. Dashti Germi, Z. Ahmadi, M. Shahedi Asl, Microstructural investigation of spark plasma sintered TiB_2 ceramics with Si_3N_4 addition, Ceram. Int. 44 (2018) 13367–13372. doi:10.1016/j.ceramint.2018.04.171.

[113] M. Dashti Germi, Z. Hamidzadeh Mahaseni, Z. Ahmadi, M. Shahedi Asl, Phase evolution during spark plasma sintering of novel Si_3N_4-doped TiB_2–SiC composite, Mater. Charact. 145 (2018) 225–232. doi:10.1016/j.matchar.2018.08.043.

[114] A. Babapoor, M.S. Asl, Z. Ahmadi, A.S. Namini, Effects of spark plasma sintering temperature on densification, hardness and thermal conductivity of titanium carbide, Ceram. Int. 44 (2018) 14541–14546. doi:10.1016/j.ceramint.2018.05.071.

[115] A. Sabahi Namini, A. Motallebzadeh, B. Nayebi, M. Shahedi Asl, M. Azadbeh, Microstructure–mechanical properties correlation in spark plasma sintered Ti–4.8 wt.% TiB_2 composites, Mater. Chem. Phys. 223 (2019) 789–796. doi:10.1016/j.matchemphys.2018.11.057.

[116] T.P. Nguyen, Z. Hamidzadeh Mahaseni, M. Dashti Germi, S.A. Delbari, Q. Van Le, Z. Ahmadi, M. Shokouhimehr, M. Shahedi Asl, A. Sabahi Namini, Densification behavior and microstructure development in TiB_2 ceramics doped with h-BN, Ceram. Int. 46 (2020) 18970–18975. doi:10.1016/j.ceramint.2020.04.223.

[117] M. Fattahi, Y. Pazhouhanfar, S.A. Delbari, S. Shaddel, A. Sabahi Namini, M. Shahedi Asl, Influence of TiB_2 content on the properties of TiC–SiCw composites, Ceram. Int. 46 (2020) 7403–7412. doi:10.1016/j.ceramint.2019.11.236.

[118] V.-H. Nguyen, S.A. Delbari, Z. Ahmadi, A. Sabahi Namini, Q. Van Le, M. Shokouhimehr, M. Shahedi Asl, M. Mohammadi, Effects of discrete and simultaneous addition of SiC and Si_3N_4 on microstructural development of TiB_2 ceramics, Ceram. Int. (2020). doi:10.1016/j.ceramint.2020.09.196.

[119] V.-H. Nguyen, M. Shahedi Asl, Z. Hamidzadeh Mahaseni, M. Dashti Germi, S.A. Delbari, Q. Van Le, Z. Ahmadi, M. Shokouhimehr, A. Sabahi Namini, M. Mohammadi, Role of co-addition of BN and SiC on microstructure of TiB_2-based composites densified by SPS method, Ceram. Int. 46 (2020) 25341–25350. doi:10.1016/j.ceramint.2020.07.001.

[120] T.P. Nguyen, S.A. Delbari, Y. Azizian-Kalandaragh, A. Babapoor, Q. Van Le, A. Sabahi Namini, M. Shokouhimehr, M. Shahedi Asl, Characteristics of quadruplet Ti–Mo–TiB_2–TiC composites prepared by spark plasma sintering, Ceram. Int. 46 (2020) 20885–20895. doi:10.1016/j.ceramint.2020.05.137.

[121] Z. Ahmadi, Z.H. Mahaseni, M.D. Germi, M.S. Asl, Microstructure of spark plasma sintered TiB_2 and TiB_2–AlN ceramics, Adv. Ceram. Prog. 5 (2019) 36–40.

[122] M. Fattahi, Y. Pazhouhanfar, S.A. Delbari, S. Shaddel, A. Sabahi Namini, M. Shahedi Asl, Strengthening of novel TiC–AlN ceramic with in-situ synthesized Ti3Al intermetallic compound, Ceram. Int. 46 (2020) 14105–14113. doi:10.1016/j.ceramint.2020.02.213.

[123] V.-H. Nguyen, S.A. Delbari, M. Shahedi Asl, Q. Van Le, H.W. Jang, M. Shokouhimehr, M. Mohammadi, A. Sabahi Namini, A novel TiC-based composite co-strengthened with AlN particulates and graphene nano-platelets, Int. J. Refract. Met. Hard Mater. 92 (2020) 105331. doi:10.1016/j.ijrmhm.2020.105331.

[124] B. Nayebi, M. Mehrabian, M. Shahedi Asl, M. Shokouhimehr, Nanostructural approach to the thickening behavior and oxidation of calcium-stabilized aluminum foams, Mater. Chem. Phys. 220 (2018) 351–359. doi:10.1016/j.matchemphys.2018.09.017.

[125] B. Nayebi, A. Bahmani, M.S. Asl, A. Rasooli, M.G. Kakroudi, M. Shokouhimehr, Characteristics of dynamically formed oxide films in aluminum–calcium foamable alloys, J. Alloys Compd. 655 (2016) 433–441. doi:10.1016/j.jallcom.2015.09.200.

[126] T.P. Nguyen, Y. Pazhouhanfar, S.A. Delbari, A. Sabahi Namini, A. Babapoor, Y. Mohammadpourderakhshi, S. Shaddel, Q. Van Le, M. Shokouhimehr, M. Shahedi Asl, Physical, mechanical and microstructural characterization of TiC–ZrN ceramics, Ceram. Int. 46 (2020) 22154–22163. doi:10.1016/j.ceramint.2020.05.292.

[127] T.P. Nguyen, Y. Pazhouhanfar, S.A. Delbari, Q. Van Le, S. Shaddel, M. Pazhouhanfar, A. Sabahi Namini, M. Shokouhimehr, M. Shahedi Asl, Characterization of spark plasma sintered TiC ceramics reinforced with graphene nano-platelets, Ceram. Int. 46 (2020) 18742–18749. doi:10.1016/j.ceramint.2020.04.189.

[128] M. Fattahi, S.A. Delbari, A. Babapoor, A. Sabahi Namini, M. Mohammadi, M. Shahedi Asl, Triplet carbide composites of TiC, WC, and SiC, Ceram. Int. 46 (2020) 9070–9078. doi:10.1016/j.ceramint.2019.12.155.

[129] M. Shahedi Asl, Z. Ahmadi, A. Sabahi Namini, A. Babapoor, A. Motallebzadeh, Spark plasma sintering of TiC–SiCw ceramics, Ceram. Int. 45 (2019) 19808–19821. doi:10.1016/j.ceramint.2019.06.236.

[130] M. Fattahi, S.A. Delbari, A. Sabahi Namini, Z. Ahmadi, M. Azadbeh, M. Shahedi Asl, Characterization of triplet Ti–TiB–TiC composites: Comparison of in-situ formation and ex-situ addition of TiC, Ceram. Int. 46 (2020) 11726–11734. doi:10.1016/j.ceramint.2020.01.204.

[131] M. Fattahi, A. Babapoor, S.A. Delbari, Z. Ahmadi, A. Sabahi Namini, M. Shahedi Asl, Strengthening of TiC ceramics sintered by spark plasma via nano-graphite addition, Ceram. Int. 46 (2020) 12400–12408. doi:10.1016/j.ceramint.2020.01.291.

[132] M. Fattahi, A. Mohammadzadeh, Y. Pazhouhanfar, S. Shaddel, M. Sha-

hedi Asl, A. Sabahi Namini, Influence of SPS temperature on the properties of TiC–SiCw composites, Ceram. Int. 46 (2020) 11735–11742. doi:10.1016/j.ceramint.2020.01.206.

[133] V.-H. Nguyen, Y. Pazhouhanfar, S.A. Delbari, S. Shaddel, A. Babapoor, Y. Mohammadpourderakhshi, Q. Van Le, M. Shokouhimehr, M. Shahedi Asl, A. Sabahi Namini, Beneficial role of carbon black on the properties of TiC ceramics, Ceram. Int. 46 (2020) 23544–23555. doi:10.1016/j.ceramint.2020.06.125.

[134] V.-H. Nguyen, S.A. Delbari, M. Shahedi Asl, Q. Van Le, M. Shokouhimehr, A. Sabahi Namini, M. Mohammadi, Microstructure–property correlation in nano-diamond and TiN added TiC-based ceramics, Ceram. Int. (2020). doi:10.1016/j.ceramint.2020.08.152.

[135] V.-H. Nguyen, S.A. Delbari, A. Sabahi Namini, A. Babapoor, Q. Van Le, H.W. Jang, M. Shokouhimehr, M. Shahedi Asl, M. Mohammadi, Microstructural, mechanical and friction properties of nano-graphite and h-BN added TiC-based composites, Ceram. Int. (2020). doi:10.1016/j.ceramint.2020.08.068.

[136] V.-H. Nguyen, S.A. Delbari, M. Shahedi Asl, Q. Van Le, H.W. Jang, M. Shokouhimehr, M. Mohammadi, A. Sabahi Namini, A novel spark plasma sintered TiC–ZrN–C composite with enhanced flexural strength, Ceram. Int. (2020). doi:10.1016/j.ceramint.2020.08.073.

[137] K. Kasraee, S.A. Tayebifard, H. Roghani, M. Shahedi Asl, Preparation of B4C–SiC–HfB2 nanocomposite by mechanically activated combustion synthesis, Ceram. Int. 46 (2020) 12288–12295. doi:10.1016/j.ceramint.2020.01.279.

[138] I. Farahbakhsh, Z. Ahmadi, M. Shahedi Asl, Densification, microstructure and mechanical properties of hot pressed ZrB_2 –SiC ceramic doped with nano-sized carbon black, Ceram. Int. 43 (2017) 8411–8417. doi:10.1016/j.ceramint.2017.03.188.

[139] M. Shahedi Asl, I. Farahbakhsh, B. Nayebi, Characteristics of multi-walled carbon nanotube toughened ZrB_2 –SiC ceramic composite prepared by hot pressing, Ceram. Int. 42 (2016) 1950–1958. doi:10.1016/j.ceramint.2015.09.165.

[140] S.A. Delbari, B. Nayebi, E. Ghasali, M. Shokouhimehr, M. Shahedi Asl, Spark plasma sintering of TiN ceramics codoped with SiC and CNT, Ceram. Int. 45 (2019) 3207–3216. doi:10.1016/j.ceramint.2018.10.223.

[141] M. Shahedi Asl, M. Ghassemi Kakroudi, Characterization of hot-pressed graphene reinforced ZrB_2 –SiC composite, Mater. Sci. Eng. A. 625 (2015) 385–392. doi:10.1016/j.msea.2014.12.028.

[142] K. Farhadi, A. Sabahi Namini, M. Shahedi Asl, A. Mohammadzadeh, M. Ghassemi Kakroudi, Characterization of hot pressed SiC whisker reinforced TiB_2 based composites, Int. J. Refract. Met. Hard Mater. 61 (2016) 84–90. doi:10.1016/j.ijrmhm.2016.08.004.

[143] A. Sabahi Namini, M. Azadbeh, M. Shahedi Asl, Effect of TiB_2 content on the characteristics of spark plasma sintered Ti–TiBw composites, Adv. Powder Technol. 28 (2017) 1564–1572. doi:10.1016/j.apt.2017.03.028.

[144] Z. Balak, M. Azizieh, H. Kafashan, M.S. Asl, Z. Ahmadi, Optimization of effective parameters on thermal shock resistance of ZrB_2 -SiC-based composites prepared by SPS: Using Taguchi design, Mater. Chem. Phys. 196 (2017) 333–340. doi:10.1016/j.matchemphys.2017.04.062.

[145] F. Sharifianjazi, M. Moradi, N. Parvin, A. Nemati, A. Jafari Rad, N. Sheysi, A. Abouchenari, A. Mohammadi, S. Karbasi, Z. Ahmadi, A. Esmaeilkhanian, M. Irani, A. Pakseresht, S. Sahmani, M. Shahedi Asl, Magnetic $CoFe_2O_4$ nanoparticles doped with metal ions: A review, Ceram. Int. 46 (2020) 18391–18412. doi:10.1016/j.ceramint.2020.04.202.

[146] H. Jangara, K. Shayesteh, M. Shahedi Asl, Mathematical modeling of absorption accompanied by a non-elementary reversible chemical reaction, Chem. Eng. Res. Des. 157 (2020) 58–64. doi:10.1016/j.cherd.2020.02.030.

[147] K. Asadi-Pakdel, R. Mehdinavaz Aghdam, M. Shahedi Asl, M.A. Faghihi Sani, Synthesis and morphology optimization of electrospun SiBNC nanofibers, Ceram. Int. 46 (2020) 6052–6059. doi:10.1016/j.ceramint.2019.11.063.

[148] M. Akhlaghi, S.A. Tayebifard, E. Salahi, M. Shahedi Asl, Spark plasma sintering of TiAl–Ti_3AlC_2 composite, Ceram. Int. 44 (2018) 21759–21764. doi:10.1016/j.ceramint.2018.08.272.

[149] S. Haji Amiri, M. Ghassemi Kakroudi, T. Rabizadeh, M. Shahedi Asl, Characterization of hot-pressed Ti_3SiC_2–SiC composites, Int. J. Refract. Met. Hard Mater. 90 (2020) 105232. doi:10.1016/j.ijrmhm.2020.105232.

[150] M. Shokouhimehr, M.S. Asl, B. Mazinani, Modulated large-pore mesoporous silica as an efficient base catalyst for the Henry reaction, Res. Chem. Intermed. 44 (2018) 1617–1626. doi:10.1007/s11164-017-3188-9.

[151] A. Sabahi Namini, S.A. Delbari, B. Nayebi, M. Shahedi Asl, S. Parvizi, Effect of B_4C content on sintering behavior, microstructure and mechanical properties of Ti-based composites fabricated via spark plasma sintering, Mater. Chem. Phys. 251 (2020) 123087. doi:10.1016/j.matchemphys.2020.123087.

[152] A. Sabahi Namini, M. Shahedi Asl, S.A. Delbari, Influence of Sintering Temperature on Microstructure and Mechanical Properties of Ti–Mo–B_4C Composites, Met. Mater. Int. (2019). doi:10.1007/s12540-019-00469-y.

[153] M. Akhlaghi, S.A. Tayebifard, E. Salahi, M. Shahedi Asl, G. Schmidt, Self-propagating high-temperature synthesis of Ti_3AlC_2 MAX phase from mechanically-activated Ti/Al/graphite powder mixture, Ceram. Int. 44 (2018) 9671–9678. doi:10.1016/j.ceramint.2018.02.195.

[154] M. Fattahi, M. Shahedi Asl, S.A. Delbari, A. Sabahi Namini, Z. Ahmadi, M. Mohammadi, Role of nano-WC addition on microstructural, mechanical and thermal characteristics of TiC–SiC composites, Int. J. Refract. Met. Hard Mater. 90 (2020) 105248. doi:10.1016/j.ijrmhm.2020.105248.

[155] F. Sharifianjazi, M. Moradi, A. Abouchenari, A.H. Pakseresht, A. Esmaeilkhanian, M. Shokouhimehr, M. Shahedi Asl, Effects of Sr and Mg dopants on biological and mechanical properties of SiO_2–CaO–P_2O_5 bioactive glass, Ceram. Int. 46 (2020) 22674–22682. doi:10.1016/j.ceramint.2020.06.030.

[156] K. Shayesteh, P. Abbasi, V. Vahid Fard, M. Shahedi Asl, Simultaneous Removal of Nickel and Cadmium During the Cold Purification of Zinc Sulfate Solution, Arab. J. Sci. Eng. 45 (2020) 587–598. doi:10.1007/s13369-019-04320-9.

[157] S.A. Delbari, A. Sabahi Namini, M. Azadbeh, Z. Ahmadi, V.-H. Nguyen, Q. Van Le, M. Shokouhimehr, M. Shahedi Asl, M. Mohammadi, Post hot rolling of spark plasma sintered Ti–Mo–B_4C composites, Mater. Sci. Eng. A. 799 (2021) 140214. doi:10.1016/j.msea.2020.140214.

[158] M. Shahedi Asl, S.A. Delbari, M. Azadbeh, A. Sabahi Namini, M. Mehrabian, V.-H. Nguyen, Q. Van Le, M. Shokouhimehr, M. Mohammadi, Nanoindentational and conventional mechanical properties of spark plasma sintered Ti–Mo alloys, J. Mater. Res. Technol. 9 (2020) 10647–10658. doi:10.1016/j.jmrt.2020.07.066.

[159] H. Roghani, S.A. Tayebifard, K. Kasraee, M. Shahedi Asl, Volume combustion synthesis of B_4C–SiC nanocomposites in tubular and spark plasma furnaces, Ceram. Int. (2020). doi:10.1016/j.ceramint.2020.08.060.

[160] Y. Azizian-Kalandaragh, J. Farazin, Ş. Altindal, M. Shahedi Asl, G. Pirgholi-Givi, S.A. Delbari, A. Sabahi Namini, Electrical and dielectric properties of Al/(PVP: Zn-TeO_2)/p-Si heterojunction structures using current–voltage (I–V) and impedance-frequency (Z–f) measurements, Appl. Phys. A. 126 (2020) 635. doi:10.1007/s00339-020-03804-y.

[161] S. Asadzadeh-Khaneghah, A. Habibi-Yangjeh, M. Shahedi Asl, Z. Ahmadi, S. Ghosh, Synthesis of novel ternary g-C_3N_4/SiC/C-Dots photocatalysts and their visible-light-induced activities in removal of various contaminants, J. Photochem. Photobiol. A Chem. 392 (2020) 112431. doi:10.1016/j.jphotochem.2020.112431.

[162] F. Sharifianjazi, A.H. Pakseresht, M. Shahedi Asl, A. Esmaeilkhanian, H. Nargesi khoramabadi, H.W. Jang, M. Shokouhimehr, Hydroxyapatite Consolidated by Zirconia: Applications for Dental Implant, J. Compos. Compd. 2 (2020) 26–34. doi:10.29252/jcc.2.1.4.

[163] H. Salimkhani, P. Palmeh, A.B. Khiabani, E. Hashemi, S. Matinpour, H. Salimkhani, M.S. Asl, Electrophoretic deposition of spherical carbonyl iron particles on carbon fibers as a microwave absorbent composite, Surfaces and Interfaces. 5 (2016) 1–7. doi:10.1016/j.surfin.2016.09.004.

[164] P. Mohamadzadeh Jahani, Simultaneous Detection of Morphine and Diclofenac Using Graphene Nanoribbon Modified Screen-Printed Electrode, Int. J. Electrochem. Sci. (2020) 9037–9048. doi:10.20964/2020.09.14.

[165] V. Sridhara, L.N. Satapathy, Effect of Nanoparticles on Thermal Properties Enhancement in Different Oils – A Review, Crit. Rev. Solid State Mater. Sci. 40 (2015) 399–424. doi:10.1080/10408436.2015.1068159.

[166] X. Li, C. Zou, X. Lei, W. Li, Stability and enhanced thermal conductivity of ethylene glycol-based SiC nanofluids, Int. J. Heat Mass Transf. 89 (2015) 613–619. doi:10.1016/j.ijheatmasstransfer.2015.05.096.

[167] Y. Hwang, J.-K. Lee, J.-K. Lee, Y.-M. Jeong, S. Cheong, Y.-C. Ahn, S.H. Kim, Production and dispersion stability of nanoparticles in nanofluids, Powder Technol. 186 (2008) 145–153. doi:10.1016/j.powtec.2007.11.020.

[168] W. Yu, D.M. France, J.L. Routbort, S.U.S. Choi, Review and Comparison of Nanofluid Thermal Conductivity and Heat Transfer Enhancements, Heat Transf. Eng. 29 (2008) 432–460. doi:10.1080/01457630701850851.

[169] Q.B. Romano, J. M., Parker, J. C., & Ford, Application opportunities for nanoparticles made from the condensation of physical vapors, Advances in Powder Metallurgy and Particulate Materials, 1997.

[170] P. Garg, J.L. Alvarado, C. Marsh, T.A. Carlson, D.A. Kessler, K. Annamalai, An experimental study on the effect of ultrasonication on viscosity and heat transfer performance of multi-wall carbon nanotube-based aqueous nanofluids, Int. J. Heat Mass Transf. 52 (2009) 5090–5101. doi:10.1016/j.ijheatmasstransfer.2009.04.029.

[171] A. Nasiri, M. Shariaty-Niasar, A. Rashidi, A. Amrollahi, R. Khodafarin, Effect of dispersion method on thermal conductivity and stability of nanofluid, Exp. Therm. Fluid Sci. 35 (2011) 717–723. doi:10.1016/j.expthermflusci.2011.01.006.

[172] S.S. Sonawane, R.S. Khedkar, K.L. Wasewar, Effect of sonication time on enhancement of effective thermal conductivity of nano TiO_2 –water, ethylene glycol, and paraffin oil nanofluids and models comparisons, J. Exp. Nanosci. 10

(2015) 310–322. doi:10.1080/17458080.2013.832421.
[173] B. Buonomo, O. Manca, L. Marinelli, S. Nardini, Effect of temperature and sonication time on nanofluid thermal conductivity measurements by nano-flash method, Appl. Therm. Eng. 91 (2015) 181–190. doi:10.1016/j.applthermaleng.2015.07.077.
[174] T.-K. Hong, H.-S. Yang, C.J. Choi, Study of the enhanced thermal conductivity of Fe nanofluids, J. Appl. Phys. 97 (2005) 064311. doi:10.1063/1.1861145.
[175] M.-S. Liu, M.C.-C. Lin, C.Y. Tsai, C.-C. Wang, Enhancement of thermal conductivity with Cu for nanofluids using chemical reduction method, Int. J. Heat Mass Transf. 49 (2006) 3028–3033. doi:10.1016/j.ijheatmasstransfer.2006.02.012.
[176] G. Paul, S. Sarkar, T. Pal, P.K. Das, I. Manna, Concentration and size dependence of nano-silver dispersed water based nanofluids, J. Colloid Interface Sci. 371 (2012) 20–27. doi:10.1016/j.jcis.2011.11.057.
[177] E. De Robertis, E.H.H. Cosme, R.S. Neves, A.Y. Kuznetsov, A.P.C. Campos, S.M. Landi, C.A. Achete, Application of the modulated temperature differential scanning calorimetry technique for the determination of the specific heat of copper nanofluids, Appl. Therm. Eng. 41 (2012) 10–17. doi:10.1016/j.applthermaleng.2012.01.003.
[178] S.U.S. Choi, Z.G. Zhang, W. Yu, F.E. Lockwood, E.A. Grulke, Anomalous thermal conductivity enhancement in nanotube suspensions, Appl. Phys. Lett. 79 (2001) 2252–2254. doi:10.1063/1.1408272.
[179] S.M.S. Murshed, K.C. Leong, C. Yang, Enhanced thermal conductivity of TiO_2—water based nanofluids, Int. J. Therm. Sci. 44 (2005) 367–373. doi:10.1016/j.ijthermalsci.2004.12.005.
[180] M.E. Meibodi, M. Vafaie-Sefti, A.M. Rashidi, A. Amrollahi, M. Tabasi, H.S. Kalal, The role of different parameters on the stability and thermal conductivity of carbon nanotube/water nanofluids, Int. Commun. Heat Mass Transf. 37 (2010) 319–323. doi:10.1016/j.icheatmasstransfer.2009.10.004.
[181] S.W. Lee, S.D. Park, S. Kang, I.C. Bang, J.H. Kim, Investigation of viscosity and thermal conductivity of SiC nanofluids for heat transfer applications, Int. J. Heat Mass Transf. 54 (2011) 433–438. doi:10.1016/j.ijheatmasstransfer.2010.09.026.
[182] P.K. Singh, P.V. Harikrishna, T. Sundararajan, S.K. Das, Experimental and numerical investigation into the hydrodynamics of nanofluids in microchannels, Exp. Therm. Fluid Sci. 42 (2012) 174–186. doi:10.1016/j.expthermflusci.2012.05.004.
[183] S.A. Fazeli, S.M. Hosseini Hashemi, H. Zirakzadeh, M. Ashjaee, Experimental and numerical investigation of heat transfer in a miniature heat sink utilizing silica nanofluid, Superlattices Microstruct. 51 (2012) 247–264. doi:10.1016/j.spmi.2011.11.017.
[184] Z.T. Tabari, S.Z. Heris, Heat Transfer Performance of Milk Pasteurization Plate Heat Exchangers Using MWCNT/Water Nanofluid, J. Dispers. Sci. Technol. 36 (2015) 196–204. doi:10.1080/01932691.2014.894917.
[185] R. Choudhary, S. Subudhi, Aspect ratio dependence of turbulent natural convection in Al_2O_3/water nanofluids, Appl. Therm. Eng. 108 (2016) 1095–1104. doi:10.1016/j.applthermaleng.2016.08.016.
[186] V. Irani, A. Maleki, A. Tavasoli, CO2 absorption enhancement in graphene-oxide/MDEA nanofluid, J. Environ. Chem. Eng. 7 (2019) 102782. doi:10.1016/j.jece.2018.11.027.
[187] W. Rashmi, A.F. Ismail, I. Sopyan, A.T. Jameel, F. Yusof, M. Khalid, N.M. Mubarak, Stability and thermal conductivity enhancement of carbon nanotube nanofluid using gum arabic, J. Exp. Nanosci. 6 (2011) 567–579. doi:10.1080/17458080.2010.487229.
[188] X.F. Li, D.S. Zhu, X.J. Wang, N. Wang, J.W. Gao, H. Li, Thermal conductivity enhancement dependent pH and chemical surfactant for Cu-H2O nanofluids, Thermochim. Acta. 469 (2008) 98–103. doi:10.1016/j.tca.2008.01.008.
[189] H. Zhu, C. Zhang, Y. Tang, J. Wang, B. Ren, Y. Yin, Preparation and thermal conductivity of suspensions of graphite nanoparticles, Carbon N. Y. 45 (2007) 226–228. doi:10.1016/j.carbon.2006.07.005.
[190] M.J. Assael, I.N. Metaxa, J. Arvanitidis, D. Christofilos, C. Lioutas, Thermal Conductivity Enhancement in Aqueous Suspensions of Carbon Multi-Walled and Double-Walled Nanotubes in the Presence of Two Different Dispersants, Int. J. Thermophys. 26 (2005) 647–664. doi:10.1007/s10765-005-5569-3.
[191] L. Jiang, L. Gao, J. Sun, Production of aqueous colloidal dispersions of carbon nanotubes, J. Colloid Interface Sci. 260 (2003) 89–94. doi:10.1016/S0021-9797(02)00176-5.
[192] Y. Xuan, Q. Li, Heat transfer enhancement of nanofluids, Int. J. Heat Fluid Flow. 21 (2000) 58–64. doi:10.1016/S0142-727X(99)00067-3.
[193] X. Peng, X. F., Yu, X. L., Xia, L. F., & Zhong, Influence factors on suspension stability of nanofluids, Journal-Zhejiang Univ. Eng. Sci. 41 (2007) 577.
[194] H.E. Patel, K.B. Anoop, T. Sundararajan, S.K. Das, A MICRO-CONVECTION MODEL FOR THERMAL CONDUCTIVITY OF NANOFLUIDS, in: Nanoscale, Begell House Inc., 2006. doi:10.1615/IHTC13.p8.240.
[195] D. Lee, J.-W. Kim, B.G. Kim, A New Parameter to Control Heat Transport in Nanofluids: Surface Charge State of the Particle in Suspension, J. Phys. Chem. B. 110 (2006) 4323–4328. doi:10.1021/jp057225m.
[196] H. Chen, Y. Ding, A. Lapkin, Rheological behaviour of nanofluids containing tube / rod-like nanoparticles, Powder Technol. 194 (2009) 132–141. doi:10.1016/j.powtec.2009.03.038.
[197] W. Yu, H. Xie, L. Chen, Y. Li, Enhancement of thermal conductivity of kerosene-based Fe3O4 nanofluids prepared via phase-transfer method, Colloids Surfaces A Physicochem. Eng. Asp. 355 (2010) 109–113. doi:10.1016/j.colsurfa.2009.11.044.
[198] M. Chandrasekar, S. Suresh, A. Chandra Bose, Experimental studies on heat transfer and friction factor characteristics of Al_2O_3/water nanofluid in a circular pipe under laminar flow with wire coil inserts, Exp. Therm. Fluid Sci. 34 (2010) 122–130. doi:10.1016/j.expthermflusci.2009.10.001.
[199] S.S.J. Aravind, P. Baskar, T.T. Baby, R.K. Sabareesh, S. Das, S. Ramaprabhu, Investigation of Structural Stability, Dispersion, Viscosity, and Conductive Heat Transfer Properties of Functionalized Carbon Nanotube Based Nanofluids, J. Phys. Chem. C. 115 (2011) 16737–16744. doi:10.1021/jp201672p.
[200] M. Shanbedi, S.Z. Heris, M. Baniadam, A. Amiri, M. Maghrebi, Investigation of Heat-Transfer Characterization of EDA-MWCNT/DI-Water Nanofluid in a Two-Phase Closed Thermosyphon, Ind. Eng. Chem. Res. 51 (2012) 1423–1428. doi:10.1021/ie202110g.
[201] M. Shanbedi, S. Zeinali Heris, M. Baniadam, A. Amiri, The Effect of Multi-Walled Carbon Nanotube/Water Nanofluid on Thermal Performance of a Two-Phase Closed Thermosyphon, Exp. Heat Transf. 26 (2013) 26–40. doi:10.1080/08916152.2011.631078.
[202] A. Amiri, R. Sadri, M. Shanbedi, G. Ahmadi, B.T. Chew, S.N. Kazi, M. Dahari, Performance dependence of thermosyphon on the functionalization approaches: An experimental study on thermo-physical properties of graphene nanoplatelet-based water nanofluids, Energy Convers. Manag. 92 (2015) 322–330. doi:10.1016/j.enconman.2014.12.051.
[203] R.M. Mostafizur, A.R. Abdul Aziz, R. Saidur, M.H.U. Bhuiyan, Investigation on stability and viscosity of SiO2–CH3OH (methanol) nanofluids, Int. Commun. Heat Mass Transf. 72 (2016) 16–22. doi:10.1016/j.icheatmasstransfer.2016.01.001.
[204] K. Cacua, R. Buitrago-Sierra, B. Herrera, F. Chejne, E. Pabón, Influence of different parameters and their coupled effects on the stability of alumina nanofluids by a fractional factorial design approach, Adv. Powder Technol. 28 (2017) 2581–2588. doi:10.1016/j.apt.2017.07.009.
[205] S.J.K. S, P.K. Nagarajan, Influence of stability and particle shape effects for an entropy generation based optimized selection of magnesia nanofluid for convective heat flow applications, Appl. Surf. Sci. 489 (2019) 560–575. doi:10.1016/j.apsusc.2019.06.038.
[206] H. Chang, C.S. Jwo, P.S. Fan, S.H. Pai, Process optimization and material properties for nanofluid manufacturing, Int. J. Adv. Manuf. Technol. 34 (2007) 300–306. doi:10.1007/s00170-006-0597-0.
[207] Y. He, Y. Jin, H. Chen, Y. Ding, D. Cang, H. Lu, Heat transfer and flow behaviour of aqueous suspensions of TiO_2 nanoparticles (nanofluids) flowing upward through a vertical pipe, Int. J. Heat Mass Transf. 50 (2007) 2272–2281. doi:10.1016/j.ijheatmasstransfer.2006.10.024.
[208] K.B. Hadjov, Modified self-consisted scheme to predict the thermal conductivity of nanofluids, Int. J. Therm. Sci. 48 (2009) 2249–2254. doi:10.1016/j.ijthermalsci.2009.05.008.
[209] L. Jorge, S. Coulombe, P.-L. Girard-Lauriault, Tetraethylenepentamine and (3-aminopropyl)triethoxysilane adsorbed on multi-walled carbon nanotubes for stable water and ethanol nanofluids, Thin Solid Films. 682 (2019) 50–56. doi:10.1016/j.tsf.2019.05.007.
[210] M. Zareei, H. Yoozbashizadeh, H.R. Madaah Hosseini, Investigating the effects of pH, surfactant and ionic strength on the stability of alumina/water nanofluids using DLVO theory, J. Therm. Anal. Calorim. 135 (2019) 1185–1196. doi:10.1007/s10973-018-7620-1.
[211] B. Bakthavatchalam, K. Habib, R. Saidur, B.B. Saha, K. Irshad, Comprehensive study on nanofluid and ionanofluid for heat transfer enhancement: A review on current and future perspective, J. Mol. Liq. 305 (2020) 112787. doi:10.1016/j.molliq.2020.112787.
[212] L. Yang, Y. Hu, Toward TiO_2 Nanofluids—Part 1: Preparation and Properties, Nanoscale Res. Lett. 12 (2017) 417. doi:10.1186/s11671-017-2184-8.
[213] J.D. Clogston, A.K. Patri, Zeta Potential Measurement, in: 2011: pp. 63–70. doi:10.1007/978-1-60327-198-1_6.
[214] L. Vandsburger, Synthesis and covalent surface modification of carbon nanotubes for preparation of stabilized nanofluid suspensions, M.Eng., Montr. McGill

Univ. (2009) 1–73.
[215] F. Mashali, E.M. Languri, J. Davidson, D. Kerns, W. Johnson, K. Nawaz, G. Cunningham, Thermo-physical properties of diamond nanofluids: A review, Int. J. Heat Mass Transf. 129 (2019) 1123–1135. doi:10.1016/j.ijheatmasstransfer.2018.10.033.
[216] I. Zakaria, W.A.N.W. Mohamed, A.M.I. Bin Mamat, R. Saidur, W.H. Azmi, R. Mamat, S.F.A. Talib, Experimental Investigation of Al_2O_3 - Water Ethylene Glycol Mixture Nanofluid Thermal Behaviour in a Single Cooling Plate for PEM Fuel Cell Application, Energy Procedia. 79 (2015) 252–258. doi:10.1016/j.egypro.2015.11.474.
[217] T. Sun, A.S. Teja, Density, Viscosity and Thermal Conductivity of Aqueous Solutions of Propylene Glycol, Dipropylene Glycol, and Tripropylene Glycol between 290 K and 460 K, J. Chem. Eng. Data. 49 (2004) 1311–1317. doi:10.1021/je049960h.
[218] N.G. Tsierkezos, I.E. Molinou, Thermodynamic Properties of Water + Ethylene Glycol at 283.15, 293.15, 303.15, and 313.15 K, J. Chem. Eng. Data. 43 (1998) 989–993. doi:10.1021/je9800914.
[219] M. Hosseinzadeh, A. Salari, M. Sardarabadi, M. Passandideh-Fard, Optimization and parametric analysis of a nanofluid based photovoltaic thermal system: 3D numerical model with experimental validation, Energy Convers. Manag. 160 (2018) 93–108. doi:10.1016/j.enconman.2018.01.006.
[220] B. Kolade, K.E. Goodson, J.K. Eaton, Convective Performance of Nanofluids in a Laminar Thermally Developing Tube Flow, J. Heat Transfer. 131 (2009). doi:10.1115/1.3013831.
[221] S.K. Das, N. Putra, P. Thiesen, W. Roetzel, Temperature Dependence of Thermal Conductivity Enhancement for Nanofluids, J. Heat Transfer. 125 (2003) 567–574. doi:10.1115/1.1571080.
[222] Q. Shou, R. Chen, S. Su, Experimental research on thermal conductivity of metal-oxide nanofluids, Appl. Mech. Mater. 148–149 (2012) 587–590. doi:10.4028/www.scientific.net/AMM.148-149.587.
[223] C.H. Chon, K.D. Kihm, S.P. Lee, S.U.S. Choi, Empirical correlation finding the role of temperature and particle size for nanofluid (Al_2O_3) thermal conductivity enhancement, Appl. Phys. Lett. 87 (2005) 153107. doi:10.1063/1.2093936.
[224] Y. Li, J. Zhou, S. Tung, E. Schneider, S. Xi, A review on development of nanofluid preparation and characterization, Powder Technol. 196 (2009) 89–101. doi:10.1016/j.powtec.2009.07.025.
[225] A.S. Dalkılıç, G. Yalçın, B.O. Küçükyıldırım, S. Öztuna, A. Akdoğan Eker, C. Jumpholkul, S. Nakkaew, S. Wongwises, Experimental study on the thermal conductivity of water-based CNT-SiO_2 hybrid nanofluids, Int. Commun. Heat Mass Transf. 99 (2018) 18–25. doi:10.1016/j.icheatmasstransfer.2018.10.002.
[226] K. Vaferi, S. Nekahi, M. Vajdi, F. Sadegh Moghanlou, M. Shokouhimehr, A. Motallebzadeh, J. Sha, M. Shahedi Asl, Heat transfer, thermal stress and failure analyses in a TiB_2 gas turbine stator blade, Ceram. Int. 45 (2019). doi:10.1016/j.ceramint.2019.06.184.
[227] M. Vajdi, F. Sadegh Moghanlou, Z. Ahmadi, A. Motallebzadeh, M. Shahedi Asl, Thermal diffusivity and microstructure of spark plasma sintered TiB_2SiC Ti composite, Ceram. Int. 45 (2019) 8333–8344. doi:10.1016/j.ceramint.2019.01.141.
[228] S. Nekahi, M. Vajdi, F. Sadegh Moghanlou, K. Vaferi, A. Motallebzadeh, M. Özen, U. Aydemir, J. Sha, M. Shahedi Asl, TiB_2–SiC-based ceramics as alternative efficient micro heat exchangers, Ceram. Int. 45 (2019) 19060–19067. doi:10.1016/j.ceramint.2019.06.150.
[229] S. Nekahi, F. Sadegh Moghanlou, M. Vajdi, Z. Ahmadi, A. Motallebzadeh, M. Shahedi Asl, Microstructural, thermal and mechanical characterization of TiB_2–SiC composites doped with short carbon fibers, Int. J. Refract. Met. Hard Mater. 82 (2019) 129–135. doi:10.1016/j.ijrmhm.2019.04.005.
[230] M. Vajdi, F. Sadegh Moghanlou, S. Nekahi, Z. Ahmadi, A. Motallebzadeh, H. Jafarzadeh, M. Shahedi Asl, Role of graphene nano-platelets on thermal conductivity and microstructure of TiB_2–SiC ceramics, Ceram. Int. 46 (2020) 21775–21783. doi:10.1016/j.ceramint.2020.05.289.
[231] F. Sadegh Moghanlou, S. Nekahi, M. Vajdi, Z. Ahmadi, A. Motallebzadeh, A. Shokouhimehr, M. Shokouhimehr, S. Jafargholinejad, M. Shahedi Asl, Effects of graphite nano-flakes on thermal and microstructural properties of TiB_2–SiC composites, Ceram. Int. 46 (2020) 11622–11630. doi:10.1016/j.ceramint.2020.01.192.
[232] S. Jana, A. Salehi-Khojin, W.-H. Zhong, Enhancement of fluid thermal conductivity by the addition of single and hybrid nano-additives, Thermochim. Acta. 462 (2007) 45–55. doi:10.1016/j.tca.2007.06.009.
[233] H. Xie, H. Lee, W. Youn, M. Choi, Nanofluids containing multiwalled carbon nanotubes and their enhanced thermal conductivities, J. Appl. Phys. 94 (2003) 4967. doi:10.1063/1.1613374.
[234] X. Wang, X. Xu, S.U.S. Choi, Thermal Conductivity of Nanoparticle - Fluid Mixture, J. Thermophys. Heat Transf. 13 (1999) 474–480. doi:10.2514/2.6486.
[235] M. Abareshi, E.K. Goharshadi, S. Mojtaba Zebarjad, H. Khandan Fadafan, A. Youssefi, Fabrication, characterization and measurement of thermal conductivity of Fe_3O_4 nanofluids, J. Magn. Magn. Mater. 322 (2010) 3895–3901. doi:10.1016/j.jmmm.2010.08.016.
[236] W.Y. Lai, S. Vinod, P.E. Phelan, R. Prasher, Convective Heat Transfer for Water-Based Alumina Nanofluids in a Single 1.02-mm Tube, J. Heat Transfer. 131 (2009). doi:10.1115/1.3133886.
[237] D. Zhu, X. Li, N. Wang, X. Wang, J. Gao, H. Li, Dispersion behavior and thermal conductivity characteristics of Al_2O_3–H_2O nanofluids, Curr. Appl. Phys. 9 (2009) 131–139. doi:10.1016/j.cap.2007.12.008.
[238] H. Xie, J. Wang, T. Xi, Y. Liu, F. Ai, Q. Wu, Thermal conductivity enhancement of suspensions containing nanosized alumina particles, J. Appl. Phys. 91 (2002) 4568–4572. doi:10.1063/1.1454184.
[239] H.E. Patel, S.K. Das, T. Sundararajan, A. Sreekumaran Nair, B. George, T. Pradeep, Thermal conductivities of naked and monolayer protected metal nanoparticle based nanofluids: Manifestation of anomalous enhancement and chemical effects, Appl. Phys. Lett. 83 (2003) 2931–2933. doi:10.1063/1.1602578.
[240] D. Wen, Y. Ding, Experimental investigation into convective heat transfer of nanofluids at the entrance region under laminar flow conditions, Int. J. Heat Mass Transf. 47 (2004) 5181–5188. doi:10.1016/j.ijheatmasstransfer.2004.07.012.
[241] S.A. Putnam, D.G. Cahill, P. V. Braun, Z. Ge, R.G. Shimmin, Thermal conductivity of nanoparticle suspensions, J. Appl. Phys. 99 (2006) 084308. doi:10.1063/1.2189933.
[242] L. Godson, B. Raja, D.M. Lal, S. Wongwises, Experimental Investigation on the Thermal Conductivity and Viscosity of Silver-Deionized Water Nanofluid, Exp. Heat Transf. 23 (2010) 317–332. doi:10.1080/08916150903564796.
[243] M. Kole, T.K. Dey, Thermal conductivity and viscosity of Al_2O_3 nanofluid based on car engine coolant, J. Phys. D. Appl. Phys. 43 (2010) 315501. doi:10.1088/0022-3727/43/31/315501.
[244] L. Colla, L. Fedele, M. Scattolini, S. Bobbo, Water-Based Fe_2O_3 Nanofluid Characterization: Thermal Conductivity and Viscosity Measurements and Correlation, Adv. Mech. Eng. 4 (2012) 674947. doi:10.1155/2012/674947.
[245] O. MANNA, S.K. SINGH, G. PAUL, Enhanced thermal conductivity of nano-SiC dispersed water based nanofluid, Bull. Mater. Sci. 35 (2012) 707–712. doi:10.1007/s12034-012-0366-7.
[246] T.-P. Teng, Thermal conductivity and phase-change properties of aqueous alumina nanofluid, Energy Convers. Manag. 67 (2013) 369–375. doi:10.1016/j.enconman.2012.12.004.
[247] M.K. Sinha, R. Madarkar, S. Ghosh, P.V. Rao, Application of eco-friendly nanofluids during grinding of Inconel 718 through small quantity lubrication, J. Clean. Prod. 141 (2017) 1359–1375. doi:10.1016/j.jclepro.2016.09.212.
[248] F. Micali, M. Milanese, G. Colangelo, A. de Risi, Experimental investigation on 4-strokes biodiesel engine cooling system based on nanofluid, Renew. Energy. 125 (2018) 319–326. doi:10.1016/j.renene.2018.02.110.
[249] R. Ranjbarzadeh, A. Moradikazerouni, R. Bakhtiari, A. Asadi, M. Afrand, An experimental study on stability and thermal conductivity of water/silica nanofluid: Eco-friendly production of nanoparticles, J. Clean. Prod. 206 (2019) 1089–1100. doi:10.1016/j.jclepro.2018.09.205.
[250] A. Riahi, S. Khamlich, M. Balghouthi, T. Khamliche, T.B. Doyle, W. Dimassi, A. Guizani, M. Maaza, Study of thermal conductivity of synthesized Al_2O_3-water nanofluid by pulsed laser ablation in liquid, J. Mol. Liq. 304 (2020) 112694. doi:10.1016/j.molliq.2020.112694.
[251] J.C. Maxwell, The Scientific Papers of James Clerk Maxwell, Cambridge University Press, Cambridge, 1890. doi:10.1017/CBO9780511698095.
[252] R.L. Hamilton, O.K. Crosser, Thermal Conductivity of Heterogeneous Two-Component Systems, Ind. Eng. Chem. Fundam. 1 (1962) 187–191. doi:10.1021/i160003a005.
[253] D.A.G. Bruggeman, Berechnung verschiedener physikalischer Konstanten von heterogenen Substanzen. III. Die elastischen Konstanten der quasiisotropen Mischkörper aus isotropen Substanzen, Ann. Phys. 421 (1937) 160–178. doi:10.1002/andp.19374210205.
[254] R.L.G. E.J. Wasp, J.P. Kenny, Solid–liquid flow: Slurry pipeline transportation. [pumps, valves, mechanical equipment, economicS], Ser. Bulk Mater. Handl.; (United States). 1:4 (1977) 1.
[255] S. Lu, H. Lin, Effective conductivity of composites containing aligned spheroidal inclusions of finite conductivity, J. Appl. Phys. 79 (1996) 6761–6769. doi:10.1063/1.361498.
[256] W. Yu, S.U.S. Choi, The role of interfacial layers in the enhanced thermal conductivity of nanofluids: A renovated Hamilton?Crosser model, J. Nanoparticle Res. 6 (2004) 355–361. doi:10.1007/s11051-004-2601-7.
[257] C.-W. Nan, Z. Shi, Y. Lin, A simple model for thermal conductivity of carbon nanotube-based composites, Chem. Phys. Lett. 375 (2003) 666–669. doi:10.1016/S0009-2614(03)00956-4.

[258] B.-X. Wang, L.-P. Zhou, X.-F. Peng, A fractal model for predicting the effective thermal conductivity of liquid with suspension of nanoparticles, Int. J. Heat Mass Transf. 46 (2003) 2665–2672. doi:10.1016/S0017-9310(03)00016-4.
[259] S.K. Kumar, D. H., Patel, H. E., Kumar, V. R., Sundararajan, T., Pradeep, T., & Das, Model for heat conduction in nanofluids, Phys. Rev. Lett. 93 (2004) 144301.
[260] H. Xie, M. Fujii, X. Zhang, Effect of interfacial nanolayer on the effective thermal conductivity of nanoparticle-fluid mixture, Int. J. Heat Mass Transf. 48 (2005) 2926–2932. doi:10.1016/j.ijheatmasstransfer.2004.10.040.
[261] P.E.P. R. Prasher, P. Bhattacharya, Thermal conductivity of nanoscale colloidal solutions (nanofluids), Phys. Rev. Lett. 94 (2005) 25901.
[262] S.M.S. Murshed, K.C. Leong, C. Yang, A model for predicting the effective thermal conductivity of nanoparticle-fluid suspensions, Int. J. Nanosci. 05 (2006) 23–33. doi:10.1142/S0219581X06004127.
[263] J. Li, Computational Analysis of Nanofluid Flow in Microchannels with Applications to Micro-heat Sinks and Bio-MEMS., (2008) 207. doi:10.1017/CBO9781107415324.004.
[264] R.S. Vajjha, D.K. Das, D.P. Kulkarni, Development of new correlations for convective heat transfer and friction factor in turbulent regime for nanofluids, Int. J. Heat Mass Transf. 53 (2010) 4607–4618. doi:10.1016/j.ijheatmasstransfer.2010.06.032.
[265] K.S. Suganthi, V. Leela Vinodhan, K.S. Rajan, Heat transfer performance and transport properties of ZnO–ethylene glycol and ZnO–ethylene glycol–water nanofluid coolants, Appl. Energy. 135 (2014) 548–559. doi:10.1016/j.apenergy.2014.09.023.
[266] Y. Gao, H. Wang, A.P. Sasmito, A.S. Mujumdar, Measurement and modeling of thermal conductivity of graphene nanoplatelet water and ethylene glycol base nanofluids, Int. J. Heat Mass Transf. 123 (2018) 97–109. doi:10.1016/j.ijheatmasstransfer.2018.02.089.
[267] R. Prasher, D. Song, J. Wang, P. Phelan, Measurements of nanofluid viscosity and its implications for thermal applications, Appl. Phys. Lett. 89 (2006) 133108. doi:10.1063/1.2356113.
[268] E.W. Woolard, A. Einstein, R. Furth, A.D. Cowper, Investigations on the Theory of the Brownian Movement., Dover Publications, Inc, 1956.
[269] S.M.S. Murshed, P. Estellé, A state of the art review on viscosity of nanofluids, Renew. Sustain. Energy Rev. 76 (2017) 1134–1152. doi:10.1016/j.rser.2017.03.113.
[270] M. Ghazvini, M.A. Akhavan-Behabadi, E. Rasouli, M. Raisee, Heat Transfer Properties of Nanodiamond–Engine Oil Nanofluid in Laminar Flow, Heat Transf. Eng. 33 (2012) 525–532. doi:10.1080/01457632.2012.624858.
[271] Y. Ding, H. Alias, D. Wen, R.A. Williams, Heat transfer of aqueous suspensions of carbon nanotubes (CNT nanofluids), Int. J. Heat Mass Transf. 49 (2006) 240–250. doi:10.1016/j.ijheatmasstransfer.2005.07.009.
[272] S. Zeinali Heris, S.G. Etemad, M. Nasr Esfahany, Experimental investigation of oxide nanofluids laminar flow convective heat transfer, Int. Commun. Heat Mass Transf. 33 (2006) 529–535. doi:10.1016/j.icheatmasstransfer.2006.01.005.
[273] C.T. Nguyen, F. Desgranges, N. Galanis, G. Roy, T. Maré, S. Boucher, H. Angue Mintsa, Viscosity data for Al_2O_3–water nanofluid—hysteresis: is heat transfer enhancement using nanofluids reliable?, Int. J. Therm. Sci. 47 (2008) 103–111. doi:10.1016/j.ijthermalsci.2007.01.033.
[274] L. Syam Sundar, M.K. Singh, A.C.M. Sousa, Investigation of thermal conductivity and viscosity of Fe_3O_4 nanofluid for heat transfer applications, Int. Commun. Heat Mass Transf. 44 (2013) 7–14. doi:10.1016/j.icheatmasstransfer.2013.02.014.
[275] M. Shanbedi, S. Zeinali Heris, A. Maskooki, Experimental investigation of stability and thermophysical properties of carbon nanotubes suspension in the presence of different surfactants, J. Therm. Anal. Calorim. 120 (2015) 1193–1201. doi:10.1007/s10973-015-4404-8.
[276] H.W. Chiam, W.H. Azmi, N.A. Usri, R. Mamat, N.M. Adam, Thermal conductivity and viscosity of Al_2O_3 nanofluids for different based ratio of water and ethylene glycol mixture, Exp. Therm. Fluid Sci. 81 (2017) 420–429. doi:10.1016/j.expthermflusci.2016.09.013.
[277] K.M. Yashawantha, A. Asif, G. Ravindra Babu, M.K. Ramis, Rheological Behavior and Thermal Conductivity of Graphite–Ethylene Glycol Nanofluid, J. Test. Eval. 49 (2021) 20190255. doi:10.1520/JTE20190255.
[278] A. Ajith, Eine neue bestimmung der moleküldimensionen, Ann. Phys. 324 (1906) 289–306.
[279] H.C. Brinkman, The Viscosity of Concentrated Suspensions and Solutions, J. Chem. Phys. 20 (1952) 571–571. doi:10.1063/1.1700493.
[280] J.D. Eshelby, The determination of the elastic field of an ellipsoidal inclusion, and related problems, Proc. R. Soc. London. Ser. A. Math. Phys. Sci. 241 (1957) 376–396. doi:10.1098/rspa.1957.0133.
[281] I.M. Krieger, T.J. Dougherty, A Mechanism for Non-Newtonian Flow in Suspensions of Rigid Spheres, Trans. Soc. Rheol. 3 (1959) 137–152. doi:10.1122/1.548848.
[282] N.A. Frankel, A. Acrivos, On the viscosity of a concentrated suspension of solid spheres, Chem. Eng. Sci. 22 (1967) 847–853. doi:10.1016/0009-2509(67)80149-0.
[283] D.J. Jeffrey, A. Acrivos, The rheological properties of suspensions of rigid particles, AIChE J. 22 (1976) 417–432. doi:10.1002/aic.690220303.
[284] A.L. Graham, On the viscosity of suspensions of solid spheres, Appl. Sci. Res. 37 (1981) 275–286. doi:10.1007/BF00951252.
[285] T.S. Chow, Viscosities of concentrated dispersions, Phys. Rev. E. 48 (1993) 1977–1983. doi:10.1103/PhysRevE.48.1977.
[286] B.C. Pak, Y.I. Cho, Hydrodynamic and heat transfer study of dispersed fluids with submicron metallic oxide particles, Exp. Heat Transf. 11 (1998) 151–170. doi:10.1080/08916159808946559.
[287] S. Liu, Particle dispersion for suspension flow, Chem. Eng. Sci. 54 (1999) 873–891. doi:10.1016/S0009-2509(98)00309-1.
[288] A. De Noni Jr, D.E. Garcia, D. Hotza, A modified model for the viscosity of ceramic suspensions, Ceram. Int. 28 (2002) 731–735. doi:10.1016/S0272-8842(02)00035-4.
[289] L.A. Dávalos Orozco, L.F. del Castillo, Hydrodynamic Behavior of Suspensions of Polar Particles, Encycl. Surf. Colloid Sci. Third Ed. (2016) 3070–3091. doi:10.1081/e-escs3-120021916.
[290] C.T. Nguyen, F. Desgranges, G. Roy, N. Galanis, T. Maré, S. Boucher, H. Angue Mintsa, Temperature and particle-size dependent viscosity data for water-based nanofluids – Hysteresis phenomenon, Int. J. Heat Fluid Flow. 28 (2007) 1492–1506. doi:10.1016/j.ijheatfluidflow.2007.02.004.
[291] S. Bobbo, L. Fedele, A. Benetti, L. Colla, M. Fabrizio, C. Pagura, S. Barison, Viscosity of water based SWCNH and TiO_2 nanofluids, Exp. Therm. Fluid Sci. 36 (2012) 65–71. doi:10.1016/j.expthermflusci.2011.08.004.
[292] S. Aberoumand, A. Jafarimoghaddam, M. Moravej, H. Aberoumand, K. Javaherdeh, Experimental study on the rheological behavior of silver-heat transfer oil nanofluid and suggesting two empirical based correlations for thermal conductivity and viscosity of oil based nanofluids, Appl. Therm. Eng. 101 (2016) 362–372. doi:10.1016/j.applthermaleng.2016.01.148.
[293] A. Karimipour, S. Ghasemi, M.H.K. Darvanjooghi, A. Abdollahi, A new correlation for estimating the thermal conductivity and dynamic viscosity of CuO/liquid paraffin nanofluid using neural network method, Int. Commun. Heat Mass Transf. 92 (2018) 90–99. doi:10.1016/j.icheatmasstransfer.2018.02.002.
[294] M. Hemmat Esfe, H. Rahimi Raki, M.R. Sarmasti Emami, M. Afrand, Viscosity and rheological properties of antifreeze based nanofluid containing hybrid nano-powders of MWCNTs and TiO_2 under different temperature conditions, Powder Technol. 342 (2019) 808–816. doi:10.1016/j.powtec.2018.10.032.
[295] A. Kumar, S. Subudhi, Preparation, characterization and heat transfer analysis of nanofluids used for engine cooling, Appl. Therm. Eng. 160 (2019) 114092. doi:10.1016/j.applthermaleng.2019.114092.
[296] B. Farajollahi, S.G. Etemad, M. Hojjat, Heat transfer of nanofluids in a shell and tube heat exchanger, Int. J. Heat Mass Transf. 53 (2010) 12–17. doi:10.1016/j.ijheatmasstransfer.2009.10.019.
[297] D. Wen, Y. Ding, Formulation of nanofluids for natural convective heat transfer applications, Int. J. Heat Fluid Flow. 26 (2005) 855–864. doi:10.1016/j.ijheatfluidflow.2005.10.005.
[298] J.-Y. Jung, H.-S. Oh, H.-Y. Kwak, Forced Convective Heat Transfer of Nanofluids in Microchannels, in: Heat Transf. Vol. 3, ASMEDC, 2006: pp. 327–332. doi:10.1115/IMECE2006-13851.
[299] S.Z. Heris, S.G. Etemad, M.N. Esfahany, Convective Heat Transfer of a Cu/Water Nanofluid Flowing Through a Circular Tube, Exp. Heat Transf. 22 (2009) 217–227. doi:10.1080/08916150902950145.
[300] D.J. Faulkner, D.R. Rector, J.J. Davidson, R. Shekarriz, Enhanced Heat Transfer Through the Use of Nanofluids in Forced Convection, in: Heat Transf. Vol. 3, ASME, 2004: pp. 219–224. doi:10.1115/IMECE2004-62147.
[301] M. Naraki, S.M. Peyghambarzadeh, S.H. Hashemabadi, Y. Vermahmoudi, Parametric study of overall heat transfer coefficient of CuO/water nanofluids in a car radiator, Int. J. Therm. Sci. 66 (2013) 82–90. doi:10.1016/j.ijthermalsci.2012.11.013.
[302] F.W. Dittus, L.M.K. Boelter, Heat transfer in automobile radiators of the tubular type, Int. Commun. Heat Mass Transf. 12 (1985) 3–22. doi:10.1016/0735-1933(85)90003-X.
[303] H.Hausen, Darstellung des Warmeuberganges in Rohren durch verallgemeinerte Potenzbeziehungen, Z. VDI Beih. Verfahrenstech. 4 (1943) 91–98.
[304] D.L. V. Lyon, R. N., & Katz, Liquid-Metals Handbook, US Gov. Print. Off. 733 (1954).

[305] S. Lubarsky, Bernard; Kaufman, Review of Experimental Investigations of Liquid-Metal Heat Transfer, Natl. Advis. Comm. Aeronaut. (1956) 1–33.
[306] S.W. Churchill, R. Usagi, A general expression for the correlation of rates of transfer and other phenomena, AIChE J. 18 (1972) 1121–1128. doi:10.1002/aic.690180606.
[307] R.H. Notter, C.A. Sleicher, A solution to the turbulent Graetz problem-III Fully developed and entry region heat transfer rates, Chem. Eng. Sci. 27 (1972) 2073–2093. doi:10.1016/0009-2509(72)87065-9.
[308] S.E.B. Maïga, C.T. Nguyen, N. Galanis, G. Roy, Heat transfer behaviours of nanofluids in a uniformly heated tube, Superlattices Microstruct. 35 (2004) 543–557. doi:10.1016/j.spmi.2003.09.012.
[309] S. Suresh, K.P. Venkitaraj, P. Selvakumar, M. Chandrasekar, Effect of Al_2O_3-Cu/water hybrid nanofluid in heat transfer, Exp. Therm. Fluid Sci. 38 (2012) 54–60. doi:10.1016/j.expthermflusci.2011.11.007.
[310] L. Syam Sundar, M.T. Naik, K. V. Sharma, M.K. Singh, T.C. Siva Reddy, Experimental investigation of forced convection heat transfer and friction factor in a tube with Fe_3O_4 magnetic nanofluid, Exp. Therm. Fluid Sci. 37 (2012) 65–71. doi:10.1016/j.expthermflusci.2011.10.004.
[311] K. Raj, R. Moskowitz, Commercial applications of ferrofluids, J. Magn. Magn. Mater. 85 (1990) 233–245. doi:10.1016/0304-8853(90)90058-X.
[312] K. V. Wong, O. De Leon, Applications of nanofluids: Current and future, Adv. Mech. Eng. 2010 (2010). doi:10.1155/2010/519659.

Journal of Composites and Compounds 2 (2020) 193-204

Available online at www.jourcc.com

Journal homepage: www.JOURCC.com

Journal of Composites and Compounds

An overview of the development of composites containing Mg and Zn for drug delivery

Firooze Niazvand[a], Amir Cheshmi[b], Maryam Zand[c], Reyhaneh NasrAzadani[d], Beena Kumari[e], Ali Raza[f], Shima Nasibi[g]*

[a] School of medicine, Abadan Faculty of Medical Sciences, Abadan, Iran
[b] Department of Materials Engineering, Babol Noshirvani University of Technology, Shariati Avenue, Babol, Islamic Republic of Iran
[c] Department of Physics, Alzahra University, Tehran, Iran
[d] Department of Biomaterials Nanotechnology and Tissue engineering, School of Advanced Technology in Medicine, Isfahan University of Medical Sciences, Isfahan, Iran
[e] Department of Pharmaceutical Sciences, Indira Gandhi University, Meerpur, Rewari, Haryana, India
[f] School of Biomedical Engineering, Shanghai Jiaotong University, 800 Dongchuan Road, Shanghai, 200240, PR China
[g] Materials Science and Engineering Department, School of Engineering, Shiraz University, Shiraz, Iran

ABSTRACT

Drug delivery is known as the administration of drugs using suitable vehicle for achieving effective treatment with no unwanted effects. In recent years, various composite materials have been developed and evaluated for being used in different biomedical fields such as wound dressings, cardiac prosthesis, tissue engineering, and drug delivery. Zinc is the second most available element after Fe in our body. Nanoparticles based on metal oxides, such as zinc oxides and Zn-containing composites, can be considered as viable platforms for some biomedical uses, especially for drug delivery applications. Mg composite biomaterials are also suggested for diverse biomedical applications due to their good mechanical properties, biocompatibility, and bioactivity. This paper highlights applications of zinc and magnesium-based composites in development of drug delivery systems.

Peer review under responsibility of jourcc

ARTICLE INFORMATION

Article history:
Received 7 November 2020
Received in revised form 3 December 2020
Accepted 18 December 2020

Keywords:
Drug delivery
Biomedical application
Zinc oxide composite
Mg composites

Table of contents

* Corresponding author: Amir Cheshmi; E-mail: amir_cheshomi@yahoo.com
https://doi.org/10.29252/jcc.2.4.4

1. Introduction

Drug delivery systems are designed for the administration of a pharmaceutical compound to promote its therapeutic effects in the animal or human body with minimum side effects [1, 2]. Through extensive studies on animals and humans, our understanding of pharmacodynamics and pharmacokinetic fundamentals has been improved widely. Based on these improvements, several attempts have been implied to improve drug effects in treatment. As a result of these attempts, controlled-release technology is developed, for instance, sustained release drug delivery systems, targeted drug delivery systems, on-demand drug delivery systems, etc. Such systems include tablets, capsules, liposomes, nanoparticles, hydrogels, microneedles and other medical devices [3, 4].

In the past few years, a wide range of composites has been developed and evaluated for different biomedical applications such as cardiac prosthesis, tissue engineering, and drug delivery [5-9]. For instance, for delivering a drug to the intestines, the structure of the composite should include an acid-resistant fatty acid surface covering the interlayers of lactate dehydrogenase (LDH) [10-12]. In recent years, there has been a great interest in the development of bioactive mesoporous materials for drug delivery and bone repair owing to their high pore volume as well as specific surface area. In this regard, a variety of bioactive mesoporous materials have been studied including mesoporous amorphous calcium silicate [13], silica-hydroxyapatite (HAp) composite [14], silica with different pore sizes [15], and $CaO–SiO_2–P_2O_5$ bioactive glasses [16-19].

Zinc is the second most abundant trace element found in our body [20, 21], 85% of which is stored in the bone and muscle [22]. It has been estimated that the zinc amount in our bone is between 110 to 300 mg/kg [23]. The combination of multifunctional properties of zinc and high bioactivity of HAp yields attractive characteristics for biomedical applications [24]. Zn has been termed 'calcium of the twenty-first century' [25]. Intrinsic physiological relevance, pro-regeneration properties, biocompatibility, and biodegradability of Zn has resulted in the emergence of Zinc-based degradable biomaterials [25]. Zn metal-organic frameworks (MOFs), Zn ceramic nanomaterials, and metallic Zn alloys are common Zn-based biomaterials [25, 26]. In the field of drug delivery systems, nanoparticles (NPs) have exhibited prospective performance resulting from facile synthesis and incorporation, high surface area, and high stability, making them suitable for targeting specific cell types and controlling drug release within various microenvironments [27]. PH-responsive drug carriers such as ZnS and ZnO nanoparticles can target tumor cells because the pH values of these cells are noticeably lower than those of normal cells [28, 29]. Nanocomposites are preferred materials for drug delivery due to their adsorption [29].

Mg alloys have attracted great interest among different biodegradable materials owing to their biosafety and desirable mechanical properties [30-32]. Several studies have concentrated on the application of magnesium alloys for temporary cardiovascular stents [33-40]. Furthermore, drug-eluting stents (DESs) have been developed after successfully placing temporary Mg-based cardiovascular stents into a preterm baby's left pulmonary artery [41]. Recently, some Mg alloy-based DESs, such as DREAMS and DREAMS 2G, have been developed, which have lower degradation rate compared to the bare Mg stent and release antiproliferative drug including paclitaxel or rapamycin. The BIOSOLVE-I and BIOSOLVE-II clinical trials of these stents were reported to be successful and no obvious scaffold thrombosis or death was observed, indicating optimal efficacy and biosafety [34, 40, 42]. The mentioned merits of biodegradable Mg-based alloys have encouraged researchers to investigate porous magnesium-based composites that offer higher fracture toughness as well as compressive strength for bone tissue engineering applications [43, 44]. Mg-based composite scaffolds have also shown favorable drug release profiles appropriate for bone infection treatment [45].

The objective of this paper is to review the progress and development of Mg and Zn-containing composites for drug delivery, their synthesis methods, mechanisms, and current challenges and future developments.

2. Drug delivery system

Controlled drug delivery systems (DDSs) are known as formulations or devices that can transport therapeutic agents in the body for their action at specific site, at desired rate, for specific time, and release of the drugs to the target location [46-48]. Therefore, these systems act as an interface between the drug and the patient and help us to develop personalized medicine including pharmaco proteomics, pharmacometrics, and pharmacogenomics. In addition to active pharmaceutical components, an improved delivery process provides a suitable pharmaceutical formulation containing a variety of inactive constituents [49, 50]. Any disease is treated by the specific concentration of therapeutic drugs in plasma with a special regimen [51], which is achieved by a specific drug dose taken at a particular interval in conventional drug therapy. The intervals and the dose of the drug are regulated only based on the half-life and therapeutic index of the drug. In general, fluctuations occur inevitably due to missed dose of the drug, improper patient compliance, over medication or under medication. In order for the drug to be released with an effective therapeutic concentration in a controlled release system, a definite drug release kinetics is required to be followed which is achieved through controlled drug delivery systems [52, 53].

The administration route also influences drug bioavailability. Various administration routes namely, parenteral (subcutaneous, intramuscular, and intravenous) or enteral (ocular, nasal, oral, or transmucosal) can influence the drug bioavailability by altering the biological barrier numbers a drug should cross or by altering the drug exposure to metabolic and pumping mechanisms [54, 55]. To overcome these limitations, it is required to use existing drug effectively and safely using concepts and techniques contributing to controlled/sustained and targeted drug delivery systems. Moreover, the attempts towards overcoming negative aspects of conventional drug delivery that are formed by compression of tablets, coating, and encapsulating bioactive drug molecules have resulted in technological advancements in drug delivery systems and revolution in medication methods [50, 56]. In this regard, computational simulations have also provided a unique insight into the mechanisms of drug diffusion and adsorption in porous carriers at the atomic level [57-60].

3. Composites in drug delivery

In recent decades, noticeable advancements have been observed in the design of chemotherapeutics. However, most chemotherapeutics have some limiting drawbacks such as high cytotoxicity, nonspecific and uncontrolled delivery, high drug dosing, lower solubility, poor absorption, and high side effects [61, 62]. Therefore, it is needed to develop ideal drug delivery systems with some particular properties such as biodegradability, biocompatibility, high drug loading capacity, and capability of drug release in a controlled way. In recent years, different drug delivery systems have been designed to address these parameters including dendrimer, liposomes, and polymers nanoparticles; however, they cannot address the mentioned factors independently [63-66].

The expected characteristics of an ideal drug delivery system could be provided by metal substrate composites. A composite system can offer some advantages like controlled drug release over a long time, stability improvement of drug delivery system, and drug bioactivity preservation in polymeric-based technology. Furthermore, in comparison with pure liposome, dendrimer, and polymeric-based systems, this integrated

system may increase the delivery efficacy [67, 68].

4. Composites containing Mg and Zn in drug delivery

4.1 Zinc and composites containing Zn in drug delivery

Owing to better biocompatibility as well as in vivo biodegradation rate for tissue therapy and regeneration, zinc is considered a preferred candidate for biodegradable metallic materials over Fe and Mg. The emerging theranostics field, such as drug delivery, cancer therapy, bioimaging, and tissue targeting, have extensively benefited from zinc-based ceramic nanomaterials [69, 70]. These ceramics possess several promising characteristics including a high surface-to-volume ratio, pH-responsive nanostructure, good biocompatibility, antibacterial activity, and photoluminescence [71]. Organic biomaterials based on Zn, mainly MOFs, are also promising materials for bioimaging, drug delivery, and cancer therapy due to pH responsiveness as well as large surface/volume ratios [25].

In mesoporous silica nanoparticles (MSNs), the ZnS and ZnO quantum dots, or nanoparticles, are incorporated to cover pores as a component in nanocomposites or cappers [25, 72-74]. In addition, ZnO can exhibit various nanostructures such as nanobels, nano rods, nano disks, nano sheets, nano spheres, quantum dots, etc. It can also be modified to provide excellent properties as a nanocomposite. The US Food and Drug Administration introduced ZnO as one of the safe metal oxides [75, 76]. Moreover, its high energy of excitation-binding around 60 meV, as well as its the wide spot gap around 3.37 eV, add positive properties to its long list of attractive features. Regarding the rewarding properties of ZnO together with its low cost, nanomaterials based on this metal oxide attracted attention in applications related to biomedicine [28, 77]. Furthermore, ZnO nanomaterials exhibit a high capacity of drug loading, have good biodegradability, and can be synthesized through different routes, making them prospective materials for drug delivery. Not only ZnO-based nanocarriers have been fabricated into various forms of nanostructures to deliver drugs to target sites but also they have designed to release the drugs in a controlled manner in response to the pathophysiological conditions [78, 79].

4.2. Magnesium and composites containing Mg in drug delivery

Mg, as one of the important elements in bone tissue and body fluids, has some key roles in the improvement of bone mineral density, reduction of bone fragility, and enhancement of the growth and adhesion of osteoblast cells leading to bony tissue development [31, 80, 81]. Because of the excellent biocompatibility, bioactivity, and mechanical properties of Mg-based biomaterials, they have been considered for local drug delivery systems as well as bone regeneration materials. These systems include forsterite (Mg_2SiO_4) [82], calcium phosphate bone cements doped by Mg [83, 84], magnesium-containing bioactive glasses, etc. [85]. To make biomaterials suitable for bone repair, they are preferred to exhibit a controllable drug delivery capacity in addition to bioactivity [86, 87]. The Mg alloy surface can be treated by bioactive agents to become suitable for this kind of application. Local drug release strategies have several advantages over traditional systemic drug delivery including avoiding systemic drug exposure as well as using a lower amount of drugs [88]. Until now, some drug release orthopedic implants based on Mg alloys have been reported containing antibiotics, e.g. antimicrobial peptide [89, 90], gentamicin [91], or gentamicin sulfate [92]. Magnesium alloy implants commonly suffer from an easy infection related to implantation along with the high rate of degradation. Dong et al [89] fabricated a surface drug delivery system based on Mg/Epoxy resin-ZnO/Polycaprolactone (PCL)-Ibuprofen using a dip coating method followed by spraying. It was suggested that the composite coating could be a promising alternative for biodegradable Mg-based drug delivery and implant applications.

5. Synthesis methods of composites containing Mg and Zn

5.1. Electrospinning method

In order to fabricate composite with well chemical composition and controlled morphology, many advanced methods have been employed. Meanwhile, electrospinning is considered the simplest and most adaptable technique. The fabrication of composites can easily be prepared via the electrospinning technique; however, the only restriction is that the second phase should be well dispersed or soluble in the primary solu-

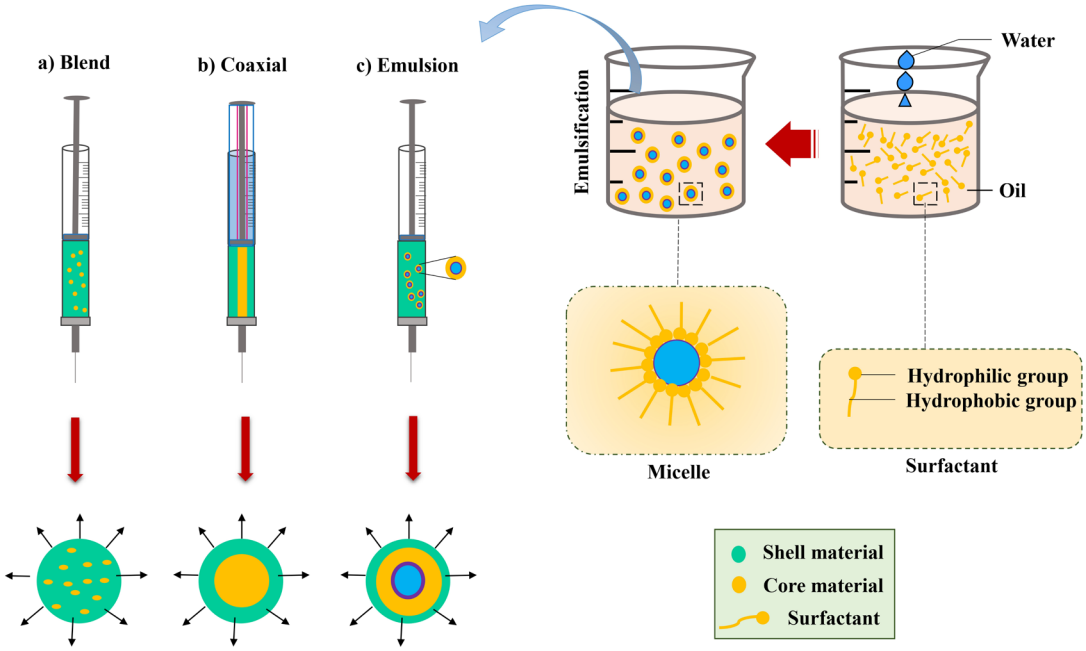

Fig. 1. Schematic illustration of composites containing bioactive agents by (a) blend, (b) coaxial, and (c) emulsion electrospinning.

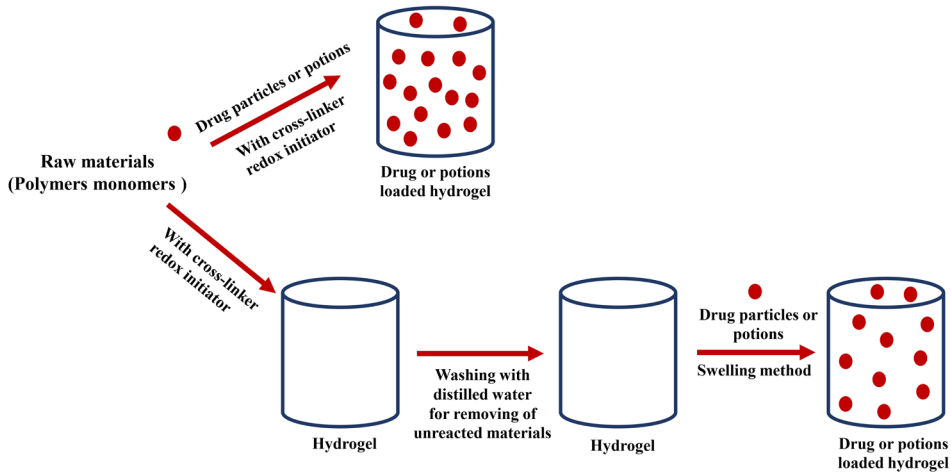

Fig. 2. Free-radical polymerization technique for the nanostructured hydrogel preparation.

tion. This technique has been developed approximately for a century and can be considered as sub-branches of the electrospray process [93-95]. During the electrospinning process, the elongation of the liquid drop occurs by increasing the electric field. A conical shape of the liquid drop is created by achieving a balance between the induced charge distribution on the drop surface and the liquid surface tension. The process is shown schematically in Fig. 1.

In the case of electrospinning, the fundamental setup is easily controlled and very simple. Mainly, it consists of an electrically conductive collector (an aluminum foil or silicon part), a high-voltage power supply, and a spinneret, however, all of these segments are not essential [96]. Therefore, to produce fibers instead of droplets, a number of processing parameters must be optimized actually e.g. fibers, droplets, or a beaded structure that depends on the different processing parameters, such as distance between collector and source [97].

5.2. Solvothermal technique

Another synthesis method for the composites is the solvothermal technique. The general procedure is similar to the hydrothermal technique, but organic solvents are utilized instead of water in the solvothermal method [98-100][96]. Through this technique, a transformation or chemical reaction occurs under supercritical temperature and pressure in an organic solvent such as toluene [101], 1, 4 butanol [102], and methanol [103]. To make the final material crystallized, it is required to perform a subsequent thermal treatment [104].

5.3. Co-precipitation method

A commonly used technique for the fabrication of layered double hydroxides (LDHs) and similar materials for drug delivery applications is co-precipitation [105-107]. For all co-precipitation variations, similar materials are required for initiation. The starting materials are composed of similar starting materials: 1) a divalent cation soluble source for the formation of the layers; 2) a trivalent cation soluble source for the formation of the layers; 3) a soluble ionic compound such as sodium nitrate and sodium carbonate as a source of interlayer anions; 4) a strong base including sodium hydroxide, urea, ammonia, and potassium hydroxide to cause LDH precipitation [105, 108, 109].

5.4. Sol-gel method

The sol-gel technique is an extensively used method to synthesize highly pure and homogeny products [93, 110, 111]. Depending on the homogeneity degree of the gel, two types of the sol-gel method are known: monophasic and diphasic. In case metal ions are dispersed at the atomic level, it is called a monophasic gel, while in diphasic one, the homogeneity scale is in the range of 1-100 nm [112]. The hybrid gel is a combination of monophasic and diphasic gels [113, 114]. The final material properties are determined by the rate of hydrolysis and condensation in the sol-gel process, which is dependent on different factors. These factors include starting materials, inorganic and organic additive addition, pH, water content, etc. [114, 115]. Recent developments in the sol-gel process have made it possible to embed organic compounds as well as other modified inorganic oxides in SiO2 and also to control the release of these compounds from the matrix into the medium [116, 117]. Despite the remarkable advantages of these sol-gel carrier systems, they are not widely known for drug delivery applications. The sol-gel method is facile and versatile; the starting materials are inexpensive, inert, stable to heat and light, and benign for the environment or humans [118-121].

5.5. Water-in-oil-in-water (w/o/w) double emulsion method

According to Sahoo et al. [122] and Jaraswekin et al. [123], the most popular method for the preparation of poly(lactic-co-glycolic acid) (PLGA) microparticles (MP) or microsphere (MS) is the solvent evaporation method. In this technique, elevated temperatures or agents for inducing phase separation are not needed, and sterile microcapsules can also be produced by scaling up microencapsulation (ME) [124, 125]. Based on the drug state in the polymer solution and the dispersion medium, the emulsion method is categorized into oil-in-water (o/w), water-in-oil (w/o), and water-in-oil-in-water (w/o/w) double emulsion methods [126, 127]. Among the methods used for MS preparation, the w/o/w solvent evaporation is the most commonly practiced technique [128]. In order to provide the controlled drug release, degradation protection of the drugs, and alleviating adverse effects of the drugs in the body, pharmaceutical industries extensively use w/o/w by evaporation removal of the emulsion solvent technique [129, 130]. In this method, to internalize the active ingredient efficiently, the stability of the primary emulsion is considered to be a critical factor [131]. Low encapsulation efficiency is the result of unstable primary emulsion [132, 133].

5.6. Microemulsion method

The microemulsion method is employed for the preparation of high-T_c oxide of $YBa_2Cu_3O_7$, nanocrystalline Al_2O_3, TiO_2, Fe_2O_3, colloidal metals, colloidal AgCl, and colloidal Fe_3O_4 [134, 135]. Microemulsions consist of at least three components including a surfactant, a nonpolar phase (usually oil), and a polar phase (usually water). Microemulsions are thermodynamically stable solutions, isotropic, and macroscopically homogeneous. The polar and the non-polar regions are separated by an interfacial film formed by the surfactant molecules [136]. This method shows some significant advantages such as thermodynamic stability,

nanoparticle monodispersity, large interfacial area, and ultralow interfacial tension [137, 138]. Microemulsion has attracted attention in the preparation of nanoparticles mainly due to the versatility of microemulsion systems like the very small droplet size production, cost-effectiveness [139-141], simple procedure, and mild reaction conditions [142, 143].

5.7. Free radical polymerization method

In bioprinting, free radical polymerization is frequently utilized for the creation of cross-linked hydrogels [144]. Through using thermal or photo-initiator or redox reaction, polymerization of a polymer consisting of vinyl groups occurs leading to the formation of a hydrogel. This method is not a suitable technique for the fabrication of end-functional polymers. On the other hand, the situation has changed by the emergence of living radical polymerization, so that the production of end-functional polymers is also possible using this technique. Free radical polymerization is employed to synthesize composites containing polymers, metal, and metal oxide used in the drug delivery systems [145]. The processing steps are presented in Fig. 2.

5.8. Microwave radiation method

As a result of several rewarding properties of microwave stimulation including controllable operability, deep tissue penetration, and good thermal efficiency, it is being increasingly used in numerous smart drug delivery investigations [146]. Microwave is composed of both magnetic and electrical components with high-frequency radiation in the range of 300 MHz-300 GHz [147]. By the use of the electromagnetic and/or heating elements of the microwave, drug delivery systems can be processed and modified. The introduction of microwave radiation can be carried out directly onto the pre-formed products and/or upon the dosage form preparation. Furthermore, the microwave can be used in the excipients processing before using them in the drug formulation in delivery systems [148].

Qiu et al. [149] designed a microwave-sensitive drug microcarrier based on Fe_3O_4@ZnO@mGd_2O_3: Eu nanoparticles using poly [(N-isopropyl acrylamide)-co-(methacrylic acid)] as the microwave stimulus gate-keeper. By using a short-time high-frequency microwave device, it is possible to avoid the bulk heating, therefore, the construction of drug delivery systems based on MSN responsive to microwave radiation is feasible [150]. Shi et al. [146] fabricated NPs for drug delivery based on a doped ZnO@Fe_3O_4 core surrounded by a mesoporous silica shell. The silica shell was used due to its large pore volume and good biocompatibility, while the core exhibited high-performance microwave absorbance.

5.9. In-situ gelling procedure

The in-situ gel forming polymeric systems have been extensively studied as carriers for sustained drug delivery. Before administration in the body, these vehicles are in the form of sol or suspension and after administration, they undergo in-situ gelation [151-153]. In the formulation of these systems, a gelling agent is used to form a stable suspension/sol system containing dispersed drugs and other excipients. Due to the pH change in the gastric environment, the gelation of the sol/suspension system is triggered. The adopted formulation is a sodium alginate solution or gellan gum containing sodium citrate and calcium chloride, in which the free calcium ions turn into complexes and released only in the stomach acidic environment. Sodium alginate/gellan gum acts as a gelling agent producing textures in the final product, which can be in the form of hard, brittle, non-elastic gels of fluid gels [153-155]. Ca ions entrapped in sodium alginate or gellan gum polymeric chains enable polymer chains crosslinking to form matrix structure. In the gelation process, double-helical junction domains are first formed, then, these domains are re-aggregated forming a three-dimensional network by hydrogen bonding with water and complexing with cations [156, 157]. Some advances in the field of in-situ gelling include: overcoming the problem of poor conventional ophthalmic solution bioavailability by using gel drops that are instilled into eyes; increasing drug contact time at the maximum absorption site; reducing systemic drug absorption through the nasolacrimal duct and the resulting side effects; reducing the frequency of administration, and drug delivery with narrow windows of absorption in the small intestinal zone. Gastro-retentive drug delivery systems are beneficial for drugs that are absorbed through the stomach such as ferrous salts and also for the ones that are used for local treatment in the stomach and peptic ulcer disease treatment (e.g. antacids) [158-160].

6. Drug delivery mechanisms of composites containing Mg and Zn

There are slightly different ways for the definition of the term "release mechanism". It has been used for describing the process that determines the rate of release and also for describing the procedure through which drug molecules are released or transported. A number of processes or mechanisms have been demonstrated to be rate-controlling in drug release [161]. In recent years, the development of novel approaches for designing new controlled-release drug delivery systems has been at the center of attention [162]. The traditional drug delivery system works in a way that causes a rapid increase in the drug dosage in the blood following by a drop in the dosage [163, 164]. Drug plasma levels are described as under level and overhead, which are inefficient and toxic, respectively [165]. In an ideal drug delivery system, a suitable drug concentration should be transmitted to targeting sites while keeping other tissues safe [166, 167].The following two formulas (Eq. 1and Eq. 2) are used for the calculation of the levels of loaded and released drug [166]:

$$Drug\ loading\ of\ carrier\ (wt\%) = \frac{the\ amount\ of\ drug\ (g)}{the\ amount\ of\ nanohybride\ and\ drug\ (g)} * 100$$

$$\text{OR} \quad \%Drug\ loading = \frac{weight\ of\ drug\ in\ a\ sample}{weight\ of\ sample\ taken} * 100 \qquad (1)$$

$$\%Drug\ release = \frac{the\ amount\ of\ released\ drug\ (g)}{the\ amount\ of\ loaded\ drug\ (g)} * 100 \qquad (2)$$

The efficiency of drug encapsulation can be determined according to Eq.(3) [168]:

$$Encapsulation\ efficiency(\%) = \frac{Initial\ drug\ weight - Drug\ weight\ in\ supernatan}{Initial\ drug\ weight} * 100 \qquad (3)$$

The drug release of nanocomposite has been studied in the literature using mathematical models [169]. Eq.4 can determine the sample liquid uptake:

$$M_s = Kt^n \qquad (4)$$

where, K and n are constants. By using the mechanism of drug release, the following power law equation is obtained:

$$M_t/M_\infty = Kt^n \qquad (5)$$

where, the drug released fraction at time t and equilibrium is represented by M_t and M_∞, respectively. The characteristic of the drug and the samples determines the value of K and the diffusion exponent of n is used for the characterization of the drug release mechanism. The values of 'k' and 'n' are obtained by calculating the intercept and slope of the plot between M_t/M_∞ [170].

Das et al. [171] designed a colon-specific drug carrier based on Zn/pectin/chitosan composite microparticles. By studying the drug release,

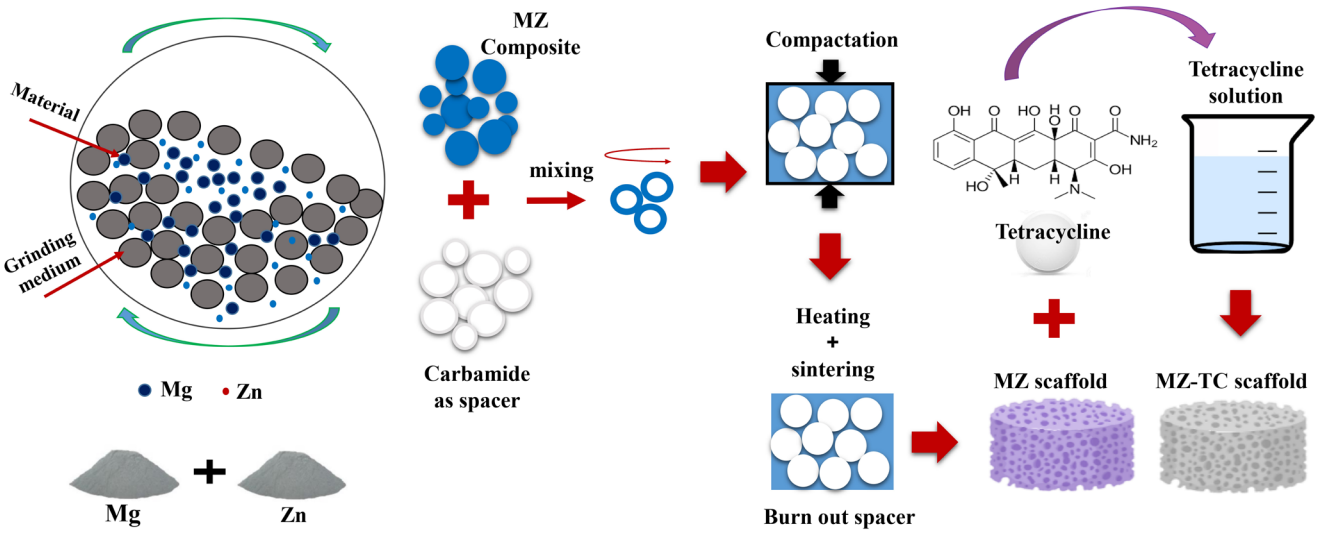

Fig. 3. Hydrogel beads containing ZnO NPs for the drug delivery application.

the formulation was optimized. The drug release pattern was shown to be significantly affected by formulation parameters. It was reported that the specific content of the colon-specific drug could be loaded without hampering its behavior. Results showed high encapsulation efficiency and stability of the drug in the formulation during storage time. Furthermore, *in vivo* drug release was observed from the optimized composite particle formulation in rats. Company et al. [172] developed a novel composite of zinc oxide nanoparticles and citric acid-based polyester elastomer (POC–ZnO). Results indicated that the original concentration of NPs in the composites affected the ZnO release kinetics for 15 days. Among all composites, POC–ZnO 5% was reported to have the zero-order release kinetics.

7. The state-of-the-art of composites containing Zn and Mg in drug delivery

Dodero et al. [173] used an electrospinning technique to embed ZnO nanoparticles within alginate-based nanofibrous membranes. In order to combine ZnO nanoparticle with the polymer through electrospinning, it is preferred to use medium-molecular-mass alginates with a low mannuronic and guluronic acid residues (M/G) ratio or low-molecular-mass alginates with a high M/G ratio. Composite scaffolds based on ZnO-polyetherimide (ZnO/PEI) with antibacterial activity were also developed by the electrospinning process [174]. The effectiveness of the developed scaffolds was reported by positive responses against gram-negative (*Escherichia coli*) bacteria as well as gram-positive (*Staphylococcus aureus*).

Javanbakht et al. [166] developed a novel drug delivery bio-nanocomposite based on carboxymethylcellulose (CMC)/zinc MOF/graphene oxide via the solvothermal method. It was reported that the prepared bio-nanocomposite could be used for anticancer drug delivery. Bhattacharjee et al. [175] successfully incorporated ZnO into Fe (III) trimesate metal-organic framework (MIL-100(Fe)) to deliver anticancer drugs of doxorubicin hydrochloride (DOX) by the one-pot in-situ method. The investigation rendered interesting insights into the incorporation of NPs into MIL-100(Fe) and its drug loading capacity as well as release rates. Kura et al. [176] loaded L-3-(3,4-dihydroxyphenyl) alanine as an anti-parkinsonian drug in a novel layered organic-inorganic nanocomposite based on Al-layered double hydroxide (LDH)/Zn via a direct co-precipitation technique. Sustained-release behavior was observed in these composites suggesting that they are suitable for controlled-release formulations. In comparison with pure levodopa, the synthesized nanocomposite showed enhanced cell viability of 3T3 cells after 72 h of exposure.

Seyfoori et al. [177] fabricated a robust nanostructure composite of $ZnFe_2O_4$ and $ZnFe_2O_4$-hydroxyapatite using the co-precipitation method for multiple applications of cancer treatment, bone filler, and drug delivery.

Nigam et al. [178] reported a successful synthesis of $Zn_xMg_{(1-x)}Fe_2O_4$ nanoparticles using the sol-gel method with the potential to be used for drug delivery. SiO_2–CaO mesoporous bioactive glass nanoparticles doped with Zn^{2+} ions were produced by Neščáková et al. [179] using the microemulsion assisted sol-gel method. It was reported that the nanoparticles have the potential for being used as drug delivery systems as well as bioactive fillers for various applications such as wound healing and bone regeneration. Thangaraj et al [180] synthesized superparamagnetic Ce_4−$xSr_{1+x}Fe_{5-x}ZnxO_{14+\delta}$ (x=0-0.45) nanocomposites by the nitrate-citrate sol-gel route for different applications such as drug delivery, sensor, dielectric, conductivity studies, and optical properties. Pathania et al. [181] studied the drug release kinetics of chitosan-*g*-poly(acrylamide)/Zn (CPA-Zn) nanocomposite synthesized by microwave radiations. The nature of the matrix and the pH of the medium were shown to affect the drug release behavior.

Zn-clinoptilolite/GO nanocomposite was introduced by Khatamian et al [182] for the preparation of drug delivery systems with high loading capacity. The reflux method and microwave-assisted hydrothermal method were used for the fabrication of the nanocomposites. As a cancer drug, the nanocomposite exhibited slow release for DOX, high loading capacity, and cytocompatibility. Nanocomposite hydrogel scaffolds based on chitosan-gelatin/ZnO with both drug delivery and inherent antibacterial properties were prepared using an in-situ method. The prepared scaffolds demonstrated high porosity and no agglomeration in the chitosan-gelatin matrix. Additionally, the nanocomposite scaffolds exhibited improved antibacterial, biodegradation, swelling properties, as well as a controlled release for naproxen [183]. Yadollahi et al [184] synthesized nanocomposite hydrogel beads of chitosan/ZnO by the in-situ generation of zinc oxide nanoparticles upon the chitosan bead formation. According to the results, the drug release from the chitosan beads was prolonged by the addition of ZnO nanoparticles. This was reported to be due to a longer drug migration path from the beads to the

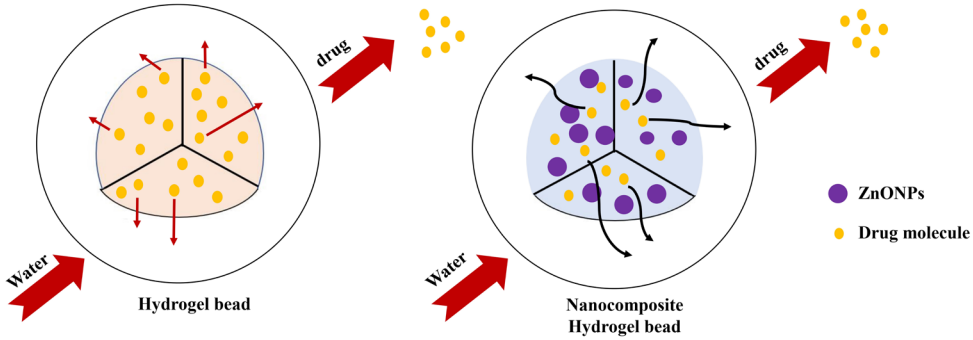

Fig. 4. Preparation of composite scaffolds by the space holder technique.

media. The nanocomposites showed promising behavior for developing controlled delivery of drugs. The drug release behavior of hydrogel beads containing ZnO particles is demonstrated in Fig. 3.

Yang et al [185] assembled flower-mesoporous carbon (FPCS)-magnetic Fe_3O_4 and pH-sensitive ZnO nanoparticles to construct the FPCS-Fe_3O_4-ZnO composite as microwave and pH bi-triggered drug carrier. Yang et al. [186] incorporated Mg particles into poly (l-lactic acid) (PLLA) microspheres to suppress inflammatory response induced by PLLA and regulate the drug release profile. It was shown that the internal connectivity of the microspheres was altered during hydrolytic degradation by changing the Mg particle sizes and contents, resulting in manipulating drug delivery with tunable release patterns. Foroughi et al. [168] developed a novel synthesis method (one-step modified reverse microemulsion) for the preparation of HAp-$MgFe_2O_4$ nanocomposite for the drug delivery application. It was demonstrated that the drug delivery rate of the nanocomposite was influenced by calcination temperature and textural properties.

In a study by Cheddadi et al. [187], the free radical polymerization method was used to synthesize poly (magnesium acrylate) hydrogel for drug delivery applications. They were suggested for oral drug delivery devices due to prospective drug release properties along with simplicity and low cost. In the work performed by Rijal et al. [188], the electrospinning technique was utilized to synthesize Mg incorporated polycaprolactone/low molecular weight chitosan (PCL/LMW-CS) composite nanofiber. They showed that the obtained nanofibrous were good candidates for applications in tissue engineering such as bone regeneration, wound healing, regenerative medicine, and drug delivery. Rijal et al. [189] used the electrospinning method to prepare composite nanofibers of MgO, chitosan (CS), and poly(ε-caprolactone) (PCL). They realized that the obtained new composite nanofibrous membranes were able to mimic the function and physical structure of the tissue extracellular matrix (ECM). This, in turn, suggested that they can be potentially used for various tissue engineering applications e.g. DDSs.

In another study, Mohammad et al. [190] prepared a composite of ethyl cellulose-magnesium hydrogen phosphate (EC-MgHPO4) via the sol-gel technique. Their results proved that the composite could be used in the fields of drug delivery, biosensor, bioanalytical, and scaffolding applications. Foroughi et al. [191] used a one-step reverse microemulsion method to synthesize nanoporous HAp-$MgFe_2O_4$ nanocomposite. They found that calcining the nanocomposite at 700 °C results in a core-shell structure with MS of ~9.5 emu/g. In addition, considering the IBU release behavior of all samples, the drug delivery rate of the nanocomposite could be altered by calcination temperature that in turn may change the textural properties of samples.

Bakhsheshi-Rad and his colleagues [45] synthesized composite scaffolds of Mg-Ca-TiO_2 (MCT). They loaded different concentrations of doxycycline (DC) in the scaffolds and used the space holder technique as a cost-effective, feasible, and novel method to have an appropriate corrosion rate, a network of interconnected pores, and appropriate compressive strength. A schematic presentation of this technique is shown in Fig. 4. Considering the drug release profiles, they found that DC loading MCT scaffolds showed sustained and burst drug release and by increasing the concentration of DC, the drug release rate was increased.

Tabia et al. [192] fabricated the Mg-doped bioactive glass nanoparticles (BG-NPs) through the sol-gel route. They loaded amoxicillin to the synthesized BG-NPs and investigated their drug release behavior. They concluded that by increasing Mg content the loading efficiency decreased. However, the release kinetics was increased by increasing magnesium content. They realized that the specific surface area and porosity were responsible for this advancement.

8. Conclusions and future insights

In this review, the drug delivery composite systems containing Mg and Zn either matrix or reinforcement are summarized. Both Zn and Mg have been applied in various areas of DDSs due to their amazing intrinsic properties i.e. biocompatible and biodegradable as well as being abundantly available. This has made them remarkably advantageous over their conventional counterparts. Besides, the synthesis methods of these excellent composites are also reviewed and their mechanism of drug release is discussed. It should be noted that studying the drug delivery properties of zinc/magnesium and their composites might lead to the realization of more effective drug delivery systems in the future.

Acknowledgments

The listed authors are highly obliged to their institutes and universities for the literature access services.

REFERENCES

[1] G. Tiwari, R. Tiwari, B. Sriwastawa, L. Bhati, S. Pandey, P. Pandey, S.K. Bannerjee, Drug delivery systems: An updated review, International journal of pharmaceutical investigation 2(1) (2012) 2.

[2] Z. Goudarzi, A. Ijadi, A. Bakhtiari, S. Eskandarinezhad, N. Azizabadi, M.A. Jazi, Sr-doped bioactive glasses for biological applications, Journal of Composites and Compounds 2(3) (2020) 105-109.

[3] X. Zhang, M. Cresswell, Inorganic controlled release technology, Inorg. Control. Release Technol. (2016).

[4] J.-H. Kang, M.-H. Chun, M.-S. Cho, Y.-B. Kwon, J.-C. Choi, D.-W. Kim, C.-W. Park, E.-S. Park, Preparation and characterization of metformin hydrochloride controlled-release tablet using fatty acid coated granules, Drug Development and Industrial Pharmacy 46(5) (2020) 852-860.

[5] C.J. Grande, F.G. Torres, C.M. Gomez, M.C. Bañó, Nanocomposites of bacterial cellulose/hydroxyapatite for biomedical applications, Acta Biomaterialia 5(5) (2009) 1605-1615.

[6] J.P. Jose, S. Thomas, J. Kuruvilla, S. Malhotra, K. Goda, M.S. Sreekala, Advances in polymer composites: macro-and microcomposites—state of the art, new challenges, and opportunities, Polymer Composites; Wiley: Weinheim, Germany 1 (2012) 3-16.

[7] H. Ullah, F. Wahid, H.A. Santos, T. Khan, Advances in biomedical and pharmaceutical applications of functional bacterial cellulose-based nanocomposites,

Carbohydrate polymers 150 (2016) 330-352.
[8] F. Sharifianjazi, A.H. Pakseresht, M.S. Asl, A. Esmaeilkhanian, H.W. Jang, M. Shokouhimehr, Hydroxyapatite consolidated by zirconia: applications for dental implant, Journal of Composites and Compounds 2(1) (2020) 26-34.
[9] L. Bazli, B. Eftekhari Yekta, A. Khavandi, Preparation and Characterization of Sn-Containing Glasses for Brachytherapy Applications, Transactions of the Indian Ceramic Society 76(4) (2017) 242-246.
[10] Y. Kameshima, H. Sasaki, T. Isobe, A. Nakajima, K. Okada, Synthesis of composites of sodium oleate/Mg–Al-ascorbic acid-layered double hydroxides for drug delivery applications, International journal of pharmaceutics 381(1) (2009) 34-39.
[11] M. Abniki, A. Moghimi, F. Azizinejad, Fabrication of bionanocomposite based on LDH using biopolymer of gum arabic and chitosan-coating for sustained drug-release, Journal of the Serbian Chemical Society 85(5) (2020).
[12] M. Abniki, A. Moghimi, F. Azizinejad, Synthesis of calcium-layered double hydroxide based nanohybrid for controlled release of an anti-inflammatory drug, Journal of the Chinese Chemical Society (2020).
[13] W.-H. Lu, K.-D. Li, C.-H. Lu, L.G. Teoh, W.H. Wu, Y.C. Shen, Synthesis and characterization of mesoporous SiO_2–CaO–P_2O_5 bioactive glass by sol–gel process, Materials transactions 54(5) (2013) 791-795.
[14] J. Andersson, S. Areva, B. Spliethoff, M. Lindén, Sol–gel synthesis of a multifunctional, hierarchically porous silica/apatite composite, Biomaterials 26(34) (2005) 6827-6835.
[15] S.P. Hudson, R.F. Padera, R. Langer, D.S. Kohane, The biocompatibility of mesoporous silicates, Biomaterials 29(30) (2008) 4045-4055.
[16] X. Li, X. Wang, H. Chen, P. Jiang, X. Dong, J. Shi, Hierarchically porous bioactive glass scaffolds synthesized with a PUF and P123 cotemplated approach, Chemistry of Materials 19(17) (2007) 4322-4326.
[17] A. López-Noriega, D. Arcos, I. Izquierdo-Barba, Y. Sakamoto, O. Terasaki, M. Vallet-Regí, Ordered mesoporous bioactive glasses for bone tissue regeneration, Chemistry of Materials 18(13) (2006) 3137-3144.
[18] X. Yan, X. Huang, C. Yu, H. Deng, Y. Wang, Z. Zhang, S. Qiao, G. Lu, D. Zhao, The in-vitro bioactivity of mesoporous bioactive glasses, Biomaterials 27(18) (2006) 3396-3403.
[19] X. Yan, C. Yu, X. Zhou, J. Tang, D. Zhao, Highly ordered mesoporous bioactive glasses with superior in vitro bone-forming bioactivities, Angewandte Chemie International Edition 43(44) (2004) 5980-5984.
[20] M. Vašák, D.W. Hasler, Metallothioneins: new functional and structural insights, Current opinion in chemical biology 4(2) (2000) 177-183.
[21] M.F. Heragh, S. Eskandarinezhad, A. Dehghan, Ni-Cu matrix composite reinforced with CNTs: preparation, characterization, wear and corrosion behavior, inhibitory effects, Journal of Composites and Compounds 2(4) (2020) 123-128.
[22] C.T. Chasapis, A.C. Loutsidou, C.A. Spiliopoulou, M.E. Stefanidou, Zinc and human health: an update, Archives of toxicology 86(4) (2012) 521-534.
[23] E. Alhava, H. Olkkonen, J. Puittinen, V. Nokso-Koivisto, Zinc content of human cancellous bone, Acta Orthopaedica Scandinavica 48(1) (1977) 1-4.
[24] H. Kim, S. Mondal, S. Bharathiraja, P. Manivasagan, M.S. Moorthy, J. Oh, Optimized Zn-doped hydroxyapatite/doxorubicin bioceramics system for efficient drug delivery and tissue engineering application, Ceramics International 44(6) (2018) 6062-6071.
[25] Y. Su, I. Cockerill, Y. Wang, Y.-X. Qin, L. Chang, Y. Zheng, D. Zhu, Zinc-based biomaterials for regeneration and therapy, Trends in biotechnology 37(4) (2019) 428-441.
[26] Z. Gao, D. Zhang, X. Li, S. Jiang, Q. Zhang, Current status, opportunities and challenges in chemical conversion coatings for zinc, Colloids and Surfaces A: Physicochemical and Engineering Aspects 546 (2018) 221-236.
[27] S. Parveen, R. Misra, S.K. Sahoo, Nanoparticles: a boon to drug delivery, therapeutics, diagnostics and imaging, Nanomedicine: Nanotechnology, Biology and Medicine 8(2) (2012) 147-166.
[28] H.M. Xiong, ZnO nanoparticles applied to bioimaging and drug delivery, Advanced Materials 25(37) (2013) 5329-5335.
[29] Z.Y. Zhang, Y.D. Xu, Y.Y. Ma, L.L. Qiu, Y. Wang, J.L. Kong, H.M. Xiong, Biodegradable ZnO@ polymer core–shell nanocarriers: pH-triggered release of doxorubicin in vitro, Angewandte Chemie 125(15) (2013) 4221-4225.
[30] G. Song, Control of biodegradation of biocompatable magnesium alloys, Corrosion science 49(4) (2007) 1696-1701.
[31] A.H. Shahbaz, M. Esmaeilian, R. NasrAzadani, K. Gavanji, The effect of MgF_2 addition on the mechanical properties of hydroxyapatite synthesized via powder metallurgy, Journal of Composites and Compounds 1(1) (2019) 18-24.
[32] S. Nasibi, K. Alimohammadi, L. Bazli, S. Eskandarinezhad, A. Mohammadi, N. Sheysi, TZNT alloy for surgical implant applications: A systematic review, Journal of Composites and Compounds 2(3) (2020) 62-68.
[33] R. Erbel, C. Di Mario, J. Bartunek, J. Bonnier, B. de Bruyne, F.R. Eberli, P. Erne, M. Haude, B. Heublein, M. Horrigan, Temporary scaffolding of coronary arteries with bioabsorbable magnesium stents: a prospective, non-randomised multicentre trial, The Lancet 369(9576) (2007) 1869-1875.
[34] M. Haude, R. Erbel, P. Erne, S. Verheye, H. Degen, D. Böse, P. Vermeersch, I. Wijnbergen, N. Weissman, F. Prati, Safety and performance of the drug-eluting absorbable metal scaffold (DREAMS) in patients with de-novo coronary lesions: 12 month results of the prospective, multicentre, first-in-man BIOSOLVE-I trial, The Lancet 381(9869) (2013) 836-844.
[35] M. Haude, H. Ince, A. Abizaid, R. Toelg, P.A. Lemos, C. von Birgelen, E.H. Christiansen, W. Wijns, F.-J. Neumann, C. Kaiser, Safety and performance of the second-generation drug-eluting absorbable metal scaffold in patients with de-novo coronary artery lesions (BIOSOLVE-II): 6 month results of a prospective, multicentre, non-randomised, first-in-man trial, The Lancet 387(10013) (2016) 31-39.
[36] B. Heublein, R. Rohde, V. Kaese, M. Niemeyer, W. Hartung, A. Haverich, Biocorrosion of magnesium alloys: a new principle in cardiovascular implant technology?, Heart 89(6) (2003) 651-656.
[37] H. Li, H. Zhong, K. Xu, K. Yang, J. Liu, B. Zhang, F. Zheng, Y. Xia, L. Tan, D. Hong, Enhanced efficacy of sirolimus-eluting bioabsorbable magnesium alloy stents in the prevention of restenosis, Journal of Endovascular Therapy 18(3) (2011) 407-415.
[38] R. Waksman, R. Erbel, C. Di Mario, J. Bartunek, B. de Bruyne, F.R. Eberli, P. Erne, M. Haude, M. Horrigan, C. Ilsley, Early-and long-term intravascular ultrasound and angiographic findings after bioabsorbable magnesium stent implantation in human coronary arteries, JACC: Cardiovascular Interventions 2(4) (2009) 312-320.
[39] R. Waksman, R. Pakala, P.K. Kuchulakanti, R. Baffour, D. Hellinga, R. Seabron, F.O. Tio, E. Wittchow, S. Hartwig, C. Harder, Safety and efficacy of bioabsorbable magnesium alloy stents in porcine coronary arteries, Catheterization and Cardiovascular Interventions 68(4) (2006) 607-617.
[40] E. Wittchow, N. Adden, J. Riedmüller, C. Savard, R. Waksman, M. Braune, Bioresorbable drug-eluting magnesium-alloy scaffold: design and feasibility in a porcine coronary model, EuroIntervention 8(12) (2013) 1441-1450.
[41] P. Zartner, R. Cesnjevar, H. Singer, M. Weyand, First successful implantation of a biodegradable metal stent into the left pulmonary artery of a preterm baby, Catheterization and Cardiovascular Interventions 66(4) (2005) 590-594.
[42] M. Haude, H. Ince, A. Abizaid, R. Toelg, P.A. Lemos, C. von Birgelen, E.H. Christiansen, W. Wijns, F.-J. Neumann, C. Kaiser, Sustained safety and performance of the second-generation drug-eluting absorbable metal scaffold in patients with de novo coronary lesions: 12-month clinical results and angiographic findings of the BIOSOLVE-II first-in-man trial, European heart journal 37(35) (2016) 2701-2709.
[43] M. Diba, O.-M. Goudouri, F. Tapia, A.R. Boccaccini, Magnesium-containing bioactive polycrystalline silicate-based ceramics and glass-ceramics for biomedical applications, Current opinion in solid state and materials science 18(3) (2014) 147-167.
[44] Y. Bi, Y. Zheng, Y. Li, Microstructure and mechanical properties of sintered porous magnesium using polymethyl methacrylate as the space holder, Materials Letters 161 (2015) 583-586.
[45] H. Bakhsheshi-Rad, E. Hamzah, M.P. Staiger, G.J. Dias, Z. Hadisi, M. Saheban, M. Kashefian, Drug release, cytocompatibility, bioactivity, and antibacterial activity of doxycycline loaded Mg-Ca-TiO_2 composite scaffold, Materials & Design 139 (2018) 212-221.
[46] K.K. Jain, Drug delivery systems-an overview, Drug delivery systems, Springer2008, pp. 1-50.
[47] M. Arefian, M. Hojjati, I. Tajzad, A. Mokhtarzade, M. Mazhar, A. Jamavari, A review of Polyvinyl alcohol/Carboxiy methyl cellulose (PVA/CMC) composites for various applications, Journal of Composites and Compounds 2(3) (2020) 69-76.
[48] P. Abasian, M. Radmansouri, M.H. Jouybari, M.V. Ghasemi, A. Mohammadi, M. Irani, F.S. Jazi, Incorporation of magnetic NaX zeolite/DOX into the PLA/chitosan nanofibers for sustained release of doxorubicin against carcinoma cells death in vitro, International journal of biological macromolecules 121 (2019) 398-406.
[49] H. Derendorf, L.J. Lesko, P. Chaikin, W.A. Colburn, P. Lee, R. Miller, R. Powell, G. Rhodes, D. Stanski, J. Venitz, Pharmacokinetic/pharmacodynamic modeling in drug research and development, The Journal of Clinical Pharmacology 40(12) (2000) 1399-1418.
[50] S. Gopi, A. Amalraj, N.P. Sukumaran, J.T. Haponiuk, S. Thomas, Biopolymers and their composites for drug delivery: a brief review, Macromolecular Symposia, Wiley Online Library, 2018, p. 1800114.
[51] G.R. Matzke, G.R. Aronoff, A.J. Atkinson Jr, W.M. Bennett, B.S. Decker, K.-U. Eckardt, T. Golper, D.W. Grabe, B. Kasiske, F. Keller, Drug dosing consideration in patients with acute and chronic kidney disease—a clinical update from

Kidney Disease: Improving Global Outcomes (KDIGO), Kidney international 80(11) (2011) 1122-1137.
[52] M.J. Munoz-Davila, Role of old antibiotics in the era of antibiotic resistance. Highlighted nitrofurantoin for the treatment of lower urinary tract infections, Antibiotics 3(1) (2014) 39-48.
[53] J.J. De Waele, S. Carrette, M. Carlier, V. Stove, J. Boelens, G. Claeys, I. Leroux-Roels, E. Hoste, P. Depuydt, J. Decruyenaere, Therapeutic drug monitoring-based dose optimisation of piperacillin and meropenem: a randomised controlled trial, Intensive care medicine 40(3) (2014) 380-387.
[54] S.K. Bardal, J.E. Waechter, D.S. Martin, Applied pharmacology, Elsevier Health Sciences2011.
[55] W. Brand, M.E. Schutte, G. Williamson, J.J. van Zanden, N.H. Cnubben, J.P. Groten, P.J. van Bladeren, I.M. Rietjens, Flavonoid-mediated inhibition of intestinal ABC transporters may affect the oral bioavailability of drugs, food-borne toxic compounds and bioactive ingredients, Biomedicine & pharmacotherapy 60(9) (2006) 508-519.
[56] A.H. Chow, H.H. Tong, P. Chattopadhyay, B.Y. Shekunov, Particle engineering for pulmonary drug delivery, Pharmaceutical research 24(3) (2007) 411-437.
[57] S. Amirhossein, A.-B. Aydin, Z. Habib, Polaroid-PET: a PET scanner with detectors fitted with polaroids for filtering unpolarized optical photons: a Monte Carlo simulation study, Physics in Medicine & Biology (2020).
[58] A. Sanaat, H. Zaidi, Depth of interaction estimation in a preclinical PET scanner equipped with monolithic crystals coupled to SiPMs using a deep neural network, Applied Sciences 10(14) (2020) 4753.
[59] A. Sanaat, H. Arabi, M.R. Ay, H. Zaidi, Novel preclinical PET geometrical concept using a monolithic scintillator crystal offering concurrent enhancement in spatial resolution and detection sensitivity: a simulation study, Physics in Medicine & Biology 65(4) (2020) 045013.
[60] A. Sanaat, H. Arabi, I. Mainta, V. Garibotto, H. Zaidi, Projection-space implementation of deep learning-guided low-dose brain PET imaging improves performance over implementation in image-space, Journal of Nuclear Medicine (2020) jnumed. 119.239327.
[61] N. Kamaly, B. Yameen, J. Wu, O.C. Farokhzad, Degradable controlled-release polymers and polymeric nanoparticles: mechanisms of controlling drug release, Chemical reviews 116(4) (2016) 2602-2663.
[62] J. Daraei, Production and characterization of PCL (Polycaprolactone) coated TCP/nanoBG composite scaffolds by sponge foam method for orthopedic applications, Journal of Composites and Compounds 2(1) (2020) 45-50.
[63] X. Huang, S. Wu, X. Ke, X. Li, X. Du, Phosphonated pillar [5] arene-valved mesoporous silica drug delivery systems, ACS Applied Materials & Interfaces 9(23) (2017) 19638-19645.
[64] N.G. Kotla, B. Chandrasekar, P. Rooney, G. Sivaraman, A. Larrañaga, K.V. Krishna, A. Pandit, Y. Rochev, Biomimetic lipid-based nanosystems for enhanced dermal delivery of drugs and bioactive agents, ACS Biomaterials Science & Engineering 3(7) (2017) 1262-1272.
[65] A. Kazemzadeh, H. Kazemzadeh, Determination of Hg^{2+} by Diphenylcarbazone Compound in Polymer Film, Journal of Composites and Compounds 1(1) (2019) 30-35.
[66] A. Nouri, B. Faraji Dizaji, N. Kianinejad, A. Jafari Rad, S. Rahimi, M. Irani, F. Sharifian Jazi, Simultaneous linear release of folic acid and doxorubicin from ethyl cellulose/chitosan/g-C_3N_4/MoS_2 core-shell nanofibers and its anticancer properties, Journal of Biomedical Materials Research Part A (2020).
[67] D. Liu, F. Yang, F. Xiong, N. Gu, The smart drug delivery system and its clinical potential, Theranostics 6(9) (2016) 1306.
[68] Z. Wang, Y. Duan, Y. Duan, Application of polydopamine in tumor targeted drug delivery system and its drug release behavior, Journal of Controlled Release 290 (2018) 56-74.
[69] J. Ma, N. Zhao, D. Zhu, Endothelial cellular responses to biodegradable metal zinc, ACS biomaterials science & engineering 1(11) (2015) 1174-1182.
[70] F.S. Jazi, N. Parvin, M. Rabiei, M. Tahriri, Z.M. Shabestari, A.R. Azadmehr, Effect of the synthesis route on the grain size and morphology of ZnO/Ag nanocomposite, Journal of Ceramic Processing Research 13(5) (2012) 523-526.
[71] J. Jiang, J. Pi, J. Cai, The advancing of zinc oxide nanoparticles for biomedical applications, Bioinorganic chemistry and applications 2018 (2018).
[72] Z. Zeng, X. Fang, W. Miao, Y. Liu, T. Maiyalagan, S. Mao, Electrochemically Sensing of Trichloroacetic Acid with Iron(II) Phthalocyanine and Zn-Based Metal Organic Framework Nanocomposites, ACS Sensors 4(7) (2019) 1934-1941.
[73] W. Liu, Y. Pan, W. Xiao, H. Xu, D. Liu, F. Ren, X. Peng, J. Liu, Recent developments on zinc (ii) metal–organic framework nanocarriers for physiological pH-responsive drug delivery, MedChemComm 10(12) (2019) 2038-2051.
[74] K. Dong, Y. Zhang, L. Zhang, Z. Wang, J. Ren, X. Qu, Facile preparation of metal− organic frameworks-based hydrophobic anticancer drug delivery nanoplatform for targeted and enhanced cancer treatment, Talanta 194 (2019) 703-708.
[75] M. Zamani, M. Rostami, M. Aghajanzadeh, H. Kheiri Manjili, K. Rostamizadeh, H. Danafar, Mesoporous titanium dioxide@ zinc oxide–graphene oxide nanocarriers for colon-specific drug delivery, Journal of Materials Science 53(3) (2018) 1634-1645.
[76] J.W. Rasmussen, E. Martinez, P. Louka, D.G. Wingett, Zinc oxide nanoparticles for selective destruction of tumor cells and potential for drug delivery applications, Expert opinion on drug delivery 7(9) (2010) 1063-1077.
[77] V. Karpina, V. Lazorenko, C. Lashkarev, V. Dobrowolski, L. Kopylova, V. Baturin, S. Pustovoytov, A.J. Karpenko, S. Eremin, P. Lytvyn, Zinc oxide–analogue of GaN with new perspective possibilities, Crystal Research and Technology: Journal of Experimental and Industrial Crystallography 39(11) (2004) 980-992.
[78] X. Huang, X. Zheng, Z. Xu, C. Yi, Zno-based nanocarriers for drug delivery application: From passive to smart strategies, International journal of pharmaceutics 534(1-2) (2017) 190-194.
[79] A.J. Rad, Synthesis of copper oxide nanoparticles on activated carbon for pollutant removal in Tartrazine structure, Journal of Composites and Compounds 2(3) (2020) 99-104.
[80] A. Moghanian, A. Ghorbanoghli, M. Kazem-Rostami, A. Pazhouheshgar, E. Salari, M. Saghafi Yazdi, T. Alimardani, H. Jahani, F. Sharifian Jazi, M. Tahriri, Novel antibacterial Cu/Mg-substituted 58S-bioglass: Synthesis, characterization and investigation of in vitro bioactivity, International Journal of Applied Glass Science 11(4) (2020) 685-698.
[81] F. Sharifianjazi, M. Moradi, A. Abouchenari, A.H. Pakseresht, A. Esmaeilkhanian, M. Shokouhimehr, M.S. Asl, Effects of Sr and Mg dopants on biological and mechanical properties of SiO_2–CaO–P_2O_5 bioactive glass, Ceramics International (2020).
[82] S. Ni, L. Chou, J. Chang, Preparation and characterization of forsterite (Mg_2SiO_4) bioceramics, Ceramics International 33(1) (2007) 83-88.
[83] N. Sezer, Z. Evis, S.M. Kayhan, A. Tahmasebifar, M. Koç, Review of magnesium-based biomaterials and their applications, Journal of Magnesium and Alloys 6(1) (2018) 23-43.
[84] A. Bordbar-Khiabani, B. Yarmand, M. Mozafari, Emerging magnesium-based biomaterials for orthopedic implantation, Thomas Telford Ltd, 2019.
[85] Z. Wu, T. Tang, H. Guo, S. Tang, Y. Niu, J. Zhang, W. Zhang, R. Ma, J. Su, C. Liu, In vitro degradability, bioactivity and cell responses to mesoporous magnesium silicate for the induction of bone regeneration, Colloids and Surfaces B: Biointerfaces 120 (2014) 38-46.
[86] A. Bigham, S.A. Hassanzadeh-Tabrizi, M. Rafienia, H. Salehi, Ordered mesoporous magnesium silicate with uniform nanochannels as a drug delivery system: The effect of calcination temperature on drug delivery rate, Ceramics International 42(15) (2016) 17185-17191.
[87] M. Vallet-Regi, Bio-ceramics with clinical applications, John Wiley & Sons2014.
[88] P. Wu, D.W. Grainger, Drug/device combinations for local drug therapies and infection prophylaxis, Biomaterials 27(11) (2006) 2450-2467.
[89] H. Dong, Q. Li, C. Tan, N. Bai, P. Cai, Bi-directional controlled release of ibuprofen and Mg^{2+} from magnesium alloys coated by multifunctional composite, Materials Science and Engineering: C 68 (2016) 512-518.
[90] J. Tian, S. Shen, C. Zhou, X. Dang, Y. Jiao, L. Li, S. Ding, H. Li, Investigation of the antimicrobial activity and biocompatibility of magnesium alloy coated with HA and antimicrobial peptide, Journal of Materials Science: Materials in Medicine 26(2) (2015) 66.
[91] J. Zhang, Z. Wen, M. Zhao, G. Li, C. Dai, Effect of the addition CNTs on performance of CaP/chitosan/coating deposited on magnesium alloy by electrophoretic deposition, Materials Science and Engineering: C 58 (2016) 992-1000.
[92] A. Morawska-Chochół, P. Domalik-Pyzik, J. Chłopek, B. Szaraniec, J. Sterna, M. Rzewuska, M. Boguń, R. Kucharski, P. Mielczarek, Gentamicin release from biodegradable poly-l-lactide based composites for novel intramedullary nails, Materials Science and Engineering: C 45 (2014) 15-20.
[93] A. Kazemzadeh, M.A. Meshkat, H. Kazemzadeh, M. Moradi, R. Bahrami, R. Pouriamanesh, Preparation of graphene nanolayers through surfactant-assisted pure shear milling method, Journal of Composites and Compounds 1(1) (2019) 25-30.
[94] W.E. Teo, S. Ramakrishna, A review on electrospinning design and nanofibre assemblies, Nanotechnology 17(14) (2006) R89.
[95] L.A. Mercante, V.P. Scagion, F.L. Migliorini, L.H. Mattoso, D.S. Correa, Electrospinning-based (bio) sensors for food and agricultural applications: A review, TrAC Trends in Analytical Chemistry 91 (2017) 91-103.
[96] M. Jiménez, C. Abradelo, J. San Román, L. Rojo, Bibliographic review on the state of the art of strontium and zinc based regenerative therapies. Recent developments and clinical applications, Journal of materials chemistry B 7(12) (2019)

1974-1985.
[97] T.J. Sill, H.A. Von Recum, Electrospinning: applications in drug delivery and tissue engineering, Biomaterials 29(13) (2008) 1989-2006.
[98] Y. Qian, Solvothermal Synthesis of Nanocrystalline III–V Semiconductors, Advanced Materials 11(13) (1999) 1101-1102.
[99] C. Wang, Z.-X. Deng, Y. Li, The synthesis of nanocrystalline anatase and rutile titania in mixed organic media, Inorganic Chemistry 40(20) (2001) 5210-5214.
[100] K. Kaviyarasu, E. Manikandan, P. Paulraj, S. Mohamed, J. Kennedy, One dimensional well-aligned CdO nanocrystal by solvothermal method, Journal of alloys and compounds 593 (2014) 67-70.
[101] C.-S. Kim, B.K. Moon, J.-H. Park, S. Tae Chung, S.-M. Son, Synthesis of nanocrystalline TiO_2 in toluene by a solvothermal route, Journal of Crystal Growth 254(3) (2003) 405-410.
[102] M. Kang, Synthesis of Fe/TiO_2 photocatalyst with nanometer size by solvothermal method and the effect of H_2O addition on structural stability and photodecomposition of methanol, Journal of Molecular Catalysis A: Chemical 197(1) (2003) 173-183.
[103] S. Yin, Y. Fujishiro, J. Wu, M. Aki, T. Sato, Synthesis and photocatalytic properties of fibrous titania by solvothermal reactions, Journal of Materials Processing Technology 137(1-3) (2003) 45-48.
[104] S.M. Gupta, M. Tripathi, A review on the synthesis of TiO_2 nanoparticles by solution route, Central European Journal of Chemistry 10(2) (2012) 279-294.
[105] F.L. Theiss, G.A. Ayoko, R.L. Frost, Synthesis of layered double hydroxides containing Mg^{2+}, Zn^{2+}, Ca^{2+} and Al^{3+} layer cations by co-precipitation methods—A review, Applied Surface Science 383 (2016) 200-213.
[106] M. Bukhtiyarova, A review on effect of synthesis conditions on the formation of layered double hydroxides, Journal of Solid State Chemistry 269 (2019) 494-506.
[107] V. Solovov, N. Nikolenko, V. Kovalenko, V. Kotok, A. Burkov, D. Kondrat'ev, O. Chernova, S. Zhukovin, Synthesis of Ni (II)-Ti (IV) layered double hydroxides using coprecipitation at high supersaturation method, ARPN Journal of Engineering and Applied Sciences 13(24) (2018) 9652-9656.
[108] X. Duan, D.G. Evans, Layered double hydroxides, Springer Science & Business Media2006.
[109] H.W. Olfs, L.O. Torres-Dorante, R. Eckelt, H. Kosslick, Comparison of different synthesis routes for Mg–Al layered double hydroxides (LDH): Characterization of the structural phases and anion exchange properties, Applied Clay Science 43(3) (2009) 459-464.
[110] L. Bazli, M. Siavashi, A. Shiravi, A review of carbon nanotube/TiO_2 composite prepared via sol-gel method, Journal of Composites and Compounds 1(1) (2019) 1-9.
[111] A. Bakhtiari, A. Cheshmi, M. Naeimi, S.M. Fathabad, M. Aliasghari, A.M. Chahardehi, S. Hassani, V. Elhami, Synthesis and characterization of the novel 80S bioactive glass: bioactivity, biocompatibility, cytotoxicity, Journal of Composites and Compounds 2(4) (2020) 110-114.
[112] L. Armelao, D. Barreca, M. Bertapelle, G. Bottaro, C. Sada, E. Tondello, A sol–gel approach to nanophasic copper oxide thin films, Thin Solid Films 442(1) (2003) 48-52.
[113] F.S. Jazi, N. Parvin, M. Tahriri, M. Alizadeh, S. Abedini, M. Alizadeh, The relationship between the synthesis and morphology of SnO_2-Ag_2O nanocomposite, Synthesis and Reactivity in Inorganic, Metal-Organic, and Nano-Metal Chemistry 44(5) (2014) 759-764.
[114] M. Alizadeh, F. Sharifianjazi, E. Haghshenasjazi, M. Aghakhani, L. Rajabi, Production of nanosized boron oxide powder by high-energy ball milling, Synthesis and Reactivity in Inorganic, Metal-Organic, and Nano-Metal Chemistry 45(1) (2015) 11-14.
[115] L.S. Cividanes, T.M. Campos, L.A. Rodrigues, D.D. Brunelli, G.P. Thim, Review of mullite synthesis routes by sol–gel method, Journal of Sol-Gel Science and Technology 55(1) (2010) 111-125.
[116] M. Gonçalves, Sol-gel silica nanoparticles in medicine: A natural choice. Design, synthesis and products, Molecules 23(8) (2018) 2021.
[117] S. Devaraju, K. Krishnadevi, E. Naveena, M. Alagar, Eco-friendly fully bio-based polybenzoxazine-silica hybrid materials by sol–gel approach, Polymer Bulletin (2020) 1-10.
[118] H. Böttcher, P. Slowik, W. Süß, Sol-gel carrier systems for controlled drug delivery, Journal of sol-gel science and technology 13(1-3) (1998) 277-281.
[119] M. Catauro, E. Tranquillo, F. Barrino, I. Blanco, F. Dal Poggetto, D. Naviglio, Drug release of hybrid materials containing Fe (II) citrate synthesized by sol-gel technique, Materials 11(11) (2018) 2270.
[120] Y. Ding, W. Li, A. Correia, Y. Yang, K. Zheng, D. Liu, D.W. Schubert, A.R. Boccaccini, H.A. Santos, J.A. Roether, Electrospun polyhydroxybutyrate/poly (ε-caprolactone)/Sol–gel-derived silica hybrid scaffolds with drug releasing function for bone tissue engineering applications, ACS applied materials & interfaces 10(17) (2018) 14540-14548.
[121] M. Catauro, F. Barrino, G. Dal Poggetto, M. Milazzo, I. Blanco, S.V. Ciprioti, Structure, drug absorption, bioactive and antibacterial properties of sol-gel SiO_2/ZrO_2 materials, Ceramics International (2020).
[122] S.K. Sahoo, S. Barik, G. Dehury, S. Dhala, S. Kanungo, B.B. Barik, K.K. Puhan, Evaluation of controlled release theophylline microspheres prepared with cellulose acetate using solvent evaporation method, Tropical Journal of Pharmaceutical Research 10(2) (2011).
[123] S. Jaraswekin, S. Prakongpan, R. Bodmeier, Effect of poly (lactide-co-glycolide) molecular weight on the release of dexamethasone sodium phosphate from microparticles, Journal of microencapsulation 24(2) (2007) 117-128.
[124] S. Freitas, H.P. Merkle, B. Gander, Microencapsulation by solvent extraction/evaporation: reviewing the state of the art of microsphere preparation process technology, Journal of Controlled Release 102(2) (2005) 313-332.
[125] J. Emami, H. Hamishehkar, A.R. Najafabadi, K. Gilani, M. Minaiyan, H. Mahdavi, A. Nokhodchi, A Novel Approach to Prepare Insulin-Loaded Poly (Lactic-Co-Glycolic Acid) Microcapsules and the Protein Stability Study, Journal of Pharmaceutical Sciences 98(5) (2009) 1712-1731.
[126] M.L. Manca, Chitosan and PLGA microspheres as drug delivery system against pulmonary mycobacteria infections, (2007).
[127] M. Hoppel, D. Mahrhauser, C. Stallinger, F. Wagner, M. Wirth, C. Valenta, Natural polymer-stabilized multiple water-in-oil-in-water emulsions: a novel dermal drug delivery system for 5-fluorouracil, Journal of Pharmacy and Pharmacology 66(5) (2014) 658-667.
[128] H. Yang, Y. Hao, Q. Liu, Z. Mi, Z. Wang, L. Zhu, Q. Feng, N. Hu, Preparation and in vitro study of hydrochloric norvancomycin encapsulated poly (d, l-lactide-co-glycolide, PLGA) microspheres for potential use in osteomyelitis, Artificial cells, nanomedicine, and biotechnology 45(7) (2017) 1326-1330.
[129] M. Li, O. Rouaud, D. Poncelet, Microencapsulation by solvent evaporation: State of the art for process engineering approaches, International Journal of Pharmaceutics 363(1) (2008) 26-39.
[130] W.M. Obeidat, Recent patents review in microencapsulation of pharmaceuticals using the emulsion solvent removal methods, Recent patents on drug delivery & formulation 3(3) (2009) 178-192.
[131] Y. Maa, C. Hsu, Effect of primary emulsions on microsphere size and protein-loading in the double emulsion process, Journal of microencapsulation 14(2) (1997) 225-241.
[132] D. Noviendri, Microencapsulation of Fucoxanthin by Water-in-Oil-in-Water (W/O/W) Double Emulsion Solvent Evaporation Method: A Review, Squalen Bulletin of Marine and Fisheries Postharvest and Biotechnology 9(3) (2014).
[133] Y.-Y. Yang, T.-S. Chung, N.P. Ng, Morphology, drug distribution, and in vitro release profiles of biodegradable polymeric microspheres containing protein fabricated by double-emulsion solvent extraction/evaporation method, Biomaterials 22(3) (2001) 231-241.
[134] R. Zhang, L. Gao, Preparation of nanosized titania by hydrolysis of alkoxide titanium in micelles, Materials research bulletin 37(9) (2002) 1659-1666.
[135] A.S. Narang, D. Delmarre, D. Gao, Stable drug encapsulation in micelles and microemulsions, International journal of pharmaceutics 345(1-2) (2007) 9-25.
[136] M.A. Malik, M.Y. Wani, M.A. Hashim, Microemulsion method: A novel route to synthesize organic and inorganic nanomaterials: 1st Nano Update, Arabian Journal of Chemistry 5(4) (2012) 397-417.
[137] S.F. Chin, A. Azman, S.C. Pang, Size Controlled Synthesis of Starch Nanoparticles by a Microemulsion Method, Journal of Nanomaterials 2014 (2014) 763736.
[138] H. Liu, J. Mei, Y. Xu, L. Tang, D. Chen, Y. Zhu, S. Huang, T.J. Webster, H. Ding, Improving The Oral Absorption Of Nintedanib By A Self-Microemulsion Drug Delivery System: Preparation And In Vitro/In Vivo Evaluation, International Journal of Nanomedicine 14 (2019) 8739.
[139] M.B. de Jesus, A. Radaic, I.S. Zuhorn, E. de Paula, Microemulsion extrusion technique: a new method to produce lipid nanoparticles, Journal of nanoparticle research 15(10) (2013) 1960.
[140] S.P. Callender, J.A. Mathews, K. Kobernyk, S.D. Wettig, Microemulsion utility in pharmaceuticals: Implications for multi-drug delivery, International journal of pharmaceutics 526(1-2) (2017) 425-442.
[141] B. Yan, Y. Gu, J. Zhao, Y. Liu, L. Wang, Y. Wang, Self-microemulsion Technology for Water-insoluble Drug Delivery, Current Nanoscience 15(6) (2019) 576-588.
[142] S.M. Dizaj, F. Lotfipour, M. Barzegar-Jalali, M.-H. Zarrintan, K. Adibkia, Physicochemical characterization and antimicrobial evaluation of gentamicin-loaded $CaCO_3$ nanoparticles prepared via microemulsion method, Journal of Drug Delivery Science and Technology 35 (2016) 16-23.

[143] M.N. Kelchen, N.K. Brogden, In vitro skin retention and drug permeation through intact and microneedle pretreated skin after application of propranolol loaded microemulsions, Pharmaceutical research 35(12) (2018) 228.
[144] L. Huang, J. Wu, M. Liu, L. Mao, H. Huang, Q. Wan, Y. Dai, Y. Wen, X. Zhang, Y. Wei, Direct surface grafting of mesoporous silica nanoparticles with phospholipid choline-containing copolymers through chain transfer free radical polymerization and their controlled drug delivery, Journal of colloid and interface science 508 (2017) 396-404.
[145] L.J. Min, T.Y.S. Edgar, Z. Zicheng, Y.W. Yee, Chapter 6 - Biomaterials for Bioprinting, in: L.G. Zhang, J.P. Fisher, K.W. Leong (Eds.), 3D Bioprinting and Nanotechnology in Tissue Engineering and Regenerative Medicine, Academic Press2015, pp. 129-148.
[146] Z. Shi, C. Yang, R. Li, L. Ruan, Microwave thermal-triggered drug delivery using thermosensitive peptide-coated core–shell mesoporous silica nanoparticles, Journal of Materials Science 55(14) (2020) 6118-6129.
[147] R.E. Mardziah, T.W. Wong, Effects of microwave on drug-release responses of spray-dried alginate microspheres, Drug development and industrial pharmacy 36(10) (2010) 1149-1167.
[148] T. Wong, Use of microwave in processing of drug delivery systems, Current Drug Delivery 5(2) (2008) 77-84.
[149] H. Qiu, B. Cui, W. Zhao, P. Chen, H. Peng, Y. Wang, A novel microwave stimulus remote controlled anticancer drug release system based on Fe_3O_4@ZnO@ mGd_2O_3: Eu@P(NIPAm-co-MAA) multifunctional nanocarriers, Journal of Materials Chemistry B 3(34) (2015) 6919-6927.
[150] J. Xu, X. Cheng, L. Tan, C. Fu, M. Ahmed, J. Tian, J. Dou, Q. Zhou, X. Ren, Q. Wu, Microwave responsive nanoplatform via P-selectin mediated drug delivery for treatment of hepatocellular carcinoma with distant metastasis, Nano letters 19(5) (2019) 2914-2927.
[151] S. Miyazaki, H. Aoyama, N. Kawasaki, W. Kubo, D. Attwood, In situ-gelling gellan formulations as vehicles for oral drug delivery, Journal of Controlled release 60(2-3) (1999) 287-295.
[152] Y. Wu, Y. Liu, X. Li, D. Kebebe, B. Zhang, J. Ren, J. Lu, J. Li, S. Du, Z. Liu, Research progress of in-situ gelling ophthalmic drug delivery system, Asian Journal of Pharmaceutical Sciences 14(1) (2019) 1-15.
[153] M. Agrawal, S. Saraf, S. Saraf, S.K. Dubey, A. Puri, U. Gupta, P. Kesharwani, V. Ravichandiran, P. Kumar, V. Naidu, Stimuli-responsive In situ gelling system for nose-to-brain drug delivery, Journal of Controlled Release (2020).
[154] K. Itoh, T. Hirayama, A. Takahashi, W. Kubo, S. Miyazaki, M. Dairaku, M. Togashi, R. Mikami, D. Attwood, In situ gelling pectin formulations for oral drug delivery at high gastric pH, International journal of pharmaceutics 335(1-2) (2007) 90-96.
[155] T.N. Nimi, D.R. Manohar, An Overview on In-Situ Nasal Gel for Drug Delivery, Journal of Pharmaceutical Sciences and Research 11(7) (2019) 2585-2589.
[156] S. Desai, S. Bolton, A floating controlled-release drug delivery system: in vitro-in vivo evaluation, Pharmaceutical research 10(9) (1993) 1321-1325.
[157] Z. Shi, X. Chen, L. Zhang, S. Ding, X. Wang, Q. Lei, W. Fang, FA-PEG decorated MOF nanoparticles as a targeted drug delivery system for controlled release of an autophagy inhibitor, Biomaterials science 6(10) (2018) 2582-2590.
[158] K. Neha, H.S. Nirmala, Insitu gelling system: A Review, J Drug Del and Therapeutics 4(4) (2014) 93-103.
[159] P. Suradkar, R. Mishra, T. Nandgude, Overview on Trends in Development of Gastroretentive Drug Delivery System, Research Journal of Pharmacy and Technology 12(11) (2019) 5633-5640.
[160] D. Bhowmik, R. Bhanot, D. Gautam, P. Rai, K. Kumar, Gastro Retentive Drug Delivery Systems-a Novel Approaches of Controlled Drug Delivery Systems, Research Journal of Science and Technology 10(2) (2018) 145-156.
[161] S. Fredenberg, M. Wahlgren, M. Reslow, A. Axelsson, The mechanisms of drug release in poly (lactic-co-glycolic acid)-based drug delivery systems—a review, International journal of pharmaceutics 415(1-2) (2011) 34-52.
[162] J. Panyam, V. Labhasetwar, Biodegradable nanoparticles for drug and gene delivery to cells and tissue, Advanced drug delivery reviews 55(3) (2003) 329-347.
[163] Y. Ma, J.C. Pacan, Q. Wang, Y. Xu, X. Huang, A. Korenevsky, P.M. Sabour, Microencapsulation of bacteriophage Felix O1 into chitosan-alginate microspheres for oral delivery, Applied and environmental microbiology 74(15) (2008) 4799-4805.
[164] J. Trygg, E. Yildir, R. Kolakovic, N. Sandler, P. Fardim, Anionic cellulose beads for drug encapsulation and release, Cellulose 21(3) (2014) 1945-1955.
[165] H. Bao, Y. Pan, Y. Ping, N.G. Sahoo, T. Wu, L. Li, J. Li, L.H. Gan, Chitosan-functionalized graphene oxide as a nanocarrier for drug and gene delivery, Small 7(11) (2011) 1569-1578.
[166] S. Javanbakht, M. Pooresmaeil, H. Namazi, Green one-pot synthesis of carboxymethylcellulose/Zn-based metal-organic framework/graphene oxide bio-nanocomposite as a nanocarrier for drug delivery system, Carbohydrate Polymers 208 (2019) 294-301.
[167] H.H.P. Duong, L.-Y.L. Yung, Synergistic co-delivery of doxorubicin and paclitaxel using multi-functional micelles for cancer treatment, International journal of pharmaceutics 454(1) (2013) 486-495.
[168] F. Foroughi, S.A. Hassanzadeh-Tabrizi, A. Bigham, In situ microemulsion synthesis of hydroxyapatite-$MgFe_2O_4$ nanocomposite as a magnetic drug delivery system, Materials Science and Engineering: C 68 (2016) 774-779.
[169] K. Drlica, Biology of bacterial deoxyribonucleic acid topoisomerases, Microbiological reviews 48(4) (1984) 273.
[170] D. Pathania, D. Gupta, N. Kothiyal, G. Eldesoky, M. Naushad, Preparation of a novel chitosan-g-poly (acrylamide)/Zn nanocomposite hydrogel and its applications for controlled drug delivery of ofloxacin, International journal of biological macromolecules 84 (2016) 340-348.
[171] S. Das, A. Chaudhury, K.Y. Ng, Preparation and evaluation of zinc-pectin-chitosan composite particles for drug delivery to the colon: role of chitosan in modifying in vitro and in vivo drug release, Int J Pharm 406(1-2) (2011) 11-20.
[172] K. Kompany, E.H. Mirza, S. Hosseini, B. Pingguan-Murphy, I. Djordjevic, Polyoctanediol citrate–ZnO composite films: Preparation, characterization and release kinetics of nanoparticles from polymer matrix, Materials Letters 126 (2014) 165-168.
[173] A. Dodero, M. Alloisio, S. Vicini, M. Castellano, Preparation of composite alginate-based electrospun membranes loaded with ZnO nanoparticles, Carbohydrate polymers 227 (2020) 115371.
[174] W. Artifon, S.M. Pasini, A. Valério, S.Y.G. González, S.M.d.A.G. Ulson, A.A.U. de Souza, Harsh environment resistant-antibacterial zinc oxide/Polyetherimide electrospun composite scaffolds, Materials Science and Engineering: C 103 (2019) 109859.
[175] A. Bhattacharjee, M.K. Purkait, S. Gumma, Loading and release of doxorubicin hydrochloride from Iron (III) trimesate MOF and zinc oxide nanoparticle composites, Dalton Transactions (2020).
[176] A.U. Kura, S.H.H. Al Ali, M.Z. Hussein, S. Fakurazi, P. Arulselvan, Development of a controlled-release anti-parkinsonian nanodelivery system using levodopa as the active agent, International Journal of Nanomedicine 8 (2013) 1103.
[177] A. Seyfoori, S.A.S. Ebrahimi, S. Omidian, S.M. Naghib, Multifunctional magnetic $ZnFe_2O_4$-hydroxyapatite nanocomposite particles for local anti-cancer drug delivery and bacterial infection inhibition: An in vitro study, Journal of the Taiwan Institute of Chemical Engineers 96 (2019) 503-508.
[178] A. Nigam, S.J. Pawar, Structural, magnetic, and antimicrobial properties of zinc doped magnesium ferrite for drug delivery applications, Ceramics International 46(4) (2020) 4058-4064.
[179] Z. Neščáková, K. Zheng, L. Liverani, Q. Nawaz, D. Galusková, H. Kaňková, M. Michálek, D. Galusek, A.R. Boccaccini, Multifunctional zinc ion doped sol – gel derived mesoporous bioactive glass nanoparticles for biomedical applications, Bioactive Materials 4 (2019) 312-321.
[180] V. Thangaraj, M. Yogapriya, K. Thirumalai, M. Swaminathan, A. Sundaramurthy, R. Nandhakumar, S. Suresh, E. Vakees, A. Araichimani, Sol–Gel Synthesis of $Ce_{4-x}Sr_{1+x}Fe_{5-x}Zn_xO_{14+\delta}$ [$0 \leq x \leq 0.45$] Superparamagnetic Oxide Systems and Its Magnetic, Dielectric, and Drug Delivery Properties, ACS omega 3(12) (2018) 16509-16518.
[181] D. Pathania, D. Gupta, N.C. Kothiyal, G. sharma, G.E. Eldesoky, M. Naushad, Preparation of a novel chitosan-g-poly(acrylamide)/Zn nanocomposite hydrogel and its applications for controlled drug delivery of ofloxacin, International Journal of Biological Macromolecules 84 (2016) 340-348.
[182] M. Khatamian, B. Divband, F. Farahmand-Zahed, Synthesis and characterization of Zinc (II)-loaded Zeolite/Graphene oxide nanocomposite as a new drug carrier, Materials Science and Engineering: C 66 (2016) 251-258.
[183] R. Rakhshaei, H. Namazi, H. Hamishehkar, H.S. Kafil, R. Salehi, In situ synthesized chitosan–gelatin/ZnO nanocomposite scaffold with drug delivery properties: Higher antibacterial and lower cytotoxicity effects, Journal of Applied Polymer Science 136(22) (2019) 47590.
[184] M. Yadollahi, S. Farhoudian, S. Barkhordari, I. Gholamali, H. Farhadnejad, H. Motasadizadeh, Facile synthesis of chitosan/ZnO bio-nanocomposite hydrogel beads as drug delivery systems, International journal of biological macromolecules 82 (2016) 273-278.
[185] Z. Yang, L. Wang, Y. Liu, S. Liu, D. Tang, L. Meng, B. Cui, ZnO capped flower-like porous carbon-Fe_3O_4 composite as carrier for bi-triggered drug delivery, Materials Science and Engineering: C 107 (2020) 110256.
[186] F. Yang, X. Niu, X. Gu, C. Xu, W. Wang, Y. Fan, Biodegradable Magnesium-Incorporated Poly(l-lactic acid) Microspheres for Manipulation of Drug Release and Alleviation of Inflammatory Response, ACS Applied Materials & Interfaces 11(26) (2019) 23546-23557.

[187] M. Cheddadi, E. López-Cabarcos, K. Slowing, E. Barcia, A. Fernández-Carballido, Cytotoxicity and biocompatibility evaluation of a poly(magnesium acrylate) hydrogel synthesized for drug delivery, International Journal of Pharmaceutics 413(1) (2011) 126-133.
[188] N.P. Rijal, U. Adhikari, N. Bhattarai, Magnesium Incorporated Polycaprolactone-Based Composite Nanofibers, ASME 2015 International Mechanical Engineering Congress and Exposition, 2015.
[189] N.P. Rijal, U. Adhikari, S. Khanal, D. Pai, J. Sankar, N. Bhattarai, Magnesium oxide-poly(ε-caprolactone)-chitosan-based composite nanofiber for tissue engineering applications, Materials Science and Engineering: B 228 (2018) 18-27.
[190] F. Mohammad, T. Arfin, H.A. Al-Lohedan, Sustained drug release and electrochemical performance of ethyl cellulose-magnesium hydrogen phosphate composite, Materials Science and Engineering: C 71 (2017) 735-743.
[191] F. Foroughi, S. Hassanzadeh-Tabrizi, A. Bigham, In situ microemulsion synthesis of hydroxyapatite-$MgFe_2O_4$ nanocomposite as a magnetic drug delivery system, Materials Science and Engineering: C 68 (2016) 774-779.
[192] Z. Tabia, K. El Mabrouk, M. Bricha, K. Nouneh, Mesoporous bioactive glass nanoparticles doped with magnesium: drug delivery and acellular in vitro bioactivity, RSC advances 9(22) (2019) 12232-12246.

Journal of Composites and Compounds 2 (2020) 205-214

Available online at www.jourcc.com

Journal homepage: www.JOURCC.com

Journal of Composites and Compounds

Recent progress in materials used towards corrosion protection of Mg and its alloys

Hadi Ghazanfari[a] , Saber Hasanizadeh[b], Sara Eskandarinezhad[c], Soheil Hassani[d], Mohsen Sheibani[e], Alireza Dordsheikh Torkamani[f], Belma Fakić[g]*

[a] *Department of Mining, Metallurgical and Materials Engineering, Université Laval, Québec G1V 0A6, QC, Canada*
[b] *Chemical Engineering Department, Kermanshah University of Technology, Kermanshah, Iran*
[c] *Department of Mining and Metallurgy, Yazd University, Yazd, Iran*
[d] *Department of Materials Engineering, Science and Research Branch, Islamic Azad University, Tehran, Iran*
[e] *Department of Materials Engineering and Metallurgy, Shiraz Branch, Islamic Azad University, Shiraz, Iran*
[f] *School of Metallurgy and Materials Engineering, Iran University of Science and Technology (IUST), Tehran, Iran*
[g] *Metallographic laboratory, Institute "Kemal Kapetanović" in Zenica, University of Zenica, B and H*

A B S T R A C T

Magnesium has little resistance to corrosion and therefore its production and use are quite limited. The problem of corrosion associated with these alloys has been alleviated to some extent by the advantages obtained from fine coatings. An additional dense barrier against corrosion is created, using coatings obtained from sol-gel. As an alternative for Cr-based conversion coatings, rare-earth elements-based ones are been increasingly investigated for Mg and its alloys due to being eco-friendly. Because of chemical inertness, low friction, and high hardness, diamond-like carbon (DLC) coatings have exhibited the best protection for Mg and its alloys. In this review, we shed light on recent advancements in novel coatings for Mg alloys including hybrid, rare-earth conversion, composite polymeric (polymer composite is a multi-phase material in which reinforcing fillers are integrated with a polymer matrix), and DLC coatings.

Peer review under responsibility of jourcc

A R T I C L E I N F O R M A T I O N

Article history:
Received 7 November 2020
Received in revised form 27 December 2020
Accepted 21 December 2020

Keywords:
Hybrid coatings
Rare-earth
Polymeric composite
DLC coatings

Table of contents

1. Introduction

The earth's 8th most abundant element is Mg, which makes up about 0.13% of the mass of oceans and 1.93% of the mass of the earth's crust. Owing to some favorable advantages of Mg, it is considered a promising metal for various applications. Mg has a high value of strength to weight ratio, which is 1/4 of that of iron and 2/3 of that of aluminum. Other properties of Mg include good dimensional stability, acceptable machinability, great thermal conductivity, good electromagnetic shielding, high damping characteristics, as well as recyclability. Because of these characteristics, Mg is used in different applications such as computer and automobile parts, household equipment, handheld tools, sporting goods, mobile phones, and aerospace components. Inherent biocompati-

* *Corresponding author: Hadi Ghazanfari; E-mail: hadi.ghazanfari.1@ulaval.ca*
https://doi.org/10.29252/jcc.2.4.5

bility and low weight of Mg made it also a suitable material for implant applications [1-4].

However, extensive use of Mg in many applications is hindered because of several undesirable features including high chemical reactivity, weak corrosion resistance, weak creep resistance, as well as poor resistance to wear. The poor corrosion resistance is the main challenge limiting the use of Mg [5, 6]. Coating the base metal is considered an effective solution for the prevention of corrosion [7, 8]. The protection of the substrate is provided by the barrier formed between the metallic substrate and the surrounding environment and/or through some chemicals that act as corrosion inhibitors [9, 10]. The coating properties for rendering satisfying corrosion protection include uniformity, good adherence, being pore-free, and having self-healing ability for the occurrence of physical damage is possible [1].

The development of sol-gel coatings based on organic-inorganic hybrids with a low thickness in the range of 0.2-10 μm has been an appealing method for alleviating corrosion problems [11, 12]. Sol-gel coatings enhance the adherence of the organic paint system to the metal surface; therefore, they create additional dense barriers for corrosive substances. Another practiced coating is rare-earth conversion coating. This process is known for its simple electrolytic substances that usually contain chloride, sulfate, and nitrate of rare-earth metals such as neodymium, lanthanum, and cerium. Because of the simple electrolyte, its maintenance and recycling are easy. Another important issue is that these coatings are eco-friendly surface treatments [13-15].

Recently, composite polymer coatings and their performance in the corrosion protection of Mg have attracted the attention of many researchers. The good corrosion resistance of super-dispersed polytetrafluoroethylene (SPTFE) [16-18], a composite of diethylenetriamine, polyetherimide, and hydroxyapatite [19], and composites graphene oxide (GO)-containing 4-ethylene dioxythiophene (PEDOT) has been reported for the protection of Mg and its alloys. Coatings based on diamond-like carbon (DLC) are also among recently-developed coatings for the protection of Mg alloys owing to their chemical inertness, low friction, and high hardness [20]. An interlayer metallic film such as Si or Cr is usually used between the substrate and DLC film for the enhancement of coating adhesion [21, 22]. In this article, new coating materials for the protection of magnesium and its alloys including rare earth conversion coatings, hybrid coatings, DLC coating, and composite polymeric coatings, have been discussed and recent advancements in these fields have been reviewed.

2. Mg and its alloys

Among engineering metals, Mg is the lightest metal and its density is 1.74 $g.cm^{-3}$ [23, 24]. Its density is about four times less than steel (7.86 $g.cm^{-3}$) and 35% less than Al (2.7 $g.cm^{-3}$) [25-28]. Mg metal is obtained by either the electrolysis of seawater magnesium chloride melts or magnesium oxide reduction with silicon. About 1.3 kg magnesium is founded in 1 m^3 of seawater

(0.3%) [29]. Mg has better vibration and noise dampening properties than Al and shows excellent castability and good ductility [30-32]. By alloying magnesium with zirconium [33], zinc [34], thorium [35], manganese [36], aluminum [37], or rare earth metals [38], the ratio of strength to weight increases, making these materials suitable choices where lightweight and the reduction of inertial forces are required. Due to this characteristic, denser cast iron, steel, copper-based alloys, and even Al-based alloys are replaced with Mg-based alloys [39, 40]. Mg is very appealing to the electronic and audio industry owing to its significant electromagnetic interference shielding [41, 42].

Important commercial Mg alloys are the AM series (Mg-Al-Mn), AZ series (Mg-Al-Zn), EZ series (Mg-RE-Zn), AE series (Mg-Al-RE), WE series (Mg-RE-Zr), and ZK series (Mg-Zn-Zr). Different casting processes are used for the production of Mg alloys. Gravity casting (permanent mold and sand casting) together with high-pressure die-casting are the most applicable fabrication techniques. Thixomolding, Thixocasting, and squeeze casting are other production methods [43-46]. According to the Mg consumption analysis by the International Magnesium Association (IMA), automotive components fabricated based on die casting Mg alloys are increasing significantly. In other words, the dominant production approach for Mg alloys with long-term potential growth is expected to be high-pressure die-casting [47].

Although the most common casting technique is die casting, the low density of Mg together with other advantages are important for aerospace applications using the sand cast method. Special Zr-containing magnesium casting alloys with yttrium, zinc, silver, and rare earth elements are utilized between 250 ˚C to 300 ˚C [48-50]. Also, wrought products including forgings, plates, sheets, and extrusions have been applied for numerous applications [39].

2.1 Application of Mg and its alloys

By applying magnesium alloys, it is possible to design lightweight engineering systems such as positive implications in reducing energy consumption. Moreover, these alloys have been used in the form of battery electrodes and viable biodegradable materials [51, 52]. The microelectronics industry benefits from Mg alloys in various components used in computer disk drives, CVD/DVD chassis, cellphone, and camera casings [53-55].

The primary reason to use Mg alloys in the automotive industry is environmental and energy concerns. As a result of a high ratio of strength/weight, Al and steel alloys can be replaced with Mg alloys in the automotive industry [56, 57]. A considerable number of research on auto manufacturing companies has been focused on the development of magnesium and its alloys [47, 58]. The first auto company that used Mg in its products was Volkswagen. The company used 22 kg of Mg in each Beetle model [59].In 1928, Porsche first used magnesium in the car engine [60]. The Mg average usage in 2005, 2010, and 2015 was 3 kg, 20 kg, and 50 kg per car, respectively [61].

In addition to fiber-reinforced polymers and composites, modern aircraft need structural metals. Al and its alloys have been already optimized as the traditional aerospace materials and there are limitations in the further enhancement of their strength together with the reduction of weight and the component dimension. Although Mg alloys have high strength-to-weight ratios and other promising properties, their high surface reactivity is a significant challenge [62-64]. In aerospace applications, the coating of Mg with nickel has also been suggested. It was shown that coating nickel on ZM21 alloy by direct electroless plating provided coatings with good soldering, optical, environmental, and mechanical characteristics [36].

Recently, Mg alloys have been of great interest as new degradable biomaterials. The properties that offer Mg alloys as promising materials for temporary implants include: (1) Mg is a necessary element for human metabolism. In terms of the abundance of the cations in the human body, cationic magnesium is in fourth place and the stored amount of this element in our body is 25 g. Half of this value is stored in the bone tissue. (2) The density of Mg and its alloys (1.74-2.0 $g.cm^{-3}$) is lower than the density of Ti alloys (4.4-4.5 $g.cm^{-3}$) and close to the density of bones (1.8-2.1 $g.cm^{-3}$). (3) The elastic moduli of Mg alloys (41-45 GPa) are close to that of the bone resulting in the alleviation of the stress shielding effect. Moreover, these alloys show greater fracture toughness compared to ceramic biomaterials. Mg is also a cofactor for different enzymes in the body and acts as a stabilizer for the structures of RNA and DNA [65-70]. (4) The standard electrode for magnesium has a potential of -2.37 V, and in a physiologic environment containing Cl, Mg

Fig. 1. Schematic of the applications of Mg and its alloys.

metal shows even poorer corrosion resistance. Hence, biodegradable Mg alloys can be developed by benefitting from their high-rate corrosion in physiologic environments [70-72]. Fig. 1 shows the schematic illustration of the Mg and its alloys applications in various fields.

2.2 Corrosion process in Mg and its alloys

Although magnesium alloys exhibit good properties suitable for different applications, the problem of their poor corrosion resistance is still a concern [73-75]. Because of the low standard electrode potential of Mg, this metal is the most reactive one. A galvanic corrosion system is formed between Mg and another metal and even micro-galvanic corrosion could occur between Mg and some secondary phases and/or impurities in aqueous environments [53, 76]. Therefore, the discussion of the possible current density of galvanic corrosion and micro galvanic corrosion over-potential is useful. The negative difference effect (NDE) of Mg and its alloys, which is different from most metals like copper and iron, lies at the center of the magnesium corrosion process. Overall, shedding light on the main causes of the Mg corrosion process could lead to progress in corrosion-related research. The galvanic current as well as its distribution can determine the galvanic corrosion rate as follows [74, 77]:

$$I_g=(\Phi_c-\Phi_a)/(R_a+R_c+R_s+R_m) \quad (1)$$

Where the galvanic current between the cathode and anode was denoted by , the potentials of the open circuit for the anode and cathode are represented by and , the anode and cathode resistances were denoted by and , respectively. is the solution resistance between the cathode and anode and is the metal resistance from the surface of anode to the surface of the cathode across a metallic path. In fact, Mg alloys are mostly used as structural materials in atmospheric environments; however, there are limited reports about the atmospheric corrosion of these alloys. Most studies are oriented towards an electrochemical approach in solutions [78, 79]. Oxygen reduction and water reduction are thought to contribute to the cathodic reaction on Mg in the atmospheric environment and under immersion condition [80]:

Anodic reaction:

$$Mg(s) \rightarrow Mg^{2+}(aq) + 2\bar{e} \quad (2)$$

Cathodic reaction:

$$2H_2O + 2\bar{e} \rightarrow H_2(g) + 2OH^-(aq) \quad (3)$$

$$O_2 + 2H_2O + 4\bar{e} \rightarrow 4OH^-(aq) \quad (4)$$

The general reaction has been shown as the following:

$$Mg^{2+}(aq) + 2H_2O(aq) \rightarrow Mg(OH)_2(s) + H_2 \quad (5)$$

$$2Mg^{2+}(aq) + 2H_2O(aq) + O_2 \rightarrow 2Mg(OH)_2(s) \quad (6)$$

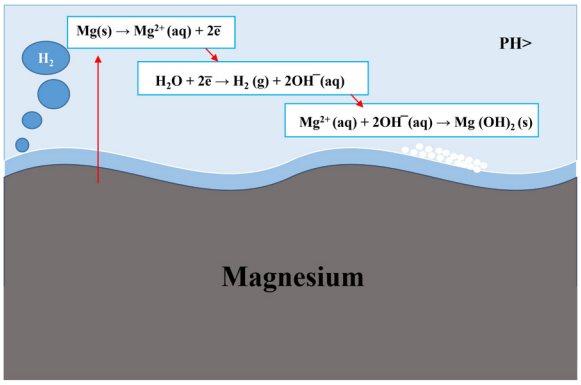

Fig. 2. Schematic of magnesium corrosion mechanism in the atmospheric environment.

At the ordinary atmosphere CO_2 level, a direct reaction occurs between brucite and CO_2, and magnesite is formed. The reaction is:

$$Mg(OH)_2(s) + CO_2 \rightarrow MgCO_3(s) + H_2O \quad (7)$$

Fig. 2 shows a schematic illustration of the magnesium corrosion mechanism in the atmospheric environment. Compared to conventional metals like Mn, Al, and Zn alloys, Mg and its alloys have higher chemical activity due to their corrosion potential between -1.73 and -1.67 V-NHE. As a result, Mg alloys often act as an anode in contact with other metals and exhibit low corrosion resistance. Hence, galvanic corrosion is prevalent in Mg alloys that are in contact with other metals. Localized corrosion, fatigue corrosion, galvanic corrosion, stress corrosion cracking (SCC), and intergranular corrosion are different kinds of corrosion in Mg alloys [1, 81, 82]. These drawbacks constrain the application of Mg alloys in various engineering fields [83]. If unprotected Mg is in contact with an aqueous solution or moisture containing SO_x or Cl ions, it will be corroded severely due to the lack of sustainability and self-healing capability of the hydroxide-oxide-carbonate film formed on the surface of Mg [79, 83, 84]. Therefore, the prominent reasons for weak corrosion of these alloys are the formation of unstable, quasi-passive hydroxide film on their surface and the presence of impurities or secondary phases in their structure leading to internal galvanic corrosion [77, 79, 85].

2.3. Corrosion-resistant coatings for Mg and its alloys

Most light metals such as Ti and Al can form a passive oxide film on their surfaces; however, Mg cannot form such a protective film. Hydroxide/oxide/carbonate films are rapidly formed on the surface of Mg when exposed to the atmospheric environment [86-88]. These films have porous structures, are inhomogeneous and poorly bonded, and are unable to inhibit the corrosion of the underlying metal [89]. The formation of a coating on the metal surface that can form or add functional barrier layers leads to the isolation of the metal from the surrounding environment. This is an effective approach for the improvement of the corrosion resistance of Mg and its alloys. Besides, a good base is formed for applying subsequent organic coatings [90]. Some other coating treatment methods have been also developed such as vapor-phase processes, hybrid coatings, anodizing, conversion coatings, and electrochemical plating (electroplating) [1, 91-93].

There are two basic problems regarding single-layer coatings applied on the surfaces of Mg alloys: Firstly, conversion coatings are unable to provide Mg alloys with prolonged protection against corrosion [1, 13]. Secondly, the presence of an interface between the substrate and coatings cannot provide long-term protection. Hydroxide/oxide/carbonate precipitate forms a layer on the magnesium surface, weakening the adherence of applied coatings to the metal substrate. Thus, as the corrosive agent penetrates the interface between the substrate and the coating, the top coat is rapidly delaminated. The high volume of corrosion products under the top coat results in the detachment of the coating from the sub-

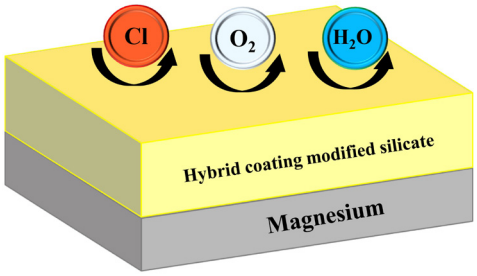

Fig. 3. Illustration of the protective effect of the silicate-modified hybrid coating against corrosion.

strate [94, 95]. Considering these issues, it is concluded that applying a single-layer coating on the surface of Mg alloys cannot provide enough corrosion protection [85].

3. New coating materials for corrosion protection

3.1 *Hybrid coatings*

Combining organic and inorganic materials in a single-phase hybrid network makes it possible to tune the desired coating characteristics for various applications [96]. The synthesis of materials containing hybrids of inorganic and organic compounds by various methods is a new field of research in materials science. The considerable attention paid to this field has led to the new hybrid material emergence with promising properties for novel applications [97-99]. The strength and nature of organic/inorganic interactions determine the properties of hybrid materials. The interaction strength increases when strong bonding, such as covalent bonding, replace weak van der Waals forces. Organic/inorganic hybrids may be categorized into two groups depending on the interaction type or the chemical bonding nature between the components: hybrids with poor interactions between the two constituents are classified into class I, and the ones with strong chemical interactions are classified into class II [100, 101]. Structural properties can be measured for distinguishing between different organic/inorganic hybrids. An ancient painting of Maya blue is an old example of a class I hybrid material made by ancient Mexican people. They prepared Maya blue by encapsulating the natural blue indigo within clay mineral channels. This approach made it resist the severe environments for more than twelve centuries; this could not be achieved by simply mixing the two components [102]. The sol-gel technique could be used as a proper synthetic process to prepare the thin-film hybrid coatings. It is possible to produce transparent hybrid coatings in which molecular-scale interactions exist between the constituents with the sol-gel process [103, 104].

A group of the hybrid materials that have the potential to be used in a variety of industrial materials is organically modified silicates (or mosils). They can be used for catalyst supports, porous materials for chromatography, corrosion protection coatings, anti-fogging coatings, anti-soiling, abrasion-resistant, colored glasses, hard coatings, and optical materials with high reflection due to the facile process depending on the molecular scale [105]. The mechanical behavior of these materials is also promising, owing to the combination of tough organic phases and rigid inorganic phases [106, 107]. In these systems, dispersed organic groups throughout the film enhance the coating hydrophobicity, render them water-repellent, and improve the corrosion resistance [108-110]. Fig.3 schematically shows the protective effect of the silicate-modified hybrid coating against corrosion.

To enhance the corrosion resistance of AZ31 Mg alloy, Li et al. [111] prepared a hybrid coating of poly(lactic-co-glycolic acid) (PLGA) and

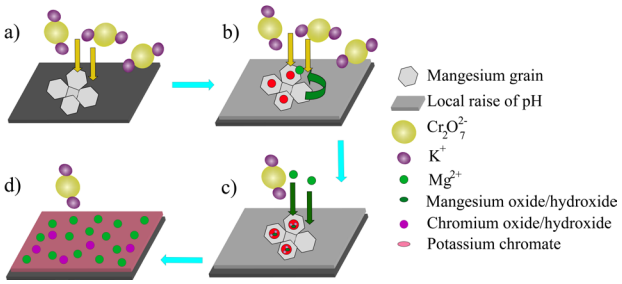

Fig. 4. Illustration the deposition mechanisms of the Cr conversion coating on the metal in the treatment bath (a) immersion of the pretreated alloy, (b) reaction of redox, (c) the coating deposition, and (d) complete coating deposition..

dicalcium phosphate dihydrate (DCPD). First, a DCPD coating was applied on the substrate using electrochemical deposition and then a PLGA coating was deposited to form the coating. This hybrid coating was effective to increase the magnesium alloy resistance against corrosion. Gao et al. [112] developed an effective biomimetic approach to coat AZ91 with a hydroxyapatite/graphene oxide (HA/GO) hybrid. According to the results, the hybrid coating decreased the corrosion current density of the metallic substrate by one order of magnitude in comparison with bare alloy.

Peres et al. [113] added different amounts of silica nanoparticles to (3-glycidoxypropyl)trimethoxysilane (GPTMS) and tetraethylorthosilicate (TEOS) hybrid films to improve the corrosion properties of AZ31. The results suggested that the hybrid coating provided corrosion protection for Mg alloys and adding the SiO_2 nanoparticles further increased the corrosion resistance. Lamaka et al. [114] used the sol-gel approach to form an organic-inorganic hybrid coating on AZ31B magnesium alloy. The coating was applied through copolymerization of Ti or Zr alkoxides and epoxy-siloxane. The additive of tris (trimethylsilyl) phosphate was also utilized for the provision of additional corrosion protection. It was proposed that hydrolytically stable chemical bonds of Mg–O–P was formed in the coating doped with tris(trimethylsilyl)-phosphate, and increased the magnesium alloy resistance to corrosion.

Zhang et al. [115] employed a chemical conversion route for applying a crack-free hybrid coating of HA/phytic acid (PA) on the AZ31 surface. After the formation of the precursor coating, the coating was hydrothermally treated in the saturated CaO solution. It was shown that the hybrid coating had stable barrier properties and could effectively protect the Mg alloy. To enhance biological behavior and obtain tunable degradation, Kang et al. [116] deposited a hybrid coating of poly(ether imide) (PEI)-SiO_2 on Mg. An increase in the content of SiO_2 resulted in the enhancement of coating hydrophilicity and thereby the corrosion rate of the substrate increased. In these systems, dispersed organic groups throughout the film enhance the coating hydrophobicity, render them water-repellent, and improve the corrosion resistance. The magnesium alloys coated with such films have a good resistance to corrosion.

3.2. Rare earth conversion coatings

Due to the simple and low-cost procedure, conversion coating treatment has been considered for different applications. The conversion coatings for Mg are typically applied for the provision of enhanced paint-base properties and corrosion protection [117]. Because of the excellent corrosion resistance as well as a simple coating process, chromate conversion coatings have been favored greatly in recent years. Nevertheless, the application of these coating is limited due to the hexavalent chromium ion toxicity. Other conversion coatings on Mg alloys such as stannate [118-121], phosphate-permanganate [122, 123], phosphate [124-126], and rare earth metals [127-130] conversion coat-

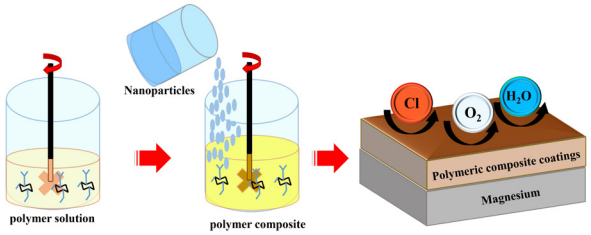

Fig. 5. Illustration of the polymer composites' production containing nanoparticles and their anti-corrosion properties.

ings have been investigated. The process of preparing rare-earth conversion coatings is accompanied by simple electrolytic constituents, mainly, chloride, sulfate, and neodymium, cerium, nitrate, and lanthanum rare earth metals. Therefore, its maintenance and recycling would be easy. Another important advantage of the rare-earth conversion coatings is that they are considered as environment-friendly treatment [13].

Rudd et al. [127] coated Mg and WE43 alloy with praseodymium, lanthanum, and cerium conversion coatings. The coating decreased the magnesium dissolution in a buffer solution with pH=8.5, however, after 60 min of immersion, a deterioration in the coating was observed. The reason was stated to be the formation of corrosion products of Mg hydroxide together with mixed coatings composed of rare earth/Mg oxide and hydroxides. In another research, Brunelli et al. [131], produced a conversion coating of cerium for the corrosion protection of Mg, AZ91, as well as AM50. It was reported that by reducing the cathodic and anodic currents and ennobling the corrosion potential, the corrosion resistance of bare Mg and its alloys could be increased. Furthermore, a further increase in the corrosion resistance was achieved by acid pre-treatment. The result of corrosion investigations in the chloride environment showed that after five days, the coated samples were unaffected while localized corrosion was observed in the untreated samples.

Montemor et al. [132] studied the effect of conversion film of rare-earth metals (cerium and lanthanum) on the corrosion behavior of the AZ31 Mg alloy. The AZ31 substrate showed reduced corrosion activity in the presence of chloride ions. Moreover, the treatment time affected the efficiency of corrosion protection. On the other hand, Li et al. [133] reported weak adhesion of cerium conversion coatings to the AZ31 substrate and limited corrosion resistance enhancement of the coating. Lin et al. [13] also found the inherent weakness in adhesion of cerium conversion coatings to the surface of AZ31 leading to coating partial detachment when dried at room temperature. Cross-sectional observations exhibited three layers with porous, compact, and fibrous structures formed sequentially on the surface of the substrate. Among the interfaces, the interface between the fibrous and compact layers was identified to be the weakest bonding.

According to Lin et al. [134], conversion coatings of lanthanum and cerium could improve the corrosion resistance of AZ63 alloy. An increment in immersion time resulted in the improvement of the inhibition effect provided by the dual rare-earth film. Laleh et al. [135] used the micro-arc oxidation (MAO) method to apply oxide coatings on AZ91D magnesium alloy and then the samples were soaked in a Ce bath for sealing the pores of the MAO coatings. The results revealed that the pore sealing for 10 min exhibited a remarkable improvement of the substrate corrosion resistance. Fig.4 shows a schematic illustration of the deposition mechanisms of the Cr conversion coating on the metal in the treatment bath.

Many works were reported on rare-earth coatings for Mg and its alloys. According to the results of corrosion studies, the rare-earth coatings can provide good corrosion resistance.

3.3. Polymeric nanocomposite coatings

Polymers and polymer composites are widely used in different engineering applications [136-139]. A range of physical and tribological features are offered by polymeric nanocomposites [140]. The addition of nanoparticles in polymers leads to the improvement of properties such as anti-corrosion performance, thermal conductivity, mechanical strength, and electronic and optical properties [141, 142]. Fig. 5 shows a schematic illustration of the production of polymer composites containing nanoparticles and their anti-corrosion properties.

Metallic components used in engineering, energy, defense, and biomedical applications are encountered with the problem of corrosion [143]. In this regard, wear and abrasion resistance, anti-corrosion resistance, and barrier properties of polymeric nanocomposite are used. Restriction of electron flow from the metallic substrate to oxidizing agents occurs within doped conducting polymers preventing corrosion of the substrate. However, neat polymers as metal coatings are unable to provide good wear properties and corrosion protection [144]. Nanoparticles such as titania, silica, nanoclay, carbon black, carbon nanotube, graphene oxide (GO), graphene, nanodiamond, and fullerene nanoparticles have been added to various polymeric matrices to improve their corrosion resistance. To enhance interfacial adhesion and load transferring of matrix/nanofiller, functionalization has been considered [145]. Functional nanoparticles can increase the strength of nanocomposites and restrict the diffusion of corrosive species within the polymer matrix to prevent corrosion [146]. The underlying material can be also protected against friction and wear [147, 148].

Nazeer et al. [149] added GO and TiO_2 nanoparticles to poly (butyl methacrylate) (poly(BMA)) to prepare a nanocomposite coating for AZ31 magnesium alloy. The results demonstrated that the nanocomposite coating was able to act as an excellent passivation layer to prevention diffusion and corrosion so that the corrosion current decreased significantly and the charge transfer resistance increased noticeably. Soleymani et al. [150] incorporated different amounts of baghdadite mineral to polycaprolactone (PCL)/chitosan (Ch) for improving the resistance to corrosion, biocompatibility, as well as bioactivity of the anodized AZ91 alloy. According to the results, the nanocomposite coating containing 3 wt % baghdadite showed hydrophobic behavior that led to decreasing the corrosion current density for the magnesium alloy and the enhancement of its corrosion resistance.

A corrosion control layer of 3,4-ethylenedioxythiphene (PEDOT)/GO nanocomposite was coated on magnesium in research by Catt et al. [151]. The results indicated that the corroding samples exhibited an increment in the polarization resistance, reduction of corrosion current, and more positive corrosion potential. It was reported that three factors contributed to corrosion protection of PEDOT/GO including redox coupling with magnesium corrosion resulting in the creation of a protective magnesium phosphate layer, inducing negative charges in the film, and the formation of an initial passive layer that prevents solution uptake. In the research of Rahimi et al. [152], cellulose nanoparticles (CNs) were added to polylactic acid (PLA) coating to protect the AZ31 alloy. The outcome of adding CNs to the coating was the enhancement of the PLA corrosion resistance. The most promising result of corrosion resistance improvement was attributed to the coating containing 5 wt. % of CNs.

Zhang et al. [153] coated AZ91D Mg alloy with polyaniline (PANI)/organophilic montmorillonite (OMMT) polymer nanocomposite. They reported that after 6000 h of immersion in the corrosive environment, the Mg alloy coated by PANI/OMMT maintained its high corrosion resistance. A dense Ch/hydroxyapatite (HA) composite coating was applied on AZ31 Mg alloy by Hahn et al. [154]. A high adhesion strength range of 24.6-27.7 MPa was reported for the coating and it exhibited higher corrosion resistance compared to the bare Mg substrate. To improve bone-implant integration and control the degradation of Mg-based

substrates, Johnson et al. [155] developed PLGA/nanostructured hydroxyapatite (nHA) coatings using the spin coating method. Nano-scale features of the coatings were retained with the dispersion of nHA in the PLGA matrix. According to the corrosion behavior studies in the revised simulated body fluid, Mg substrates coated by the composite showed an enhancement of the corrosion potential and reduction of the corrosion current.

Nanocomposite coatings of the addition of inorganic nanofillers into the polymer matrix are a new method for corrosion protection that exhibit excellent mechanical performance and corrosion resistance in comparison to conventional composite coatings

3.4. DLC coatings

DLC involves a broad range of amorphous carbon coatings having different hydrogen levels and sp^2 and sp^3 bonded carbon ratios. A variety of properties can be obtained by changing the ratio of the three components. There are similarities in the properties of DLC and diamond, however, DLC has an amorphous matrix in which sp^3 nodules exist in a matrix of bonded sp^2 [156, 157]. DLC coatings have a dense microstructure, chemical inertness, and high mechanical hardness [158]. Due to the structure of DLC coatings, high residual stress is built within these coatings [159]. Consequently, surface adhesion would be weak resulting in the delamination of the coatings at early stages. By the deposition of interlayers, the surface adhesion can be improved. The interlayers are thin coating layers that are applied for the promotion of DLC adhesion [160, 161]. The interlayer is required to have a strong bonding with both the DLC top coat and the substrate. Silicon nitride (Si_3N_4), chromium carbide (CrC), and titanium (Ti) are common interlayer materials. The interlayer can also contribute to the enhancement of the corrosion resistance because DLC could be both conductive and porous. Hence, the layer can act as a physical barrier between the corrosive environment and the substrate and decrease the delamination risk [162].

Recently, DLC coatings have been considered by many researchers for the promotion of the anti-corrosion and mechanical properties of magnesium alloys [161, 163]. Nevertheless, the direct deposition of hard materials like DLC coatings on Mg-based soft substrates is a challenge. Considerable differences in physical properties including thermal expansion coefficient, plasticity, and elastic modulus between the coating and substrate lie at the center of the problem [164-166]. Wu et al. [164] applied a three-layer coating composed of aluminum, aluminum nitride, and diamond-like carbon (from bottom to top) on the surface of AZ31. The results indicated the enhancement of the corrosion resistance of the coated alloy so that the presence of 3.5 wt% NaCl in solution reduces the current density from 2.25×10^{-5} A.cm^{-2} to 1.28×10^{-6} A.cm^{-2}. Anti-corrosion behavior of the Si-incorporated DLC (Si-DLC) films on AZ31 Mg alloy was studied by Choi et al. [20]. The prepared Si-DLC films yielded noticeable corrosion protection for the Mg alloy. The improved anti-corrosion performance of the Si-DLC films is the result of very low internal stress within the coatings. Wu et al. [167] deposited columnar layers of Cr and CrN with preferred textures of (110) and (111), respectively as interlayers for applying a DLC coating on AZ31. Although the adhesion between the substrate and coating was improved significantly by applying the interlayers, the enhancement of the DLC/AZ31 corrosion resistance was not observed. This was reported to be the result of the galvanic cell formation between interlayer and substrate in the through-thickness defects in a solution of 3.5 wt. % NaCl.

Masami et al. [168] also incorporated Si into DLC coatings to provide corrosion protection for AZ91 magnesium alloy. Results indicated that the Si-DLC coating had higher corrosion resistance in comparison with DLC coating. Applying Ti interlayer promoted adhesion between the AZ91 substrate and DLC coating, however, it negatively affected corrosion protection. Corrosion resistance, as well as adhesion strength of Mg alloy, was improved by treating the surface of the substrate with ozone. In a research study by Uematsu et al. [169], it was shown that the corrosion fatigue strength of AZ80A in distilled water was not improved by applying single-layer and multilayer DLC films. The films contained some defects facilitating the access of the corrosive water to the substrate. The thicker multilayer DLC coating showed no degradation of fatigue strength in the corrosive environment revealing its effectiveness for corrosion protection. According to the reports of Yamauchi et al. [170], it was found that the diamond-like carbon coating on the Mg-14 mass% Li alloy could not withstand the corrosive alkaline and acidic solutions.

4. Conclusions and future insights

Mg and its alloys suffer from low corrosion resistance. Mg alloys, unlike other light metals such as Ti and Al, are not capable of forming naturally passivating oxide films. Porous, poor-bonded oxide/hydroxide/carbonate layers are rapidly developed on the Mg surface under atmospheric exposure that are unable to protect the substrate. Different coatings are being used for Mg alloys to isolate the substrate from corrosive environments. Organic-inorganic hybrid coatings, polymeric nanocomposite, rare earth conversion coatings, and DLC coatings have been demonstrated to have great impacts on the promotion of corrosion resistance of Mg alloys. These new coatings have shown promising results in terms of corrosion protection of Mg alloys in different corrosive environments, however, they still need to be improved. Future studies might concentrate on the promotion of these coatings as well as the development of novel coating materials for the corrosion protection of magnesium and magnesium-based alloys. The development of inexpensive coating processes and accessible coating materials are favored for the industry and this issue should be considered in future research.

REFERENCES

[1] J. Gray, B. Luan, Protective coatings on magnesium and its alloys—a critical review, Journal of alloys and compounds 336(1-2) (2002) 88-113.

[2] A.H. Shahbaz, M. Esmaeilian, R. NasrAzadani, K. Gavanji, The effect of MgF_2 addition on the mechanical properties of hydroxyapatite synthesized via powder metallurgy, Journal of Composites and Compounds 1(1) (2019) 18-24.

[3] A. Moghanian, A. Ghorbanoghli, M. Kazem-Rostami, A. Pazhouheshgar, E. Salari, M. Saghafi Yazdi, T. Alimardani, H. Jahani, F. Sharifian Jazi, M. Tahriri, Novel antibacterial Cu/Mg-substituted 58S-bioglass: Synthesis, characterization and investigation of in vitro bioactivity, International Journal of Applied Glass Science 11(4) (2020) 685-698.

[4] H. Liu, F. Cao, G.-L. Song, D. Zheng, Z. Shi, M.S. Dargusch, A. Atrens, Review of the atmospheric corrosion of magnesium alloys, Journal of Materials Science & Technology 35(9) (2019) 2003-2016.

[5] D. Tawil, Corrosion and surface protection developments, magnesium technology, Proceedings of the Conference, 1986.

[6] M. Shahin, K. Munir, C. Wen, Y. Li, Magnesium matrix nanocomposites for orthopedic applications: a review from mechanical, corrosion, and biological perspectives, Acta biomaterialia 96 (2019) 1-19.

[7] M.F. Heragh, S. Eskandarinezhad, A. Dehghan, Ni-Cu matrix composite reinforced with CNTs: preparation, characterization, wear and corrosion behavior, inhibitory effects, Journal of Composites and Compounds 2(4) (2020) 123-128.

[8] M. Amiri, V.T. Targhi, S. Padervand, S.M.M. Khoei, Corrosion behavior of aluminum oxide coatings created by electrolytic plasma method under different potential regimes, Journal of Composites and Compounds 2(4) (2020) 129-137.

[9] M. Amiri, S. Padervand, V.T. Targhi, S.M.M. Khoei, Investigation of aluminum oxide coatings created by electrolytic plasma method in different potential regimes, Journal of Composites and Compounds 2(4) (2020) 115-122.

[10] A. Abuchenari, H. Ghazanfari, M. Siavashi, M. Sabetzadeh, S. Talebi, Z.K. Chemeh, A. Jamavari, A review on development and application of self-healing thermal barrier composite coatings, Journal of Composites and Compounds 2(4) (2020) 147-154.

[11] S. Lamaka, M. Montemor, A. Galio, M. Zheludkevich, C. Trindade, L. Dick, M. Ferreira, Novel hybrid sol–gel coatings for corrosion protection of AZ31B

magnesium alloy, Electrochimica Acta 53(14) (2008) 4773-4783.
[12] F.S. Jazi, N. Parvin, M. Rabiei, M. Tahriri, Z.M. Shabestari, A.R. Azadmehr, Effect of the synthesis route on the grain size and morphology of ZnO/Ag nanocomposite, Journal of Ceramic Processing Research 13(5) (2012) 523-526.
[13] C. Lin, S. Fang, Formation of cerium conversion coatings on AZ31 magnesium alloys, Journal of the Electrochemical Society 152(2) (2004) B54.
[14] F.S. Jazi, N. Parvin, M. Tahriri, M. Alizadeh, S. Abedini, M. Alizadeh, The relationship between the synthesis and morphology of SnO_2-Ag_2O nanocomposite, Synthesis and Reactivity in Inorganic, Metal-Organic, and Nano-Metal Chemistry 44(5) (2014) 759-764.
[15] Q. Cheng, X. Guo, X. Hao, Z. Shi, S. Zhu, Z. Cui, Fabrication of Robust Antibacterial Coatings Based on an Organic–Inorganic Hybrid System, ACS applied materials & interfaces 11(45) (2019) 42607-42615.
[16] S.V. Gnedenkov, S.L. Sinebryukhov, D.V. Mashtalyar, V.S. Egorkin, M.V. Sidorova, A.S. Gnedenkov, Composite polymer-containing protective coatings on magnesium alloy MA8, Corrosion Science 85 (2014) 52-59.
[17] J. Daraei, Production and characterization of PCL (Polycaprolactone) coated TCP/nanoBG composite scaffolds by sponge foam method for orthopedic applications, Journal of Composites and Compounds 2(1) (2020) 45-50.
[18] M. Arefian, M. Hojjati, I. Tajzad, A. Mokhtarzade, M. Mazhar, A. Jamavari, A review of Polyvinyl alcohol/Carboxiy methyl cellulose (PVA/CMC) composites for various applications, Journal of Composites and Compounds 2(3) (2020) 69-76.
[19] A. Zomorodian, M. Garcia, T.M. e Silva, J. Fernandes, M. Fernandes, M. Montemor, Corrosion resistance of a composite polymeric coating applied on biodegradable AZ31 magnesium alloy, Acta Biomaterialia 9(10) (2013) 8660-8670.
[20] J. Choi, S. Nakao, J. Kim, M. Ikeyama, T. Kato, Corrosion protection of DLC coatings on magnesium alloy, Diamond and Related Materials 16(4) (2007) 1361-1364.
[21] X.-J. Cui, C.-M. Ning, L.-L. Shang, G.-A. Zhang, X.-Q. Liu, Structure and anticorrosion, friction, and wear characteristics of Pure Diamond-Like Carbon (DLC), Cr-DLC, and Cr-H-DLC films on AZ91D Mg alloy, Journal of Materials Engineering and Performance 28(2) (2019) 1213-1225.
[22] T. Nakatani, H. Takeuchi, A. Wada, S. Yamashita, Investigation of Anti-Corrosive Performance of a Si-Doped DLC-Coated Magnesium Alloy Stent Deposited by RF-Plasma CVD, Journal of Photopolymer Science and Technology 32(3) (2019) 511-517.
[23] K. Zhanga, Q. Van Leb, Journal of Composites and Compounds, (2019).
[24] C. Niranjan, S. Srinivas, M. Ramachandra, An experimental study on depth of cut of AZ91 Magnesium Alloy in abrasive water jet cutting, Materials Today: Proceedings 5(1) (2018) 2884-2890.
[25] N. Studio, Magnesium and exercise-Blog, (2020).
[26] L.S. Fard, N.S. Peighambardoust, H.W. Jang, A. Dehghan, N.N.K. Saligheh, M. Iranpour, M.I. Rajabi, The rechargeable aluminum-ion battery with different composite cathodes: A review, Journal of Composites and Compounds 2(4) (2020) 138-146.
[27] S. Nasibi, K. Alimohammadi, L. Bazli, S. Eskandarinezhad, A. Mohammadi, N. Sheysi, TZNT alloy for surgical implant applications: A systematic review, Journal of Composites and Compounds 2(3) (2020) 62-68.
[28] K. Zhang, H.W. Jang, Q. Van Le, Production methods of ceramic-reinforced Al-Li matrix composites: A review, Journal of Composites and Compounds 2(3) (2020) 77-84.
[29] J.-L. Kuo, S. Sugiyama, S.-H. Hsiang, J. Yanagimoto, Investigating the characteristics of AZ61 magnesium alloy on the hot and semi-solid compression test, The International Journal of Advanced Manufacturing Technology 29(7-8) (2006) 670-677.
[30] X. He, B. Dong, Y. Chen, R. Li, F. Wang, J. Li, Z. Cai, Analysis of magnesium and copper in aluminum alloys with high repetition rate laser-ablation spark-induced breakdown spectroscopy, Spectrochimica Acta Part B: Atomic Spectroscopy 141 (2018) 34-43.
[31] I. Tajzad, E. Ghasali, Production methods of CNT-reinforced Al matrix composites: a review, Journal of Composites and Compounds 2(1) (2020) 1-9.
[32] F. Sharifianjazi, M. Moradi, A. Abouchenari, A.H. Pakseresht, A. Esmaeilkhanian, M. Shokouhimehr, M.S. Asl, Effects of Sr and Mg dopants on biological and mechanical properties of SiO_2–CaO–P_2O_5 bioactive glass, Ceramics International (2020).
[33] A. Bordbar-Khiabani, B. Yarmand, M. Mozafari, Emerging magnesium-based biomaterials for orthopedic implantation, Thomas Telford Ltd, 2019.
[34] K. Singh, G. Singh, H. Singh, Review on friction stir welding of magnesium alloys, Journal of magnesium and alloys 6(4) (2018) 399-416.
[35] K. Singh, G. Singh, H. Singh, Investigation of microstructure and mechanical properties of friction stir welded AZ61 magnesium alloy joint, Journal of Magnesium and Alloys 6(3) (2018) 292-298.
[36] H. Somekawa, A. Kinoshita, A. Kato, Effect of alloying elements on room temperature stretch formability in Mg alloys, Materials Science and Engineering: A 732 (2018) 21-28.
[37] R. Galun, A. Weisheit, B. Mordike, Laser surface alloying of magnesium base alloys, Journal of Laser Applications 8(6) (1996) 299-305.
[38] M. Easton, M.A. Gibson, S. Zhu, T. Abbott, J.-F. Nie, C.J. Bettles, G. Savage, Development of magnesium-rare earth die-casting alloys, TMS Annual Meeting & Exhibition, Springer, 2018, pp. 329-336.
[39] E. Aghion, B. Bronfin, Magnesium alloys development towards the 21st century, Materials Science Forum, Trans Tech Publ, 2000, pp. 19-30.
[40] A. Abuchenari, M. Moradi, The Effect of Cu-substitution on the microstructure and magnetic properties of Fe-15% Ni alloy prepared by mechanical alloying, Journal of Composites and Compounds 1(1) (2019) 11-17.
[41] R. Pandey, S. Tekumalla, M. Gupta, Effect of defects on electromagnetic interference shielding effectiveness of magnesium, Journal of Materials Science: Materials in Electronics 29(11) (2018) 9728-9739.
[42] S. Ben Zaken, O. Simantov, A. Abenstein, Z. Radomysky, G. Koren, Water desalination, serum magnesium and dementia: a population-based study, Journal of Water and Health 18(5) (2020) 722-727.
[43] A.A. Luo, Magnesium casting technology for structural applications, journal of Magnesium and Alloys 1(1) (2013) 2-22.
[44] H. Hu, Squeeze casting of magnesium alloys and their composites, Journal of materials science 33(6) (1998) 1579-1589.
[45] H. Dieringa, K.U. Kainer, Magnesium and Magnesium Alloys, Springer Handbook of Materials Data, Springer2018, pp. 151-159.
[46] R.H. Buzolin, P. Volovitch, A. Maltseva, S. Lamaka, C. Blawert, C.L. Mendis, A. Lohmüller, K.U. Kainer, N. Hort, Thixomolded AZ91D and MRI153M magnesium alloys and their enhanced corrosion resistance, Materials and corrosion 71(3) (2020) 339-351.
[47] B. Viswanadhapalli, V.B. Raja, Application of Magnesium Alloys in Automotive Industry-A Review, International Conference on Emerging Current Trends in Computing and Expert Technology, Springer, 2019, pp. 519-531.
[48] R. Viswanathan, N. Sivashankar, S. Chandrakumar, R. Karthik, Improving Corrosion Resistance of Magnesium Alloy for Aerospace Applications, International Journal of Mechanical and Production Engineering Research and Development 9(3) (2019) 769-774.
[49] O.I. Velikokhatnyi, P.N. Kumta, First-principles studies on alloying and simplified thermodynamic aqueous chemical stability of calcium-, zinc-, aluminum-, yttrium-and iron-doped magnesium alloys, Acta Biomaterialia 6(5) (2010) 1698-1704.
[50] M. Bian, X. Huang, Y. Chino, Improving flame resistance and mechanical properties of magnesium–silver–calcium sheet alloy by optimization of calcium content, Journal of Alloys and Compounds (2020) 155551.
[51] M. Esmaily, J. Svensson, S. Fajardo, N. Birbilis, G. Frankel, S. Virtanen, R. Arrabal, S. Thomas, L. Johansson, Fundamentals and advances in magnesium alloy corrosion, Progress in Materials Science 89 (2017) 92-193.
[52] A. Toulabifard, M. Rahmati, K. Raeissi, A. Hakimizad, M. Santamaria, The Effect of Electrolytic Solution Composition on the Structure, Corrosion, and Wear Resistance of PEO Coatings on AZ31 Magnesium Alloy, Coatings 10(10) (2020) 937.
[53] R. Ambat, N.N. Aung, W. Zhou, Evaluation of microstructural effects on corrosion behaviour of AZ91D magnesium alloy, Corrosion science 42(8) (2000) 1433-1455.
[54] C.H. Chang, K.-T. Wu, C.-T. Lin, Magnesium Alloy Substrate, Google Patents, 2018.
[55] C. Li, H. Huang, J. Zhao, S. Ruan, A high strength magnesium alloy-based rotating mirror for an ultra-high speed camera, Optik 157 (2018) 85-92.
[56] G. Song, A.L. Bowles, D.H. StJohn, Corrosion resistance of aged die cast magnesium alloy AZ91D, Materials Science and Engineering: A 366(1) (2004) 74-86.
[57] D. Klaumünzer, J.V. Hernandez, S. Yi, D. Letzig, S.-h. Kim, J.J. Kim, M.H. Seo, K. Ahn, Magnesium process and alloy development for applications in the automotive industry, Magnesium Technology 2019, Springer2019, pp. 15-20.
[58] G. Demir, A.U. Malcıoğlu, S. Sağdiç, A. Ulus, S. Aslanlar, E. İlhan, Optimization of Thermo-Mechanical Processes of Continuous Casting Products Using High Magnesium Aluminum Alloys in Automotive Industry Applications, Light Metals 2020, Springer2020, pp. 386-399.
[59] H. Friedrich, S. Schumann, Research for a “new age of magnesium” in the automotive industry, Journal of Materials Processing Technology 117(3) (2001) 276-281.
[60] S. Schumann, The paths and strategies for increased magnesium applications

in vehicles, Materials Science Forum, Trans Tech Publ, 2005, pp. 1-8.
[61] M.K. Kulekci, Magnesium and its alloys applications in automotive industry, The International Journal of Advanced Manufacturing Technology 39(9-10) (2008) 851-865.
[62] F. Czerwinski, Controlling the ignition and flammability of magnesium for aerospace applications, Corrosion Science 86 (2014) 1-16.
[63] T. Kaneko, M. Suzuki, Automotive applications of magnesium alloys, Materials science forum, Trans Tech Publications Ltd., Zurich-Uetikon, Switzerland, 2003, pp. 67-72.
[64] P.R. Matli, A.V. Krishnan, V. Manakari, G. Parande, B. Chua, S. Wong, C. Lim, M. Gupta, A new method to lightweight and improve strength to weight ratio of magnesium by creating a controlled defect, Journal of Materials Research and Technology (2020).
[65] M.P. Staiger, A.M. Pietak, J. Huadmai, G. Dias, Magnesium and its alloys as orthopedic biomaterials: a review, Biomaterials 27(9) (2006) 1728-1734.
[66] N.-E.L. Saris, E. Mervaala, H. Karppanen, J.A. Khawaja, A. Lewenstam, Magnesium: an update on physiological, clinical and analytical aspects, Clinica chimica acta 294(1-2) (2000) 1-26.
[67] J.M. Seitz, R. Eifler, F.W. Bach, H. Maier, Magnesium degradation products: effects on tissue and human metabolism, Journal of biomedical materials research Part A 102(10) (2014) 3744-3753.
[68] T.C. Wallace, Combating COVID-19 and building immune resilience: a potential role for magnesium nutrition?, Journal of the American College of Nutrition (2020) 1-9.
[69] F. Ahmed, A. Mohammed, Magnesium: the forgotten electrolyte—a review on hypomagnesemia, Medical Sciences 7(4) (2019) 56.
[70] D. Song, C. Li, N. Liang, F. Yang, J. Jiang, J. Sun, G. Wu, A. Ma, X. Ma, Simultaneously improving corrosion resistance and mechanical properties of a magnesium alloy via equal-channel angular pressing and post water annealing, Materials & Design 166 (2019) 107621.
[71] D. Seifzadeh, A. Haghighat, Formation of rare earth-permanganate conversion coating on AZ61 magnesium alloy and its properties, (2013).
[72] S. Kamrani, C. Fleck, Biodegradable magnesium alloys as temporary orthopaedic implants: a review, BioMetals 32(2) (2019) 185-193.
[73] K. Jafarzadeh, T. Shahrabi, S. Hadavi, M. Hosseini, EIS study on corrosion behavior of AA5083-H321 aluminum-magnesium alloys in stagnant NaCl solution, (2008).
[74] L. Liu, M. Schlesinger, Corrosion of magnesium and its alloys, Corrosion Science 51(8) (2009) 1733-1737.
[75] F. Gao, Y. Hu, Z. Gong, T. Liu, T. Gong, S. Liu, C. Zhang, L. Quan, B. Kaveendran, C. Pan, Fabrication of chitosan/heparinized graphene oxide multilayer coating to improve corrosion resistance and biocompatibility of magnesium alloys, Materials Science and Engineering: C 104 (2019) 109947.
[76] I. Apachitei, L. Fratila-Apachitei, J. Duszczyk, Microgalvanic activity of an Mg–Al–Ca-based alloy studied by scanning Kelvin probe force microscopy, Scripta Materialia 57(11) (2007) 1012-1015.
[77] G. Song, B. Johannesson, S. Hapugoda, D. StJohn, Galvanic corrosion of magnesium alloy AZ91D in contact with an aluminium alloy, steel and zinc, Corrosion Science 46(4) (2004) 955-977.
[78] R. Ambat, N.N. Aung, W. Zhou, Effect of pH and chloride ion concentration on the corrosion and electrochemical behaviour of AZ91D magnesium alloy, Journal of Applied Electrochemistry 30 (2000) 865-874.
[79] S. Mathieu, C. Rapin, J. Steinmetz, P. Steinmetz, A corrosion study of the main constituent phases of AZ91 magnesium alloys, Corrosion Science 45(12) (2003) 2741-2755.
[80] M. Jönsson, D. Persson, D. Thierry, Corrosion product formation during NaCl induced atmospheric corrosion of magnesium alloy AZ91D, Corrosion Science 49(3) (2007) 1540-1558.
[81] X. Gu, Y. Zheng, Y. Cheng, S. Zhong, T. Xi, In vitro corrosion and biocompatibility of binary magnesium alloys, Biomaterials 30(4) (2009) 484-498.
[82] S. Abbasi, M. Aliofkhazraei, H. Mojiri, M. Amini, M. Ahmadzadeh, M. Shourgeshty, Corrosion behavior of pure Mg and AZ31 magnesium alloy, Protection of Metals and Physical Chemistry of Surfaces 53(3) (2017) 573-578.
[83] N. Liu, W. Huang, DSC study on temperature memory effect of NiTi shape memory alloy, Transactions of Nonferrous Metals Society of China 16 (2006) s37-s41.
[84] A. Coy, F. Viejo, P. Skeldon, G. Thompson, Susceptibility of rare-earth-magnesium alloys to micro-galvanic corrosion, Corrosion Science 52(12) (2010) 3896-3906.
[85] M. Toorani, M. Aliofkhazraei, Review of electrochemical properties of hybrid coating systems on Mg with plasma electrolytic oxidation process as pretreatment, Surfaces and Interfaces 14 (2019) 262-295.
[86] T. Cain, L. Bland, N. Birbilis, J. Scully, A compilation of corrosion potentials for magnesium alloys, Corrosion 70(10) (2014) 1043-1051.
[87] P. Huang, J.-A. Latham, D.R. MacFarlane, P.C. Howlett, M. Forsyth, A review of ionic liquid surface film formation on Mg and its alloys for improved corrosion performance, Electrochimica Acta 110 (2013) 501-510.
[88] L. Yan, M. Zhou, X. Pang, K. Gao, One-step in situ synthesis of reduced graphene oxide/Zn–Al layered double hydroxide film for enhanced corrosion protection of magnesium alloys, Langmuir 35(19) (2019) 6312-6320.
[89] R. Arrabal, A. Pardo, M. Merino, S. Merino, P. Casajús, M. Mohedano, P. Rodrigo, Corrosion behavior of mg-al alloys with aluminum thermal spray coatings in humid and saline environments, Corrosion 65(12) (2009) 817-830.
[90] M.M. Avedesian, H. Baker, ASM specialty handbook: magnesium and magnesium alloys, ASM international1999.
[91] J. Li, Y. He, Y. Sun, X. Zhang, W. Shi, D. Ge, Synthesis of Polypyrrole/V_2O_5 Composite Film on the Surface of Magnesium Using a Mild Vapor Phase Polymerization (VPP) Method for Corrosion Resistance, Coatings 10(4) (2020) 402.
[92] R. Molak, K. Topolski, M. Spychalski, I. Dulińska-Molak, B. Morończyk, Z. Pakieła, L. Nieużyła, M. Mazurkiewicz, M. Wojucki, A. Gebeshuber, Functional properties of the novel hybrid coatings combined of the oxide and DLC layer as a protective coating for AZ91E magnesium alloy, Surface and Coatings Technology 380 (2019) 125040.
[93] V.Z. Asl, J. Zhao, M.J. Anjum, S. Wei, W. Wang, Z. Zhao, The effect of cerium cation on the microstructure and anti-corrosion performance of LDH conversion coatings on AZ31 magnesium alloy, Journal of Alloys and Compounds 821 (2020) 153248.
[94] R.-G. Hu, S. Zhang, J.-F. Bu, C.-J. Lin, G.-L. Song, Recent progress in corrosion protection of magnesium alloys by organic coatings, Progress in Organic Coatings 73(2-3) (2012) 129-141.
[95] J. Scully, S. Hensley, Lifetime prediction for organic coatings on steel and a magnesium alloy using electrochemical impedance methods, Corrosion 50(9) (1994) 705-716.
[96] S. Pandey, S.B. Mishra, Sol–gel derived organic–inorganic hybrid materials: synthesis, characterizations and applications, Journal of sol-gel science and technology 59(1) (2011) 73-94.
[97] M. Faustini, L. Nicole, E. Ruiz-Hitzky, C. Sanchez, History of organic–inorganic hybrid materials: prehistory, art, science, and advanced applications, Advanced Functional Materials 28(27) (2018) 1704158.
[98] R. Zandi-Zand, A. Ershad-Langroudi, A. Rahimi, Organic–inorganic hybrid coatings for corrosion protection of 1050 aluminum alloy, Journal of Non-Crystalline Solids 351(14-15) (2005) 1307-1311.
[99] F. García-Galván, M. Mezour, G. Hickman, I. Soliman, A. Jiménez-Morales, V. Barranco, J. Galván, C. Perry, Organic-inorganic hybrid coatings containing phosphorus precursors prepared by sol–gel on Ti6Al4V alloy: Electrochemical and in-vitro biocompatibility evaluation, Progress in Organic Coatings 148 (2020) 105834.
[100] N. Farhadyar, A. Rahimi, A. Ershad Langroudi, Synthesis and chracterization of inorganic-organic hybrid produced from tetraethoxysilane and epoxy-aromatic amine, IUPAC World Polymer Congress Macro, 2004, p. 2.
[101] Z.R. ZANDI, L.A. ERSHAD, A. RAHIMI, Improvement of corrosion resistance of organic-inorganic hybrid coatings based on epoxy-silica via aromatic diol curing agent, (2005).
[102] C. Sanchez, B. Julián, P. Belleville, M. Popall, Applications of hybrid organic–inorganic nanocomposites, Journal of Materials Chemistry 15(35-36) (2005) 3559-3592.
[103] J.C.B. Alcázar, R.M.J. Lemos, M.C.M. Conde, L.A. Chisini, M.M.S. Salas, B.S. Noremberg, F.V. da Motta, F.F. Demarco, S.B.C. Tarquinio, N.L.V. Carreño, Preparation, characterization, and biocompatibility of different metal oxide/PEG-based hybrid coating synthesized by sol–gel dip coating method for surface modification of titanium, Progress in Organic Coatings 130 (2019) 206-213.
[104] M. Masudi, A. Rahimi, R.P. Astaneh, Synthesis, Characterization, and Investigation of Inhibitor Release of the Anticorrosion Sol–Gel Hybrid Nanocomposite Coatings, Protection of Metals and Physical Chemistry of Surfaces 55(2) (2019) 363-370.
[105] Z.R. Zandi, L.A. ERSHAD, A. Rahimi, Synthesis and characterization of nano-composite hybrid coatings based on 3-glycidoxypropyl-trimethoxysilane and bisphenol A, (2005).
[106] M. Ochi, R. Takahashi, Phase structure and thermomechanical properties of primary and tertiary amine-cured epoxy/silica hybrids, Journal of Polymer Science Part B: Polymer Physics 39(11) (2001) 1071-1084.
[107] Y. Ma, L. Chen, Y. Ye, H. Wan, H. Zhou, J. Chen, Preparation and tribological behaviors of a novel organic-inorganic hybrid resin bonded solid lubricating coating cured by ultraviolet radiation, Progress in Organic Coatings 127 (2019)

348-358.
[108] S. Amiri, A. Rahimi, Hybrid nanocomposite coating by sol–gel method: A review, Iranian Polymer Journal 25(6) (2016) 559-577.
[109] C.L. Chiang, C.C.M. Ma, D.L. Wu, H.C. Kuan, Preparation, characterization, and properties of novolac-type phenolic/SiO_2 hybrid organic–inorganic nanocomposite materials by sol–gel method, Journal of Polymer Science Part A: Polymer Chemistry 41(7) (2003) 905-913.
[110] D. Balgude, A. Sabnis, Sol–gel derived hybrid coatings as an environment friendly surface treatment for corrosion protection of metals and their alloys, Journal of sol-gel science and technology 64(1) (2012) 124-134.
[111] X. Li, Z. Weng, W. Yuan, X. Luo, H.M. Wong, X. Liu, S. Wu, K.W.K. Yeung, Y. Zheng, P.K. Chu, Corrosion resistance of dicalcium phosphate dihydrate/poly(-lactic-co-glycolic acid) hybrid coating on AZ31 magnesium alloy, Corrosion Science 102 (2016) 209-221.
[112] F. Gao, C. Xu, H. Hu, Q. Wang, Y. Gao, H. Chen, Q. Guo, D. Chen, D. Eder, Biomimetic synthesis and characterization of hydroxyapatite/graphene oxide hybrid coating on Mg alloy with enhanced corrosion resistance, Materials Letters 138 (2015) 25-28.
[113] R.N. Peres, E.S.F. Cardoso, M.F. Montemor, H.G. de Melo, A.V. Benedetti, P.H. Suegama, Influence of the addition of SiO_2 nanoparticles to a hybrid coating applied on an AZ31 alloy for early corrosion protection, Surface and Coatings Technology 303 (2016) 372-384.
[114] S.V. Lamaka, M.F. Montemor, A.F. Galio, M.L. Zheludkevich, C. Trindade, L.F. Dick, M.G.S. Ferreira, Novel hybrid sol–gel coatings for corrosion protection of AZ31B magnesium alloy, Electrochimica Acta 53(14) (2008) 4773-4783.
[115] M. Zhang, S. Cai, S. Shen, G. Xu, Y. Li, R. Ling, X. Wu, In-situ defect repairing in hydroxyapatite/phytic acid hybrid coatings on AZ31 magnesium alloy by hydrothermal treatment, Journal of Alloys and Compounds 658 (2016) 649-656.
[116] M.-H. Kang, T.-S. Jang, H.-D. Jung, S.-M. Kim, H.-E. Kim, Y.-H. Koh, J. Song, Poly (ether imide)-silica hybrid coatings for tunable corrosion behavior and improved biocompatibility of magnesium implants, Biomedical Materials 11(3) (2016) 035003.
[117] F. Pan, X. Yang, D. Zhang, Chemical nature of phytic acid conversion coating on AZ61 magnesium alloy, Applied Surface Science 255(20) (2009) 8363-8371.
[118] D. Hawake, D. Albright, Metal Finishing, October l995 (1995) 34-38.
[119] H. Umehara, M. Takaya, Y. Kojima, An investigation of the structure and corrosion resistance of permanganate conversion coatings on AZ91D magnesium alloy, Materials Transactions 42(8) (2001) 1691-1699.
[120] M. Gonzalez-Nunez, P. Skeldon, G. Thompson, H. Karimzadeh, Kinetics of the development of a nonchromate conversion coating for magnesium alloys and magnesium-based metal matrix composites, Corrosion 55(12) (1999) 1136-1143.
[121] M. Gonzalez-Nunez, C. Nunez-Lopez, P. Skeldon, G. Thompson, H. Karimzadeh, P. Lyon, T. Wilks, A non-chromate conversion coating for magnesium alloys and magnesium-based metal matrix composites, Corrosion Science 37(11) (1995) 1763-1772.
[122] A. Simaranov, A. Marshakov, Y. Mikhailovskii, Formation of Conversion Coatings on Magnesium in Moderately Acidic Chromate Solutions, Zashch. Met. 25(5) (1989) 766-774.
[123] S. Ono, K. Asami, N. Masuko, Mechanism of chemical conversion coating film growth on magnesium and magnesium alloys, Materials transactions 42(7) (2001) 1225-1231.
[124] C. Lin, C. Lee, W. Li, Y. Chen, G. Fang, Formation of phosphate/permanganate conversion coating on AZ31 magnesium alloy, Journal of The Electrochemical Society 153(3) (2006) B90.
[125] W. Zhou, D. Shan, E.-H. Han, W. Ke, Structure and formation mechanism of phosphate conversion coating on die-cast AZ91D magnesium alloy, Corrosion Science 50(2) (2008) 329-337.
[126] Y. Song, D. Shan, R. Chen, F. Zhang, E.-H. Han, Biodegradable behaviors of AZ31 magnesium alloy in simulated body fluid, Materials Science and Engineering: C 29(3) (2009) 1039-1045.
[127] A.L. Rudd, C.B. Breslin, F. Mansfeld, The corrosion protection afforded by rare earth conversion coatings applied to magnesium, Corrosion Science 42(2) (2000) 275-288.
[128] M. Dabala, K. Brunelli, E. Napolitani, M. Magrini, Cerium-based chemical conversion coating on AZ63 magnesium alloy, Surface and Coatings Technology 172(2-3) (2003) 227-232.
[129] B.R. Fazal, S. Moon, Formation of cerium conversion coatings on AZ31 magnesium alloy, Korean Society of Surface Engineering 49(1) (2016) 1-13.
[130] Y. Xiang, W. Hu, X. Liu, C. Zhao, W. Ding, A study on surface state during the pretreatment of electroless nickel plating on magnesium alloys, Transactions of the IMF 79(1) (2001) 27-29.
[131] K. Brunelli, M. Dabalà, I. Calliari, M. Magrini, Effect of HCl pre-treatment on corrosion resistance of cerium-based conversion coatings on magnesium and magnesium alloys, Corrosion Science 47(4) (2005) 989-1000.
[132] M.F. Montemor, A.M. Simões, M.J. Carmezim, Characterization of rare-earth conversion films formed on the AZ31 magnesium alloy and its relation with corrosion protection, Applied Surface Science 253(16) (2007) 6922-6931.
[133] L. Li, J. Lei, S. Yu, Y. Tian, Q. Jiang, F. Pan, Formation and characterization of cerium conversion coatings on magnesium alloy, Journal of Rare Earths 26(3) (2008) 383-387.
[134] C. Lin, C. Changguo, W. Ningning, W. Jimin, D. Ling, Study of Cerium and Lanthanum Conversion Coatings on AZ63 Magnesium Alloy Surface, Rare Metal Materials and Engineering 44(2) (2015) 333-338.
[135] M. Laleh, F. Kargar, A.S. Rouhaghdam, Investigation of rare earth sealing of porous micro-arc oxidation coating formed on AZ91D magnesium alloy, Journal of Rare Earths 30(12) (2012) 1293-1297.
[136] M. Bazli, L. Bazli, R. Rahmani, S. Mansoor, M. Ahmadi, R. Pouriamanesh, Concrete filled FRP–PVC tubular columns used in the construction sector: A review, Journal of Composites and Compounds 2(4) (2020) 155-162.
[137] L. Bazli, M.H. Bagherian, M. Karrabi, F. Abbassi-Sourki, H. Azizi, Effect of starch ratio and compatibilization on the viscoelastic behavior of POE/starch blends, Journal of Applied Polymer Science 137(29) (2020) 48877.
[138] S.O. Omid, Z. Goudarzi, L.M. Kangarshahi, A. Mokhtarzade, F. Bahrami, Self-expanding stents based on shape memory alloys and shape memory polymers, Journal of Composites and Compounds 2(3) (2020) 92-98.
[139] P. Abasian, M. Radmansouri, M.H. Jouybari, M.V. Ghasemi, A. Mohammadi, M. Irani, F.S. Jazi, Incorporation of magnetic NaX zeolite/DOX into the PLA/chitosan nanofibers for sustained release of doxorubicin against carcinoma cells death in vitro, International journal of biological macromolecules 121 (2019) 398-406.
[140] L. Bazli, A. Khavandi, M.A. Boutorabi, M. Karrabi, Morphology and viscoelastic behavior of silicone rubber/EPDM/Cloisite 15A nanocomposites based on Maxwell model, Iranian Polymer Journal 25(11) (2016) 907-918.
[141] L. Bazli, A. Khavandi, M.A. Boutorabi, M. Karrabi, Correlation between viscoelastic behavior and morphology of nanocomposites based on SR/EPDM blends compatibilized by maleic anhydride, Polymer 113 (2017) 156-166.
[142] S. Pourhashem, F. Saba, J. Duan, A. Rashidi, F. Guan, E.G. Nezhad, B. Hou, Polymer/Inorganic Nanocomposite Coatings with Superior Corrosion Protection Performance: A Review, Journal of Industrial and Engineering Chemistry (2020).
[143] A. Uriondo, M. Esperon-Miguez, S. Perinpanayagam, The present and future of additive manufacturing in the aerospace sector: A review of important aspects, Proceedings of the Institution of Mechanical Engineers, Part G: Journal of Aerospace Engineering 229(11) (2015) 2132-2147.
[144] A. Kausar, A review of filled and pristine polycarbonate blends and their applications, Journal of Plastic Film & Sheeting 34(1) (2018) 60-97.
[145] M. Quaresimin, M. Salviato, M. Zappalorto, Strategies for the assessment of nanocomposite mechanical properties, Composites Part B: Engineering 43(5) (2012) 2290-2297.
[146] F. Awaja, S. Zhang, M. Tripathi, A. Nikiforov, N. Pugno, Cracks, microcracks and fracture in polymer structures: Formation, detection, autonomic repair, Progress in Materials Science 83 (2016) 536-573.
[147] A. Kausar, Corrosion prevention prospects of polymeric nanocomposites: A review, Journal of Plastic Film & Sheeting 35(2) (2019) 181-202.
[148] C. Min, P. Nie, W. Tu, C. Shen, X. Chen, H. Song, Preparation and tribological properties of polyimide/carbon sphere microcomposite films under seawater condition, Tribology International 90 (2015) 175-184.
[149] A.A. Nazeer, E. Al-Hetlani, M.O. Amin, T. Quiñones-Ruiz, I.K. Lednev, A poly(butyl methacrylate)/graphene oxide/TiO_2 nanocomposite coating with superior corrosion protection for AZ31 alloy in chloride solution, Chemical Engineering Journal 361 (2019) 485-498.
[150] F. Soleymani, R. Emadi, S. Sadeghzade, F. Tavangarian, Applying baghdadite/PCL/chitosan nanocomposite coating on AZ91 magnesium alloy to improve corrosion behavior, bioactivity, and biodegradability, Coatings 9(12) (2019) 789.
[151] K. Catt, H. Li, X.T. Cui, Poly (3,4-ethylenedioxythiophene) graphene oxide composite coatings for controlling magnesium implant corrosion, Acta Biomaterialia 48 (2017) 530-540.
[152] N. Rahimi Roshan, H. Hassannejad, A. Nouri, Corrosion and mechanical behaviour of biodegradable PLA-cellulose nanocomposite coating on AZ31 magnesium alloy, Surface Engineering (2020) 1-10.
[153] Y. Zhang, Y. Shao, T. Zhang, G. Meng, F. Wang, High corrosion protection of a polyaniline/organophilic montmorillonite coating for magnesium alloys, Progress in Organic Coatings 76(5) (2013) 804-811.
[154] B.-D. Hahn, D.-S. Park, J.-J. Choi, J. Ryu, W.-H. Yoon, J.-H. Choi, H.-E. Kim, S.-G. Kim, Aerosol deposition of hydroxyapatite–chitosan composite coat-

ings on biodegradable magnesium alloy, Surface and Coatings Technology 205(8) (2011) 3112-3118.
[155] I. Johnson, K. Akari, H. Liu, Nanostructured hydroxyapatite/poly(lactic-co-glycolic acid) composite coating for controlling magnesium degradation in simulated body fluid, Nanotechnology 24(37) (2013) 375103.
[156] Y. Wang, N. Yamada, J. Xu, J. Zhang, Q. Chen, Y. Ootani, Y. Higuchi, N. Ozawa, M.-I.D.B. Bouchet, J.M. Martin, Triboemission of hydrocarbon molecules from diamond-like carbon friction interface induces atomic-scale wear, Science advances 5(11) (2019) eaax9301.
[157] H. Yoshinaka, S. Inubushi, T. Wakita, T. Yokoya, Y. Muraoka, Formation of Q-carbon by adjusting sp3 content in diamond-like carbon films and laser energy density of pulsed laser annealing, Carbon 167 (2020) 504-511.
[158] Z. Ren, H. Qin, Y. Dong, G. Doll, C. Ye, A boron-doped diamond like carbon coating with high hardness and low friction coefficient, Wear 436 (2019) 203031.
[159] Y. Lei, J. Jiang, Y. Wang, T. Bi, L. Zhang, Structure evolution and stress transition in diamond-like carbon films by glancing angle deposition, Applied Surface Science 479 (2019) 12-19.
[160] A. Moreno-Bárcenas, J. Alvarado-Orozco, J.G. Carmona, G. Mondragón-Rodríguez, J. González-Hernández, A. García-García, Synergistic effect of plasma nitriding and bias voltage on the adhesion of diamond-like carbon coatings on M2 steel by PECVD, Surface and Coatings Technology 374 (2019) 327-337.
[161] N. Konkhunthot, P. Photongkam, P. Wongpanya, Improvement of thermal stability, adhesion strength and corrosion performance of diamond-like carbon films with titanium doping, Applied Surface Science 469 (2019) 471-486.
[162] C.A. Love, R.B. Cook, T.J. Harvey, P.A. Dearnley, R.J.K. Wood, Diamond like carbon coatings for potential application in biological implants—a review, Tribology International 63 (2013) 141-150.
[163] A. Mazare, A. Anghel, C. Surdu-Bob, G. Totea, I. Demetrescu, D. Ionita, Silver doped diamond-like carbon antibacterial and corrosion resistance coatings on titanium, Thin Solid Films 657 (2018) 16-23.
[164] G. Wu, W. Dai, H. Zheng, A. Wang, Improving wear resistance and corrosion resistance of AZ31 magnesium alloy by DLC/AlN/Al coating, Surface and Coatings Technology 205(7) (2010) 2067-2073.
[165] Y.L. Wei, L.L. Huang, L.J. Han, Y.S. Chen, Corrosion resistance and surface biocompatibility of diamond-like carbon coating on AZ31D magnesium alloy, International Journal of Surface Science and Engineering 10(2) (2016) 101-115.
[166] C.-M. Ning, X.-J. Cui, L.-L. Shang, Y.-J. Zhang, G.-A. Zhang, Structure and properties of different elements doped diamond-like carbon on micro-arc oxidation coated AZ31B Mg alloy, Diamond and Related Materials (2020) 107832.
[167] G. Wu, L. Sun, W. Dai, L. Song, A. Wang, Influence of interlayers on corrosion resistance of diamond-like carbon coating on magnesium alloy, Surface and Coatings Technology 204(14) (2010) 2193-2196.
[168] I. Masami, N. Setsuo, S. Tsutomu, C. Junho, Improvement of corrosion protection property of Mg-alloy by DLC and Si–DLC coatings with PBII technique and multi-target DC–RF magnetron sputtering, Nuclear Instruments and Methods in Physics Research Section B: Beam Interactions with Materials and Atoms 267(8) (2009) 1675-1679.
[169] Y. Uematsu, T. Kakiuchi, T. Teratani, Y. Harada, K. Tokaji, Improvement of corrosion fatigue strength of magnesium alloy by multilayer diamond-like carbon coatings, Surface and Coatings Technology 205(8) (2011) 2778-2784.
[170] N. Yamauchi, N. Ueda, A. Okamoto, T. Sone, M. Tsujikawa, S. Oki, DLC coating on Mg–Li alloy, Surface and Coatings Technology 201(9) (2007) 4913-4918.

Available online at www.jourcc.com

Journal homepage: www.JOURCC.com

Journal of Composites and Compounds

Nanodiamond-containing composites for tissue scaffolds and surgical implants: A review

*Yasamin Zamani[a], Ali Zareein[b], Leila Bazli[c], Reyhaneh NasrAzadani[d], Babar Pasha Mahammod[e], Shima Nasibi[f], Amir Modarresi Chahardehi[g]**

[a] *Department of Biology, Tehran Medical Sciences Branch, Islamic Azad University, Tehran, Iran*
[b] *Department of Biomedical Engineering, Tabriz Branch, Islamic Azad University, Tabriz, Iran*
[c] *School of Metallurgy and Materials Engineering, Iran University of Science and Technology, Tehran, Iran*
[d] *Department of Biomaterials Nanotechnology and Tissue engineering, School of Advanced Technology in Medicine, Isfahan University of Medical Sciences, Isfahan, Iran*
[e] *National Institute of Technology Warangal, Warangal, India*
[f] *Department of Materials Science and Engineering, School of Engineering, Shiraz University, Shiraz, Iran*
[g] *Integrative Medicine Cluster, Advanced Medical and Dental Institute, Universiti Sains Malaysia, Bertam, 13200, Kepala Batas, Penang, Malaysia*

A B S T R A C T

Due to promising properties such as low toxicity against different cell lines, being highly stable fluorescent without showing photobleaching, and good surface properties, nanodiamonds have gained ever-increasing attention for various biomedical applications including bioimaging and therapeutic applications. Various methods are used for the fabrication of nanostructured diamond, the commonly used of which is the denotation technique. Newer approaches are being practiced for the modification and functionalization of their surfaces by different biomolecules suitable for interaction with considered targets. In this review, the scope and recent advancement in the field of nanodiamonds for biomedical applications particularly their application for nanocomposite scaffold and implants are discussed.

Peer review under responsibility of jourcc

A R T I C L E I N F O R M A T I O N

Article history:
Received 4 November 2020
Received in revised form 15 December 2020
Accepted 24 December 2020

Keywords:
Nanodiamonds
Surface modification
Biomedical application
Nanocomposite scaffold
Implants

Table of contents

1. Introduction

Nanocarbons involve a diverse structural family, one of which is nanodiamonds (NDs). NDs can be found in the form of nano-sized diamondoids, fullerenes, amorphous carbon, foam, platelets, whiskers, bells, peapods, cones, rods, horns, onions, and tubes [1-4]. A detailed investigation of NDs was initiated in Russia in the 1960s. Since then, these nanoparticles have attracted significant attention because they can be produced on large scale by cost-effective processes based on the detonation process of carbon-containing explosives. Moreover, nanodi-

* *Corresponding author: Amir Modarresi Chahardehi; E-mail: amirmch@gmail.com*
https://doi.org/10.29252/jcc.2.4.6

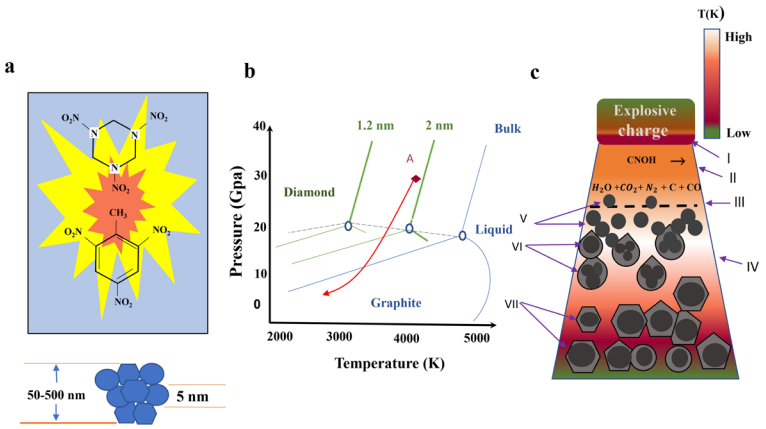

Fig. 1. Fabrication of nanodiamonds through detonation.

amonds are highly biocompatible, they can be easily functionalized like bioconjugation, and they have a small particle size of about 5 nm. A few products based on carbon nanomaterial such as derivatized fullerenes [5-8] or adamantane derivatives (e.g. memantine, amantadine, and rimantadine) have found ways to medicinal practice; however, ND suspensions have offered promising outcomes when used in animals and human patients suffering from cancer [9-12].

Similar to other nanoparticles such as metallic nanoparticles, carbon nanoparticles, and quantum dots, NDs can be used for the production of therapeutic agents for tissue scaffolds, anti-bacterial treatments, anti-viral treatments, gene therapy, delivery vehicles, diagnostic probes, as well as the preparation of new medical devices like nanorobots [13-19]. Moreover, the prospective exploitation of nanodiamonds can be applied for bioanalytical purposes including purification of proteins or biolabeling by the application of NDs with high fluorescence properties [20, 21]. The limitless potential of bio nanotechnology is demonstrated by the interaction of engineered nanostructured materials (e.g. ceramic, metallic, polymeric, and composite materials) at the molecular level which acts highly specific [22, 23] Nevertheless, the establishment of novel analytical methods, development of diverse nanofabrication approaches, and miniaturization of devices, e. g. BioMEMS is required for taking advantage of the advances of NDs in clinical trials [24-29].

This paper presents an overview of the processing and purification of nanodiamond particles, their properties, as well as their biomedical applications. In this review, the focus will be on the biological applications of NDs, especially in scaffolds and implants. Lastly, existing challenges and prospective directions in the development of NDs in biotechnology, engineering, and medicine will be discussed.

2. Nanodiamonds

At ambient pressure and temperature, the most stable allotrope of carbon is known to be graphite and diamond has a metastable state [30-32]. Besides the subtle difference in the energy state of graphite and diamond (0.02 eV), the energy barrier existing between the two phases is high (~0.4 eV per atom). Therefore, the transformation of the phases requires high pressure and temperature and/or catalyst [33, 34]. Due to the dependence of the Gibbs free energy on the surface energy, the cluster size should be included in the nanoscale carbon phase diagram in addition to temperature and pressure[35, 36]. Nanoscale diamonds consist of a core with sp^3 carbon structures together with disorder/defect and sp^2 carbon on the surface, which is available with single-digit nanoscale individual particles in colloidal suspension [37-39].

Diamond nanostructures in the size range of 1 to 100 nm are in the forms of pure-phase particles, 2-D diamond nanoplatelets, 1-D diamond nanorods, and diamond films. Ultra-nanocrystalline diamond (UNCD) is a special group of nanodiamonds with a size of a few nanometers, and their characteristics can be distinguished from other nanostructured diamonds with sizes larger than 10 nm [40-42]. In the 1960s, "detonation nanodiamond" (DND) or ultradispersed diamond" (UDD) with characteristic sizes of 4 to 5 nanometer were fabricated in the former USSR using detonation of carbon-containing explosives. At the end of the 1990s, Argon National Laboratory in the U. S. developed pure-phase UNCD films via chemical vapor deposition (CVD). Their characteristic grain sizes were between 2 to 5 nm [42-44].

Today, baffling nanodiamond arrays are available for investigations. Various methods have been developed for the fabrication of these nanomaterials including the detonation method (Fig. 1), high-energy ball milling of diamond microcrystals produced at high temperature and high pressure (HPHT) [45, 46], laser ablation [47], ultrasound cavitation [48], electron irradiation of carbon 'onions' [49], ion irradiation of graphite [50], chlorination of carbides [51], autoclave preparation from supercritical fluids [52], and chemical vapor deposition (CVD) with plasma assistance [53]. Among these techniques, the first three methods are employed commercially.

According to astronomical observations, the presence of NDs in the protoplanetary disks of some star types has been demonstrated [54, 55]. However, scientists are still investigating the origins of these cosmic sources. For using NDs for research and industrial applications, the large-scale production of nanodiamonds is needed. In this paper, we will review the production, modification, and applications of NDs, while concentrating on their application for tissue engineering.

3. Synthesis and purification of nanodiamonds

Carbon-containing explosives can provide a source of energy for the transformation of carbon to nanodiamonds (Fig. 1a) [34, 56, 57]. This method is eco-friendly and by using this technique, we can dispose of old munitions, like Composition B, while using other explosives might be possible. The detonation of explosives occurs in a closed chamber that is filled by water/ice coolant (wet synthesis) or an inert gas coolant (dry synthesis). Detonation soot that is used for naming the resultant products is composed of diamond particles in the range of 4 to 5 nm (~75 wt%) accompanied by other allotropes of carbon and impurities. Based on cooling media, the carbon yield is about 4 to 10 wt% of the explosive [56-59].

The mechanism of ND formation by detonation was proposed by Danilenko [34, 56]. The Jouguet point temperature and pressure (point

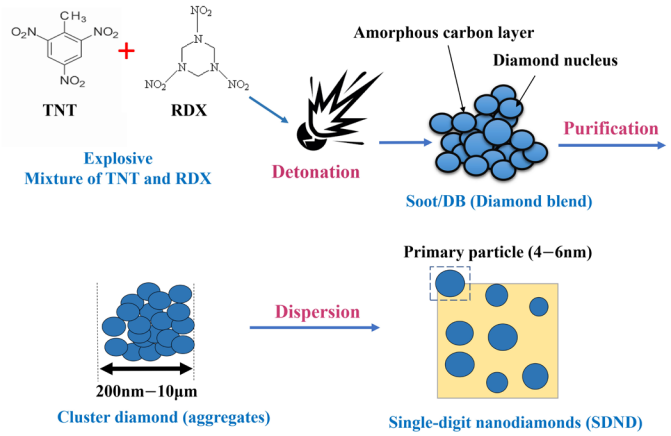

Fig. 2. Processing stages of NDs.

A in Fig. 1b) do not reach the point to form liquid bulk carbon, however, they are enough for the production of liquid carbon at the nanoscale (Fig. 1b). For nanocarbon, the liquid carbon region is shifted to lower temperatures, and there is a slight shift in the nanodiamond stability region to higher pressures (Fig. 1b). Therefore, the nucleation of NDs occurs by liquid carbon condensation and crystallization in the supersaturated carbon vapor (Fig. 1c). Other explosive-based methods, such as using waves for the production of NDs from graphite, fabricate NDs with crystallite sizes greater than 10 nanometers.

As mentioned, about 25–85 wt% of the detonation soot is graphitic carbon, and about 1–8 wt% of that is composed of incombustible impurities such as metals and oxides. Therefore, for most applications, it is required to be purified [57, 60]. The sources of the metallic impurities are the steel walls of the chamber (iron and other metals) where detonation occurs and the igniter that initiates detonation (typical azides of copper, lead, or silver). These impurities can be found on the outer surface of ND aggregates or inside them; hence, the aggregates must be disintegrated for the removal of the trapped impurities [61, 62].

For the removal of non-diamond carbon on an industrial scale, liquid oxidants such as HNO_3, $HClO_4$, H_2O_2/HNO_3 under pressure, Na_2O_2, KOH/KNO_3, $K_2Cr_2O_7$ in H_2SO_4, or a mixture of HNO_3 and H_2SO_4, are used for the purification of detonation soot [56, 57]. To reduce the concentration of non-carbon impurities to less than 0.5 wt%, further exposure to HCl and other treatments are carried out. Using a liquid phase for purification is hazardous and expensive so that 40% of the product cost is contributed to this process. An alternative environmentally-friendly approach for the removal of non-diamond carbon is its oxidation by air or ozone-enriched air at a high temperature [60, 63]. Oxidizing in the air is an eco-friendly, robust, and cost-effective purification method, which can change the content of diamond from ~25 wt% to more than 95 wt%. Because of oxidation, different presented functional groups are removed from the surface of NDs, and oxygen-containing surface functional groups, mainly carboxylic acids and anhydrides are produced. Consequently, different nanodiamond grades can be converted to materials that contain a high diamond content with unified surface chemistry [3, 60].

In comparison with the acid-purified NDs, the aggregate size of ozone-purified ones in aqueous dispersions is about 160-180 nm and a higher amount of faceted particles in the range of 3 to 5 nm is produced [63, 64]. Moreover, due to highly acidic surface groups in the hydrosols purified by ozone, their pH is very low; for instance, the pH value for 10 wt% hydrosol is between 1.6 and 2. Additionally, the electrokinetic potential (ζ-potential) varies from -50 mV for polydispersed specimens to -100 mV for the fraction with the size of 20-30 nm and the potential remains constant between the pH values of 2 to 12. Thus, the most promising technique for the purification of NDs is gas oxidation. The reduction of surface in a hydrogen atmosphere has been practiced, however, the removal of non-diamond carbon was not complete [65].

4. Surface modification and de-agglomeration of nanodiamonds

Commercial NDs are often required to undergo further processing and modification. This is due to their high content of non-diamond carbon and incombustible impurities, the large average size of aggregates, and unsuitable surface chemistry for proposed applications [19, 66, 67].

Even though the diameter of NDs is between 4 to 5 nm, there is a tendency to aggregation in the particles and the size of the aggregates is larger in common commercial ND suspensions, which are sometimes resistant to ultrasonic treatment. Even though the presence of the aggregates could be beneficial for some application such as drug delivery [68] or chromatography [69], de-aggregation of the particles into individual primary ones are often required for exploiting the advantages of NDs [70].

Osawa et al. [71] developed a microbead (SiO_2 or ZrO_2)-assisted ultrasonic de-aggregation process using the suspension of NDs, which was reported to be able to yield individual ND colloidal solutions with diameters of 4-5 nm. Using microbeads bring about some complications, mainly contamination with bead material and the graphite layer that forms on the surfaces of nanodiamonds [72]. It is also required to remove metal contaminants and amorphous carbon that was released from the aggregates during milling. On the other hand, the re-aggregation of the particles occurs during the purification of milled diamonds with the help of liquid oxidizers [72]. According to recent studies, sufficiently purified and oxidized particles in the air are allowed for subsequent isolation of stable hydrosol nanoparticles with a diameter of 4-5 nm by centrifugation [73].

Recently, the de-aggregation of particles from microscale aggregates to stable nanoparticles with a diameter in the range of 5-20 nm has been practiced by dry milling in cheap and abundant media like sugar and water-soluble salts. These media do not produce contaminants [74]. The reduction of NDs in borane with the help of ultrasonic treatment was reported to yield finer aggregates [75]. Aggregates with a diameter of ~20 nm were also obtained with surface graphitization and subsequent functionalization [76]. Nanodiamond aqueous colloids containing stable single particles were also obtained by hydrogen treatment at high temperatures and the nanoparticles with the size of 2-4 nm were isolated using a centrifugation process at above 10,000 rpm [77, 78].

Re-aggregation of NDs after additional surface functionalization is a concern regarding the processing of nanodiamonds. Because of capil-

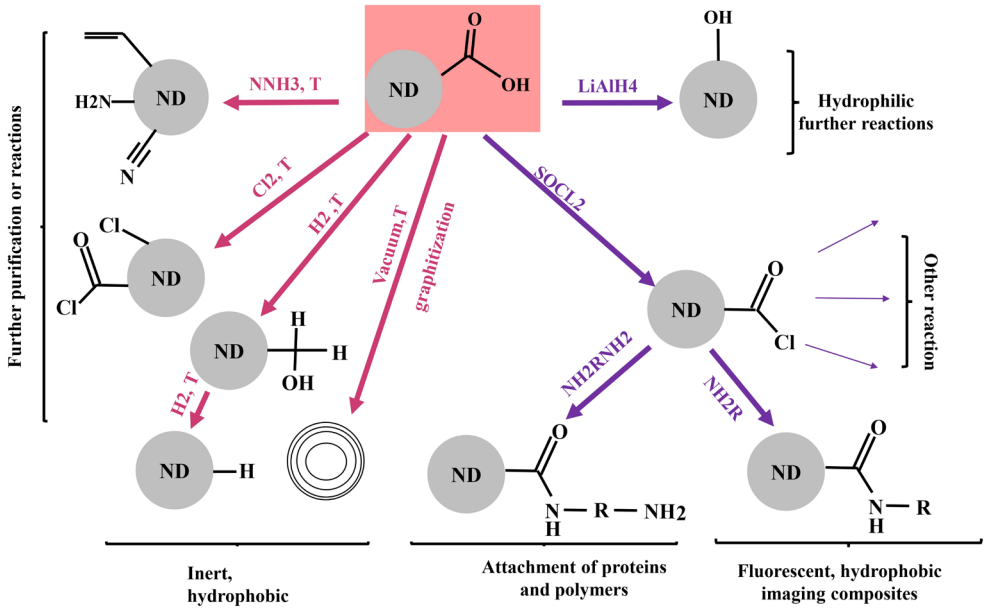

Fig. 3. Surface modification of NDs.

lary forces that attract the particles together, re-aggregation may also be promoted by drying (for storage). It could be caused by attractive van der Waals forces, which make the functionalization an arduous task. An approach for the prevention of re-aggregation after drying is the treatment of NDs in NaCl solution with the assistance of ultrasound [61, 79]. The prevention results from the attachment of Na^+ ions to the surfaces of NDs. Halting re-aggregation of NDs fabricated via NaCl-assisted milling can also be explained by this reason [74].

NDs can be separated into fractions by their size and weight using centrifugation [80, 81]. Unlike methods that introduce contamination (e.g. bead milling), centrifugation is contamination-free and ND fractions (different sizes) are possible to be isolated suitable for various applications. For instance, only small particles can be used for drug delivery, while NDs that can form photonic structures for light diffraction are required to have aggregate sizes above 100 nm [82]. Obtaining small NDs by centrifugation is economically feasible when NDs purified by air or ozone are used rather than acid-purified NDs. This is because of a higher fraction of fine aggregates achieved by the former approaches. Although single-digit NDs can be extracted by ultracentrifugation, the yield is low. Therefore, the dispersion of NDs into individual particles requires the development of facile, scalable, and non-contaminating techniques. The processing of NDs from synthesis to de-aggregation is illustrated in Fig. 2.

NDs are superior to carbon nanotubes (CNTs) and other graphite-based nanoparticles in terms of the possibility to attach various functional groups to their surfaces [44]. This capability not only provides complex surface functionalizations but also preserves the promising characteristics of the diamond core [83]. Nevertheless, understanding their interaction mechanism with their surrounding materials and the alleviation of adverse effects such as aggregation is essential [84, 85]. The different functional groups that exist on the surface of commercial NDs can be utilized for covalent functionalization; however, starting with carboxylated NDs prepared by ozone and air purification methods, and then making use of the COOH groups' rich chemistry is more convenient. As a result of the hydrogen microwave chemical vapor deposition plasma treatment at temperatures higher than 700 °C, COOH groups are completely removed and hydrogenated NDs are produced by the complete removal of oxygen from the surface [86].

In comparison with gas treatments in the temperature range of 400-850 °C, milder conditions are required for wet chemistry. An enhanced selectivity is provided by this approach through the conversion of plenty of functional groups known in organic chemistry (Fig. 3). In several wet chemical reactions, reactive C–Cl and C–F bonds on the surface generated by photochemical chlorination and halogen annealing have also been used [87, 88]. Long alkyl chain terminations were produced on the surface of NDs by esterification of O-H terminations with acylchlorides [89]. O-H terminates are also involved in silanization/de-aggregation [90]. Also, the modification of NDs by taking advantage of the graphitic carbon chemistry can be performed. Graphite carbon can be either intrinsically present or formed by surface graphitization. Strong bonds of C–C can be formed between the surface group and the graphitic shell, while C–X bonds (where X is S, O, N, etc.) are created by methods that work based on the chemistry of ND functional groups [91, 92].

Diazonium chemistry and Diels–Alder reactions have been used for the functionalization of nanodiamond graphitic shells. Diazonium chemistry has been utilized with hydroxylated nanodiamond for the production of C–O–C bonds between the diamond core and the attached moiety, and also with hydrogenated NDs for the C–C bond formation [93]. Even though there are different options for surface functionalization of NDs, the uniformity and purity of the starting materials surface chemistry strongly affect the outcome [94, 95]. The development of quantitative analysis for the evaluation of different groups present on the surface of NDs is a challenge in this regard.

5. Properties of nanodiamond

5.1. Fluorescence

The promising fluorescence properties of NDs results from nitrogen atoms next to a vacancy called nitrogen-vacancy (NV) centers in NDs. To create NV centers, NDs are irradiated with high-energy particles such as protons, electrons, and helium ions, and then vacuum annealed at 600-800 °C [96, 97]. During irradiation, vacancies are formed in the diamond structure, and the annealing treatment leads to the migration of the vacancies and their entrapment by N atoms present in NDs [98]. Different spectra are emitted based on the NV center types that would be either negatively charged (NV^-) or neutral (NV^0). The spin ground state of $S = 1$ of NV^- centers provide the possibility of spin polarization by

optical pumping and manipulation through electron paramagnetic resonance. Additionally, NV^- centers possess long spin coherence times. In isotopically clean diamonds, fluorescent NV centers have been favored for quantum computing [99], while in NDs, NV centers are being studied for biomedical imaging [96], high-resolution magnetic sensing [100-102], and fluorescence resonance energy transfer applications [103].

Diamond synthesized at high temperatures and high pressures contain about hundreds of ppm of native substitutional nitrogen and thereby they are the candidate for developing bright photoluminescent [45, 96]. These materials are then ground to nanoparticles containing single-digit NDs [45]. The concentration of electron-irradiation-generated fluorescent NV defects is not significantly affected by the nanocrystal size; however, the produced fraction of NV-defects is reduced with the decrease in the nanodiamond size due to electron traps at the surface [104].

With the help of medical imaging, it is possible to detect and diagnose a variety of diseases, and thereby the healthcare industry is seeking innovations in the imaging field [105-108]. Up to now, NDs fabricated by explosives have not been considered as promising materials for NV-center-based imaging applications. In recent years, individual pristine NDs with a diameter of 5 nm synthesized by the detonation of TNT and hexogen precursors have shown NV-center-based intermittent luminescence [102]. Additionally, larger NDs (above 20 nm) with trapped NV centers fabricated by graphite and hexogen [109] and TNT and hexogen [110] precursors have exhibited stable luminescence. Doping of nitrogen into the ND core and the *in situ* creation of NV centers are influenced by numerous factors including the cooling conditions and the nitrogen amount in the precursors. The reasons for the low intensity of fluorescence in NDs synthesized from explosives are the existence of internal defects and the proximity of surface defects dependent on their size [102, 109].

Adsorbing [111] or linking [66, 112] of different fluorophores onto NDs can also produce fluorescent particles. NDs with fluorophore linkage can move through cellular sections with varying pH values without changing cell viability or causing degradation of fluorophore linked to the surface over a long period [113]. Octadecylamine was linked to carboxylic groups on the surfaces of NDs and thus, bright blue fluorescent NDs were formed [114]. Not only do fluorescent NDs benefit from the promising properties of semiconductor quantum dots, namely, high photostability, small size, and bright multicolor fluorescence, but also they show rich surface chemistry, biocompatibility, and non-toxicity. These properties would probably revolutionize *in vivo* imaging [96, 115, 116].

Zhang et al. [117] prepared the multimodal nanodiamonds by attaching monoclonal antibodies and drug-oligonucleotide conjugates labeled by fluorescent onto the surface of ND. They reported that by these linkers, it is possible to quantify the ND conjugates and observe intercellular regions. Dong et al. [118] prepared fluorescent nanodiamond-based composites by a simple and novel method. The hydrophilic polymer/ functionalized ND composite was reported to be suitable for different biomedical applications because of their good potential and physicochemical properties. Also, they reported that these samples have strong fluorescence intensity, low toxicity, and high water dispersibility. According to the result of cell uptakes, the cells could internalize the fluorescent nanodiamond-based composites. Sarkar et al. [119] used a new background-free imaging method and reported that this technique enhances the ratio of signal-to-background up to 100 times. Also, an improvement was observed in the fluorescent nanodiamond imaging capabilities on diverse fluorescence imaging platforms.

5.2. Biocompatibility

Although glassy carbon and diamond are not toxic, carbon nanoparticles cannot be assumed also non-toxic. Because of a variety of processes for purification and different options for surface modification used by various manufacturers, the toxicity caused by NDs is a concern [120-122]. *In vitro* and *in vivo* properties such as gene program activity, cell viability, and *in vivo* physiological and mechanistic behavior in the presence of NDs have been investigated [66, 120, 123-127].

Researchers demonstrated that instilled NDs within the trachea had a low level of pulmonary toxicity. The ND amount decreased with time in the alveolar region. Moreover, after 28 days after exposure, ND-burdened macrophages were observed in the bronchia [9, 125, 128, 129]. Systemic toxicity and serum indicators of the liver were not affected by using high dosages of intravenously administered ND complexes [127].

Mohan et al [126] studied worm reproduction, cytotoxicity, and stress response activity of fluorescent NDs with an average hydrodynamic size of about 120 nanometers in *Caenorhabditis elegans* worm. They reported that bare ND particles remained in the lumen of the worm, while NDs coated with bovine serum albumin or dextran were adsorbed into its intestinal cells. Transferring NDs injected into worm gonads to the larvae and offspring was observed, however, this did not affect the survival or reproductivity of the worms. It was also indicated that fluorescent NDs are non-toxic and do not cause stress in the worm, thus, they are suitable for *in vivo* imaging. Overall, the biocompatibility and toxicity of newly developed NDs should be carefully investigated.

6. General applications

ND additives have been utilized for metal plating (electrolytic/electroless) for a long time [130, 131]. In recent years, these particles have found ways to other applications. In this section, different applications of NDs are addressed.

Tribology and lubrication: Adding detonation soot containing diamond to lubricants causes about 5% reduction in fuel consumption and prolongs the engine life [130]. Two reasons contribute to this effect: 1) the existing graphite has a lubrication effect: 2) friction is reduced on sliding surfaces by NDs through polishing away asperities. The enhancement in tribological performance is provided when purified NDs are dispersed alone or together with metal nanoparticles or polytetrafluoroethylene (PTFE) in oils or greases [132]. The initial assumption about the lubrication mechanism was acting as 'ball bearings', however, recent studies suggested different contributing mechanisms. For instance, the wear mechanism for Al alloys is significantly affected by the viscosity of the ND suspension, while a decrease in wear and friction of carbon steel is the result of the embedment of NDs from the lubricant into the surface of the carbon steel [114]. It is possible to tailor the surface chemistry of NDs so that they can be dispersed in various systems such as water and oil [133].

Because of the microscopic ball-bearing effect, carbon onions can offer an efficient lubrication effect. Generally, in contrast to expectations, the lubrication mechanism is more complex, but it can be accepted that both carbon onions and NDs embed into the surfaces of metals and thereby leading to the separation of sliding surfaces and prevention of wear resulting from metal-metal adhesion [134, 135].

Nanocomposites: Nanocomposites have shown promising properties suitable for a variety of applications [136-139]. NDs have been suggested as excellent fillers for composites owing to their rich surface chemistry, and good thermal and mechanical characteristics. Also, the fillers can tailor these composites for biomedical applications due to the diamond core's chemical stability and biocompatibility. It has been reported that the ND addition to polymers caused the enhancement of their thermal conductivity [140, 141], electromagnetic shielding [142], adhesion [143], wear resistance [144], and mechanical strength [47, 141, 145-148]. On the other hand, in the case of using aggregated or non-purified NDs, degradation in properties has been observed, which confirms the necessity of proper functionalization and well dispersion

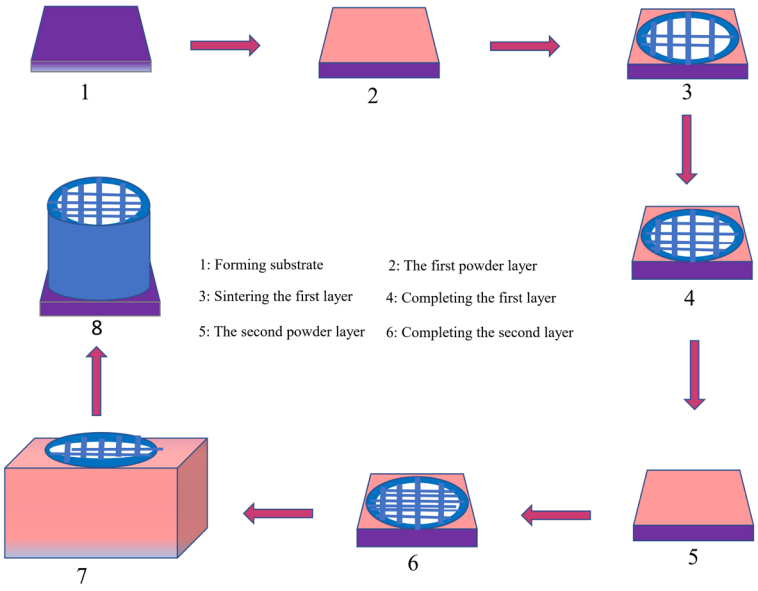

Fig. 4. Schematic illustration of the selective laser sintering method.

of these particles.

The addition of small amounts of NDs to transparent poly(vinyl alcohol) showed improved mechanical properties [149]. Surface chemistry can control the interfacial interaction between the matrix and NDs as well as their dispersion in the matrix. If NDs are modified, they can covalently bond with metal, ceramic, polymeric matrices, and further enhancement can be provided for composites [146, 150, 151].

Drug delivery: A drug delivery system is required to have some properties including scalability, dispersibility in water, the capability of carrying various therapeutics, and biocompatibility [152-156]. Another important property is the targeted therapy potential combined with imaging possibility. Most of these requirements are met by NDs [157-161].

Delivery of doxorubicin (Dox) by ND-based systems has been shown to be safe and effective [162-164]. ND-Dox complexes were utilized for the treatment of liver cancer (LT2-M) and breast cancer (4T1) models. The application of ND-Dox complexes increased the circulation half-time to 10 times of unmodified doxorubicin, and the doxorubicin expelling capacity of tumors decreased. Other benefits of drug delivery systems based on ND-Dox are reported to be a noticeable decrease in the tumor size, the absence of myelosuppression, and the absence of mortality in the case of high delivery doses [123, 165, 166]. Besides, delivering small molecules polyethyleneimine 800 (PEI800)-coated NDs were investigated for the delivery of nucleic acids. Different loadings have been delivered by NDs such as siRNA for specific cancers [158], small molecules in acidic environment [3], proteins [3, 157], and covalently bonded drugs [167, 168].

The functional groups are present on the surface of ND, especially oxygenated moieties including hydroxyl, ether, ketone, lactone, carboxylic acid. ND is a widely applicable nanocrystalline due to its structural stability, natural biocompatibility, and non-toxic nature. According to previous works, ND has a role as a drug carrier of dexamethasone, 4-hydroxytamoxifen, purvalanol A, and doxorubicin for blood cancer, breast cancer, liver cancer, and colon cancer therapies, respectively [169].

Protein mimics: Owing to promising properties such as low cytotoxicity, ability to self-assemble, rich surface chemistry, stable core, and small size, NDs are being used for mimicking globular proteins [170, 171]. Besides the ability to deliver drugs, other molecules such as genetic material can be delivered across cellular membranes. NDs are also able to mimic other functions of proteins. For instance, proteins that are involved in the folding/unfolding of DNA are highly alkaline histones. During this process, a nucleosome that contains histones in its core, spool the DNA strand around itself. NDs not only can be increased close to the size of histones by selective air oxidation [172] but also by employing covalent bonding of amino groups, their surface alkalization is possible [146]. The alkaline NDs can then be folded with DNA to form artificial nucleosomes. Functionalized NDs can also mimic some proteins' enzymatic functions due to their catalytic properties [173].

Tissue scaffolds and surgical implants: Due to the restoring potential for damaged tissue, regenerative medicine, and tissue engineering are of great interest [174-177]. Like protein-coated materials, ND monolayers have been indicated to act as a suitable platform for the growth of neuronal cells [178]. Reinforcement of biodegradable polymers with NDs provides prospective advantages for the synthesis of multifunctional tissue engineering scaffolds due to their biocompatibility, superior mechanical properties, delivering biologically active molecules and drugs, and tunable surface chemistry [179]. One of the ND-containing polymer composites studied for biomedical applications is ND octadecylamine (ODA)-poly (l-lactic acid) (PLLA). PLLA is a biodegradable and biocompatible polymer, however, its mechanical properties cannot satisfy the requirements for load-bearing implants. It has been reported that the incorporation of ND-ODA and its good dispersion enhanced Young's modulus and hardness of the composites close to those obtained for human cortical bone. Also, no changes in proliferation and morphology of murine 7F2 osteoblast cells cultured on the ND-ODA-PLLA scaffold were observed. Therefore, clinically relevant properties are obtained by these composites while offering high scalability and non-toxicity [123, 179-181]. The remarkable enhancement of properties caused by the addition of NDs could suggest these materials to be used in a wider range of biomaterials.

7. Scaffolds based on nanodiamond composites

7.1. Fabrication methods

Selective laser sintering (SLS): In this method, polymer/ND powders first are poured on a workbench, and then the powders are sintered selectively by laser-based layer-by-layer sintering following a pre-designed scaffold model. At the final step, the sintered scaffold is achieved by removing the residual powder [67]. This process is schematically illustrated in Fig. 4.

Feng et al. [182] synthesized poly(3-hydroxybutyrate-co-3-hydroxyvalerate) PHBV/ND, PHBV/MoS_2, and PHBV/ND/MoS_2 composite

powders via a solution mixing technique. Selective laser sintering with laser power of 2 W, scanning speed of 200 mm/s, and a spot diameter of 50 μm was used for the fabrication of cylindrical scaffolds with a height of 10 mm and a diameter of 8 mm. PLLA/ND composite scaffolds were also prepared by Shuai et al. [67] using the selective laser sintering method.

Electrospinning: This technique is a facile, efficient, fast, and cost-effective route for the production of nanofibers from a polymeric melt or solution via applying electrostatic forces [183, 184]**.** This method is used for the fabrication of fibrous polymeric scaffolds [185, 186]. In this technique, ND particles are dispersed in a polymer solution, and then the polymeric solutions are loaded into a syringe equipped with a metallic needle. The electric potential is applied to the metallic needle and aluminum foil is used to collect the as-spun nanofibers. The parameters that contribute to the electrospinning method are temperature, feed rate, polymer concentration, voltage, and distance between the collector and needle [179, 187, 188]. The synthesis of poly (lactic-co-glycolic acid)/nanodiamond (PLGA-ND) composite was reported using the electrospinning of a dimethylformamide and methylene chloride solution. In comparison with pure PLGA fibers, PLGA-ND fibers were noticeably thicker. The results demonstrated that cell spreading of human mesenchymal stem cells (hMSCs) improved compared to pure PLGA. This is due to the presence of oxygen termination of NDs that provides hydrophilicity in ND-containing scaffolds [189, 190]. Houshyar et al. [187] performed wound healing dresses based on polycaprolactone (PCL) and ND using electrospinning. Enhanced moisture and wicking management in NDs results from different hydrophilic groups on their surfaces. Furthermore, excellent cellular activities and no cytotoxicity were exhibited by the composites**.**

In-situ polymerization: ND nanocomposite scaffolds can be prepared by in-situ polymerization. ND particles are usually functionalized and the nanodispersion is added to a monomer-containing solution. Finally, self-assembly and polymerization of monomers occur in the presence of functionalized ND [179, 191]. Alishiri et al. [192] polymerized acrylate-terminated polyurethane-acrylate diluents (APUA) in the presence of 2- hydroxyethyl methacrylate (HEMA)-grafted ND. This method led NDs to well dispersion in APUA resulting in the enhancement of mechanical properties. Ultra-high molecular weight polyethylene (UHMWPE)/ND nanocomposites were also successfully synthesized by in-situ polymerization based on bi-supported Ziegler-Natta catalyst. The results showed that the mechanical properties of both silane-modified and unmodified NDs were improved [193].

Solvent casting: Due to the solubility of biopolymers in various solvents, solvent casting has been considered as a facile and commonly used technique for biopolymer film synthesis. Solubilization, casting, and drying are the steps that are involved in this approach [167]. For the preparation of ND-containing nanocomposites by solvent casting, nanodiamonds are first ultrasonically dispersed in a solution. The polymer then is added to the prepared solution; afterward, the mixture is poured on a glass substrate or in a mold followed by the complete evaporation of the solvent [194].

Maitra et al. [195] incorporated acid purified ND in a PVA film to improve the mechanical properties of the polymer for applications in broader biomedical areas [196]. Fox et al. [148] also used the solvent casting method to reinforce the polycaprolactone (PCL) film with fluorescent ND. In this regard, a mixture of PCL and fluorescent ND in methanol was prepared followed by casting for the production of free-standing films. Sun et al. [144] synthesized chitosan and ND-COOH composite films by using a solvent of acetic acid. The results showed the improvement of mechanical properties owing to a strong interaction between chitosan polymer chains and carboxyl groups of ND. Zhang et al. [123] added ODA-grafted ND to a mixture of chloroform and PLLA and showed that the addition of nanodiamonds enhanced Young's modulus and hardness of PLLA.

The preparation of nanocomposites by solvent casting is a suitable method; however, selecting an appropriate solvent that can dissolve both ND particles and polymer would be a critical issue affecting ND aggregation. Thus, the functionalization of ND is necessary in most cases to achieve uniform distribution in polymeric films [197, 198].

7.2. Nanocomposite scaffolds and implants

ND-containing composite scaffolds are gaining increasing attention for biomedical research and applications. Shuai et al. [67] modified ND by phospholipid and incorporated the modified particles in PLLA scaffolds using selective laser sintering. The hydrophilic head (–OH) of phospholipid was adsorbed on ND surfaces (–COOH), while its hydrophobic tails were arranged toward the polymeric PLLA matrix. Therefore, a layer of phospholipid covered ND particles. Because of the repulsive force between the hydrophobic tails, phospholipids are forced away from each other leading to better dispersion of NDs in the PLLA matrix. Compared to unmodified scaffolds, phospholipid-modified composite scaffolds showed an increase in Vickers hardness, the compressive modulus, and compressive strength by 88.2%, 163.2%, and 162.8%, respectively. It was reported that the prepared scaffolds acted as a proper platform for cell adhesion, growth, and migration, indicating their potential for bone tissue engineering.

Houshyar et al. [187] used the electrospinning technique for the fabrication of PCL/ND nanofibrous scaffolds. It was proposed that the scaffolds possessed the requirements for wound healing including the restriction of microbial activities and the promotion of epithelial cell proliferation. The outcomes of adding ND to PCL were a delay in the scaffolds' thermal degradation, better moisture management, and higher thermal stability. The proliferation of Chinese hamster ovarian (CHO) cells for PCL-5%ND after 1, 3, and 7 incubation days exhibited 43%, 38%, and 22% enhancement. Also, microbial activity decreased with the increase in the ND content. Fox et al. [177] also reported the synthesis of PCL/ND composites by the solvent casting method. The results demonstrated that hydrophilicity and surface roughness of the ND-PCL composite films were higher than those of PCL alone. Moreover, their degradation was slightly enhanced and the tensile strength decreased. Osteoblast adhesion increased with an increase in the ND loading. Finally, a 3D composites scaffold was produced by extrusion revealing the promising potential for tissue regeneration.

Apicella et al. [199] fabricated bio-mechanical scaffolds based on ND and poly (hydroxy-ethyl-methacrylate) hydrophilic matrix for tissue engineering. The hybrid material was reported to be potent for biomimetic, osteoinductive, and osteoconductive applications as biomechanical bones. Owing to the enhanced mechanical strength, these hybrid materials can be a replacement for traditional hydrogels with lower mechanical properties for bone regeneration; they can also be used as coatings onto metal trabecular scaffolds. Recreation of micro-and macro-distribution of bone deformations and stresses occur in osteoinductive ceramic/polymer-coated micro-trabecular metal scaffolds.

Nunes-Pereira et al. [143] used solvent casting to add different types of ND into Poly (vinylidene fluoride) (PVDF). According to the results, the thermodynamic stability as well as the optical properties of the samples could be tailored by the addition of ND nanofillers. Also, the dielectric losses of the nanocomposites remained constant, and the dielectric constant increased while was independent of the filler concentration. Moreover, ND nanoparticles were found to be non-toxic. It was concluded that the prepared nanocomposites were promising material for biomedical applications owing to cell culture properties of the polymer and nanodiamond potential for drug delivery and protein functionalization.

Feng et al. [182] embedded ND particles into MoS_2 nanosheets and

Table 1.
ND-containing composites for scaffolds and implants

Matrix	ND size (nm)	Functionalization	Fabrication method	Cell type	Conclusion	Ref.
PCL	45	-	Solvent Casting	Human osteoblasts	Incorporation of ND resulted in increased hydrophilicity and tailored degradation of the composites compared to base PCL No cytotoxicity	[177]
PCL	-	Acid treatment+octadecylamine	Electrospinning	Human lens epithelial (HLE)	Tensile Strength of FND/PCL composites increased compared to pure PCL No cytotoxicity	[151]
PVDF	<10	-	Solvent casting	MC3T3-E1 pre-osteoblast cells	No toxicity	[143]
PLGA	-	-	Electrospinning	Human mesenchymal stromal cells (hMSCs)	PLGA-ND membranes exhibited higher hardness and Young's modulus. No cytotoxicity	[189]
PVDF/bioglass scaffold	5–10	-	Selective laser sintering	MG 63 cells	Tensile strength of the scaffolds increased by 23.01% Bioactivity of the samples increased Improved osteoinductive properties	[201]
Chitosan	5	Acid treatment	Solvent casting	Cell wall of fungi	Addition of 1 wt % nanodiamond improved the young's modulus and hardness of the composites by 239% and 69% respectively.	[144]
PCL	<10	-	Electrospinning	CHO	The surface energy of the PCL-ND composite increased by the addition of ND which resulted in better moisture management, proliferation, and cell attachments. No cytotoxicity More thermal stability Increased crystallization temperature	[187]
Polydiallyldimethylammonium chloride (PDDA)	4	-	Coating of NDs using Polyelectrolyte multilayers (PEMs)	Human fetal osteoblasts (hFOBs)	Cell Viability increased by 40% Increased cell adhesion Feasibility of NDs as a coating material for biomedical applications and drug delivery vehicles.	[202]
Magnesium	<10	-	Powder metallurgy	Fibroblast (L-929)	The corrosion resistance of the MG-5ND composites increased by 4.5% compared to pure Mg Biocompatible and No Cytotoxicity	[203]
PLLA	5	-	Solution casting followed by compression molding	-	10 wt% of ND-ODA led to an increase in the strain to failure by 280% and an increase in fracture energy by 310% in comparison to pure PLLA. Bonelike apatite is formed on the ND-ODA/PLLA scaffolds when tested in SBF Solution, which may increase the osteoinductive properties.	[204]
PCL	-		Electrospinning	NIH/3 T3 cells	The addition of 1 wt% of ND resulted in increased young's modulus, Tensile Strength, and percentage elongation to break. High cell proliferation rate for 1 wt% ND/PCL No cytotoxicity	[205]
Poly(lactic acid) (PLA)	<10	-	Electrospinning	-	Incorporation of 1 wt % nanodiamond in PLA improved the tensile strength and young's modulus of the composites by 239% and 161% respectively.	[161]
Poly (L-lactide-co-e-caprolactone) (poly(LLA-co-CL))		-	Anionic polymerization	stem cell line UE7T-13	Young's modulus of 10 wt% composites increased by 6 times. Biocompatible and no cytotoxicity for all contents (i.e. 1, 5, 10, 50 wt%)	[206]
APU	-	Quaternary ammonium	In-situ polymerization	MC3T3-E1 cells	Improved mechanical properties Hydrophilicity increased by incorporation of NDs Crystallinity improved which resulted in tailored degradation rates No cytotoxicity	[200]
Gelatin	-	-	Electrospinning	Human adipose-derived stem cells (hASCs)	Enhanced cell viability and proliferation Increased scaffold stiffness No cytotoxicity	[207]

then the co-dispersion nanostructure was added to poly(3-hydroxybutyrate-co-3-hydroxyvalerate) (PHBV) by selective laser sintering to produce scaffolds for bone regeneration. The restacking of the molybdenum oxide nanosheets was restrained by the placement of NDs between adjacent nanosheets. Additionally, the aggregation of NDs was prevented by the steric hindrance effect of the MoS_2 nanosheets. Consequently, the compressive and tensile strengths of scaffolds containing ND and MoS_2 were increased by 52% and 94%, respectively. The mechanisms that contribute to the strengthening of the scaffolds include crack pinning, crack bridging, crack deflection, as well as pulling out of ND particles and MoS_2 nanosheets. Moreover, the scaffolds showed good cell viability.

Wang et al. [200] added polycation-modified ND loaded with Ag to acrylate-terminated polyurethanes (APU) for cartilage tissue implants using in-situ polymerization. The results indicated that the crystallinity of the nanocomposites increased compared to pure APU, showing a strong interaction between APU and nanodiamonds. Release-killing of the Ag nanoparticles and contact-killing of cationic polymers resulted in excellent antibacterial activity of the nanocomposites. Additionally, the addition of polyethylene glycol to APU increased its degradability rates significantly. Moreover, the synthesized scaffolds showed low toxicity. Overall, the combined effects of hydrophilicity and crystallinity provided proper degradation rates for APU, which was reported to be adaptable to the cartilage tissue-healing rate. Some research studies focusing on the development of ND-containing composites for scaffolds and implants have been summarized in Table 1.

Table 1. ND-containing composites for scaffolds and implants

8. Conclusions and Future insights

NDs have shown all the ideal properties needed for biomedical applications. Many research activities in various biomedical applications have focused on the application of nanodiamonds. However, some challenges should be addressed including re-aggregation prevention, cost reduction, poor cell affinity, controlling by-product degradation, and controlling surface chemistry. As a result, scientists continuously study NDs to shed light on the surface structure and chemistry to develop functional materials with improved properties. Composites containing biopolymers and NDs are also attracting the attention of scientists leading to the introduction of novel materials and methods into this area. In the near future, the approval of ND application in implants is expected. Therefore, a new era for the application of nanodiamonds in the biomedical field will be opened. The prospective applications of nanodiamonds will be in various multifunctional devices for simultaneous cell targeting, drug delivery, and image reactions.

REFERENCES

[1] O. Shenderova, V. Zhirnov, D. Brenner, Solid State Mater, Sci 27(3/4) (2002) 227.

[2] J. Sung, Diamond nanotechnology: Synthesis and applications, CRC Press2019.

[3] Y. Zhang, K.Y. Rhee, D. Hui, S.-J. Park, A critical review of nanodiamond based nanocomposites: Synthesis, properties and applications, Composites Part B: Engineering 143 (2018) 19-27.

[4] W. Ahmed, S. Gul, M. Awais, Z.U. Hassan, S. Jabeen, M. Farooq, A review: novel nanohybrids of epoxy/polyamide with carbon nanotube/nano-diamond, Polymer-Plastics Technology and Materials (2020) 1-22.

[5] H. Schwertfeger, A.A. Fokin, P.R. Schreiner, Diamonds are a chemist's best friend: diamondoid chemistry beyond adamantane, Angewandte Chemie International Edition 47(6) (2008) 1022-1036.

[6] T. Da Ros, M. Prato, Medicinal chemistry with fullerenes and fullerene derivatives, Chemical Communications (8) (1999) 663-669.

[7] S. Ong, R. Van Harmelen, N. Norouzi, F. Offens, I. Venema, M.H. Najafi, R. Schirhagl, Interaction of nanodiamonds with bacteria, Nanoscale 10(36) (2018) 17117-17124.

[8] H.-S. Jung, K.-J. Cho, S.-J. Ryu, Y. Takagi, P.A. Roche, K.C. Neuman, Biocompatible Fluorescent Nanodiamonds as Multifunctional Optical Probes for Latent Fingerprint Detection, ACS Applied Materials & Interfaces 12(5) (2020) 6641-6650.

[9] K. van der Laan, M. Hasani, T. Zheng, R. Schirhagl, Nanodiamonds for in vivo applications, Small 14(19) (2018) 1703838.

[10] E. Perevedentseva, Y.-C. Lin, C.-L. Cheng, A review of recent advances in nanodiamond-mediated drug delivery in cancer, Expert Opinion on Drug Delivery (2020) 1-14.

[11] M. Abnikia, Z. Azizi, H. Ahmad-Panahib, A. Pashaeia, Modification of zinc sulfide nanoparticle by allyl glycidyl ether for adsorption of famotidine in biological sample, (2013).

[12] E. Krok, S. Balakin, J. Jung, F. Gross, J. Opitz, G. Cuniberti, Modification of titanium implants using biofunctional nanodiamonds for enhanced antimicrobial properties, Nanotechnology 31(20) (2020) 205603.

[13] S. Szunerits, R. Boukherroub, Diamond nanoparticles. A review of selected surface modification. Methods for bioconjugation, biology and medicine, Applied Surface Chemistry of Nanomaterials (2013) 3.

[14] A.J. Rad, Synthesis of copper oxide nanoparticles on activated carbon for pollutant removal in Tartrazine structure, Journal of Composites and Compounds 2(3) (2020) 99-104.

[15] L. Bazli, M. Siavashi, A. Shiravi, A review of carbon nanotube/TiO_2 composite prepared via sol-gel method, Journal of Composites and Compounds 1(1) (2019) 1-9.

[16] E. Asadi, A.F. Chimeh, S. Hosseini, S. Rahimi, B. Sarkhosh, L. Bazli, R. Bashiri, A.H.V. Tahmorsati, A review of clinical applications of graphene quantum dot-based composites, Journal of Composites and Compounds 1(1) (2019) 36-47.

[17] M. Alizadeh, F. Sharifianjazi, E. Haghshenasjazi, M. Aghakhani, L. Rajabi, Production of nanosized boron oxide powder by high-energy ball milling, Synthesis and Reactivity in Inorganic, Metal-Organic, and Nano-Metal Chemistry 45(1) (2015) 11-14.

[18] K. Zhang, Q. Zhao, S. Qin, Y. Fu, R. Liu, J. Zhi, C. Shan, Nanodiamonds conjugated upconversion nanoparticles for bio-imaging and drug delivery, Journal of colloid and interface science 537 (2019) 316-324.

[19] H. Tinwala, S. Wairkar, Production, surface modification and biomedical applications of nanodiamonds: A sparkling tool for theranostics, Materials Science and Engineering: C 97 (2019) 913-931.

[20] J.F.Y. Fong, Y.H. Ng, S. MukNg, Recent Advances in Carbon Dots for Bioanalysis and the Future Perspectives, Carbon Nanomaterials for Bioimaging, Bioanalysis, and Therapy (2019) 203-264.

[21] M. Fujiwara, S. Sun, A. Dohms, Y. Nishimura, K. Suto, Y. Takezawa, K. Oshimi, L. Zhao, N. Sadzak, Y. Umehara, Real-time nanodiamond thermometry probing\textit {in-vivo} thermogenic responses, arXiv preprint arXiv:2001.02844 (2020).

[22] K. Gonsalves, C. Halberstadt, C.T. Laurencin, L. Nair, Biomedical nanostructures, John Wiley & Sons2007.

[23] V. Labhasetwar, D.L. Leslie-Pelecky, Biomedical applications of nanotechnology, John Wiley & Sons2007.

[24] O.V. Salata, Applications of nanoparticles in biology and medicine, Journal of nanobiotechnology 2(1) (2004) 3.

[25] E. BioMEMS, By GA Urban, Springer, 2006.

[26] M.T. Castaneda, A. Merkoçi, M. Pumera, S. Alegret, Electrochemical genosensors for biomedical applications based on gold nanoparticles, Biosensors and Bioelectronics 22(9-10) (2007) 1961-1967.

[27] A. Merkoçi, Electrochemical biosensing with nanoparticles, The FEBS journal 274(2) (2007) 310-316.

[28] O. Shoseyov, I. Levy, Nanobiotechnology Overview, NanoBioTechnology, Springer2008, pp. 3-15.

[29] V. Balouchi, F.S. Jazi, A. Saidi, Developing (W, Ti) C-(Ni, Co) nanocomposite by SHS method, Journal of Ceramic Processing Research 16(5) (2015) 605-608.

[30] I. Tajzad, E. Ghasali, Production methods of CNT-reinforced Al matrix composites: a review, Journal of Composites and Compounds 2(1) (2020) 1-9.

[31] M.F. Heragh, S. Eskandarinezhad, A. Dehghan, Ni-Cu matrix composite reinforced with CNTs: preparation, characterization, wear and corrosion behavior, inhibitory effects, Journal of Composites and Compounds 2(4) (2020) 123-128.

[32] S.J. Cobb, F.H. Laidlaw, G. West, G. Wood, M.E. Newton, R. Beanland, J.V. Macpherson, Assessment of acid and thermal oxidation treatments for removing sp2 bonded carbon from the surface of boron doped diamond, Carbon (2020).

[33] J. Viecelli, S. Bastea, J. Glosli, F. Ree, Phase transformations of nanometer size carbon particles in shocked hydrocarbons and explosives, The Journal of Chemical Physics 115(6) (2001) 2730-2736.

[34] V. Danilenko, Synthesis, properties and applications of ultrananocrystalline

diamond, Proceedings of the NATO Advanced Research Workshop, 2005, pp. 181-198.
[35] S.O. Omid, Z. Goudarzi, L.M. Kangarshahi, A. Mokhtarzade, F. Bahrami, Self-expanding stents based on shape memory alloys and shape memory polymers, Journal of Composites and Compounds 2(3) (2020) 92-98.
[36] F. Sharifianjazi, A.H. Pakseresht, M.S. Asl, A. Esmaeilkhanian, H.W. Jang, M. Shokouhimehr, Hydroxyapatite consolidated by zirconia: applications for dental implant, Journal of Composites and Compounds 2(1) (2020) 26-34.
[37] E. Perevedentseva, Y.-C. Lin, M. Jani, C.-L. Cheng, Biomedical applications of nanodiamonds in imaging and therapy, Nanomedicine 8(12) (2013) 2041-2060.
[38] D.-K. Lee, S. Ha, S. Jeon, J. Jeong, D.-J. Kim, S.W. Lee, W.-S. Cho, The sp^3/sp^2 carbon ratio as a modulator of in vivo and in vitro toxicity of the chemically purified detonation-synthesized nanodiamond via the reactive oxygen species generation, Nanotoxicology (2020) 1-14.
[39] F.S. Boi, X. Zhang, D. Medranda, Evidence of sp^3-rich nano-diamond-like characteristics in amorphous carbon foam continuously filled with α-Fe, Diamond and Related Materials 84 (2018) 190-195.
[40] O. Shenderova, V. Zhirnov, D. Brenner, Carbon nanostructures, Critical reviews in solid state and material sciences 27(3-4) (2002) 227-356.
[41] D.M. Gruen, Ultrananocrystalline Diamond, William Andrew2006.
[42] D.M. Gruen, Nanocrystalline diamond films, Annual Review of Materials Science 29(1) (1999) 211-259.
[43] V.Y. Dolmatov, The Amount of Impurity Elements in Diamond-Containing Soot and Detonation Nanodiamonds upon Nitric Acid Treatment, Journal of Superhard Materials 40(2) (2018) 143-154.
[44] A.A. Vozniakovskii, T.S. Kol'tsova, A.P. Voznyakovskii, A.L. Kumskov, S.V. Kidalov, Powder hybrid nanomaterial: Detonation nanodiamonds–Carbon nanotubes and its stable reversible water nanofluids, Journal of Colloid and Interface Science 565 (2020) 305-314.
[45] J.-P. Boudou, P.A. Curmi, F. Jelezko, J. Wrachtrup, P. Aubert, M. Sennour, G. Balasubramanian, R. Reuter, A. Thorel, E. Gaffet, High yield fabrication of fluorescent nanodiamonds, Nanotechnology 20(23) (2009) 235602.
[46] I.M. Abdullahi, M. Langenderfer, O. Shenderova, N. Nunn, M.D. Torelli, C. Johnson, V.N. Mochalin, Explosive fragmentation of luminescent diamond particles, Carbon (2020).
[47] G.-W. Yang, J.-B. Wang, Q.-X. Liu, Preparation of nano-crystalline diamonds using pulsed laser induced reactive quenching, Journal of Physics: Condensed Matter 10(35) (1998) 7923.
[48] E. Galimov, A. Kudin, V. Skorobogatskii, V. Plotnichenko, O. Bondarev, B. Zarubin, V. Strazdovskii, A. Aronin, A. Fisenko, I. Bykov, Experimental corroboration of the synthesis of diamond in the cavitation process, Doklady Physics, Springer, 2004, pp. 150-153.
[49] F. Banhart, P.M. Ajayan, Carbon onions as nanoscopic pressure cells for diamond formation, Nature 382(6590) (1996) 433-435.
[50] T. Daulton, M. Kirk, R. Lewis, L. Rehn, Production of nanodiamonds by high-energy ion irradiation of graphite at room temperature, Nuclear Instruments and Methods in Physics Research Section B: Beam Interactions with Materials and Atoms 175 (2001) 12-20.
[51] S. Welz, Y. Gogotsi, M.J. McNallan, Nucleation, growth, and graphitization of diamond nanocrystals during chlorination of carbides, Journal of applied physics 93(7) (2003) 4207-4214.
[52] Y.G. Gogotsi, K.G. Nickel, D. Bahloul-Hourlier, T. Merle-Mejean, G.E. Khomenko, K.P. Skjerlie, Structure of carbon produced by hydrothermal treatment of β-SiC powder, Journal of Materials Chemistry 6(4) (1996) 595-604.
[53] M. Frenklach, W. Howard, D. Huang, J. Yuan, K. Spear, R. Koba, Induced nucleation of diamond powder, Applied physics letters 59(5) (1991) 546-548.
[54] O. Guillois, G. Ledoux, C. Reynaud, Diamond infrared emission bands in circumstellar media, The astrophysical journal letters 521(2) (1999) L133.
[55] M. Goto, T. Henning, A. Kouchi, H. Takami, Y. Hayano, T. Usuda, N. Takato, H. Terada, S. Oya, C. Jäger, Spatially resolved 3 μm spectroscopy of Elias 1: Origin of diamonds in protoplanetary disks, The Astrophysical Journal 693(1) (2009) 610.
[56] O.A. Shenderova, D.M. Gruen, Ultrananocrystalline diamond: synthesis, properties and applications, William Andrew2012.
[57] V.Y. Dolmatov, Detonation synthesis ultradispersed diamonds: properties and applications, Russian Chemical Reviews 70(7) (2001) 607-626.
[58] C. Torres-Sanchez, N. Balodimos, Effective and Eco-friendly Lubrication Protocol Using Nanodiamonds in a Dry Regime for Conveyor Systems in the Beverage Industry, Packaging Technology and Science 30(5) (2017) 209-218.
[59] I. Senthilnathan, Surface analysis of Detonation Nanodiamond thin films fabricated using automated spray coating technique, (2018).
[60] S. Osswald, G. Yushin, V. Mochalin, S.O. Kucheyev, Y. Gogotsi, Control of sp^2/sp^3 carbon ratio and surface chemistry of nanodiamond powders by selective oxidation in air, Journal of the American Chemical Society 128(35) (2006) 11635-11642.
[61] S. Kumar, M. Nehra, D. Kedia, N. Dilbaghi, K. Tankeshwar, K.-H. Kim, Nanodiamonds: Emerging face of future nanotechnology, Carbon 143 (2019) 678-699.
[62] F.S. Jazi, N. Parvin, M. Rabiei, M. Tahriri, Z.M. Shabestari, A.R. Azadmehr, Effect of the synthesis route on the grain size and morphology of ZnO/Ag nanocomposite, Journal of Ceramic Processing Research 13(5) (2012) 523-526.
[63] O. Shenderova, A. Koscheev, N. Zaripov, I. Petrov, Y. Skryabin, P. Detkov, S. Turner, G. Van Tendeloo, Surface chemistry and properties of ozone-purified detonation nanodiamonds, The Journal of Physical Chemistry C 115(20) (2011) 9827-9837.
[64] M. Sievänen, Agglomeration of nanodiamonds during deposition, (2017).
[65] O.A. Williams, J. Hees, C. Dieker, W. Jäger, L. Kirste, C.E. Nebel, Size-dependent reactivity of diamond nanoparticles, ACS nano 4(8) (2010) 4824-4830.
[66] A.M. Schrand, S.A.C. Hens, O.A. Shenderova, Nanodiamond particles: properties and perspectives for bioapplications, Critical reviews in solid state and materials sciences 34(1-2) (2009) 18-74.
[67] C. Shuai, Y. Li, G. Wang, W. Yang, S. Peng, P. Feng, Surface modification of nanodiamond: Toward the dispersion of reinforced phase in poly-l-lactic acid scaffolds, International Journal of Biological Macromolecules 126 (2019) 1116-1124.
[68] H. Huang, E. Pierstorff, E. Osawa, D. Ho, Active nanodiamond hydrogels for chemotherapeutic delivery, Nano letters 7(11) (2007) 3305-3314.
[69] O. Fedyanina, P. Nesterenko, Regularities of chromatographic retention of phenols on microdispersed sintered detonation nanodiamond in aqueous—organic solvents, Russian Journal of Physical Chemistry A 84(3) (2010) 476-480.
[70] D.H. Jariwala, D. Patel, S. Wairkar, Surface functionalization of nanodiamonds for biomedical applications, Materials Science and Engineering: C (2020) 110996.
[71] M. Ozawa, M. Inaguma, M. Takahashi, F. Kataoka, A. Krueger, E. Ōsawa, Preparation and behavior of brownish, clear nanodiamond colloids, Advanced Materials 19(9) (2007) 1201-1206.
[72] E. Ōsawa, Recent progress and perspectives in single-digit nanodiamond, Diamond and Related Materials 16(12) (2007) 2018-2022.
[73] A. Aleksenskiy, E. Eydelman, A.Y. Vul, Deagglomeration of detonation nanodiamonds, Nanoscience and Nanotechnology Letters 3(1) (2011) 68-74.
[74] A. Pentecost, S. Gour, V. Mochalin, I. Knoke, Y. Gogotsi, Deaggregation of nanodiamond powders using salt-and sugar-assisted milling, ACS applied materials & interfaces 2(11) (2010) 3289-3294.
[75] A. Krueger, J. Stegk, Y. Liang, L. Lu, G. Jarre, Biotinylated nanodiamond: simple and efficient functionalization of detonation diamond, Langmuir 24(8) (2008) 4200-4204.
[76] Y. Liang, T. Meinhardt, G. Jarre, M. Ozawa, P. Vrdoljak, A. Schöll, F. Reinert, A. Krueger, Deagglomeration and surface modification of thermally annealed nanoscale diamond, Journal of Colloid and Interface Science 354(1) (2011) 23-30.
[77] M. Gu, T.B. Toh, L. Hooi, J.J. Lim, X. Zhang, E.K.-H. Chow, Nanodiamond-mediated delivery of a G9a inhibitor for hepatocellular carcinoma therapy, ACS Applied Materials & Interfaces 11(49) (2019) 45427-45441.
[78] A. Shvidchenko, E. Eidelman, A.Y. Vul, N. Kuznetsov, D.Y. Stolyarova, S. Belousov, S. Chvalun, Colloids of detonation nanodiamond particles for advanced applications, Advances in Colloid and Interface Science 268 (2019) 64-81.
[79] V. Bondar', A. Puzyr', Nanodiamonds for biological investigations, Physics of the Solid State 46 (2004) 716-719.
[80] O. Shenderova, I. Petrov, J. Walsh, V. Grichko, V. Grishko, T. Tyler, G. Cunningham, Modification of detonation nanodiamonds by heat treatment in air, Diamond and related materials 15(11-12) (2006) 1799-1803.
[81] I. Larionova, V. Kuznetsov, A. Frolov, O. Shenderova, S. Moseenkov, I. Mazov, Properties of individual fractions of detonation nanodiamond, Diamond and related materials 15(11-12) (2006) 1804-1808.
[82] V. Grichko, T. Tyler, V.I. Grishko, O. Shenderova, Nanodiamond particles forming photonic structures, Nanotechnology 19(22) (2008) 225201.
[83] T. Meinhardt, D. Lang, H. Dill, A. Krueger, Pushing the functionality of diamond nanoparticles to new horizons: orthogonally functionalized nanodiamond using click chemistry, Advanced Functional Materials 21(3) (2011) 494-500.
[84] A. Krueger, Diamond nanoparticles: jewels for chemistry and physics, Advanced Materials 20(12) (2008) 2445-2449.
[85] A. Krueger, The structure and reactivity of nanoscale diamond, Journal of Materials Chemistry 18(13) (2008) 1485-1492.
[86] J.-C. Arnault, T. Petit, H. Girard, A. Chavanne, C. Gesset, M. Sennour, M. Chaigneau, Surface chemical modifications and surface reactivity of nanodiamonds hydrogenated by CVD plasma, Physical Chemistry Chemical Physics 13(24) (2011) 11481-11487.

[87] Y. Liu, Z. Gu, J.L. Margrave, V.N. Khabashesku, Functionalization of nanoscale diamond powder: fluoro-, alkyl-, amino-, and amino acid-nanodiamond derivatives, Chemistry of materials 16(20) (2004) 3924-3930.
[88] G. Lisichkin, V. Korol'kov, B. Tarasevich, I. Kulakova, A. Karpukhin, Photochemical chlorination of nanodiamond and interaction of its modified surface with C-nucleophiles, Russian chemical bulletin 55(12) (2006) 2212-2219.
[89] A. Krueger, T. Boedeker, Deagglomeration and functionalisation of detonation nanodiamond with long alkyl chains, Diamond and related materials 17(7-10) (2008) 1367-1370.
[90] Y. Liang, M. Ozawa, A. Krueger, A general procedure to functionalize agglomerating nanoparticles demonstrated on nanodiamond, ACS nano 3(8) (2009) 2288-2296.
[91] P. Gaur, S. Banerjee, C-N cross coupling: Novel approach towards effective aryl secondary amines modification on nanodiamond surface, Diamond and Related Materials 98 (2019) 107468.
[92] G. Reina, L. Zhao, A. Bianco, N. Komatsu, Chemical functionalization of nanodiamonds: opportunities and challenges ahead, Angewandte Chemie 131(50) (2019) 18084-18095.
[93] W.S. Yeap, S. Chen, K.P. Loh, Detonation nanodiamond: an organic platform for the suzuki coupling of organic molecules, Langmuir 25(1) (2009) 185-191.
[94] L. Lai, A.S. Barnard, Modeling the thermostability of surface functionalisation by oxygen, hydroxyl, and water on nanodiamonds, Nanoscale 3(6) (2011) 2566-2575.
[95] L. Lai, A.S. Barnard, Stability of nanodiamond surfaces exposed to N, NH, and NH_2, The Journal of Physical Chemistry C 115(14) (2011) 6218-6228.
[96] Y.-R. Chang, H.-Y. Lee, K. Chen, C.-C. Chang, D.-S. Tsai, C.-C. Fu, T.-S. Lim, Y.-K. Tzeng, C.-Y. Fang, C.-C. Han, Mass production and dynamic imaging of fluorescent nanodiamonds, Nature nanotechnology 3(5) (2008) 284-288.
[97] L. Rondin, G. Dantelle, A. Slablab, F. Grosshans, F. Treussart, P. Bergonzo, S. Perruchas, T. Gacoin, M. Chaigneau, H.-C. Chang, Surface-induced charge state conversion of nitrogen-vacancy defects in nanodiamonds, Physical Review B 82(11) (2010) 115449.
[98] B. Slepetz, I. Laszlo, Y. Gogotsi, D. Hyde-Volpe, M. Kertesz, Characterization of large vacancy clusters in diamond from a generational algorithm using tight binding density functional theory, Physical Chemistry Chemical Physics 12(42) (2010) 14017-14022.
[99] P. Neumann, J. Beck, M. Steiner, F. Rempp, H. Fedder, P.R. Hemmer, J. Wrachtrup, F. Jelezko, Single-shot readout of a single nuclear spin, Science 329(5991) (2010) 542-544.
[100] J.R. Maze, P.L. Stanwix, J.S. Hodges, S. Hong, J.M. Taylor, P. Cappellaro, L. Jiang, M.G. Dutt, E. Togan, A. Zibrov, Nanoscale magnetic sensing with an individual electronic spin in diamond, Nature 455(7213) (2008) 644-647.
[101] G. Balasubramanian, I. Chan, R. Kolesov, M. Al-Hmoud, J. Tisler, C. Shin, C. Kim, A. Wojcik, P.R. Hemmer, A. Krueger, Nanoscale imaging magnetometry with diamond spins under ambient conditions, Nature 455(7213) (2008) 648-651.
[102] C. Bradac, T. Gaebel, N. Naidoo, M. Sellars, J. Twamley, L. Brown, A. Barnard, T. Plakhotnik, A. Zvyagin, J. Rabeau, Observation and control of blinking nitrogen-vacancy centres in discrete nanodiamonds, Nature nanotechnology 5(5) (2010) 345-349.
[103] J. Tisler, R. Reuter, A. Lämmle, F. Jelezko, G. Balasubramanian, P.R. Hemmer, F. Reinhard, J.r. Wrachtrup, Highly efficient FRET from a single nitrogen-vacancy center in nanodiamonds to a single organic molecule, Acs Nano 5(10) (2011) 7893-7898.
[104] J. Tisler, G. Balasubramanian, B. Naydenov, R. Kolesov, B. Grotz, R. Reuter, J.-P. Boudou, P.A. Curmi, M. Sennour, A. Thorel, Fluorescence and spin properties of defects in single digit nanodiamonds, ACS nano 3(7) (2009) 1959-1965.
[105] A. Sanaat, H. Arabi, I. Mainta, V. Garibotto, H. Zaidi, Projection Space Implementation of Deep Learning-Guided Low-Dose Brain PET Imaging Improves Performance over Implementation in Image Space, Journal of nuclear medicine : official publication, Society of Nuclear Medicine 61(9) (2020) 1388-1396.
[106] A. Sanaat, H. Arabi, M.R. Ay, H. Zaidi, Novel preclinical PET geometrical concept using a monolithic scintillator crystal offering concurrent enhancement in spatial resolution and detection sensitivity: a simulation study, Physics in Medicine & Biology 65(4) (2020) 045013.
[107] A. Sanaat, H. Zaidi, Depth of interaction estimation in a preclinical PET scanner equipped with monolithic crystals coupled to SiPMs using a deep neural network, Applied Sciences 10(14) (2020) 4753.
[108] A. Sanaat, A. Ashrafi-Belgabad, H. Zaidi, Polaroid-PET: a PET scanner with detectors fitted with polaroids for filtering unpolarized optical photons: a Monte Carlo simulation study, Physics in Medicine & Biology (2020).
[109] O.A. Shenderova, I.I. Vlasov, S. Turner, G. Van Tendeloo, S.B. Orlinskii, A.A. Shiryaev, A.A. Khomich, S.N. Sulyanov, F. Jelezko, J. Wrachtrup, Nitrogen control in nanodiamond produced by detonation shock-wave-assisted synthesis, The Journal of Physical Chemistry C 115(29) (2011) 14014-14024.
[110] I.I. Vlasov, O. Shenderova, S. Turner, O.I. Lebedev, A.A. Basov, I. Sildos, M. Rähn, A.A. Shiryaev, G. Van Tendeloo, Nitrogen and luminescent nitrogen-vacancy defects in detonation nanodiamond, Small 6(5) (2010) 687-694.
[111] L.-C.L. Huang, H.-C. Chang, Adsorption and immobilization of cytochrome c on nanodiamonds, Langmuir 20(14) (2004) 5879-5884.
[112] S.C. Hens, G. Cunningham, T. Tyler, S. Moseenkov, V. Kuznetsov, O. Shenderova, Nanodiamond bioconjugate probes and their collection by electrophoresis, Diamond and related materials 17(11) (2008) 1858-1866.
[113] A.M. Schrand, J.B. Lin, S.C. Hens, S.M. Hussain, Temporal and mechanistic tracking of cellular uptake dynamics with novel surface fluorophore-bound nanodiamonds, Nanoscale 3(2) (2011) 435-445.
[114] V.N. Mochalin, Y. Gogotsi, Wet chemistry route to hydrophobic blue fluorescent nanodiamond, Journal of the American Chemical Society 131(13) (2009) 4594-4595.
[115] O. Faklaris, V. Joshi, T. Irinopoulou, P. Tauc, M. Sennour, H. Girard, C. Gesset, J.-C. Arnault, A. Thorel, J.-P. Boudou, Photoluminescent diamond nanoparticles for cell labeling: study of the uptake mechanism in mammalian cells, ACS nano 3(12) (2009) 3955-3962.
[116] L.P. McGuinness, Y. Yan, A. Stacey, D.A. Simpson, L.T. Hall, D. Maclaurin, S. Prawer, P. Mulvaney, J. Wrachtrup, F. Caruso, Quantum measurement and orientation tracking of fluorescent nanodiamonds inside living cells, Nature nanotechnology 6(6) (2011) 358-363.
[117] X.Q. Zhang, R. Lam, X. Xu, E.K. Chow, H.J. Kim, D. Ho, Multimodal nanodiamond drug delivery carriers for selective targeting, imaging, and enhanced chemotherapeutic efficacy, Advanced materials 23(41) (2011) 4770-4775.
[118] J. Dong, R. Jiang, H. Huang, J. Chen, J. Tian, F. Deng, Y. Dai, Y. Wen, X. Zhang, Y. Wei, Facile preparation of fluorescent nanodiamond based polymer nanoparticles via ring-opening polymerization and their biological imaging, Materials Science and Engineering: C 106 (2020) 110297.
[119] Wide-field in vivo background free imaging by selective magnetic modulation of nanodiamond fluorescence, Biomed. Opt. Express 5(4) (2014) 1190-1202.
[120] A. Schrand, J. Johnson, L. Dai, S.M. Hussain, J. Schlager, L. Zhu, Y. Hong, E. Osawa, Safety of Nanoparticles, From Manufacturing to Medical Applications, Nanostructure Science and Technology (2009) 159-187.
[121] J. Kowalczyk, M. Madej, D. Ozimina, K. Milewski, The influence of non-toxic cutting fluid on the diamond-like carbon coatings, AIP Conference Proceedings, AIP Publishing LLC, 2018, p. 020009.
[122] K.-H. Yang, R.J. Narayan, Biocompatibility and functionalization of diamond for neural applications, Current Opinion in Biomedical Engineering 10 (2019) 60-68.
[123] Q. Zhang, V.N. Mochalin, I. Neitzel, I.Y. Knoke, J. Han, C.A. Klug, J.G. Zhou, P.I. Lelkes, Y. Gogotsi, Fluorescent PLLA-nanodiamond composites for bone tissue engineering, Biomaterials 32(1) (2011) 87-94.
[124] A.M. Schrand, H. Huang, C. Carlson, J.J. Schlager, E. Ōsawa, S.M. Hussain, L. Dai, Are diamond nanoparticles cytotoxic?, The journal of physical chemistry B 111(1) (2007) 2-7.
[125] Y. Yuan, X. Wang, G. Jia, J.-H. Liu, T. Wang, Y. Gu, S.-T. Yang, S. Zhen, H. Wang, Y. Liu, Pulmonary toxicity and translocation of nanodiamonds in mice, Diamond and Related Materials 19(4) (2010) 291-299.
[126] N. Mohan, C.-S. Chen, H.-H. Hsieh, Y.-C. Wu, H.-C. Chang, In vivo imaging and toxicity assessments of fluorescent nanodiamonds in Caenorhabditis elegans, Nano letters 10(9) (2010) 3692-3699.
[127] E.K. Chow, X.-Q. Zhang, M. Chen, R. Lam, E. Robinson, H. Huang, D. Schaffer, E. Osawa, A. Goga, D. Ho, Nanodiamond therapeutic delivery agents mediate enhanced chemoresistant tumor treatment, Science translational medicine 3(73) (2011) 73ra21-73ra21.
[128] K. Yonezawa, M. Kawaguchi, A. Kaneuji, T. Ichiseki, Y. Iinuma, K. Kawamura, K. Shintani, S. Oda, M. Taki, N. Kawahara, Evaluation of Antibacterial and Cytotoxic Properties of a Fluorinated Diamond-Like Carbon Coating for the Development of Antibacterial Medical Implants, Antibiotics 9(8) (2020) 495.
[129] L. Moore, J. Yang, T.T.H. Lan, E. Osawa, D.-K. Lee, W.D. Johnson, J. Xi, E.K.-H. Chow, D. Ho, Biocompatibility assessment of detonation nanodiamond in non-human primates and rats using histological, hematologic, and urine analysis, ACS nano 10(8) (2016) 7385-7400.
[130] S. Kurtz, S. Kurtz, A Primer on UHMWPE UHMWPE biomaterials handbook: ultra high molecular weight polyethylene in total joint replacement and medical devices, Boston: Elsevier/Academic Press, 2009.
[131] Z. Karaguiozova, J. Kaleicheva, V. Mishev, G. Nikolcheva, Enhancement in the Tribological and Mechanical Properties of Electroless Nickel-Nanodiamond Coatings Plated on Iron, Tribology in Industry 39(4) (2017).

[132] T. Takimoto, T. Chano, S. Shimizu, H. Okabe, M. Ito, M. Morita, T. Kimura, T. Inubushi, N. Komatsu, Preparation of fluorescent diamond nanoparticles stably dispersed under a physiological environment through multistep organic transformations, Chemistry of materials 22(11) (2010) 3462-3471.
[133] O. Shenderova, N. Nunn, T. Oeckinghaus, M. Torelli, G. McGuire, K. Smith, E. Danilov, R. Reuter, J. Wrachtrup, A. Shames, Commercial quantities of ultrasmall fluorescent nanodiamonds containing color centers, Advances in Photonics of Quantum Computing, Memory, and Communication X, International Society for Optics and Photonics, 2017, p. 1011803.
[134] L. Joly-Pottuz, N. Matsumoto, H. Kinoshita, B. Vacher, M. Belin, G. Montagnac, J. Martin, N. Ohmae, Diamond-derived carbon onions as lubricant additives, Tribology International 41(2) (2008) 69-78.
[135] V.N. Mochalin, O. Shenderova, D. Ho, Y. Gogotsi, The properties and applications of nanodiamonds, Nature nanotechnology 7(1) (2012) 11-23.
[136] L. Bazli, A. Khavandi, M.A. Boutorabi, M. Karrabi, Correlation between viscoelastic behavior and morphology of nanocomposites based on SR/EPDM blends compatibilized by maleic anhydride, Polymer 113 (2017) 156-166.
[137] L. Bazli, A. Khavandi, M.A. Boutorabi, M. Karrabi, Morphology and viscoelastic behavior of silicone rubber/EPDM/Cloisite 15A nanocomposites based on Maxwell model, Iranian Polymer Journal 25(11) (2016) 907-918.
[138] S. Saadi, B. Nazari, Recent developments and applications of nanocomposites in solar cells: a review, Journal of Composites and Compounds 1(1) (2019) 48-58.
[139] H.W. Jang, A. Zareidoost, M. Moradi, A. Abuchenari, A. Bakhtiari, R. Pouriamanesh, B. Malekpouri, A.J. Rad, D. Rahban, Photosensitive nanocomposites: environmental and biological applications, Journal of Composites and Compounds 2(1) (2020) 50-60.
[140] O. Shenderova, A. Panich, S. Moseenkov, S. Hens, V. Kuznetsov, H.-M. Vieth, Hydroxylated detonation nanodiamond: FTIR, XPS, and NMR studies, The Journal of Physical Chemistry C 115(39) (2011) 19005-19011.
[141] W. Ma, X. Yu, X. Qu, Q. Zhang, Functionalization of agglomerating nanodiamonds with biodegradable poly (ε-caprolactone) through surface-initiated polymerization, Diamond and Related Materials 62 (2016) 14-21.
[142] A. Krüger, Y. Liang, G. Jarre, J. Stegk, Surface functionalisation of detonation diamond suitable for biological applications, Journal of Materials Chemistry 16(24) (2006) 2322-2328.
[143] J. Nunes-Pereira, A. Silva, C. Ribeiro, S. Carabineiro, J. Buijnsters, S. Lanceros-Méndez, Nanodiamonds/poly (vinylidene fluoride) composites for tissue engineering applications, Composites Part B: Engineering 111 (2017) 37-44.
[144] Y. Sun, Q. Yang, H. Wang, Synthesis and characterization of nanodiamond reinforced chitosan for bone tissue engineering, Journal of functional biomaterials 7(3) (2016) 27.
[145] A. Stacey, I. Aharonovich, S. Prawer, J.E. Butler, Controlled synthesis of high quality micro/nano-diamonds by microwave plasma chemical vapor deposition, Diamond and related materials 18(1) (2009) 51-55.
[146] V.N. Mochalin, Y. Gogotsi, Nanodiamond–polymer composites, Diamond and Related Materials 58 (2015) 161-171.
[147] D. Wang, Y. Tong, Y. Li, Z. Tian, R. Cao, B. Yang, PEGylated nanodiamond for chemotherapeutic drug delivery, Diamond and related materials 36 (2013) 26-34.
[148] K. Fox, P.A. Tran, D.W. Lau, T. Ohshima, A.D. Greentree, B.C. Gibson, Nanodiamond-polycaprolactone composite: A new material for tissue engineering with sub-dermal imaging capabilities, Materials Letters 185 (2016) 185-188.
[149] A.D. Salaam, M. Mishra, E. Nyairo, D. Dean, Electrospun polyvinyl alcohol/nanodiamond composite scaffolds: morphological, structural, and biological analysis, Journal of biomaterials and tissue engineering 4(3) (2014) 173-180.
[150] H. Gomez, M.K. Ram, F. Alvi, E. Stefanakos, A. Kumar, Novel synthesis, characterization, and corrosion inhibition properties of nanodiamond− polyaniline films, The Journal of Physical Chemistry C 114(44) (2010) 18797-18804.
[151] L. Cao, Y. Hou, K. Lafdi, K. Urmey, Fluorescent composite scaffolds made of nanodiamonds/polycaprolactone, Chemical Physics Letters 641 (2015) 123-128.
[152] M. Abniki, A. Moghimi, F. Azizinejad, Fabrication of bionanocomposite based on LDH using biopolymer of gum arabic and chitosan-coating for sustained drug-release, Journal of the Serbian Chemical Society 85(5) (2020).
[153] M. Abniki, A. Moghimi, F. Azizinejad, Synthesis of calcium-layered double hydroxide based nanohybrid for controlled release of an anti-inflammatory drug, Journal of the Chinese Chemical Society (2020).
[154] A. Bakhtiari, A. Cheshmi, M. Naeimi, S.M. Fathabad, M. Aliasghari, A.M. Chahardehi, S. Hassani, V. Elhami, Synthesis and characterization of the novel 80S bioactive glass: bioactivity, biocompatibility, cytotoxicity, Journal of Composites and Compounds 2(4) (2020) 110-114.
[155] B.F. Dizaji, M.H. Azerbaijan, N. Sheisi, P. Goleij, T. Mirmajidi, F. Chogan, M. Irani, F. Sharafian, Synthesis of PLGA/chitosan/zeolites and PLGA/chitosan/metal organic frameworks nanofibers for targeted delivery of Paclitaxel toward prostate cancer cells death, International Journal of Biological Macromolecules 164 (2020) 1461-1474.
[156] A. Nouri, B. Faraji Dizaji, N. Kianinejad, A. Jafari Rad, S. Rahimi, M. Irani, F. Sharifian Jazi, Simultaneous linear release of folic acid and doxorubicin from ethyl cellulose/chitosan/g-C_3N_4/MoS_2 core-shell nanofibers and its anticancer properties, Journal of Biomedical Materials Research Part A (2020).
[157] N. Nunn, M. Torelli, G. McGuire, O. Shenderova, Nanodiamond: a high impact nanomaterial, Current Opinion in Solid State and Materials Science 21(1) (2017) 1-9.
[158] T. Kondo, I. Neitzel, V.N. Mochalin, J. Urai, M. Yuasa, Y. Gogotsi, Electrical conductivity of thermally hydrogenated nanodiamond powders, Journal of Applied Physics 113(21) (2013) 214307.
[159] S. Mukhopadhyay, B. Deopura, High-modulus polypropylene fibers—through postspinning operations, Structure and Properties of High-Performance Fibers, Elsevier2017, pp. 187-198.
[160] M. Mahdavi, N. Mahmoudi, F. Rezaie Anaran, A. Simchi, Electrospinning of nanodiamond-modified polysaccharide nanofibers with physico-mechanical properties close to natural skins, Marine drugs 14(7) (2016) 128.
[161] N. Cai, Q. Dai, Z. Wang, X. Luo, Y. Xue, F. Yu, Preparation and properties of nanodiamond/poly (lactic acid) composite nanofiber scaffolds, Fibers and Polymers 15(12) (2014) 2544-2552.
[162] J. Xiao, X. Duan, Q. Yin, Z. Zhang, H. Yu, Y. Li, Nanodiamonds-mediated doxorubicin nuclear delivery to inhibit lung metastasis of breast cancer, Biomaterials 34(37) (2013) 9648-9656.
[163] T.-F. Li, K. Li, Q. Zhang, C. Wang, Y. Yue, Z. Chen, S.-J. Yuan, X. Liu, Y. Wen, M. Han, Dendritic cell-mediated delivery of doxorubicin-polyglycerol-nanodiamond composites elicits enhanced anti-cancer immune response in glioblastoma, Biomaterials 181 (2018) 35-52.
[164] A.N. Bokarev, I.L. Plastun, Possibility of drug delivery due to hydrogen bonds formation in nanodiamonds and doxorubicin: molecular modeling, Наносистемы: физика, химия, математика 9(3) (2018).
[165] M. Radmansouri, E. Bahmani, E. Sarikhani, K. Rahmani, F. Sharifianjazi, M. Irani, Doxorubicin hydrochloride-Loaded electrospun chitosan/cobalt ferrite/titanium oxide nanofibers for hyperthermic tumor cell treatment and controlled drug release, International journal of biological macromolecules 116 (2018) 378-384.
[166] P. Abasian, M. Radmansouri, M.H. Jouybari, M.V. Ghasemi, A. Mohammadi, M. Irani, F.S. Jazi, Incorporation of magnetic NaX zeolite/DOX into the PLA/chitosan nanofibers for sustained release of doxorubicin against carcinoma cells death in vitro, International journal of biological macromolecules 121 (2019) 398-406.
[167] J.W. Rhim, A.K. Mohanty, S.P. Singh, P.K. Ng, Effect of the processing methods on the performance of polylactide films: Thermocompression versus solvent casting, Journal of applied polymer science 101(6) (2006) 3736-3742.
[168] N. Bhardwaj, S.C. Kundu, Electrospinning: a fascinating fiber fabrication technique, Biotechnology advances 28(3) (2010) 325-347.
[169] U. Roy, V. Drozd, A. Durygin, J. Rodriguez, P. Barber, V. Atluri, X. Liu, T.G. Voss, S. Saxena, M. Nair, Characterization of Nanodiamond-based anti-HIV drug Delivery to the Brain, Scientific reports 8(1) (2018) 1-12.
[170] M.H. Alkahtani, F. Alghannam, L. Jiang, A. Almethen, A.A. Rampersaud, R. Brick, C.L. Gomes, M.O. Scully, P.R. Hemmer, Fluorescent nanodiamonds: past, present, and future, Nanophotonics 7(8) (2018) 1423-1453.
[171] J. Liu, L. Cui, D. Losic, Graphene and graphene oxide as new nanocarriers for drug delivery applications, Acta biomaterialia 9(12) (2013) 9243-9257.
[172] P. Chandrasekhar, CNT applications in drug and biomolecule delivery, Conducting Polymers, Fundamentals and Applications, Springer2018, pp. 61-64.
[173] H. Girard, T. Petit, S. Perruchas, T. Gacoin, C. Gesset, J.-C. Arnault, P. Bergonzo, Surface properties of hydrogenated nanodiamonds: a chemical investigation, Physical chemistry chemical physics 13(24) (2011) 11517-11523.
[174] S. Nasibi, K. Alimohammadi, L. Bazli, S. Eskandarinezhad, A. Mohammadi, N. Sheysi, TZNT alloy for surgical implant applications: A systematic review, Journal of Composites and Compounds 2(3) (2020) 62-68.
[175] Z. Goudarzi, A. Ijadi, A. Bakhtiari, S. Eskandarinezhad, N. Azizabadi, M.A. Jazi, Sr-doped bioactive glasses for biological applications, Journal of Composites and Compounds 2(3) (2020) 105-109.
[176] J. Daraei, Production and characterization of PCL (Polycaprolactone) coated TCP/nanoBG composite scaffolds by sponge foam method for orthopedic applications, Journal of Composites and Compounds 2(1) (2020) 45-50.
[177] K. Fox, R. Ratwatte, M.A. Booth, H.M. Tran, P.A. Tran, High Nanodiamond Content-PCL Composite for Tissue Engineering Scaffolds, Nanomaterials 10(5)

(2020) 948.
[178] O.S. Adeyemi, F.A. Sulaiman, Evaluation of metal nanoparticles for drug delivery systems, Journal of biomedical research 29(2) (2015) 145.
[179] P. Karami, S.S. Khasraghi, M. Hashemi, S. Rabiei, A. Shojaei, Polymer/nanodiamond composites-a comprehensive review from synthesis and fabrication to properties and applications, Advances in Colloid and Interface Science 269 (2019) 122-151.
[180] Q. Zhang, I. Neitzel, V.N. Mochalin, I. Knoke, D.M. Wootton, Y. Gogotsi, P.I. Lelkes, J.G. Zhou, PLLA-nanodiamond composites and their application in bone tissue engineering, Global Congress on NanoEngineering for Medicine and Biology, 2010, pp. 241-242.
[181] X. Xu, X. Wang, L. Yang, H. Yu, H. Chang, Structure and surface characterization of co-adsorbed layer of oleic acid and octadecylamine on detonation nanodiamond, Diamond and Related Materials 60 (2015) 50-59.
[182] P. Feng, Y. Kong, L. Yu, Y. Li, C. Gao, S. Peng, H. Pan, Z. Zhao, C. Shuai, Molybdenum disulfide nanosheets embedded with nanodiamond particles: co-dispersion nanostructures as reinforcements for polymer scaffolds, Applied Materials Today 17 (2019) 216-226.
[183] T.C. Yadav, A.K. Srivastava, P. Mishra, D. Singh, N. Raghuwanshi, N.K. Singh, A.K. Singh, S.K. Tiwari, R. Prasad, V. Pruthi, Electrospinning: An Efficient Biopolymer-Based Micro-and Nanofibers Fabrication Technique, Next Generation Biomanufacturing Technologies, ACS Publications2019, pp. 209-241.
[184] B. Pant, M. Park, S.-J. Park, Drug delivery applications of core-sheath nanofibers prepared by coaxial electrospinning: a review, Pharmaceutics 11(7) (2019) 305.
[185] I. Jun, H.-S. Han, J.R. Edwards, H. Jeon, Electrospun fibrous scaffolds for tissue engineering: Viewpoints on architecture and fabrication, International journal of molecular sciences 19(3) (2018) 745.
[186] F. Pereira, G. Salles, B. Rodrigues, F. Marciano, C. Pacheco-Soares, A. Lobo, Diamond nanoparticles into poly (lactic acid) electrospun fibers: Cytocompatible and bioactive scaffolds with enhanced wettability and cell adhesion, Materials Letters 183 (2016) 420-424.
[187] S. Houshyar, G.S. Kumar, A. Rifai, N. Tran, R. Nayak, R.A. Shanks, R. Padhye, K. Fox, A. Bhattacharyya, Nanodiamond/poly-ε-caprolactone nanofibrous scaffold for wound management, Materials Science and Engineering: C 100 (2019) 378-387.
[188] L. Bazli, B. Eftekhari Yekta, A. Khavandi, Preparation and Characterization of Sn-Containing Glasses for Brachytherapy Applications, Transactions of the Indian Ceramic Society 76(4) (2017) 242-246.
[189] M.A. Brady, A. Renzing, T.E. Douglas, Q. Liu, S. Wille, M. Parizek, L. Bacakova, A. Kromka, M. Jarosova, G. Godier, Development of composite poly (lactide-co-glycolide)-nanodiamond scaffolds for bone cell growth, Journal of nanoscience and nanotechnology 15(2) (2015) 1060-1069.
[190] M. Parizek, T.E. Douglas, K. Novotna, A. Kromka, M.A. Brady, A. Renzing, E. Voss, M. Jarosova, L. Palatinus, P. Tesarek, Nanofibrous poly (lactide-co-glycolide) membranes loaded with diamond nanoparticles as promising substrates for bone tissue engineering, International journal of nanomedicine 7 (2012) 1931.
[191] V. Kumar, R. Mahajan, I. Kaur, K.-H. Kim, Simple and mediator-free urea sensing based on engineered nanodiamonds with polyaniline nanofibers synthesized in situ, ACS Applied Materials & Interfaces 9(20) (2017) 16813-16823.
[192] M. Alishiri, A. Shojaei, M.J. Abdekhodaie, Biodegradable polyurethane acrylate/HEMA-grafted nanodiamond composites with bone regenerative potential applications: structure, mechanical properties and biocompatibility, RSC advances 6(11) (2016) 8743-8755.
[193] S.A. Haddadi, A.R. SA, M. Amini, A. Kheradmand, In-situ preparation and characterization of ultra-high molecular weight polyethylene/diamond nanocomposites using Bi-supported Ziegler-Natta catalyst: Effect of nanodiamond silanization, Materials Today Communications 14 (2018) 53-64.
[194] J. Nunes-Pereira, A.R. Silva, C. Ribeiro, S.A.C. Carabineiro, J.G. Buijnsters, S. Lanceros-Méndez, Nanodiamonds/poly(vinylidene fluoride) composites for tissue engineering applications, Composites Part B: Engineering 111 (2017) 37-44.
[195] U. Maitra, K.E. Prasad, U. Ramamurty, C.N.R. Rao, Mechanical properties of nanodiamond-reinforced polymer-matrix composites, Solid State Communications 149(39) (2009) 1693-1697.
[196] U. Maitra, K.E. Prasad, U. Ramamurty, C. Rao, Mechanical properties of nanodiamond-reinforced polymer-matrix composites, Solid State Communications 149(39-40) (2009) 1693-1697.
[197] O. Shenderova, T. Tyler, G. Cunningham, M. Ray, J. Walsh, M. Casulli, S. Hens, G. McGuire, V. Kuznetsov, S. Lipa, Nanodiamond and onion-like carbon polymer nanocomposites, Diamond and related materials 16(4-7) (2007) 1213-1217.
[198] E. Tamburri, V. Guglielmotti, S. Orlanducci, M.L. Terranova, D. Sordi, D. Passeri, R. Matassa, M. Rossi, Nanodiamond-mediated crystallization in fibers of PANI nanocomposites produced by template-free polymerization: Conductive and thermal properties of the fibrillar networks, Polymer 53(19) (2012) 4045-4053.
[199] A. Apicella, R. Aversa, F.I. Petrescu, Hybrid Ceramo-Polymeric Nano-Diamond Composites, American Journal of Engineering and Applied Sciences 11(2) (2018) 766.782.
[200] L. Wang, W. Cao, X. Wang, P. Li, J. Zhou, G. Zhang, X. Li, X. Xing, Biodegradable silver-loaded polycation modified nanodiamonds/polyurethane scaffold with improved antibacterial and mechanical properties for cartilage tissue repairing, Journal of Materials Science: Materials in Medicine 30(4) (2019) 41.
[201] C. Shuai, W. Huang, P. Feng, C. Gao, D. Gao, Y. Deng, Q. Wang, P. Wu, X. Guo, Nanodiamond reinforced polyvinylidene fluoride/bioglass scaffolds for bone tissue engineering, Journal of Porous Materials 24(1) (2017) 249-255.
[202] S. Balakin, Y.-S. Yun, J. Lee, E.-H. Kang, J. Spohn, I.-S. Yun, J. Opitz, G. Cuniberti, J.-S. Yeo, In vitro characterization of osteoblast cells on polyelectrolyte multilayers containing detonation nanodiamonds, Biomedical Materials (2020).
[203] H. Gong, B. Anasori, C.R. Dennison, K. Wang, E.C. Kumbur, R. Strich, J.G. Zhou, Fabrication, biodegradation behavior and cytotoxicity of Mg-nanodiamond composites for implant application, Journal of Materials Science: Materials in Medicine 26(2) (2015) 110.
[204] Q. Zhang, V.N. Mochalin, I. Neitzel, K. Hazeli, J. Niu, A. Kontsos, J.G. Zhou, P.I. Lelkes, Y. Gogotsi, Mechanical properties and biomineralization of multifunctional nanodiamond-PLLA composites for bone tissue engineering, Biomaterials 33(20) (2012) 5067-5075.
[205] G.Y. Ahn, T.-K. Ryu, Y.R. Choi, J.R. Park, M.J. Lee, S.-W. Choi, Fabrication and optimization of Nanodiamonds-composited poly (ε-caprolactone) fibrous matrices for potential regeneration of hard tissues, Biomaterials research 22(1) (2018) 1-8.
[206] Y. Sun, A. Finne-Wistrand, T. Waag, Z. Xing, M. Yassin, A. Yamamoto, K. Mustafa, D. Steinmüller-Nethl, A. Krueger, A.C. Albertsson, Reinforced degradable biocomposite by homogenously distributed functionalized nanodiamond particles, Macromolecular Materials and Engineering 300(4) (2015) 436-447.
[207] A. Şelaru, D.-M. Drăguşin, E. Olăreț, A. Serafim, D. Steinmüller-Nethl, E. Vasile, H. Iovu, I.-C. Stancu, M. Costache, S. Dinescu, Fabrication and biocompatibility evaluation of nanodiamonds-gelatin electrospun materials designed for prospective tissue regeneration applications, Materials 12(18) (2019) 2933.

Available online at www.jourcc.com

Journal homepage: www.JOURCC.com

Journal of Composites and Compounds

Application of composite conducting polymers for improving the corrosion behavior of various substrates: A Review

Leila Bazli[a], Mohammad Yusuf[b], Ali Farahani[c], Morvarid Kiamarzi[d], Zahra Seyedhosseini[e], Mehran Nezhadmansari[f], Maryam Aliasghari[g], Marjan Iranpoor[h]*

[a] *School of Metallurgy and Materials Engineering, Iran University of Science and Technology, Tehran, Iran*
[b] *Department of Chemical Engineering, Universiti Teknologi PETRONAS, Bandar Seri Iskandar, 32610, Malaysia*
[c] *Department of Textile Engineering, Amirkabir University of Technology, Tehran, Iran*
[d] *Department of Polymer Engineering and Color Technology, Amirkabir University of Technology, Tehran, Iran*
[e] *Department of Chemistry, Amirkabir University of Technology, Tehran, Iran*
[f] *Department of Engineering and Materials Science, Sharif University of Technology, Tehran, Iran*
[g] *Department of Chemistry, College of Science, Yadegar-e-Imam Khomeini (RAH) Shahre Rey Branch, Islamic Azad University, Tehran, Iran*
[h] *Department of Agricultural Machinery Mechanics, University of Tehran, Alborz, Iran*

ABSTRACT

One of the most important problems in the manufacturing industry is metal corrosion. Recently, conductive polymers (CPs) have attracted attention due to their economic viability and widespread industrial applications. Upon adsorption, long-chain carbon bonds of polymers provide a blockage for large surface areas of corroding metals. The adsorbed thin films create a barrier between the surrounding environment and the metal substrate. Polypyrrole (PPy), polyaniline (PANI), and polythiophene (PTh) are conducting polymers that are utilized to protect metals and metal alloys against corrosion. A proper selection of synthesis parameters for CPs can improve the anticorrosion behavior of the coatings for metals and metal alloys. This paper has an overview of conducting polymer composite coatings on substrates based on steel, copper, magnesium, aluminum, and their alloys.

Peer review under responsibility of jourcc

ARTICLE INFORMATION

Article history:
Received 8 November 2020
Received in revised form 9 December 2020
Accepted 23 December 2020

Keywords:
Corrosion resistance
Polyaniline
Polypyrrole
Polythiophene
Metal substrates

Table of contents

1. Introduction

In the electronic and metallurgical industries, corrosion control is a challenge with great importance worldwide [1]. To protect metals from corrosion, various methods have been used. A widely practiced technique is the application of conducting polymer coatings [2, 3]. An active area of research in electrochemistry in the last decades has been the electrodeposition of CPs on the surfaces of metallic electrodes. In contrast to other coatings, such as paints, CPs do not contain toxic and hazardous constituents for the environment. Additionally, compared to other coatings that only provide physical barriers against corrosive envi-

* *Corresponding author: Leila Bazli; E-mail: leilabazli64@gmail.com*
https://doi.org/10.29252/jcc.2.4.7

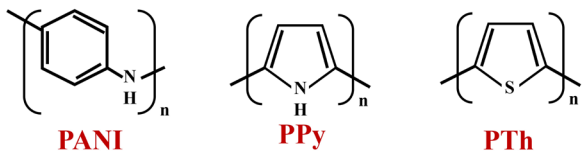

Fig. 1. FChemical composition of PANI, PPy, and PTh.

ronments, CPs provide physical and electronic barrier effects and electromagnetic interference (EMI) shielding which enhances the protection behavior [4-6].

These composite materials are strongly adsorbed onto active sites of the metal substrate leading to suppression of the dissolution process and production of a protective film layer. In fact, corrosion protection of CPs is a kind of anodic protection. According to studies, coating a metal with a conducting polymer places the potential of the electrode in the passive zone in the absence of redox reactions [7]. CPs have been applied on the surface of metals such as zinc [5], copper [6, 7], aluminum [8, 9], iron [10, 11], stainless steel (SS) [12], mild steel (MS) [13], etc. Mostly, polyaniline, polypyrrole, and polythiophene are used for coating metal substrates [8-19]. This review article has an overview of conducting polymers and composites and the state-of-the-art findings in the field of composite conducting polymers coated on various metal substrates are presented.

2.1. Conducting polymers

CPs can be used as a protective coating for the prevention of metal surface corrosion and enhancement of PE values [20]. Intrinsically conducting polymers are organic polymers with electrical conductivity. These compounds can either be semiconductors or show metallic conductivity. Their great advantage is the processability of conductive polymers, mainly by dispersion. Generally, these polymers are not thermoplastics and thereby they are not thermoformable. However, they are organic compounds like insulating polymers. Mechanical properties of conducting polymers are not similar to other commercial polymers, but they exhibit high electrical conductivity [21]. Using organic synthesis methods as well as advanced dispersion techniques, the electrical properties of these polymers can be fine-tuned [22, 23].

Different CPs are commercially available including PANI, PPy, PTh [24-26]. The chemical composition of these polymers is illustrated in Fig. 1. To synthesize CPs, electrochemical or chemical oxidation methods are used [27, 28]. PANI and its derivatives are extensively utilized for anticorrosion coatings due to facile synthesis, enhanced environmental stability, as well as various redox states that allow property regulation. Localized/delocalized polarons and bipolarons may be present in the PANI structure in various proportions, which depends on the methods of synthesis and isolation. PANI is practically applied to protect concrete steel bar reinforcement [28, 29].

Among all known CPs, one can consider PPy as promising material due to its high conductivity, easy and flexible preparation, good mechanical properties, and stability. Potential technological application of PPy include membrane separation [30], electronic and electrochromic devices [31], light-weight batteries [32], chromatographic stationary phases [33], sensors [34], and counterelectrode in electrolytic capacitors [35]. In recent years, it has been reported in several studies that PPy can protect metals and their alloys from corrosion [36-38].

An important class of conjugated polymers is PTh polymers that have a wide range of applications including field-effect transistors, electrochromic, and conducting films [39]. Few reports have demonstrated the use of PTh for the corrosion protection of metals. Among CPs, some PTh derivatives have shown good performance, which ultimately depends on the environment nature that CPs are in contact with. It is feasible to generate PTh and its derivatives on other CPs such as PPy by applying proper voltage. The combination of these two conducting polymers has led to better corrosion performance [40].

It is possible to formulate CP-based coatings to inhibit corrosion of metals even in damaged areas where the surface of the metal is directly exposed to the corrosive environment. Conducting polymers can be whether in the reduction-nonconductive state or oxidation conductive state. Under appropriate conditions, they can easily switch between the two states. Redox processes occur in CPs; therefore, the expelling/binding of dopants (counterions) is conducted in response to the metal surface potential variation. The potential variation is initiated by local electrochemical reactions resulting from the corrosion. Based on the local corrosive conditions, the dopants can be expelled or inserted by the CP, which often act as inhibitors that prevent the local corrosion reactions upon release [41, 42]. This is considered as a strategy suggested for taking advantage of CP-based corrosion-resistant coatings [43].

3. Corrosion protection mechanisms of CPs

For the provision of electronic conductivity in CPs, oxidative polymerization and anion doping are performed into the polymer. The penetration of aggressive anions into CP coating is prevented by controlling the doping ions. When CP-coated metal substrates are immersed in aggressive environments, such as the sodium chloride solution, the chloride anions present in the medium is exchanged with doped anions in the CP coating. The corrosion protection mechanisms of CPs have not been precisely revealed. Four possible hypotheses have been proposed:

I) Mechanism of controlled inhibitor release: In this mechanism, the anion dopant may be released upon reduction from the oxidized and hence doped CP-based coating on a metallic substrate, which is driven by a coating defect. As far as doped PANI is concerned, the anions are released either through a reduction mechanism or a simple acid-dopant elimination if it is soluble in water [44, 45].

II) Mechanism of anodic protection: according to this mechanism, protective metal oxide layers are formed on the metal surface as a result of CPs providing corrosion protection [46].

III) It is proposed that an electric field is produced when there is a contact between a doped semiconductor or a conducting polymer and a metal resulting in a reduction in the corrosion rate due to the restriction of the electron flow from the metal to an oxidizing species [47].

IV) CPs create an adherent, dense, low porosity film on the metal surface limiting the access of oxidant agents and prevent metal surface oxidation [48] (Fig 2).

A denser CP layer provides a better barrier effect and decreases the rate of H_2O and O_2 transport into the polymer. The reaction site on which O_2 reduction occurs moves from the metal/CP interface to the CP/solution interface by the enhancement of the compactness of the coating and its adherence to the substrate [49]. The change in the O_2 reduction site on the surface of the polymer leads to a decrease in reduction products such as OH across the metal/CP interface, and thereby prevent the coating disbondment and delamination [50]. Furthermore, oxygen reduction requires the local reoxidation of the coating and its active role in the case that local small-size defects or pinholes are generated. Therefore, the improvement of the barrier effect should not inactivate CPs. The open-circuit potential of the metal/CP-based coating/solution system will be is in the passive state as far as the conducting polymer is in the conductive form. The site of the O_2 reduction and its kinetics are important factors to determine the prolonged protective properties of the coating. Generally, it has been reported that the barrier effect is improved by

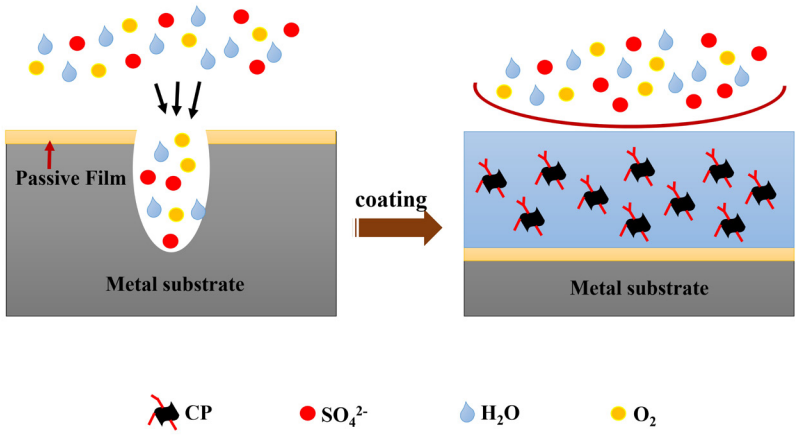

Fig. 2. Barrier effect of CPs for the diffusion of corrosive agents.

the dehydration of CP film electrodeposited on metal surfaces from an aqueous medium [43].

Mechanisms I and II are the most important contributing mechanisms that can rationalize corrosion inhibition by CPs. For a specific metal substrate/CP-based coating/solution system, the other two mechanisms contribute to the corrosion process simultaneously with the controlled inhibitor release or the anodic protection mechanism [10, 43].

3.1. Corrosion inhibitors

Different ways of CP doping can be used for controlling the electrolytic environment near the surface of the metal substrate in case a scratch is formed. In this condition, a galvanic coupling exists between the CP coating and the metal. The anodic reaction involves the metal oxidation, while the cathodic reaction is the CP reduction resulting in the release of the doping anions. However, oxygen is reduced simultaneously on both the metal surfaces and CP coating resulting in the OH production and the CP reoxidation, respectively. Based on the nature of doping anions and the metal, a self-healing process may be triggered. In some metals such as steel, copper, and aluminum, the doping anions such as molybdates and phosphonic acid derivatives act as inhibitors, or oxide formation is initiated [43].

In the inhibition mechanism, a monomolecular barrier is formed by the organic species adsorption onto the surface of the metal. The presence of the adsorbed molecules results in the limitation of the cathodic and/or anodic corrosion reactions such as electron transfer and decreases the rate of corrosion [51, 52]. According to Brycki et al. [53], the inhibitor action involves the replacement of the adsorbed water from the surface of the metal by soluble organic species (Org):

$$Org_{sol}+nH_2O_{ads} \rightarrow Org_{ads}+nH_2O_{sol} \quad (1)$$

Several investigations have reported that monomeric aniline, as well as functionalized aniline derivatives, act as potential corrosion inhibitors for steel and iron [54-56].

3.2. Anodic protection

The anodic protection activity involved the ways wherein general corrosion of the metal substrates and alloys is prevented by CPs mostly in solutions free of halides [43]. According to Kinlen et al. [57], the electroactive conducting polymer (ECPs) electrochemistry provides anodic protection for the substrate and also prevents cathodic debonding of the polymer coating. In this protection mechanism, the corrosion potential of the metal substrate in the electrolyte of interest moves to the passive region. The proposed reaction between the metal (M) and the oxidized state of the polymer coating (ECP^{m+}) is:

$$\frac{1}{n}M+\frac{1}{m}ECP^{m}+\frac{y}{n}H_2O \rightarrow \frac{1}{n}M(OH)_y^{(n-y)}+\frac{1}{m}ECP^{0}+\frac{y}{n}H \quad (2)$$

reoxidation of the ECP can occur by dissolved or atmospheric oxygen:

$$\frac{m}{4}O_2+\frac{m}{2}H_2O+ECP^{0} \rightarrow ECP^{m+}+mOH^{-} \quad (3)$$

4. Composite conducting polymers (CCPs)

Polymer nanocomposites have found increasing attention in various engineering applications [58-60]. The essential characteristic of this procedure is that CPs make it possible to maintain the substrate surface potential into a passive state wherein a protective oxide film is generated on the surface of metal substrates [43, 61]. As a result, CPs-based coatings are pinhole and defect resistant in such a way as that of the hexavalent chromium coatings. It is due to the replenishing of CP charges consumed by oxidation of metal by O_2 reduction within the CP coating. The corrosion process of metal is prevented by switching the CP-based coating into the oxidation state and thereby changing the potential into the passive region [62].

Expanded studies have focused on the anti-corrosive features of CPs; however, there are still numerous problems to be resolved regarding the fulfillment of mechanical and physico-electrochemical requirements of high performance anticorrosive CP-based coatings exposed to various practical conditions. Anticorrosive CP-based coatings have some limitations such as poor adhesion to the metallic substrate, anion-exchange properties, poor barrier effect due to porous structure, and irreversible consumption of stored charges within the coating, which can oxidize the substrate and form a passive oxide layer. The mentioned drawbacks show their effect more significantly under harsh environments. In case chloride ions are present, these ions can either penetrate through the CP coating or undergo anion-exchange (replacement of chlorides with CP doping anions) and reach the metal-substrate interface. Extended localized corrosion may be induced by chloride ions and during the redox reactions, the charge stored in the CP layer might be irreversibly consumed.

Using CP-based composites consisting of a conducting polymer and different inorganic fillers like metal oxides has been offered as an efficient strategy for the elimination of the disadvantages. In CP-based composites, the CP self-healing properties are combined with qualities of inorganic materials. Therefore, the composite coatings exhibit improved physicochemical and mechanical properties including enhanced hydrophobicity, barrier effect, and adhesion [43, 63-65]. The improvement of these properties leads to the enhancement of corrosion protection. Nano-

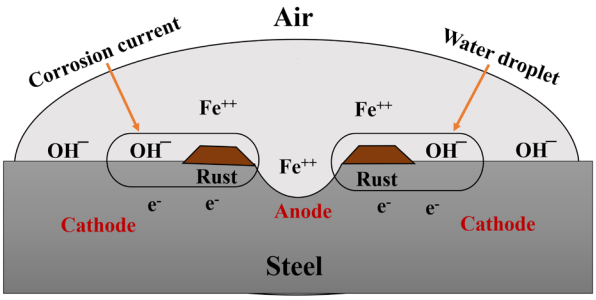

Fig. 3. Corrosion mechanism of steel.

technology has gained dramatic attention in recent years and is expected to make advancements in the design and development of commercially viable CP-based composite coatings [66]. It seems that CP-based nanocomposite can combine the properties of CPs and inorganic materials more effectively compared to microcomposites [67].

5. CCPs coatings on metals

5.1. CCPs coated on steels

Structural steel is corroded through an electrochemical process in the presence of oxygen and moisture. Rust is produced by the oxidation of iron in the steel, which has a volume of six times the original material [68]. The corrosion mechanism is presented in Fig. 3. There are numerous reported focusing on the corrosion protection effect of CP coatings on metals, especially iron and mild steel, and stainless steel and significant advancements have been made [69-76]. Most conducting polymers form conducting films directly on the substrate surface by anodic oxidation [77, 78]. Changing from an insulating state to a conducting state by different doping methods including injection of charge at the interface of a metal and the conducting polymer, photo doping, electrochemical doping, and chemical doping by charge transfer [71]. Due to the capability of these polymers in charge storing and transport, they can anodically protect metals against fast corrosion [79]. The corrosion protection mechanisms of CPs are complex and affected by various parameters [80-85]. Some theories have proposed that a passive oxide film is formed on the metal surface by oxidation-reduction processes, while others have predicted that the barrier mechanism is responsible for provided protection [61, 86, 87].

There are many studies targeting to investigate the corrosion protection of steel by CPs and CCPs. Sathiyanarayanan et al. [88] synthesized the PANI-TiO_2 composite coating (PTC) on steel and studied its corrosion protection behavior. To prepare PTC, aniline and TiO_2 were chemically oxidized by ammonium persulfate in a medium containing phosphoric acid. According to the results, the redox property of PTC led to maintaining the steel potential in the passive region. The resistance of the PTC coating in a 3% NaCl solution after 60 days was more than 107 cm^2 and in the salt spray test for 35 days was 109 cm^2. However, in both cases, the resistance of the coating was less than 104 cm^2. It was proposed that the corrosion protection is due to the passivation of steel resulting from the presence of polyaniline. Lenz et al. [73] incorporated TiO_2 pigment into PPy during the electrochemical synthesis of the CP-based coating on AISI 1010 steel. Weight loss and salt spray tests demonstrated that the PPy/TiO_2 composite significantly increased anti-corrosion properties compared to PPy films. The composite coatings were suggested as a primary coating that can be applied on mild steel instead of phosphatized layers.

According to Radhakrishnan et al. [89], composite coatings composed of PANI and nano-TiO_2 prepared by in-situ polymerization on steel plates showed superior corrosion resistance than did PANI coatings in aggressive environments. It was reported that the corrosion resistance improvement for the nanocomposite coating containing 4.18 wt% TiO_2 nanoparticles was beyond 100 times. It was proposed that the improvement is the result of the high surface area accessible for the dopant release due to nano-size additive, redox properties of PANI, charge transport prevention by the TiO_2 nanoparticles, and an increase in diffusion barrier. In a research study by Patil et al. [90], polyvinyl acetate (PVAc)-ZnO-PANI hybrid composite coatings (PVAc as the major matrix) were deposited on steel plates by the dip-coating method. In comparison with the coatings that contained either ZnO or PANI, the coatings that contained both the components exhibited higher corrosion resistance. The PVAc-ZnO-PANI coating showed the I_{corr} value of two-order lower than that of PVAc–ZnO and PVAc coatings. The improvement was reported to be the result of the redox behavior of PANI, enhancement of barrier properties by nanoparticles, as well as the formation of protective oxide layers near the substrate. Hosseini et al. [91] electrodeposited the polypyrrole phosphate (PPy-P) coating by cyclic voltammetry (CV) method on ST12 mild steel. The deposited PPy–P films demonstrated higher corrosion resistance compared to the PPy coating.

To coat 304 stainless steel for bipolar plates used in a proton exchange membrane fuel cell, Ren et al. [92] used galvanostatic deposition to produce an inner layer of PPy with large groups of dodecylsulfate ions, and then a PANI external layer containing small groups of SO_4^{2-} was applied via cyclic voltammetric deposition. According to results, the increase in pitting corrosion potential and corrosion potential of the bare steel for the single PPy and PPy/PANI coatings was more than 500 mV and 400 mV (saturated calomel electrode), respectively. Compared to the single PPy coating, the bilayer composite coating showed more effective corrosion reduction through providing passivity protection as well as a physical barrier with acceptable contact resistance.

Jiang et al. [46] deposited PPy-graphene oxide (GO) composite coatings on 304 stainless steel bipolar plates by in-situ electrodeposition to protect them against aggressive environments. The analysis in the simulated PEMFC environment exhibited that during potentiostatic polarization, the polarization current density of the substrate was significantly reduced by the conductive PPy-GO composite coating. The addition of GO to the PPy matrix led to the enhancement of the adhesion strength and an increase in the diffusion pathway of corrosive agents and therefore, restriction of their inward penetration. The best corrosion resistance was obtained for the composite coating containing 1 mg mL^{-1} of GO in the electrodeposition electrolyte. The corrosion enhancement in the composites is the result of the improved anodic protection and physical barrier. Jadhave et al. [93] added poly-o-anisidine (POA) and PANI nanoparticles to alkyd paint formulation for protecting the mild steel surface. In comparison with the POA/alkyd coatings, corrosion protection of the PANI/Alkyd coatings was remarkably higher.

Epoxy/graphene composite coatings with hydrophobic surfaces were prepared by Chang et al. [94]. The water droplet's contact angle with the epoxy surface and hydrophobic epoxy/graphene surface were 82° and 127°, respectively. The improvement of the corrosion resistance by applying the composite coating was reported to be due to the physical barrier effect, a decrease in the adsorption of water/corrosive media resulting from the coating hydrophobicity, and high aspect ratio of graphene nanosheets leading to enhancement of the oxygen barrier property. Sumi et al. [95] synthesized PANI-Fe_2O_3 composite by an *In-situ* method and added it to a commercial alkyd resin as an anti-corrosive coating for mild steel. The composite coating was proposed to offer passivation protection and better barrier performance. The complimentary cathodic reaction of the nonconductive leuco-PANI to the conductive emeraldine-PANI was explained to be also responsible for the improved corrosion resistance in the acidic medium. Table 1 summarized research

Table 1.
Research reports on using CCPs for corrosion protection of steel

Authors	CPs	Additive	Coating technique	Medium	Corrosion behavior
Jadhav et al. (2020) [96]	PPy	Fe_2O_3	Electrochemical method	NaCl	Better corrosion resistance was observed by the coating of Fe_2O_3/PPy.
Sun et al. (2020) [97]	PANI	-	Electrochemical deposition	NaCl	The density of corrosion current decreased 5 times and the coating exhibited effective protection for 140 days.
Deyab et al. (2020) [98]	PANI	Zn-Porphyrin	Electrochemical deposition	H_2SO_4	The composite of PANI/Zn-Pr with 1.0% of Zn- Pr rendered the highest anti-corrosion activity (99.41%).
Chen et al. (2020) [24]	PPy	Polydopamine –functionalized carbon powders	Electropolymerization	H_2SO_4	The PPy/C-PDA coating showed good protection performance for the 304SS bipolar plate in PEMFC.
Rajkumar et al. (2020) [99]	PPy	TiO_2, ZnO, and SiO_2	Incorporation in resin	NaCl	The PPy coating provides the denser passivation film at the interface of PPy and TiO_2.
Chen et al. (2019) [100]	PPy	TiO_2 and V-TiO_2	Electrochemical method	HCl	comparing V-TiO_2/PPy and TiO_2/PP composite coatings, the V-TiO_2/PPy showed better corrosion resistance performance.
Kong et al. (2019) [101]	PANI	Chitosan	-	HCl	Using the PANI/CTS in 0.5 M HCl solution was effective for corrosion protection of Q235 steel and at high PANI/CTS concentrations, the highest inhibition efficiency was obtained.
Babaei-Sati et al. (2019) [102]	PPy	Al_2O_3	Electrodeposition	H_2SO_4	PPy/Al_2O_3 nanocomposite with declining the density of corrosion current by 18 times, exhibited excellent performance in the protection of MS.
Shi et al. (2019) [26]	PANI	SiO2	Drop casting technique	H_2SO_4	The silicone-SiO_2@PANI coating with a 4:1 weight ratio of SiO_2/PANI exhibited the highest resistance against corrosion (2.24×107 Ω cm^2) after immersion in a corrosive medium for about 180 days.
Jaouhari et al. (2019) [103]	PPy	Zinc phosphate	Galvanostatic electrodeposition	NaCl	The ZP/PPy coatings showed excellent corrosion resistance and increased the ZP/PPy coating thickness.
Liu et al. (2019) [104]	PANI	TiO_2	Electrochemical deposition	NaCl	The epoxy coating with TiO_2/PANI particles showed high corrosion protection compared to the blank coating after subjecting to a corrosive environment.
Wang et al. (2019) [38]	PANI	Nb: TiO_2 nanofibers	galvanostatic method	HCl	The presence of Nb: TiO_2 nanofibers in the coating of PANI led to the provision of better in-situ anodic protection and physical barrier effect.
Abd El-Lateef et al. (2019) [105]	PANI	Tl_2O_3-SiO_2	Electrochemical deposition	HCl	The PANI coating could prevent the carbon steel corrosion and provide maximum yielding of 89% and this amount after the modification with Tl_2O_3-SiO_2 nanocomposites was improved and reached 96%.
Ramezanzadeh et al. (2018) [83]	PANI	GO-CeO_2	Electrodeposition	NaCl	The deposition of CeO_2 and PAni improved the properties of active and barrier corrosion inhibition of GO nanosheets.
Contri et al. (2018) [106]	PPy	Montmorillonite (Mt)	Electrodeposition	H_2SO_4	The Epoxy/Mt-PPy (5 wt%) could prevent carbon steel corrosion.
Jadhav et al. (2018) [107]	PPy	Mica	Incorporation in resin	NaCl	The pigment-based composite coating of Mo-doped PPy/mica exhibited better protection against corrosion with the steel passivation by the anions of molybdate.
Salem et al. (2018) [108]	PANI	-	Electrochemical deposition	NaCl	The possibility of delamination and blister formations were reduced by composite coatings.
Jiang et al. (2018) [109]	PANI	$Ni(OH)_2$	Cyclic voltammetry technique	NaCl	The $Ni(OH)_2$ particle deposition in a matrix of PANI prevented access to aggressive media. Also exhibited long-term anti-corrosive behavior.
Arabzadeh et al. (2017) [110]	PPy	-	Cyclic voltammetry method	HCl	The sample synthesized with the scan rate of polymerization equal to100 mV/s was the best coating.
Ladan et al. (2017) [111]	PPy	TiO_2	Dip coating	NaCl	Co doping TiO_2/PPy decreased the charge transfer across the interface of electrolyte/AISI 1018 steel.
Yan et al. (2017) [112]	PPy	Al_2O_3	Cyclic voltammetry technique	NaCl	The PPy-Al_2O_3 composite coating exhibited good performance in the corrosion protection of 316SS.
Yan et al. (2017) [113]	PPy	SiO_2	Cyclic voltammetry technique	NaCl	The PPy-SiO_2 coating exhibited good performance in the corrosion protection of 316SS.
Qiu et al. (2017) [114]	PANI	GO	Pulse-current deposition	Phosphate buffer	The 98.4% corrosion inhibition efficiency and 99.3% protection efficiency was obtained by using the PANI-GO composite coating.

investigation on using CCPs for corrosion protection of steel substrates.

5.2. CCPs coated on magnesium and its alloys

Because of biocompatibility, easy biodegradation, and excellent mechanical properties, Mg alloys have been extensively investigated for biomedical applications. Nevertheless, in a physiological environment, these alloys show a high corrosion rate leading to an increase in the pH value, which adversely affects cell differentiation, proliferation, and viability on the implant surface and thereby induces blood clots together with chronic tissue inflammatory responses [115-119]. Two main strategies for the improvement of the corrosion resistance of Mg and its alloys are surface modification and alloying [120, 121]. CPs and CP-based composites have been developed for the corrosion reduction of Mg-based substrates. The corrosion mechanism of Mg with and without CP coatings is shown in Fig. 4. PANI-TiO_2 composites were deposited on the ZM 21 alloy by Sathiyanarayanan et al. [122]. To synthesize the coatings, aniline underwent oxidative polymerization in phosphoric acid with $(NH_4)_2S_2O_8$, in the presence of TiO_2. Compared to the PANI coating, the composite coating exhibited more effective protection performance as a coating for the ZM 21 alloy. In another research, Guo et al. [123] applied a composite coating of PPy/ZnO to protect biodegradable Mg alloys for orthopedic implant applications. Results indicated the improved corrosion protection, antibacterial property, as well as cytocompatibility of the composite coating suggesting it as proper material for orthopedic implants.

Wang et al. [124] presented the corrosion protection performance of composite coatings based on PANI and coal. PANI/coal powder was synthesized by *in situ* polymerization, the coatings were composed of epoxy, and PANI/coal was deposited on the surfaces of Mg alloys. A significant decrease in the corrosion rate and corrosion current density of the PANI/coal coatings was observed suggesting that the coating is a promising candidate for the enhancement of corrosion resistance of Mg alloys in aggressive environments. In a research study by Li et al. [125], a PPy/V_2O_5 composite film was deposited on magnesium by mild vapor phase polymerization (VPP) technique. Corrosion investigations in 3.5 wt% NaCl revealed that the prepared composite film reduced the corrosion rate of Mg. The VPP method was offered as a technique with great potential to synthesize CP-based coating for the protection of reactive metals. Table 2 summarized research investigation on using CCPs for corrosion protection of Mg-based substrates.

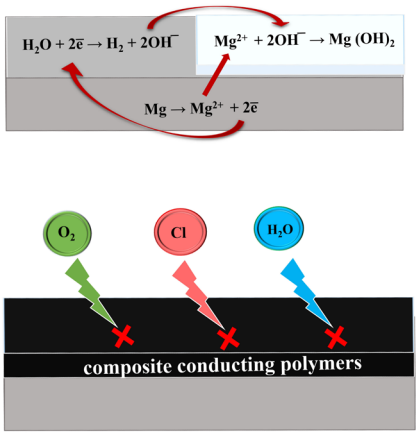

Fig. 4. Corrosion mechanism of brae Mg and CP-coated Mg.

5.3. CCPs coated on alumnum and its alloys

Al is an important metal due to its high technological value and its application in the household and aerospace industries [134-137]. Al-

Table 2.
Research reports on using CCPs for corrosion protection of Mg and its alloys

Authors	CPs	Additive	Coating technique	Medium	Corrosion behavior
Najibzad et al. (2020) [126]	PANI	Praseodymium	Dip coating	NaCl	The improvement in the performance was observed with applying 2000 ppm concentration compared to other concentrations.
Guo et al. (2020) [123]	PPy	ZnO_2	Cyclic voltammetry technique	NaCl	An increase in the resistance of the corrosion was observed.
Jothi et al. (2020) [127]	PPy	Gelatin	Electrodeposition	NaCl	The coating exhibited good performance in providing the corrosion resistance of AZ31.
Samadi et al. (2020) [128]	PANI	Praseodymium	Electrochemical methods	NaCl	The composite of PANI/Pr31 that exhibits anti-corrosion behavior can be used as environmentally-friendly and non-toxic corrosion protective coating.
Li et al. (2020) [125]	PPy	V_2O_5	Vapor phase polymerization (VPP)	NaCl	For the synthesis of the protective coating of CPs on reactive metals, the method of mild VPP may be effective.
Maurya et al. (2019) [129]	PANI	Graphene	Incorporation as pigments in epoxy resin	NaCl	The amount of the resistance value $>10^6$ Ω cm^2 was estimated using the composite coatings.
Yufeng Li et al. (2018) [130]	PANI	SiO_2	Electrochemical methods	NaCl	For the Mg-Li alloy, the good resistance was obtained with the coating and the density of the corrosion current and impedance value was 6.7×10^{-7} A cm^{-2} and 5×10^4 Ω cm^2, respectively.
Gao et al. (2018) [131]	PANI	-	Electrochemical methods	NaCl	The improvement was observed with the PANI-PhA addition because of the synergistic effect of silane, PhA, and PANI.
Wang et al. (2017) [124]	PANI	Coal	Electrodeposition	NaCl	This sample exhibited excellent resistance to corrosion.
Saremi et al. (2016) [132]	PPy	NaF and polyethylene glycol (PEG)	Cyclic voltammetry technique	NaCl	The observed improvement in the corrosion behavior of the PPy coating with PEG and NaF was due to the inhibition fluoride effect, which is considered a barrier for magnesium alloys.
Chen et al. (2010) [133]	PANI	SiO_2	Electrochemical methods	NaCl	In the solution of 3.0 wt% NaCl, the coating of PANI-SiO_2 showed better performance in keeping the potential values in the noble potential compared to the coating of pure epoxy.
Sathiyanarayanan. (2007) [122]	PANI	TiO_2	Electrodeposition	NaCl	For the protection of the Mg ZM 21 alloy, the composite coating was better than Polyaniline coating.

Table 3.
Research reports on using CCPs for corrosion protection of Al and its alloys

Authors	CPs	Additives	Coating technique	Medium	Corrosion behavior
Tomaev et al. (2019) [146]	PPy	Aluminum Oxide	Galvanostatic	H_2SO_4	The improvement in the electrochemical potential was obtained by PP coating, and the incensement in the surface impedance was provided by oxide coating.
Kumar et al. (2017) [147]	PPy	CeO_2	Galvanostatic	NaCl	For the corrosion protection of the Al in aircraft infrastructures, the nanocomposites of PPy with nanoparticles of CeO_2 could be effective.
Hosseini et al. (2017) [144]	PPy	TiO_2, Mn_2O_3, and ZnO	Cyclic voltammetry technique	oxalic acid	An excellent improvement in the corrosion protection was observed by applying the synthesized polypyrrole with nanoparticles of TiO_2.
Hussein et al. (2016) [143]	PANI / PPy	CNT and Ni_2LaO_4	Cyclic voltammetry technique	oxalic acid	The barrier effect increased with the nanoparticles of NiLa oxide. Also, the reaction of oxygen reduction catalyzed by these particles led to improving the Al passive state.
Ates et al. (2015) [148]	PANI	TiO_2, Ag, and Zn	Cyclic voltammetry method	NaCl	The nanocomposite film of PANI/Ag exhibited the highest efficiency of protection (PE = 97.54%).
Ates et al. (2015) [149]	PANI / PPy	TiO_2	Cyclic voltammetry	oxalic acid	According to the results, the efficiency of corrosion protection of the nanocomposites coated on the electrode of Al1050 was larger compared to PPy (94.9 %), PANI (96.4 %), and uncoated Al1050 electrodes.
Alvi et al. (2015) [150]	PANI	ZnO	Cyclic voltammetry method	HCl	Due to the electronic properties and chain conformation of the ZnO-PANI, it provided excellent protection against corrosion for Al and steel.
Jensen et al. (2014) [151]	PPy	Aluminum flake	Electrochemical methods	KCl	The composite coatings exhibited the reduction of dissolved oxygen over the scribe with no corrosion product concomitant buildup.
Gupta et al. (2013) [152]	PANI	Lignosulfonate	-	NaCl	The low corrosion amount was obtained with the coating of 5 wt% Pani-LGS/epoxy.
Jadhav et al. (2013) [153]	PPy	Aluminum flake	Incorporation in epoxy resin	Electrolyte solution	For the larger defect protection of the AA 2024-T3 substrate, the composite of the wire PPy/Al flake was effective.
Yan et al. (2013) [142]	PPy	Al flake	Incorporation in epoxy resin	DHS solution	The best performance of the protection was obtained by doping the vanadate in the composite coating.
Shabani et al. (2011) [154]	PANI	Montmorillonite	Electrosynthesis	NaCl	Using nanocomposite-coated compared to uncoated Al led to a decrease in the amount of the corrosion current (i_{corr}) from 6.55 μA cm^{-2} to 0.102 μA cm^{-2}.
Hosseini et al. (2011) [134]	PANI	Montmorillonite	Electrochemical methods	NaCl	Epoxy blend with polyaniline and MMT showed the highest corrosion protection for 100h.
Castagno et al. (2010) [155]	PPy	Montmorillonite (MT)	Electrochemical techniques	NaCl	The PPy/MT films with 1% clay provided good performance in the protection of corrosion for Al.
Hosseini et al. (2009) [156]	PPy	Montmorillonite	Electrochemical methods	NaCl	The coating provided good protection of Al corrosion with a combination of epoxyblend with MT and PPy advantages.
Wu et al. (2007) [157]	PANI	Silicate–NiZn ferrite	Electrochemical and salt-spray	NaCl	With the incorporation of the NiZn ferrite/PANI particles, the denser configuration of the ormosil hybrids was obtained which could prevent the Al alloy substrate corrosion.
Shah et al. (2001) [145]	PANI/ PPy	-	Galvanostatic and potentiostatic technique	oxalic acid	The low corrosion rates were observed in moderate to high applied electrochemical current densities.

though on the surface of reactive metals such as Al, a thin oxide film is formed protecting them from further corrosion, localized corrosion occurs on the surface of Al when it is exposed to corrosive environments containing complexing agents such as halides [138-141]. There have been several studies regarding the deposition of CP-based coatings on Al-based substrates to enhance their corrosion resistance. In a study by Yan et al. [142], PPy was first deposited on Al flakes in the presence of inhibiting dopants including vanadate, molybdate, or phosphate oxyanions. Then, the modified Al flakes were added to an epoxy primer to protect the AA 2024-T3 alloy. The composite coating showed good protection performance for the Al alloy through the mechanism of oxygen scavenger protection provided by PPy in the composite coating.

Hussein et al. [143] used the cyclic voltammetry technique to deposit PANI-NiLa and PPy-carbon nanotubes (CNTs) nanocomposite coating on aluminum. The thermal stability of PPy was enhanced by the addition of CNTs, while decreased in the presence of NiLa. The addition of CNTs and NiLa particles improved the protection role and adhesion of the PPy coating for aluminum. Compared to the PPy layer, the nanocomposite coatings had higher protection property for Al in the NaCl solution. PPy-NiLa nanocomposite coating demonstrated the highest corrosion protection. In another study by Hosseini et al. [144], ZnO, Mn_2O_3, and TiO_2, nanoparticles were dispersed in PPy by in-situ electropolymerization to

protect Al electrodes. It was found that the corrosion resistance of the nanocomposites was higher than that of bare PPy in harsh environments. The PPy/TiO_2 composite coating exhibited a remarkable improvement in corrosion protection. The great enhancement of protection properties was reported to be due to the high surface area of nano-additives for the dopant release, charge transport prevention by the TiO_2 nanoparticles, redox properties of PPy together with increased barrier effect to diffusion.

Kunal et al. [145] coated Al-2024-T3 substrate with PPy, PANI, and PPy/PANI composites via potentiostatic and galvanostatic techniques. Results showed that the corrosion rate reduction in the presence of CPs was about three orders of magnitude. Deposition time and applied current density as electrochemical processing variables were found to noticeably affect the corrosion behavior of the coated substrate so that low corrosion rates were achieved by applying moderate to high current densities. Table 3 summarized research investigation on using CCPs for corrosion protection of Al-based substrates.

5.4. CCPs coated on copper and its alloys

Cu is used in industrial and technological applications on a large scale because of its outstanding processability, thermal and electrical conductivity, wear and shock resistance, and ductility. Cu is the best selection for integrates circuits, especially microprocessors due to its improved electromigration performance as well as low resistivity [158-162]. Under neutral pH conditions, protective oxide or hydroxide layers form on the surface of Cu substrates [163-167]. In chloride-containing environments, the copper corrosion process and the protective layer formation are more complex [168, 169]. In oxidative environments, the mechanism of corrosion for copper involves the electrochemical reduction of water and oxygen at local cathodic zones and the dissolution of Cu at local anodic zones. The rates of reduction and dissolution reactions are slowed down by the formation of the protective film formation, and the diffusion rate of Cu chloride ions into the chloride solution influences the rate of these reactions. However, the diffusion and reduction of corrosive species like oxygen cannot be prohibited by the oxides or hydroxide layers [170, 171].

The enhancement of the corrosion resistance of copper has been an attractive topic for researchers [172, 173]. Applying CPs on copper substrates and their corrosion behaviors have been reported in the literature [174-182]. Beikmohammadi et al. [37] used the in situ electropolymerization technique to deposit PPy/TiO_2 composite coating on copper electrodes. It was proved that the addition of TiO_2 nanoparticles promoted the corrosion protection behavior of the coating compared to bare PPy in a harsh environment. As reported for the similar coatings for other metals, an increment of barrier to diffusion, charge transport prevention by the TiO_2 particles, high surface area of the titanium oxide nanoparticles for the dopant liberation, as well as redox properties of polypyrrole are responsible for the improvement.

Pan et al. [183] used Cu as substrate and electrochemically synthesized the conductive composite coating consisting of an outer PANI layer and an inner PPy layer. They found that the corrosion potential of Cu substrate increased via both the single PPy coating and the bilayered PPy/PANI. In addition, the corrosion current density decreased by an order of magnitude compared to uncoated Cu substrate. They also evaluated the Long-term protection of the coatings. It was shown that the PPy/PANI bilayer coating was better than the single polypyrrole coating that can be an effective physical barrier for inhibiting the penetration of corrosive species.

In another study, Çakmakcı et al. [184] fabricated the poly(pyrrole)/

Table 4.
Research reports on using CCPs for corrosion protection of Cu and its alloys

Authors	CPs	Additive	Coating technique	Medium	Corrosion behavior
Badi et al. (2020) [94]	PANI	Silver nanoparticles	Electrochemical methods	HCl	The coating containing the nanoparticles of PANI-Ag exhibited corrosion protection for 6061 Al alloys used in solar panel frames.
Wan et al (2019) [189]	PPy	Benzotriazole (BTA) or/ and silica	Cyclic voltammetry technique	NaCl	The composite film exhibited good performance in corrosion protection due to the synergetic effect of silica physical barrier and BTA active protection.
Beikmohammadi et al. (2018) [37]	PPy	TiO_2	Cyclic voltammetry technique	NaCl	Nanoparticles of TiO_2 exhibited good performance in the improvement of polypyrrole films for the protection of copper.
Jafari et al. (2016) [190]	PPy	Graphene	Cyclic voltammetry technique	H_2SO_4	The number of polymer pores decreased and the nanocomposite morphology after immersion in NaCl solution at a concentration of 5000 ppm for 2 hours, remained constant and unchanged.
Shabani et al. (2015) [191]	PPy	Zeolite	Electrodeposition	NaCl	By using this coating the corrosion current density declined and reached 0.34 μA cm^{-2} and also the potential of corrosion shifted from −0.314 V to −0.141 V.
Pan et al. (2015) [183]	PPy/ PANI	-	Cyclic voltammetric and galvanostatic	acidic medium	The PPy/PANI bilayered coating provided better protection for the copper substrate than the PPy coating.
Davoodi et al. (2015) [192]	PPy	Multi-walled carbon nanotubes	Cyclic voltammetry technique	NaCl	Higher protection of corrosion was obtained by using the nanocomposite of PPy/functionalized MWCNT compared to PPy/MWCNT.
Dhibar et al. (2013) [193]	PANI	-	Electrochemical methods	HCl	The promising electrochemical properties were exhibited with doping of 2 wt% PANI.
Ozkazanc et al. (2013) [209]	PPy	Zinc and nickel	Electrodeposited	H_2SO_4	The protection degree for electrodes of copper was enhanced.
K. Wu et al. (2009) [93]	PANI	Silicate/carbon black	Electrochemical methods	NaCl	The resistance of corrosion and barrier properties were enhanced by using the system of PANI/CB.

poly(N methyl pyrrole) bilayer and poly(pyrrole-co-N-methyl pyrrole) copolymer composites via electrochemical synthesis. They applied them on Cu substrate through cyclic voltammetry from an aqueous solution of 0.1 M monomer and 0.3 M oxalic acid. They suggested that the monomer feed ratio strongly affects the performance of coatings, in which the most protective property was illustrated by copolymer fabricated with 8:2 concentration ratio. Electrochemical impedance spectroscopy and anodic polarization using 0.1 M H_2SO_4 solution were employed to evaluate the corrosion behavior of polymer composites. They implied that the bilayer and copolymer coatings had a higher protection effect than that of single PPy coatings.

Branzoi et al. [185] investigated the electropolymerized monolayer poly (N, N' dimethylaniline) (PNDMA), bilayer PNDMA/PANI, polyaniline (PANI), PANI/PNDMA coatings on Cu substrate.

They found that good corrosion protection was obtained by PNDMA-SDS/PANI coatings in aggressive media. In addition, better corrosion inhibition efficiencies were observed for bilayer coatings.

Singh et al. [186] used electrophoretic deposition (EPD), as a less time-consuming, inexpensive, and fairly facile method, to fabricate hydrophobic graphene oxide-polymer composite (GOPC) on copper. The efficacy of the coating under stringent environmental conditions was investigated via EIS and potentiodynamic polarization investigation. They implied that electrochemical degradation of the bare copper substrate was three orders of magnitude higher than GOPC coating. They realized that the GOPC coatings were impermeable to ion diffusion of corrosive liquid solution and oxidizing gas.

In another study, Kim et al. [187] fabricated graphene/polysiloxane (PSX) nanocomposite films possessing superior corrosion protection, high electrical, and dual function. A facile bar coating method using a metering rod was employed for the better in-plane ordering of filler networks in the coating. It was found that PSX-G composite coating films improved the charge transfer resistance dramatically (20,000%), higher electrical conductivity (1700 Sm^{-1}), and decreased rate of corrosion (1/40 th). This was due to complementary effects between the covering agent of graphene defects and inorganic polymer matrix as the anticorrosive layer as well as graphene conductive filler. They implied that the system could be potentially employed in industrial fields including energy storage systems, electromagnetic shielding (EMI), and anti-icing.

Singh et al. [188] applied a cathodic electrophoretic deposition (EPD) technique to fabricate anticorrosive graphene reinforced composite coating. They implied that the Cu substrate became resistant to electrochemical degradation by applying the composite coating. In this regard, the Tafel analysis showed that composite coating reduced the corrosion rate about an order of magnitude lower than that of bare substrate. Table 4 summarizes the studies focusing on the application of CCPs for corrosion protection of steel, Cu, Al, and Mg.

6. Conclusions and future insights

CCPs have been widely investigated for the protection of metal substrates such as steel, Al, Cu, and Mg. PANI, PPy, and PTh are common conducting polymers that have been developed as protective coatings for metals. Composite conducting polymers have been prepared with the incorporation of different components such as ZnO_2, TiO_2, NiLa, Mn_2O_3, etc. Corrosion inhibiting and anodic protection is the most important contributing mechanisms to the reduction of the corrosion rate of metals. It has been demonstrated that CCPs have superior corrosion protection properties than do conducting polymer coatings. This is the result of the high surface area of nano-additives for the dopant release, and the promotion of barrier effect against diffusion. It is expected that in future investigations, a variety of reinforcements will be at the center of attention and more focus will be placed on the application of CCPs on other metallic substrates and in different fields. Moreover, since the protection against corrosion by CPs is mostly based on the mechanism of anodic protection, the stabilization of the passive oxide film under the polymer coating and inhibition of the aggressive anions from penetration into the polymer film must be carefully considered.

REFERENCES

[1] B. Yao, G. Wang, J. Ye, X. Li, Corrosion inhibition of carbon steel by polyaniline nanofibers, Materials Letters 62(12-13) (2008) 1775-1778.
[2] M. Hosseini, M. Sabouri, T. Shahrabi, Corrosion protection of mild steel by polypyrrole phosphate composite coating, Progress in Organic Coatings 60(3) (2007) 178-185.
[3] S. Das, T. Yokozeki, Polyaniline-based multifunctional glass fiber reinforced conductive composite for strain monitoring, Polymer Testing (2020) 106547.
[4] P. Herrasti, F. Recio, P. Ocon, E. Fatás, Effect of the polymer layers and bilayers on the corrosion behaviour of mild steel: Comparison with polymers containing Zn microparticles, Progress in Organic Coatings 54(4) (2005) 285-291.
[5] S. Das, S. Sharma, T. Yokozeki, S. Dhakate, Conductive Layer-based Multifunctional Structural Composites for Electromagnetic Interference Shielding, Composite Structures (2020) 113293.
[6] V. Kumar, S. Das, T. Yokozeki, Frequency independent AC electrical conductivity and dielectric properties of polyaniline-based conductive thermosetting composite, Journal of Polymer Engineering 38(10) (2018) 955-961.
[7] H. Zhu, L. Zhong, S. Xiao, F. Gan, Accelerating effect and mechanism of passivation of polyaniline on ferrous metals, Electrochimica acta 49(28) (2004) 5161-5166.
[8] S. Aeiyach, B. Zaid, P. Lacaze, A one-step electrosynthesis of PPy films on zinc substrates by anodic polymerization of pyrrole in aqueous solution, Electrochimica acta 44(17) (1999) 2889-2898.
[9] T. Zhang, C. Zeng, Corrosion protection of 1Cr18Ni9Ti stainless steel by polypyrrole coatings in HCl aqueous solution, Electrochimica Acta 50(24) (2005) 4721-4727.
[10] G.M. Spinks, A.J. Dominis, G.G. Wallace, D.E. Tallman, Electroactive conducting polymers for corrosion control, Journal of Solid State Electrochemistry 6(2) (2002) 85-100.
[11] N. Ogurtsov, A. Pud, P. Kamarchik, G. Shapoval, Corrosion inhibition of aluminum alloy in chloride mediums by undoped and doped forms of polyaniline, Synthetic Metals 143(1) (2004) 43-47.
[12] K. Shah, J. Iroh, Electrochemical synthesis and corrosion behavior of poly (N-ethyl aniline) coatings on Al-2024 alloy, Synthetic metals 132(1) (2002) 35-41.
[13] A.R. Elkais, M.M. Gvozdenović, B. Jugović, T. Trišović, M. Maksimović, B. Grgur, Electrochemical synthesis and corrosion behavior of thin polyaniline film on mild steel, copper and aluminum, Hemijska industrija 65(1) (2011) 15-21.
[14] J. Martins, M. Bazzaoui, T. Reis, E. Bazzaoui, L. Martins, Electrosynthesis of homogeneous and adherent polypyrrole coatings on iron and steel electrodes by using a new electrochemical procedure, Synthetic metals 129(3) (2002) 221-228.
[15] S. Jafarzadeh, P.M. Claesson, P.-E. Sundell, E. Tyrode, J. Pan, Active corrosion protection by conductive composites of polyaniline in a UV-cured polyester acrylate coating, Progress in organic coatings 90 (2016) 154-162.
[16] A. Ali Fathima Sabirneeza, S. Subhashini, A novel water-soluble, conducting polymer composite for mild steel acid corrosion inhibition, Journal of applied polymer science 127(4) (2013) 3084-3092.
[17] J. Stejskal, M. Trchová, J. Kovářová, J. Prokeš, M. Omastová, Polyaniline-coated cellulose fibers decorated with silver nanoparticles, Chemical Papers 62(2) (2008) 181-186.
[18] S.S. Najar, A. Kaynak, R.C. Foitzik, Conductive wool yarns by continuous vapour phase polymerization of pyrrole, Synthetic metals 157(1) (2007) 1-4.
[19] S.A. Kumar, K.S. Meenakshi, T. Sankaranarayanan, S. Srikanth, Corrosion resistant behaviour of PANI–metal bilayer coatings, Progress in Organic Coatings 62(3) (2008) 285-292.
[20] T. Li, X. Zeng, J. Xu, Preparation and characterization of conductive polypyrrole/organophilic montorillonite nanocomposite, Polymer-Plastics Technology and Engineering 46(8) (2007) 751-757.
[21] S. Das, V. Kumar, T. Yokozeki, Strain sensing behavior of multifunctional polyaniline-based thermoset polymer under static loading conditions, Polymer Testing 77 (2019) 105916.
[22] T.F. Otero, Conducting Polymers: Bioinspired Intelligent Materials and Devices, Royal Society of Chemistry2016.
[23] I. György, Conducting polymers: A new era in electrochemistry, Springer2008.

[24] Z. Chen, G. Zhang, W. Yang, B. Xu, Y. Chen, X. Yin, Y. Liu, Superior conducting polypyrrole anti-corrosion coating containing functionalized carbon powders for 304 stainless steel bipolar plates in proton exchange membrane fuel cells, Chemical Engineering Journal (2020) 124675.
[25] M. Bouabdallaoui, Z. Aouzal, A. El Guerraf, S.B. Jadi, M. Bazzaoui, R. Wang, E. Bazzaoui, Influence of polythiophene overoxidation on its physicochemical properties and corrosion protection performances, Materials Today: Proceedings 31 (2020) S69-S74.
[26] S. Shi, Y. Zhao, Z. Zhang, L. Yu, Corrosion protection of a novel SiO_2@ PANI coating for Q235 carbon steel, Progress in Organic Coatings 132 (2019) 227-234.
[27] G. Inzelt, Conducting polymers: a new era in electrochemistry, Springer Science & Business Media2012.
[28] G. Ćirić-Marjanović, Recent advances in polyaniline research: Polymerization mechanisms, structural aspects, properties and applications, Synthetic metals 177 (2013) 1-47.
[29] B. Bhanvase, S. Sonawane, New approach for simultaneous enhancement of anticorrosive and mechanical properties of coatings: Application of water repellent nano CaCO3–PANI emulsion nanocomposite in alkyd resin, Chemical Engineering Journal 156(1) (2010) 177-183.
[30] X. Tan, C. Hu, Z. Zhu, H. Liu, J. Qu, Electrically Pore-Size-Tunable Polypyrrole Membrane for Antifouling and Selective Separation, Advanced Functional Materials 29(35) (2019) 1903081.
[31] V.K. Thakur, G. Ding, J. Ma, P.S. Lee, X. Lu, Hybrid materials and polymer electrolytes for electrochromic device applications, Advanced materials 24(30) (2012) 4071-4096.
[32] I. Sultana, M. Rahman, S. Li, J. Wang, C. Wang, G.G. Wallace, H.-K. Liu, Electrodeposited polypyrrole (PPy)/para (toluene sulfonic acid)(pTS) free-standing film for lithium secondary battery application, Electrochimica acta 60 (2012) 201-205.
[33] J. Wu, Z. Mester, J. Pawliszyn, Speciation of organoarsenic compounds by polypyrrole-coated capillary in-tube solid phase microextraction coupled with liquid chromatography/electrospray ionization mass spectrometry, Analytica chimica acta 424(2) (2000) 211-222.
[34] S. Navale, G. Khuspe, M. Chougule, V. Patil, Camphor sulfonic acid doped PPy/α-Fe_2O_3 hybrid nanocomposites as NO_2 sensors, RSC Advances 4(53) (2014) 27998-28004.
[35] C. Bu, Q. Tai, Y. Liu, S. Guo, X. Zhao, A transparent and stable polypyrrole counter electrode for dye-sensitized solar cell, Journal of power sources 221 (2013) 78-83.
[36] E. Armelin, R. Pla, F. Liesa, X. Ramis, J.I. Iribarren, C. Alemán, Corrosion protection with polyaniline and polypyrrole as anticorrosive additives for epoxy paint, Corrosion science 50(3) (2008) 721-728.
[37] M. Beikmohammadi, L. Fotouhi, A. Ehsani, M. Naseri, Potentiodynamic and electrochemical impedance spectroscopy study of anticorrosive properties of p-type conductive polymer/TiO_2 nanoparticles, Solid State Ionics 324 (2018) 138-143.
[38] Y. Wang, S. Zhang, P. Wang, S. Chen, Z. Lu, W. Li, Electropolymerization and corrosion protection performance of the Nb:TiO_2 nanofibers/polyaniline composite coating, Journal of the Taiwan Institute of Chemical Engineers 103 (2019) 190-198.
[39] I.F. Perepichka, D.F. Perepichka, H. Meng, F. Wudl, Light-emitting polythiophenes, Advanced Materials 17(19) (2005) 2281-2305.
[40] L. Ai, Y. Liu, X. Zhang, X. Ouyang, Z. Ge, A facile and template-free method for preparation of polythiophene microspheres and their dispersion for waterborne corrosion protection coatings, Synthetic metals 191 (2014) 41-46.
[41] P.J. Kinlen, V. Menon, Y. Ding, A mechanistic investigation of polyaniline corrosion protection using the scanning reference electrode technique, Journal of the Electrochemical Society 146(10) (1999) 3690.
[42] P. Kinlen, Y. Ding, D. Silverman, Corrosion protection of mild steel using sulfonic and phosphonic acid-doped polyanilines, Corrosion 58(6) (2002) 490-497.
[43] P.P. Deshpande, N.G. Jadhav, V.J. Gelling, D. Sazou, Conducting polymers for corrosion protection: a review, Journal of Coatings Technology and Research 11(4) (2014) 473-494.
[44] D. Sazou, P.P. Deshpande, Conducting polyaniline nanocomposite-based paints for corrosion protection of steel, Chemical Papers 71(2) (2017) 459-487.
[45] G. Paliwoda-Porebska, M. Rohwerder, M. Stratmann, U. Rammelt, W. Plieth, Release mechanism of electrodeposited polypyrrole doped with corrosion inhibitor anions, Journal of Solid State Electrochemistry 10(9) (2006) 730-736.
[46] L. Jiang, J.A. Syed, H. Lu, X. Meng, In-situ electrodeposition of conductive polypyrrole-graphene oxide composite coating for corrosion protection of 304SS bipolar plates, Journal of Alloys and Compounds 770 (2019) 35-47.
[47] P. Chandrasekhar, Conducting polymers, fundamentals and applications, (1999).
[48] R. Hasanov, S. Bilgiç, Monolayer and bilayer conducting polymer coatings for corrosion protection of steel in 1 M H_2SO_4 solution, Progress in Organic Coatings 64(4) (2009) 435-445.
[49] A. Michalik, M. Rohwerder, Conducting polymers for corrosion protection: a critical view, Zeitschrift für Physikalische Chemie 219(11) (2005) 1547-1559.
[50] G. Paliwoda-Porebska, M. Stratmann, M. Rohwerder, K. Potje-Kamloth, Y. Lu, A.Z. Pich, H.-J. Adler, On the development of polypyrrole coatings with self-healing properties for iron corrosion protection, Corrosion science 47(12) (2005) 3216-3233.
[51] Y.I. Kuznetsov, Organic corrosion inhibitors: where are we now? A review. Part IV. Passivation and the role of monoand diphosphonates, International Journal of Corrosion and Scale Inhibition 6(4) (2017) 384-427.
[52] M.A.A. Ali, Inhibition of mild steel corrosion in cooling systems by low-and non-toxic corrosion inhibitors, The University of Manchester (United Kingdom), 2017.
[53] B.E. Brycki, I.H. Kowalczyk, A. Szulc, O. Kaczerewska, M. Pakiet, Organic corrosion inhibitors, InTech Open, Corrosion Inhibitors, Principles and Recent Applications2017.
[54] M. Quraishi, S.K. Shukla, Poly (aniline-formaldehyde): a new and effective corrosion inhibitor for mild steel in hydrochloric acid, Materials Chemistry and Physics 113(2-3) (2009) 685-689.
[55] R. Karthikaiselvi, S. Subhashini, Study of adsorption properties and inhibition of mild steel corrosion in hydrochloric acid media by water soluble composite poly (vinyl alcohol-o-methoxy aniline), Journal of the Association of Arab Universities for Basic and Applied Sciences 16 (2014) 74-82.
[56] D.K. Yadav, D. Chauhan, I. Ahamad, M. Quraishi, Electrochemical behavior of steel/acid interface: adsorption and inhibition effect of oligomeric aniline, RSC advances 3(2) (2013) 632-646.
[57] P. Kinlen, D. Silverman, C. Jeffreys, Corrosion protection using polyanujne coating formulations, Synthetic Metals 85(1-3) (1997) 1327-1332.
[58] L. Bazli, A. Khavandi, M.A. Boutorabi, M. Karrabi, Correlation between viscoelastic behavior and morphology of nanocomposites based on SR/EPDM blends compatibilized by maleic anhydride, Polymer 113 (2017) 156-166.
[59] L. Bazli, A. Khavandi, M.A. Boutorabi, M. Karrabi, Morphology and viscoelastic behavior of silicone rubber/EPDM/Cloisite 15A nanocomposites based on Maxwell model, Iranian Polymer Journal 25(11) (2016) 907-918.
[60] M. Bazli, L. Bazli, R. Rahmani, S. Mansoor, M. Ahmadi, R. Pouriamanesh, Concrete filled FRP–PVC tubular columns used in the construction sector: A review, Journal of Composites and Compounds 2(4) (2020) 155-162.
[61] S.A. Umoren, M.M. Solomon, Protective polymeric films for industrial substrates: A critical review on past and recent applications with conducting polymers and polymer composites/nanocomposites, Progress in Materials Science 104 (2019) 380-450.
[62] M.H. Naveen, N.G. Gurudatt, H.B. Noh, Y.B. Shim, Dealloyed AuNi dendrite anchored on a functionalized conducting polymer for improved catalytic oxygen reduction and hydrogen peroxide sensing in living cells, Advanced Functional Materials 26(10) (2016) 1590-1601.
[63] L. Zhang, W. Du, A. Nautiyal, Z. Liu, X. Zhang, Recent progress on nanostructured conducting polymers and composites: synthesis, application and future aspects, Science China Materials 61(3) (2018) 303-352.
[64] M. Tomczykowa, M.E. Plonska-Brzezinska, Conducting polymers, hydrogels and their composites: preparation, properties and bioapplications, Polymers 11(2) (2019) 350.
[65] L. Fu, Q. Qu, R. Holze, V.V. Kondratiev, Y. Wu, Composites of metal oxides and intrinsically conducting polymers as supercapacitor electrode materials: the best of both worlds?, Journal of Materials Chemistry A 7(25) (2019) 14937-14970.
[66] A. Eftekhari, Nanostructured conductive polymers. 2010, Chichester, West Sussex, UK; Hoboken, NJ: Wiley. xxiii.
[67] H. Bhandari, S.A. Kumar, S. Dhawan, Conducting polymer nanocomposites for anticorrosive and antistatic applications, Nanocomposites: New Trends and Developments (2012) 73-96.
[68] C. Cao, M.M. Cheung, Non-uniform rust expansion for chloride-induced pitting corrosion in RC structures, Construction and Building Materials 51 (2014) 75-81.
[69] M. Bernard, A. Hugot-Le Goff, S. Joiret, N.N. Dinh, N.N. Toan, Polyaniline layer for iron protection in sulfate medium, Journal of the Electrochemical Society 146(3) (1999) 995.
[70] D.E. Tallman, G. Spinks, A. Dominis, G.G. Wallace, Electroactive conducting polymers for corrosion control, Journal of Solid State Electrochemistry 6(2) (2002) 73-84.
[71] D. Tallman, M. Dewald, C. Vang, G. Wallace, G. Bierwagen, Electrodeposi-

tion of conducting polymers on active metals by electron transfer mediation, Current Applied Physics 4(2-4) (2004) 137-140.
[72] D.M. Lenz, M. Delamar, C.A. Ferreira, Improvement of the anticorrosion properties of polypyrrole by zinc phosphate pigment incorporation, Progress in Organic Coatings 58(1) (2007) 64-69.
[73] D.M. Lenz, M. Delamar, C.A. Ferreira, Application of polypyrrole/TiO_2 composite films as corrosion protection of mild steel, Journal of Electroanalytical Chemistry 540 (2003) 35-44.
[74] T. Schauer, A. Joos, L. Dulog, C. Eisenbach, Protection of iron against corrosion with polyaniline primers, Progress in Organic Coatings 33(1) (1998) 20-27.
[75] O. Zubillaga, F. Cano, I. Azkarate, I. Molchan, G. Thompson, A. Cabral, P. Morais, Corrosion performance of anodic films containing polyaniline and TiO_2 nanoparticles on AA3105 aluminium alloy, Surface and Coatings Technology 202(24) (2008) 5936-5942.
[76] K. Thompson, Los Alamos National Laboratory Report LA-UR-92-360; DA Wrobleski, BC Benicewicz, KG. Thompson, and CJ Bryan, Polymer Preprints 35 (1994) 265.
[77] S.P. Sitaram, J.O. Stoffer, T.J. O'Keefe, Application of conducting polymers in corrosion protection, Journal of Coatings Technology 69(866) (1997) 65-69.
[78] A.J. Heeger, Semiconducting and metallic polymers: the fourth generation of polymeric materials, ACS Publications, 2001.
[79] M. Qiang, T. Chen, R.-p. Yao, Effect of Preparation Condition of Polyaniline/Monmorillonite Nanocomposite Material on the Anticorrosion Property, MATERIALS PROTECTION-WUHAN- 36(7) (2003) 25-27.
[80] B. Wessling, Dispersion as the link between basic research and commercial applications of conductive polymers (polyaniline), Synthetic Metals 93(2) (1998) 143-154.
[81] O.L. Gribkova, A.A. Nekrasov, V.A. Cabanova, T.V. Krivenko, N.V. Nekrasova, S.A. Yakovlev, E.I. Terukov, A.R. Tameev, Water-processable nanocomposite based on polyaniline and 2D molybdenum disulfide for NIR-transparent ambipolar transport layers, Chemical Papers 72(7) (2018) 1741-1752.
[82] N.N. Taheri, B. Ramezanzadeh, M. Mahdavian, Application of layer-by-layer assembled graphene oxide nanosheets/polyaniline/zinc cations for construction of an effective epoxy coating anti-corrosion system, Journal of Alloys and Compounds 800 (2019) 532-549.
[83] B. Ramezanzadeh, G. Bahlakeh, M. Ramezanzadeh, Polyaniline-cerium oxide (PAni-CeO_2) coated graphene oxide for enhancement of epoxy coating corrosion protection performance on mild steel, Corrosion Science 137 (2018) 111-126.
[84] A. Baldissera, M. Silveira, C. Beraldo, N. Tocchetto, C. Ferreira, Evaluation of the expandable graphite/polyaniline combination in intumescent coatings, Synthetic Metals 256 (2019) 116141.
[85] M.J. Mazumder, L. Goni, S. Ali, M. Nazal, Inhibition of mild steel corrosion in hydrochloric acid medium by polymeric inhibitors containing residues of essential amino acid methionine, Iranian Polymer Journal 27(12) (2018) 979-995.
[86] B. Wessling, From conductive polymers to organic metals, Chemical innovation 31(1) (2001) 34-40.
[87] J. Stenger-Smith, 'A General Review of Intrinsically Conducting Polymers as Coatings for Corrosion Protection, Proc. US Navy & Industry Corrosion Technology Information Exchange (2000).
[88] S. Sathiyanarayanan, S.S. Azim, G. Venkatachari, A new corrosion protection coating with polyaniline–TiO_2 composite for steel, Electrochimica Acta 52(5) (2007) 2068-2074.
[89] S. Radhakrishnan, C.R. Siju, D. Mahanta, S. Patil, G. Madras, Conducting polyaniline–nano-TiO_2 composites for smart corrosion resistant coatings, Electrochimica Acta 54(4) (2009) 1249-1254.
[90] R.C. Patil, S. Radhakrishnan, Conducting polymer based hybrid nano-composites for enhanced corrosion protective coatings, Progress in Organic Coatings 57(4) (2006) 332-336.
[91] M.G. Hosseini, M. Sabouri, T. Shahrabi, Corrosion protection of mild steel by polypyrrole phosphate composite coating, Progress in Organic Coatings 60(3) (2007) 178-185.
[92] Y.J. Ren, C.L. Zeng, Effect of conducting composite polypyrrole/polyaniline coatings on the corrosion resistance of type 304 stainless steel for bipolar plates of proton-exchange membrane fuel cells, Journal of Power Sources 182(2) (2008) 524-530.
[93] R.S. Jadhav, D.G. Hundiwale, P.P. Mahulikar, Synthesis of nano polyaniline and poly-o-anisidine and applications in alkyd paint formulation to enhance the corrosion resistivity of mild steel, Journal of coatings technology and research 7(4) (2010) 449-454.
[94] K.-C. Chang, M.-H. Hsu, H.-I. Lu, M.-C. Lai, P.-J. Liu, C.-H. Hsu, W.-F. Ji, T.-L. Chuang, Y. Wei, J.-M. Yeh, W.-R. Liu, Room-temperature cured hydrophobic epoxy/graphene composites as corrosion inhibitor for cold-rolled steel, Carbon 66 (2014) 144-153.
[95] V.S. Sumi, S.R. Arunima, M.J. Deepa, M. Ameen Sha, A.H. Riyas, M.S. Meera, V.S. Saji, S.M.A. Shibli, PANI-Fe_2O_3 composite for enhancement of active life of alkyd resin coating for corrosion protection of steel, Materials Chemistry and Physics 247 (2020).
[96] N. Jadhav, S. Kasisomayajula, V. Gelling, Polypyrrole/Metal oxides-based composites/nanocomposites for corrosion protection, Frontiers in Materials 7 (2020) 95.
[97] M. Sun, Z. Ma, G. Zhu, Y. Zhang, Anticorrosive performance of polyaniline/waterborne epoxy/poly (methylhydrosiloxane) composite coatings, Progress in Organic Coatings 139 (2020) 105462.
[98] M. Deyab, G. Mele, Stainless steel bipolar plate coated with polyaniline/Zn-Porphyrin composites coatings for proton exchange membrane fuel cell, Scientific Reports 10(1) (2020) 1-8.
[99] R. Rajkumar, C. Vedhi, Study of the corrosion protection efficiency of polypyrrole/metal oxide nanocomposites as additives in anticorrosion coating, Anti-Corrosion Methods and Materials (2020).
[100] Z. Chen, W. Yang, B. Xu, Y. Chen, M. Qian, X. Su, Z. Li, X. Yin, Y. Liu, Corrosion protection of carbon steels by electrochemically synthesized V-TiO2/polypyrrole composite coatings in 0.1 M HCl solution, Journal of Alloys and Compounds 771 (2019) 857-868.
[101] P. Kong, H. Feng, N. Chen, Y. Lu, S. Li, P. Wang, Polyaniline/chitosan as a corrosion inhibitor for mild steel in acidic medium, RSC advances 9(16) (2019) 9211-9217.
[102] R. Babaei-Sati, J.B. Parsa, M. Vakili-Azghandi, Electrodeposition of polypyrrole/metal oxide nanocomposites for corrosion protection of mild steel—A comparative study, Synthetic Metals 247 (2019) 183-190.
[103] A. El Jaouhari, A. Chennah, S.B. Jaddi, H.A. Ahsaine, Z. Anfar, Y.T. Alaoui, Y. Naciri, A. Benlhachemi, M. Bazzaoui, Electrosynthesis of zinc phosphate-polypyrrole coatings for improved corrosion resistance of steel, Surfaces and Interfaces 15 (2019) 224-231.
[104] X. Liu, P. Hou, X. Zhao, X. Ma, B. Hou, The polyaniline-modified TiO_2 composites in water-based epoxy coating for corrosion protection of Q235 steel, Journal of Coatings Technology and Research 16(1) (2019) 71-80.
[105] H.M. Abd El-Lateef, M.M. Khalaf, Novel dispersed Tl_2O_3-SiO_2/polyaniline nanocomposites: in-situ polymerization, characterization and enforcement as a corrosion protective layer for carbon-steel in acidic chloride medium, Colloids and Surfaces A: Physicochemical and Engineering Aspects 573 (2019) 95-111.
[106] G. Contri, G. Barra, S. Ramoa, C. Merlini, L. Ecco, F. Souza, A. Spinelli, Epoxy coating based on montmorillonite-polypyrrole: Electrical properties and prospective application on corrosion protection of steel, Progress in Organic Coatings 114 (2018) 201-207.
[107] N. Jadhav, T. Matsuda, V. Gelling, Mica/polypyrrole (doped) composite containing coatings for the corrosion protection of cold rolled steel, Journal of Coatings Technology and Research 15(2) (2018) 363-374.
[108] A.A. Salem, B.N. Grgur, The influence of the polyaniline initial oxidation states on the corrosion of steel with composite coatings, Progress in Organic Coatings 119 (2018) 138-144.
[109] L. Jiang, J.A. Syed, Y. Gao, H. Lu, X. Meng, Electrodeposition of $Ni(OH)_2$ reinforced polyaniline coating for corrosion protection of 304 stainless steel, Applied Surface Science 440 (2018) 1011-1021.
[110] H. Arabzadeh, M. Shahidi, M.M. Foroughi, Electrodeposited polypyrrole coatings on mild steel: Modeling the EIS data with a new equivalent circuit and the influence of scan rate and cycle number on the corrosion protection, Journal of Electroanalytical Chemistry 807 (2017) 162-173.
[111] M. Ladan, W.J. Basirun, S.N. Kazi, F.A. Rahman, Corrosion protection of AISI 1018 steel using Co-doped TiO2/polypyrrole nanocomposites in 3.5% NaCl solution, Materials Chemistry and Physics 192 (2017) 361-373.
[112] Q. Yan, C. Li, T. Huang, F. Yang, Electrochemical synthesis of polypyrrole-Al_2O_3 composite coating on 316 stainless steel for corrosion protection, AIP Conference Proceedings, AIP Publishing LLC, 2017, p. 030005.
[113] Q. Yan, C. Li, Electrochemical synthesis of polypyrrole-SiO_2 composite coating on 316 stainless steel for corrosion protection, Anti-Corrosion Methods and Materials (2017).
[114] C. Qiu, D. Liu, K. Jin, L. Fang, G. Xie, J. Robertson, Electrochemical functionalization of 316 stainless steel with polyaniline-graphene oxide: Corrosion resistance study, Materials Chemistry and Physics 198 (2017) 90-98.
[115] S. Lu, H. Yeh, T. Tian, W. Lee, Degradation of magnesium alloys in biological solutions and reduced phenotypic expression of endothelial cell grown on these alloys, 3rd Kuala Lumpur International Conference on Biomedical Engineering 2006, Springer, 2007, pp. 98-101.
[116] C. Seal, K. Vince, M. Hodgson, Biodegradable surgical implants based on

magnesium alloys–A review of current research, IOP conference series: materials science and engineering, IOP Publishing, 2009, p. 012011.
[117] A.H. Shahbaz, M. Esmaeilian, R. NasrAzadani, K. Gavanji, The effect of MgF_2 addition on the mechanical properties of hydroxyapatite synthesized via powder metallurgy, Journal of Composites and Compounds 1(1) (2019) 18-24.
[118] F. Sharifianjazi, M. Moradi, A. Abouchenari, A.H. Pakseresht, A. Esmaeilkhanian, M. Shokouhimehr, M.S. Asl, Effects of Sr and Mg dopants on biological and mechanical properties of SiO_2–CaO–P_2O_5 bioactive glass, Ceramics International (2020).
[119] M. Rahmati, K. Raeissi, M.R. Toroghinejad, A. Hakimizad, M. Santamaria, Effect of pulse current mode on microstructure, composition and corrosion performance of the coatings produced by plasma electrolytic oxidation on AZ31 Mg alloy, Coatings 9(10) (2019) 688.
[120] M. Rahmati, K. Raeissi, M.R. Toroghinejad, A. Hakimizad, M. Santamaria, The multi-effects of K_2TiF_6 additive on the properties of PEO coatings on AZ31 Mg alloy, Surface and Coatings Technology (2020) 126296.
[121] X.-N. Gu, Y.-F. Zheng, A review on magnesium alloys as biodegradable materials, Frontiers of Materials Science in China 4(2) (2010) 111-115.
[122] S. Sathiyanarayanan, S.S. Azim, G. Venkatachari, Corrosion protection of magnesium ZM 21 alloy with polyaniline–TiO_2 composite containing coatings, Progress in Organic Coatings 59(4) (2007) 291-296.
[123] Y. Guo, S. Jia, L. Qiao, Y. Su, R. Gu, G. Li, J. Lian, A multifunctional polypyrrole/zinc oxide composite coating on biodegradable magnesium alloys for orthopedic implants, Colloids Surf B Biointerfaces 194 (2020) 111186.
[124] Y. Wang, The Electrochemical Corrosion Properties of PANI/Coal Composites on Magnesium Alloys, International Journal of Electrochemical Science (2017) 4044-4055.
[125] J. Li, Y. He, Y. Sun, X. Zhang, W. Shi, D. Ge, Synthesis of Polypyrrole/V_2O_5 Composite Film on the Surface of Magnesium Using a Mild Vapor Phase Polymerization (VPP) Method for Corrosion Resistance, Coatings 10(4) (2020).
[126] A.S. Najibzad, R. Amini, M. Rostami, P. Kardar, M. Fedel, Active corrosion performance of magnesium by silane coatings reinforced with polyaniline/praseodymium, Progress in Organic Coatings 140 (2020) 105504.
[127] V. Jothi, A.Y. Adesina, A.M. Kumar, M.M. Rahman, J.S.N. Ram, Enhancing the biodegradability and surface protective performance of AZ31 Mg alloy using polypyrrole/gelatin composite coatings with anodized Mg surface, Surface and Coatings Technology 381 (2020) 125139.
[128] A. Samadi, R. Amini, M. Rostami, P. Kardar, M. Fedel, Preparation of polyaniline-modified praseodymium nanofibers as a novel eco-friendly corrosion inhibitor to protect AZ31 magnesium alloy, Pigment & Resin Technology (2020).
[129] R. Maurya, A.R. Siddiqui, P.K. Katiyar, K. Balani, Mechanical, tribological and anti-corrosive properties of polyaniline/graphene coated Mg-9Li-7Al-1Sn and Mg-9Li-5Al-3Sn-1Zn alloys, Journal of Materials Science & Technology 35(8) (2019) 1767-1778.
[130] Y. Li, J. Li, X. Gao, S. Qi, J. Ma, J. Zhu, Synthesis of stabilized dispersion covalently-jointed SiO_2@ polyaniline with core-shell structure and anticorrosion performance of its hydrophobic coating for Mg-Li alloy, Applied Surface Science 462 (2018) 362-372.
[131] X. Gao, X. Jing, Y. Li, J. Zhu, M. Zhang, Synthesis and characterization of phosphorized polyaniline doped with phytic acid and its anticorrosion properties for Mg-Li alloy, Journal of Macromolecular Science, Part A 55(1) (2018) 24-35.
[132] M. Saremi, S.H. Mortazavi, Effect of polypyrrole coating modified by sodium fluoride and polyethylene glycol on corrosion behaviour of AZ31 magnesium alloy, Micro & Nano Letters 11(12) (2016) 866-869.
[133] X. Chen, K. Shen, J. Zhang, Preparation and anticorrosion properties of polyaniline-SiO_2-containing coating on Mg-Li alloy, Pigment & Resin Technology (2010).
[134] M. Hosseini, M. Jafari, R. Najjar, Effect of polyaniline–montmorillonite nanocomposite powders addition on corrosion performance of epoxy coatings on Al 5000, Surface and Coatings Technology 206(2-3) (2011) 280-286.
[135] M. Ghafaripoor, K. Raeissi, M. Santamaria, A. Hakimizad, The corrosion and tribocorrosion resistance of PEO composite coatings containing α-Al_2O_3 particles on 7075 Al alloy, Surface and Coatings Technology 349 (2018) 470-479.
[136] I. Tajzad, E. Ghasali, Production methods of CNT-reinforced Al matrix composites: a review, Journal of Composites and Compounds 2(1) (2020) 1-9.
[137] S. Nasibi, K. Alimohammadi, L. Bazli, S. Eskandarinezhad, A. Mohammadi, N. Sheysi, TZNT alloy for surgical implant applications: A systematic review, Journal of Composites and Compounds 2(3) (2020) 62-68.
[138] K. Kamaraj, S. Sathiyanarayanan, G. Venkatachari, Electropolymerised polyaniline films on AA 7075 alloy and its corrosion protection performance, Progress in Organic Coatings 64(1) (2009) 67-73.
[139] E. Akbari, F. Di Franco, P. Ceraolo, K. Raeissi, M. Santamaria, A. Hakimizad, Electrochemically-induced TiO_2 incorporation for enhancing corrosion and tribocorrosion resistance of PEO coating on 7075 Al alloy, Corrosion Science 143 (2018) 314-328.
[140] K. Zhang, H.W. Jang, Q. Van Le, Production methods of ceramic-reinforced Al-Li matrix composites: A review, Journal of Composites and Compounds 2(3) (2020) 77-84.
[141] E. Asadi, A.F. Chimeh, S. Hosseini, S. Rahimi, B. Sarkhosh, L. Bazli, R. Bashiri, A.H.V. Tahmorsati, A review of clinical applications of graphene quantum dot-based composites, Journal of Composites and Compounds 1(1) (2019) 36-47.
[142] M. Yan, C.A. Vetter, V.J. Gelling, Corrosion inhibition performance of polypyrrole Al flake composite coatings for Al alloys, Corrosion Science 70 (2013) 37-45.
[143] M. A. Hussein, Electrodeposition and Corrosion Protection Performance of Polypyrrole Composites on Aluminum, International Journal of Electrochemical Science (2016) 3938-3951.
[144] M. Hosseini, L. Fotouhi, A. Ehsani, M. Naseri, Enhancement of corrosion resistance of polypyrrole using metal oxide nanoparticles: Potentiodynamic and electrochemical impedance spectroscopy study, J Colloid Interface Sci 505 (2017) 213-219.
[145] K. Shah, Y. Zhu, G.S. Akundy, J.O. Iroh, O. Popoola, Corrosion and Bonding Behaviors of Intrinsically Conductive Polymers on Aluminum (AI 2024-T3), Key Engineering Materials 197 (2001) 111-120.
[146] V. Tomaev, K. Levin, T. Stoyanova, A. Syrkov, Synthesis and Study of a Polypyrrole–Aluminum Oxide Nanocomposite Film on an Aluminum Surface, Glass Physics and Chemistry 45(4) (2019) 291-297.
[147] A.M. Kumar, R.S. Babu, S. Ramakrishna, A.L. de Barros, Electrochemical synthesis and surface protection of polypyrrole-CeO_2 nanocomposite coatings on AA2024 alloy, Synthetic Metals 234 (2017) 18-28.
[148] M. Ates, E. Topkaya, Nanocomposite film formations of polyaniline via TiO_2, Ag, and Zn, and their corrosion protection properties, Progress in Organic Coatings 82 (2015) 33-40.
[149] M. Ates, O. Kalender, E. Topkaya, L. Kamer, Polyaniline and polypyrrole/TiO_2 nanocomposite coatings on Al1050: electrosynthesis, characterization and their corrosion protection ability in saltwater media, Iranian Polymer Journal 24(7) (2015) 607-619.
[150] F. Alvi, N. Aslam, S.F. Shaukat, Corrosion inhibition study of zinc oxide-polyaniline nanocomposite for aluminum and steel, American Journal of Applied Chemistry 3(2) (2015) 57-64.
[151] M.B. Jensen, M.J. Peterson, N. Jadhav, V.J. Gelling, SECM investigation of corrosion inhibition by tungstate-and vanadate-doped polypyrrole/aluminum flake composite coatings on AA2024-T3, Progress in Organic Coatings 77(12) (2014) 2116-2122.
[152] G. Gupta, N. Birbilis, A.B. Cook, A.S. Khanna, Polyaniline-lignosulfonate/epoxy coating for corrosion protection of AA2024-T3, Corrosion Science 67 (2013) 256-267.
[153] N. Jadhav, C.A. Vetter, V.J. Gelling, The effect of polymer morphology on the performance of a corrosion inhibiting polypyrrole/aluminum flake composite pigment, Electrochimica acta 102 (2013) 28-43.
[154] M. Shabani-Nooshabadi, S.M. Ghoreishi, M. Behpour, Direct electrosynthesis of polyaniline–montmorrilonite nanocomposite coatings on aluminum alloy 3004 and their corrosion protection performance, Corrosion Science 53(9) (2011) 3035-3042.
[155] K.R. Castagno, V. Dalmoro, R.S. Mauler, D.S. Azambuja, Characterization and corrosion protection properties of polypyrrole/montmorillonite electropolymerized onto aluminium alloy 1100, Journal of polymer research 17(5) (2010) 647-655.
[156] M. Hosseini, M. Raghibi-Boroujeni, I. Ahadzadeh, R. Najjar, M.S. Dorraji, Effect of polypyrrole–montmorillonite nanocomposites powder addition on corrosion performance of epoxy coatings on Al 5000, Progress in organic coatings 66(3) (2009) 321-327.
[157] K. Wu, C. Chao, C. Liu, T. Chang, Characterization and corrosion resistance of organically modified silicate–NiZn ferrite/polyaniline hybrid coatings on aluminum alloys, Corrosion science 49(7) (2007) 3001-3014.
[158] D. Wrobleski, Corrosion resistant coatings from conducting polymers, Meeting of the Division of Polymer Chemistry, 1994, pp. 265-266.
[159] A. Cascalheira, S. Aeiyach, P. Lacaze, L. Abrantes, Electrochemical synthesis and redox behaviour of polypyrrole coatings on copper in salicylate aqueous solution, Electrochimica acta 48(17) (2003) 2523-2529.
[160] Y. Meng, J. Yin, T. Jiao, J. Bai, L. Zhang, J. Su, S. Liu, Z. Bai, M. Cao, Q. Peng, Self-assembled copper/cobalt-containing polypyrrole hydrogels for highly efficient ORR electrocatalysts, Journal of Molecular Liquids 298 (2020) 112010.
[161] W.N. Nyairo, Y.R. Eker, C. Kowenje, I. Akin, H. Bingol, A. Tor, D.M.

Ongeri, Efficient adsorption of lead (II) and copper (II) from aqueous phase using oxidized multiwalled carbon nanotubes/polypyrrole composite, Separation Science and Technology 53(10) (2018) 1498-1510.
[162] M. Menkuer, H. Ozkazanc, Electrodeposition of polypyrrole on copper surfaces in OXA-DBSA mix electrolyte and their corrosion behaviour, Progress in Organic Coatings 130 (2019) 149-157.
[163] L.A. Cheah, G. Manohara, M.M. Maroto-Valer, S. Garcia, Layered Double Hydroxide (LDH)-Derived Mixed Metal Oxides (MMOs): A Systematic Crystal-Chemical Approach to Investigating the Chemical Composition and its Effect on High Temperature CO_2 capture, ChemistrySelect 5(19) (2020) 5587-5594.
[164] A.J. Rad, Synthesis of copper oxide nanoparticles on activated carbon for pollutant removal in Tartrazine structure, Journal of Composites and Compounds 2(3) (2020) 99-104.
[165] M. Arefian, M. Hojjati, I. Tajzad, A. Mokhtarzade, M. Mazhar, A. Jamavari, A review of Polyvinyl alcohol/Carboxiy methyl cellulose (PVA/CMC) composites for various applications, Journal of Composites and Compounds 2(3) (2020) 69-76.
[166] A. Abuchenari, M. Moradi, The Effect of Cu-substitution on the microstructure and magnetic properties of Fe-15% Ni alloy prepared by mechanical alloying, Journal of Composites and Compounds 1(1) (2019) 11-17.
[167] A. Moghanian, A. Ghorbanoghli, M. Kazem-Rostami, A. Pazhouheshgar, E. Salari, M. Saghafi Yazdi, T. Alimardani, H. Jahani, F. Sharifian Jazi, M. Tahriri, Novel antibacterial Cu/Mg-substituted 58S-bioglass: Synthesis, characterization and investigation of in vitro bioactivity, International Journal of Applied Glass Science (2019).
[168] G. Kilincceker, B. Yazici, A. Yilmaz, M. Erbil, Effect of phosphate ions on electrochemical behaviour of copper in sulphate solutions, British Corrosion Journal 37(1) (2002) 23-30.
[169] B. Tan, S. Zhang, Y. Qiang, L. Guo, L. Feng, C. Liao, Y. Xu, S. Chen, A combined experimental and theoretical study of the inhibition effect of three disulfide-based flavouring agents for copper corrosion in 0.5 M sulfuric acid, Journal of colloid and interface science 526 (2018) 268-280.
[170] H. Alhumade, A. Abdala, A. Yu, A. Elkamel, L. Simon, Corrosion inhibition of copper in sodium chloride solution using polyetherimide/graphene composites, The Canadian Journal of Chemical Engineering 94(5) (2016) 896-904.
[171] A. Asan, M. Kabasakaloglu, M. Işıklan, Z. Kılıç, Corrosion inhibition of brass in presence of terdentate ligands in chloride solution, Corrosion Science 47(6) (2005) 1534-1544.
[172] B.M. Thethwayo, A.M. Garbers-Craig, Laboratory scale investigation into the corrosion of copper in a sulphur-containing environment, Corrosion science 53(10) (2011) 3068-3074.
[173] J. Chen, Z. Qin, D. Shoesmith, Long-term corrosion of copper in a dilute anaerobic sulfide solution, Electrochimica acta 56(23) (2011) 7854-7861.
[174] A.M. Fenelon, C.B. Breslin, The electrochemical synthesis of polypyrrole at a copper electrode: corrosion protection properties, Electrochimica Acta 47(28) (2002) 4467-4476.
[175] T. Tüken, B. Yazıcı, M. Erbil, Polypyrrole/polythiophene coating for copper protection, Progress in organic coatings 53(1) (2005) 38-45.
[176] A. Guenbour, A. Kacemi, A. Benbachir, Corrosion protection of copper by polyaminophenol films, Progress in organic coatings 39(2-4) (2000) 151-155.
[177] M. Redondo, C.B. Breslin, Polypyrrole electrodeposited on copper from an aqueous phosphate solution: Corrosion protection properties, Corrosion science 49(4) (2007) 1765-1776.
[178] W. Prissanaroon, N. Brack, P. Pigram, J. Liesegang, Electropolymerisation of pyrrole on copper in aqueous media, Synthetic metals 142(1-3) (2004) 25-34.
[179] M. Bazzaoui, J. Martins, E. Bazzaoui, T. Reis, L. Martins, Pyrrole electropolymerization on copper and brass in a single-step process from aqueous solution, Journal of applied electrochemistry 34(8) (2004) 815-822.
[180] L.M. Dos Santos, J. Lacroix, K. Chane-Ching, A. Adenier, L. Abrantes, P. Lacaze, Electrochemical synthesis of polypyrrole films on copper electrodes in acidic and neutral aqueous media, Journal of Electroanalytical Chemistry 587(1) (2006) 67-78.
[181] P. Herrasti, A. Del Rio, J. Recio, Electrodeposition of homogeneous and adherent polypyrrole on copper for corrosion protection, Electrochimica acta 52(23) (2007) 6496-6501.
[182] M.M. Gvozdenović, B.Z. Jugović, J.S. Stevanović, B. Grgur, T.L. Trišović, Z.S. Jugović, Electrochemical synthesis and corrosion behavior of polyaniline-benzoate coating on copper, Synthetic Metals 161(13-14) (2011) 1313-1318.
[183] T.J. Pan, X.W. Zuo, T. Wang, J. Hu, Z.D. Chen, Y.J. Ren, Electrodeposited conductive polypyrrole/polyaniline composite film for the corrosion protection of copper bipolar plates in proton exchange membrane fuel cells, Journal of Power Sources 302 (2016) 180-188.
[184] İ. Çakmakcı, B. Duran, G. Bereket, Influence of electrochemically prepared poly(pyrrole-co-N-methyl pyrrole) and poly(pyrrole)/poly(N-methyl pyrrole) composites on corrosion behavior of copper in acidic medium, Progress in Organic Coatings 76(1) (2013) 70-77.
[185] F. Branzoi, V. Branzoi, Z. Pahom, Monolayer and bilayer conducting polymer coatings for corrosion protection of copper in 0.5 M H_2SO_4 solutions, Rev. Roum. Chim 58(1) (2013) 49-58.
[186] B.P. Singh, B.K. Jena, S. Bhattacharjee, L. Besra, Development of oxidation and corrosion resistance hydrophobic graphene oxide-polymer composite coating on copper, Surface and Coatings Technology 232 (2013) 475-481.
[187] H. Kim, H. Lee, H.-R. Lim, H.-B. Cho, Y.-H. Choa, Electrically conductive and anti-corrosive coating on copper foil assisted by polymer-nanocomposites embedded with graphene, Applied Surface Science 476 (2019) 123-127.
[188] B.P. Singh, S. Nayak, K.K. Nanda, B.K. Jena, S. Bhattacharjee, L. Besra, The production of a corrosion resistant graphene reinforced composite coating on copper by electrophoretic deposition, Carbon 61 (2013) 47-56.
[189] S. Wan, C.-H. Miao, R.-M. Wang, Z.-F. Zhang, Z.-H. Dong, Enhanced corrosion resistance of copper by synergetic effects of silica and BTA codoped in polypyrrole film, Progress in Organic Coatings 129 (2019) 187-198.
[190] Y. Jafari, S. Ghoreishi, M. Shabani-Nooshabadi, Polyaniline/graphene nanocomposite coatings on copper: electropolymerization, characterization, and evaluation of corrosion protection performance, Synthetic Metals 217 (2016) 220-230.
[191] M. Shabani-Nooshabadi, F. Karimian-Taheri, Electrosynthesis of a polyaniline/zeolite nanocomposite coating on copper in a three-step process and the effect of current density on its corrosion protection performance, RSC advances 5(117) (2015) 96601-96610.
[192] A. Davoodi, S. Honarbakhsh, G.A. Farzi, Evaluation of corrosion resistance of polypyrrole/functionalized multi-walled carbon nanotubes composite coatings on 60Cu–40Zn brass alloy, Progress in Organic Coatings 88 (2015) 106-115.
[193] S. Dhibar, S. Sahoo, C. Das, R. Singh, Investigations on copper chloride doped polyaniline composites as efficient electrode materials for supercapacitor applications, Journal of Materials Science: Materials in Electronics 24(2) (2013) 576-585.